

Oleic acid-based polyamides for sustainable fibers

DISSERTATION

zur Erlangung des akademischen Grades
eines Doktors der Naturwissenschaften (Dr. rer. nat.)
in der Bayreuther Graduiertenschule
für Mathematik und Naturwissenschaften (BayNAT)
der Universität Bayreuth

vorgelegt von

Maximilian Rist

aus Wangen im Allgäu

Bayreuth, 2023

This thesis was written in the period from January 2020 to November 2023 in Bayreuth at the research group Macromolecular Chemistry II under the supervision of Prof. Dr. Andreas Greiner.

This is a full reprint of the thesis submitted to obtain the academic degree of Doctor of Natural Sciences (Dr. rer. nat.) and approved by the Bayreuth Graduate School of Mathematical and Natural Sciences (BayNAT) of the University of Bayreuth.

Date of submission: 27.11.2023

Date of defence: 08.04.2024

Acting director: Prof. Dr. Jürgen Köhler

Doctoral committee:

Prof. Dr. Andreas Greiner (reviewer)

Prof. Dr.-Ing. Holger Ruckdäschel (reviewer)

Prof. Dr. Matthias Breuning (chairman)

Prof. Dr. Anna Schenk

Table of contents

Zusammenfassung	1
Summary	4
1 Introduction	6
1.1 Polyamides	6
1.1.1 Bio-based Polyamides	11
1.1.2 Oleic acid as a platform chemical	16
1.2 Fiber-spinning	21
1.2.1 Melt-spun fibers and applications	21
1.2.2 Electrospun fibers and applications.....	23
2 Synopsis	29
2.1 Aim.....	29
2.2 Overview	30
2.3 Synthesis, Characterization, and the Potential for Closed Loop Recycling of Plant Oil-Based PA X.19 Polyamides	32
2.4 Toughening of bio-based PA 6.19 by copolymerization with PA 6.6 – synthesis and production of melt-spun monofilaments and knitted fabrics	35
2.5 Bio-based electrospun polyamide membrane – sustainable multipurpose filter membranes for microplastic filtration	39
3 Contribution to the work	42
3.1 Publication 1.....	42
3.2 Publication 2.....	42
3.3 Publication 3.....	43
4 Publications	44
4.1 Publication 1.....	44
4.2 Publication 2.....	60
4.3 Publication 3.....	81

5	List of publications.....	101
6	Supplementary Information.....	102
7	References	104
8	Conclusion.....	128
9	Outlook.....	129
10	Acknowledgements	130
11	Eidesstattliche Versicherungen und Erklärungen	131

Zusammenfassung

Die weltweite Produktion von Kunststoffen hat in den letzten Jahren stetig zugenommen, so dass die Suche nach alternativen Ressourcen immer wichtiger wird. Die Verwendung bio-basierter Materialien hat sich als vielversprechende Lösung für die Herstellung nachhaltiger Kunststoffe erwiesen. Trotz ihrer Verwendung ist der Einsatz bio-basierter Rohstoffe bei der Herstellung von synthetischen Fasern jedoch noch begrenzt. Ziel dieser Arbeit war es, diese Lücke zu schließen. Hierzu wurde die Machbarkeit der Synthese von Monomeren und Polymeren aus Rohstoffen, die aus Mikroalgen gewonnen wurden, für die Herstellung nachhaltiger Kunstfasern untersucht. Mikroalgen bieten mehrere Vorteile gegenüber herkömmlichen Pflanzen, darunter schnelle Wachstumsraten und die Möglichkeit des Anbaus auf nicht bebaubaren Flächen und mit Abwasser. Außerdem binden sie Kohlendioxid und konkurrieren nicht mit der Nahrungsmittelproduktion.

In dieser Arbeit wurde Ölsäure, eine Fettsäure, die in der Natur reichlich vorkommt und von Mikroalgen leicht produziert werden kann, als Ausgangskemikalie für die Synthese von Disäuren gewählt. Diese Disäuren mussten linear sein und durften keine Seitenketten oder Verzweigungen aufweisen, um die für die Herstellung von Kunstfasern erforderliche mechanische Stabilität zu gewährleisten. Um den gesamten verfügbaren Kohlenstoff der Ölsäure zu nutzen, wurde die langkettige 1,19-Nonadecandisäure durch isomerisierende Methoxycarbonylierung synthetisiert. Die oxidative Spaltung der Ölsäure ergab die kürzere Azelainsäure, bei der nur 50 % des verfügbaren Kohlenstoffs genutzt wurden. Diese ist bereits aus nicht-algenbasierten Rohstoffen kommerziell erhältlich. Die Homopolymere PA X.19 und PA 6.9 wurden durch Schmelzpolykondensation unter Verwendung der Disäure zusammen mit Hexamethyldiamin und anderen linearen aliphatischen Diaminen synthetisiert. Die Struktur-Eigenschafts-Beziehung der resultierenden PA X.19 in Abhängigkeit vom verwendeten Diamin wurde untersucht, um ihr Potenzial für die Faserherstellung abzuschätzen.

Das bio-basierte PA X.19 wies eine wesentlich geringere Wasseraufnahme auf als die kommerziellen Polyamide PA 10.10 und PA 6 und bietet daher eine höhere Dimensionsstabilität. Sie konnten außerdem bei niedrigeren Temperaturen verarbeitet werden, was ihre Schmelzverarbeitung energieeffizienter macht. Das chemische Recycling der synthetisierten Polyamide wurde beispielhaft durch die mikrowellenunterstützte Hydrolyse von PA 6.19 gezeigt. Die 1,19-Nonadecandisäure wurde in nahezu quantitativer Ausbeute von 99%

und in hoher Reinheit zurückgewonnen. Die Synthese von PA 6.19 unter Verwendung der rezyklierten Disäure und Hexamethyldiamin wurde erfolgreich durchgeführt, um das Potenzial zur Kreislaufwirtschaft zu demonstrieren.

Die mangelnde Zugfestigkeit des Homopolymers PA 6.19 wurde durch Copolymerisation mit PA 6.6 verbessert. Die Struktur-Eigenschafts-Beziehung der resultierenden Copolyamide wurde untersucht, um eine geeignete Formulierung für die Herstellung von schmelzgesponnenen Monofilamenten zu finden. Die Einführung der kurzkettigen Adipinsäure führte zu einer Verbesserung der Zugfestigkeit um 58 %. Da die erhöhte Zugfestigkeit nicht mit einer geringeren Bruchdehnung einherging, war die Zähigkeit der Copolyamide um bis zu 64% besser als die des PA 6.19-Homopolymers. Die insgesamt beste Kombination aus Bio-Anteil und mechanischen Eigenschaften wurde in einem Scale-up-Verfahren erfolgreich synthetisiert. Das Copolyamid wurde erfolgreich für Schmelzspinnversuche bei verschiedenen Verstreckungsverhältnissen verwendet, um Monofilamente zu erhalten. Das Schmelzspinnen bei Verstreckungsverhältnissen, die für das industrielle Spinnen von teilverstreckten Garnen (POY) verwendet werden, wurde erfolgreich durchgeführt und somit die Eignung des Materials für die Verarbeitung auf industriellen Spinnanlagen nachgewiesen. Die durch Schmelzspinnen des Copolyamids gewonnenen Monofilamente zeigten eine gute Festigkeit, waren aber dem handelsüblichen PA 6 unterlegen. Aus den feinsten Monofilamenten wurden erfolgreich Strickmuster hergestellt, um die Eignung dieser Copolyamide für die Herstellung nachhaltiger Textilien weiter zu unterstreichen.

PA 6.9 wurde aus der kommerziell erhältlicher, fettsäure-basierter Azelainsäure synthetisiert und Vliese wurden erfolgreich durch Elektrospinnen hergestellt. Diese Membranen wurden vollständig charakterisiert, um eine mögliche Anpassung des Faserdurchmessers und der Porengröße in Abhängigkeit von der Polymerkonzentration aufzuzeigen. Die elektrogewonnenen Filtermembranen (EFMs) wurden erfolgreich für die Filtration von in Wasser suspendierten Polystyrol-Mikropartikeln eingesetzt. Alle Membranen zeigten eine ausgezeichnete Filtrationseffizienz und eine stabile Durchlässigkeit über einen längeren Zeitraum. Auch die Filtration von Aerosolen aus der Luft war mit hohen Filtrationseffizienzen möglich, welche internationalen Standards entsprechen. Aufgrund ihrer hydrophoben Oberfläche zeigten die EFMs eine sehr hohe Durchlässigkeit für organische Lösungsmittel wie Chloroform. Die schwerkraftgetriebene Trennung von Wasser und Chloroform war mit einer Trennleistung von 99,9 % möglich. Sie kombinieren daher eine hohe Durchlässigkeit mit einer

hohen Trennleistung. Darüber hinaus konnten die Membranen mindestens zehnmal wiederverwendet werden, ohne dass sich ihre Filtrationseigenschaften wesentlich veränderten.

Insgesamt unterstreicht diese Arbeit das Potenzial von Polyamiden auf Ölsäurebasis für die Herstellung von Kunstfasern. Die umfassende Charakterisierung der resultierenden Polyamide und die Herstellung von Makro- und Submikrofasern mit verschiedenen Spinnverfahren lieferten Einblicke in ihre potenziellen Anwendungen in Textilien und Membranen. Darüber hinaus zeigte die Untersuchung des chemischen Recyclings und der Wiederverwendbarkeit die Möglichkeit eines geschlossenen Kreislaufs auf, der die Nachhaltigkeit der Fasern weiter erhöht.

Summary

The global production of plastics has been steadily increasing, making the exploration of alternative resources more and more important. The use of bio-based materials has emerged as a promising solution for the production of sustainable plastics. However, despite the growing application of bio-based plastics, their utilization in the production of synthetic fibers remains limited. This thesis aimed to bridge this gap by investigating the feasibility of microalgae-derived feedstock for the synthesis of monomers and polymers, leading to the production of sustainable synthetic fibers. Microalgae offer several advantages over traditional crops including rapid growth rates and possibility of cultivation on non-arable land and with wastewater. Furthermore, they capture carbon dioxide and do not compete with food production.

In this thesis, oleic acid, an abundant fatty acid found in nature and readily produced by microalgae, was chosen as the platform chemical for the synthesis of the diacids. These diacids were required to be linear, devoid of side-chains or branching points, to ensure the mechanical stability necessary for the production of synthetic fibers. In order to utilize all available carbon of the oleic acid, the long-chain 1,19-nonadecanedioic acid was synthesized by isomerizing methoxycarbonylation. Oxidative cleavage of the oleic acid yielded the shorter azelaic acid, which only utilized 50% of the available carbon and is already commercially available from non-algae-based feedstock. Homopolymers PA X.19 and PA 6.9 were synthesized by melt polycondensation using these diacids together with hexamethylene diamine and other linear aliphatic diamines. The structure-property relationship of the resulting PA X.19 depending on the diamine used was investigated to assess their potential for fiber production.

The bio-based PA X.19 exhibited much lower water uptake than commercial polyamides PA 10.10 and PA 6 and therefore offer higher dimensional stability. They were also processable at a lower temperature making their melt processing more energy efficient. Chemical recycling of the synthesized polyamides was exemplary shown by microwave-assisted hydrolysis of PA 6.19. The 1,19-nonadecanedioic acid was recovered in almost quantitative yields of 99% and in high purity. Synthesis of PA 6.19 using the recycled diacid and hexamethylene diamine was successfully performed to demonstrate the potential for closed-loop recycling.

The lacking mechanical strength of the homopolymer PA 6.19 was improved by copolymerization with PA 6.6. The structure-property relationship of the resulting copolyamides was investigated in order to find a suitable formulation for the production of

melt-spun monofilaments. Introduction of the shorter-chain adipic acid resulted in an improved tensile strength by 58%. As the increased tensile strength was not accompanied by a lower elongation at break, the toughness of the copolyamides was up to 64% better than for the PA 6.19 homopolymer. The overall best combination of bio-content and mechanical properties was successfully synthesized in a scaled up reaction. The copolyamide was successfully used for melt spinning trials at different draw-down ratios to receive monofilaments. Melt spinning at draw-down ratios used for industrial spinning of partially oriented yarns (POY) was successfully performed to prove the suitability of the material for processing on industrial spinning lines. The monofilaments obtained by melt spinning of the copolyamide showed good tenacity, but were inferior to the commercial PA 6. Knitted swatches were successfully prepared from the finest monofilaments to further emphasize the suitability of these copolyamides for the production of sustainable textiles.

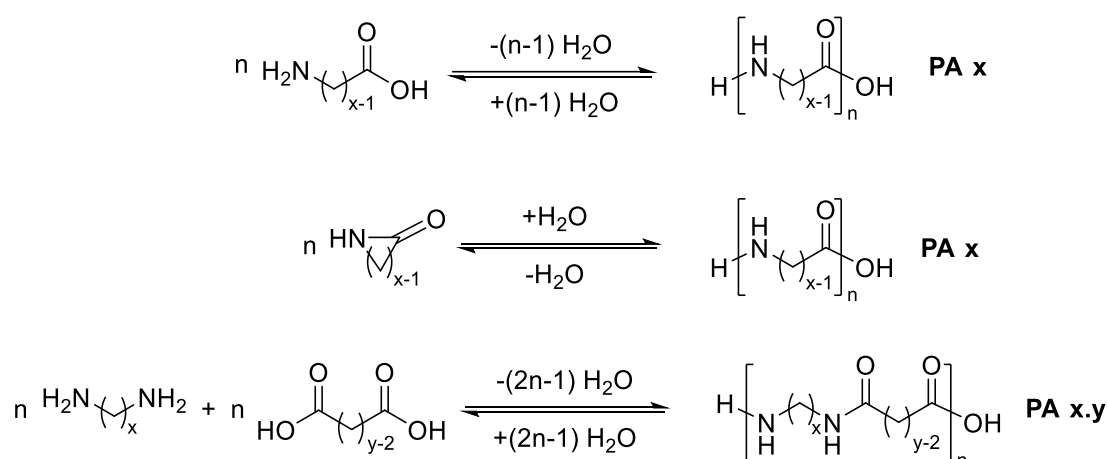
PA 6.9 was synthesized from the commercially available fatty acid-based azelaic acid and nonwovens were successfully prepared by electrospinning. These membranes were fully characterized to show possible tailoring of the fiber diameter and pore size influenced by the polymer concentration. The electrospun filter membranes (EFMs) were successfully used for the filtration of polystyrene microparticles suspended in water. All membranes showed excellent filtration efficiencies accompanied by a stable permeability over a longer duration. Aerosol filtration from air was also possible with high filtration efficiencies meeting international standards. Due to their hydrophobic surface the EFMs showed very high permeability for organic solvents like chloroform. Gravity-driven separation of water and chloroform was possible with a separation efficiency of 99.9%. They combine high permeability with a high separation efficiency. Additionally, the membranes could be reused at least ten times without significant influence on their filtration properties.

Overall, this thesis highlights the potential of oleic acid-based polyamides for the production of synthetic fibers. The comprehensive characterization of the resulting polyamides and the production of macro- and submicro-fibers using different spinning techniques provided insights into their potential applications in textiles and membranes. Moreover, the investigation of chemical recycling and reusability highlighted the possibility of adopting a closed-loop approach, further enhancing their environmental sustainability.

1 Introduction

1.1 Polyamides

The family of polyamides (PA) contains a broad variety of polymers with very different properties. On the one hand there are the naturally occurring polyamides, commonly referred to as polypeptides, which are critical for many functions in a living body. And on the other hand, the synthetic polyamides, first introduced in 1929 by CAROTHERS.^{1,2} Polyamides are typically synthesized by a polycondensation reaction of an amine and a carboxylic acid to produce an amide and water. The amine and carboxylic acid can be in the same molecule, like as in the case of amino acids. Alternatively, a dicarboxylic acid and a diamine can be used together to synthesize a polyamide (**Scheme 1**). The resulting polyamides are classified as AB-type or AABB-type, depending on the monomer(s) used, with A and B representing amine and carboxylic acid. AB-type polyamides may also be made by ring-opening polymerization of lactams, which are basically cyclized amino acids. For AABB-type polyamides the first number is corresponding to the carbon atoms in the main chain of the diamine and the second number corresponds to the carbon atoms in the diacid main chain. Depending if the carbon atoms in the dicarboxylic acid and diamine are aromatic or aliphatic, the AABB-type polyamides can be further classified into aliphatic polyamides (fully aliphatic), polyphthalamides (semi-aromatic) and polyaramides (fully aromatic).



Scheme 1. Polycondensation reaction of an amino acid and ring-opening polymerization of a lactam to form AB-type polyamides as well as polycondensation of a dicarboxylic acid and diamine to form an AABB-type polyamide.

Polyamides are, with some exceptions, semi crystalline thermoplastics with the ability to form hydrogen bonds, resulting in strong interactions between the polymer chains. This sets them

apart from other commodity polymers like polyethylene, polystyrene or polyester, where only van der Waals interactions and pi-stacking are present. Many of polyamides biggest advantages can be attributed to their intermolecular hydrogen bonding as for example their high melting temperature and high mechanical strength. These properties can be even more increased by additional attraction forces like pi-stacking in the case of polyphthalamides and polyaramides (**Table 1**). Evidently, there is a strong relationship between the structure of the polyamide and its properties.

Table 1. Melting temperature and ultimate tensile strength of different commodity polymers in comparison with polyamide 6, polyamide 6.T and *Kevlar*®.³⁻⁶ These values may vary depending on the molecular weight and crystallinity of the polymers.

Polymer	T_m [°C]	F_{max} [MPa]
Poly(paraphenylene terephthalamide) (<i>Kevlar</i> ®)	560	3620
Poly(hexamethylene terephthalamide) (PA 6.T)	371	175
Polyamide 6 (PA 6)	220	70-85
Polycaprolactone (PCL)	58	32
Polystyrene (PS)	n. a.	45-65
High density polyethylene (HDPE)	132	18-35

For aliphatic polyamides the melting temperature (T_m) is strongly influenced by the density and the orientation of the amide-groups.⁷ A decreasing density results in a lower amount of hydrogen bonds along the polymer chain and therefore a lower T_m . PA 6.12, for example, shows a much lower T_m of 215 °C than PA 6.6 (265 °C), which is due to the higher amount of methylene units in the diacid, reducing the amide-group density.⁸ The same applies for AB-type polyamides like PA 6 (220 °C) and PA 12 (179 °C). Although they have the same amide-group density, PA 6 and PA 6.6 exhibit very different T_m . This is due to the orientation of the amide-groups. In even numbered polyamides of the AB-type, such as PA 6, the orientation of the amide groups alternates. Therefore, the intramolecular distance between the hydrogen bond donor (amine) and hydrogen bond acceptor (carbonyl) of adjacent chains is not matching, which limits the formation of hydrogen bonds. For even-even numbered AABB-type polyamides like PA 6.6 the amide group orientation is also alternating, but due to the symmetry of the monomers the donors and acceptors of adjacent polymer chains are always matching. The opposite is true for odd-numbered AB-type and odd-odd and odd-even/even-odd numbered AABB-type polyamides like PA 7 (233 °C) and PA 5.6 (223 °C).^{7,8}

Much like the melting temperature, the mechanical properties of polyamides are also closely related to the amide-group density. Of course, crystallinity, molecular weight and the type of polyamide also strongly influence the mechanical properties. Aromatic units make the material stiffer and also increase the tensile strength due to the additional intermolecular pi-stacking (**Table 1**). But, the increased stiffness results in a lower elongation at break, making the material less ductile. The same result can be achieved by increasing the density of the amide-groups of aliphatic polyamides by using shorter chain diacids and diamines. For example, the tensile strength of PA 6.12 (61 MPa) is 25% lower than that of PA 6.6 (83 MPa) due to the additional six methylene-units in the diacid and the resulting lower amide-group density.⁸ A higher amide-group density results in higher crystallinity of the polyamide, which increases the flexural, compressive, tensile and shear strength of the material. Polyamides having lower crystallinity exhibit lower tensile strength but higher impact strength and toughness, due to the higher proportion of amorphous regions. A higher molecular weight also leads to higher impact strength without affecting tensile strength, but results in a lower elongation at break.⁷ The mechanical properties of polyamides are also affected by the moisture content of the material. Owing to the polarity of the amide-group, polyamides tend to absorb a relatively great amount of water when in contact to moisture. Since water is known to act as a plasticizer, increasing moisture content leads to lower tensile strength but higher elongation, which increases impact strength.^{9,10} However, the magnitude again depends on the amide-group density, since it directly influences the water uptake of the polyamide. For example, the Young's modulus for PA 6.6 drops by 55% from 3100 MPa in the dry state to 1400 MPa at 50% humidity.¹⁰ For PA 6.12, on the other hand, the change is much smaller (2400 to 1700 MPa), due to the lower water uptake. The absorbed water also affects the dimensional stability and causes deformation of the intended geometry.^{9,10} Textile fibers made from polyamide, for example, can expand in high humidity, causing the fabric to become loose. This limits the application of polyamides in deep-sea applications, where long term durability is essential.^{11,12} Additionally, hydrolytic cleavage of the amide-bond can happen during melt processing if moisture is present.⁷ Thorough drying of the polyamide is necessary before injection molding or melt spinning.

The first synthetic polyamides ever made are PA 6.6¹³ and PA 6,¹⁴ invented by CAROTHERS and SCHLACK, respectively. Both were originally used for the production of strong fibers for textiles and fishing rods. Due to their high abrasion resistance and good mechanical properties, they were quickly used as plastics as well. Today, this is the main application for polyamides, followed by the production of textile fibers.¹⁵ Following the invention of PA 6.6 and PA 6,

longer-chain AB-type polyamides, like PA 11¹⁶ and PA 12,¹⁷ were commercialized. They exhibit a significantly lower water uptake and melting temperature than PA 6 and PA 6.6, while retaining the good mechanical properties.⁷ Due to their increased dimensional stability, these polyamides are mainly used in tubing and packaging films. They are also the main polyamides used for 3D printing applications.¹⁸ Longer-chain aliphatic polyamides have so far also been synthesized up to PA 12.34.¹⁹ With increasing chain-length their melting temperature approaches that of high density polyethylene (132 °C), although a minimum was found at 110 °C for polyamides having a amide group density of approximately 35 per 1000 methylene units, corresponding theoretically to PA 29.29 (**Figure 1**).²⁰ A lower melting temperature results in low energy consumption during processing on the one hand, while limiting the application temperature on the other. For high-temperature applications, AABB-type polyamides made from short-chain diamines and diacids are preferred. For example, PA 4.6 made from diamino butane and adipic acid exhibiting a melting temperature of 295 °C may be used at temperatures up to 250 °C.²¹ Polyamides made from shorter-chain diamines and diacids either degrade before melting or exhibit too high melting temperature, making melt processing uneconomical.^{8,21} Although many different polyamides have been developed since their invention, PA 6.6 and PA 6 still dominate the market and account for over 90% of worldwide production.²²

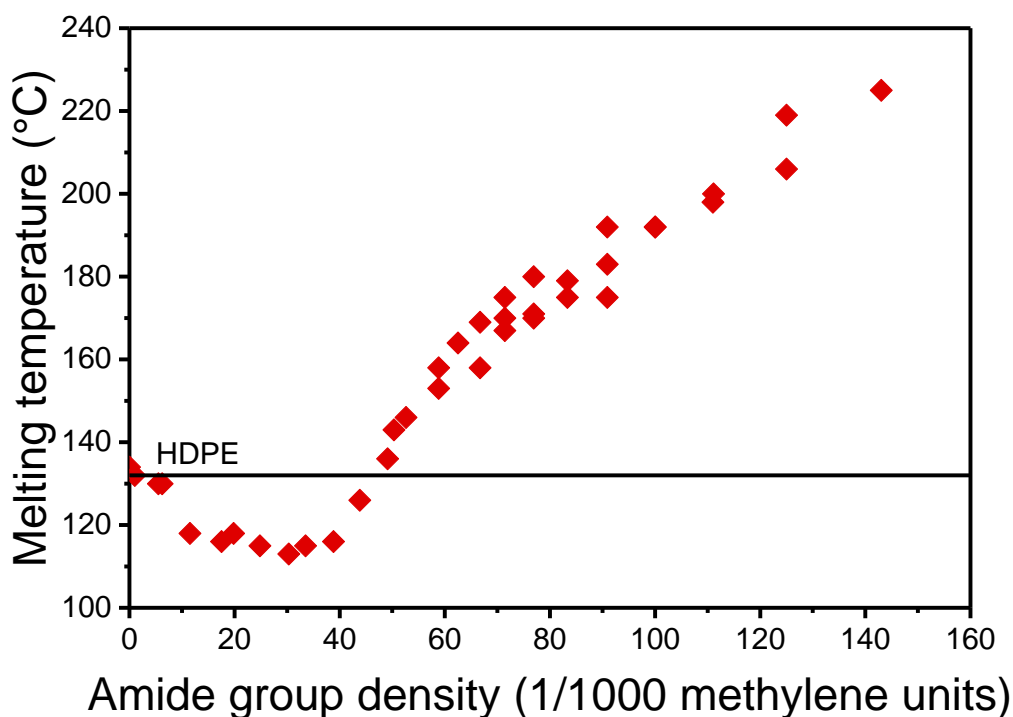


Figure 1. Melting temperature of aliphatic polyamides in dependence of the amide group density.^{20,23}

Tailoring the properties of a polyamide can also be achieved by copolymerization of two or more polyamides. The resulting copolymer exhibits a combination of the properties of its homopolymers, depending on the ratio. Since most polyamide copolymers are prepared by polycondensation of the different diacids and diamines together, the resulting copolyamide generally has a statistical distribution.²¹ Block copolymers of polyamides are challenging to synthesize due to several side reactions requiring special techniques.²⁴ Another method to yield a polyamide with combined properties is blending of homopolymers. Here, the desired homopolymers are mixed together in the melt to yield a so-called blend. A polyamide blend is a physical mixture of polyamides, whereas copolyamides are a chemical mixture.²¹ While both techniques result in a mixture of homopolymers, the resulting properties of the mixed polyamides can vary greatly. For example, the melting temperature and tensile strength of a 40:60 PA 6/6.9 blend (218 °C, 67 MPa) were found to be significantly higher than those of a PA 6/6.9 copolyamide having the same ratio (156 °C, 43 MPa).²⁵

By adjusting the ratio of the homopolymers, the melting temperature of the resulting copolyamide can be tailored. With increasing PA 6 content in the PA 6/6.6 copolyamide, the melting point decreases from 260 °C to 200 °C, passing through a minimum of 155 °C at 60 wt%.²⁶ This melting point minimum is common for statistical copolymers and due to the disruption of the crystalline structure of the copolyamide, resulting in a reduced crystallinity. The PA 6/6.6 copolyamides indeed exhibit a minimum in crystallinity for the composition having 50 mol% PA 6.²⁷ Similar observations were made for different copolyamides including PA 6/6.9,²⁸ PA 6/7²⁹ and PA 6/11.³⁰

While the melting temperature can be tailored by copolymerization, the main focus for the synthesis of copolyamides relies on tailoring the mechanical properties. The tensile strength, for example, can be improved by increasing the proportion of the tougher polyamide in the copolyamide. Thus, the copolyamides of PA 6/12 exhibit increasing tensile strength with increasing content of the tougher PA 6.^{31,32} Copolymerization also influences the elongation at break, resulting often in more pronounced changes with the copolymer ratio. For the PA 6/12 copolymers, a sharp increase from 21% for PA 6 to 560% can be observed with increasing the PA 12 content to 50% (**Figure 2a**).³¹ A similar trend was found for PA 6/6.9 copolymers, where an increasing PA 6 content led to an increase in elongation at break from 80% to >180% already at 20% PA 6.²⁵ For the copolyamides synthesized from dimerized oleic acid (C36-DA), hexamethylene diamine and adipic acid (PA 6.36/6.6) a different trend can be observed. While the tensile strength increases as before with the content of the stronger PA 6.6, the elongation

at break, however, decreases with the PA 6.6 content (**Figure 2b**).^{33,34} This is due to the long side chains of the C36-DA, causing deformation of the copolyamide chain, as well as the increased intermolecular hydrogen bonding due to the increasing PA 6.6 content.

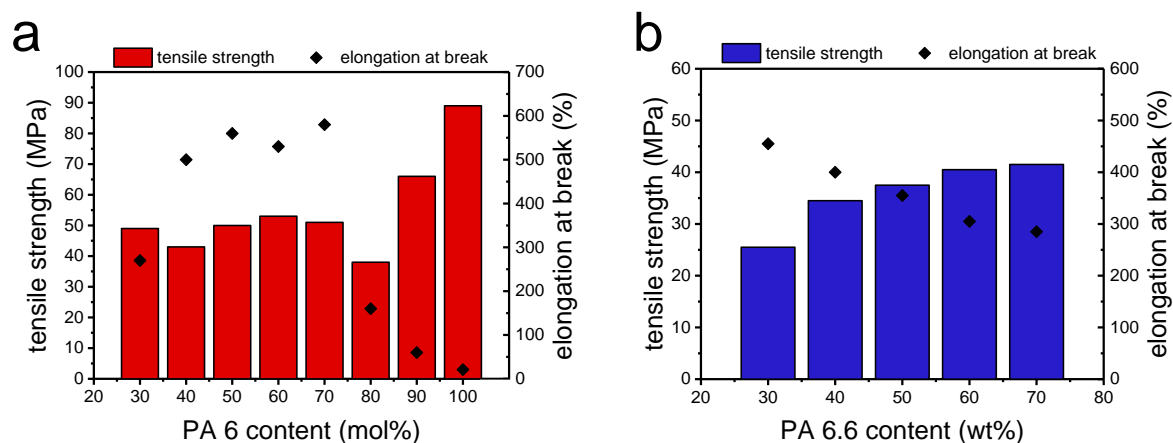
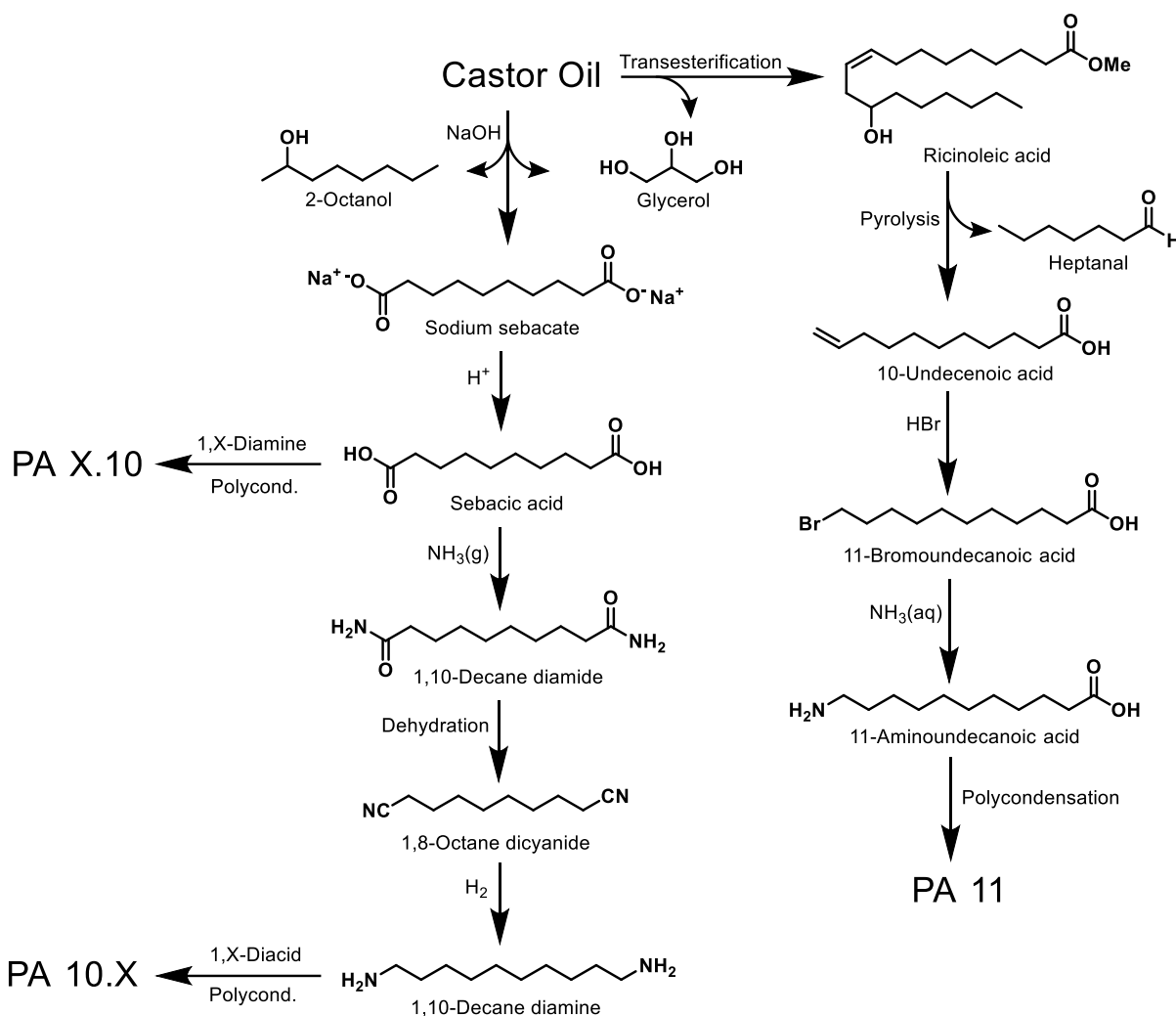


Figure 2. Mechanical properties of a) PA 6/12 copolyamides³¹ and b) PA 6.36/6.6 copolyamides³³ depending on the PA 6, respectively PA 6.6 content.

1.1.1 Bio-based Polyamides

Most of the above mentioned polyamides are conventional polymers, meaning their monomers are synthesized from crude oil. Since the invention of synthetic polymers by BAEKELAND the production volumes are steadily increasing without any sign of slowing down.³⁵ The combination of a never ending increase in production combined with a feedstock of limited supply creates the problem of finding new feedstocks to fuel the production of plastics, like polyamides, in the future. The utilization of bio-based feedstocks offers great potential for a truly sustainable production of so-called bioplastics. Additionally, the use of new resources enables the synthesis of new materials having unique and even improved properties compared to conventional plastics. For polyamides this was already realized early on by the synthesis of the fully bio-based PA 11 by GENAS in the 1950s.¹⁶ This castor oil-based polyamide offered better dimensional stability due to reduced water absorption than the conventional polyamides PA 6 and PA 6.6. Castor oil plays an important role in the synthesis of bio-based polyamides, as virtually all commercially available bio-based polyamides are made from it today. This has mainly to do with the special fatty acid profile of this plant oil. Unlike other common plant oils, castor oil contains mainly triglycerides of ricinoleic acid, which makes up about 90% of the fatty acids.³⁶ This facilitates isolation and purification of the desired fatty acid for the synthesis of monomers for polyamides. Additionally, the structure of ricinoleic acid contains a hydroxyl-

function at the C12 position giving it unique properties, as most naturally occurring fatty acids do not contain such a functionality.³⁷ Pyrolysis and subsequent hydrolysis of the methyl ester of ricinoleic acid yields 10-undecenoic acid, the platform chemical for the synthesis of monomers for bio-based polyamides (**Scheme 2**).³⁸ Reaction with gaseous hydrogen bromide in the presence of a radical initiator selectively gives the anti-markovnikov product 11-bromoundecanoic acid in high yields. Nucleophilic substitution of the bromide with aqueous ammonia gives 11-aminoundecanoic acid, the monomer for PA 11. On the other hand, reaction of castor oil with sodium hydroxide in water results in a cleavage of the fatty acid chain yielding sodium sebacate and 2-octanol. Hydrolysis of the sodium sebacate yields sebacic acid, which can be used to synthesize different partially or fully bio-based PA X.10. Amidation of the sebacic acid using gaseous ammonia and dehydration to form 1,8-octane dicyanide yields bio-based 1,10-decane diamine upon hydrogenation of the dicyanide (**Scheme 2**).³⁹ Fully bio-based PA 10.10 can be synthesized by combining the two castor oil-based monomers, as well as other partially or fully bio-based PA 10.X. For now, commercial production of castor oil-based polyamides is limited to PA 11 and the sebacic acid-based PA 4.10, 5.10, 6.10 and 10.10.⁴⁰



Scheme 2. Reaction pathways for the synthesis of monomers and polyamides from castor oil.^{38,39}

For fully bio-based ABB-type polyamides also the diamines need to be sourced from nature. This is however more difficult than for bio-based diacids.⁴¹ So far, the only commercially available chemically synthesized bio-based linear aliphatic diamine is the castor oil based 1,10-decane diamine. Other commercially available bio-based aliphatic diamines are 1,4-butane- and 1,5-pentane diamine. Although commercial 1,4-butane diamine is mostly synthesized from petrol-based succinonitrile, biochemical synthesis from glucose via L-arginine and L-ornithine also offers a bio-based route (**Scheme 3**).^{42,43} The synthesis of bio-based 1,5-pentane diamine revolves around the decarboxylation of the platform chemical L-lysine, which is easily obtained by fermentation with an annual production of over one million metric tons (**Scheme 3**).^{44,45} Chemical synthesis routes for 1,5-pentane diamine have been established in the past, but they usually lack in selectivity due to the presence of two amine functionalities.^{46–48} Commercial production therefore relies on biochemical fermentation of glucose by genetically engineered *Escherichia coli*.^{49–51} Cyclization and deamination of L-lysine also yields ϵ -caprolactam in good

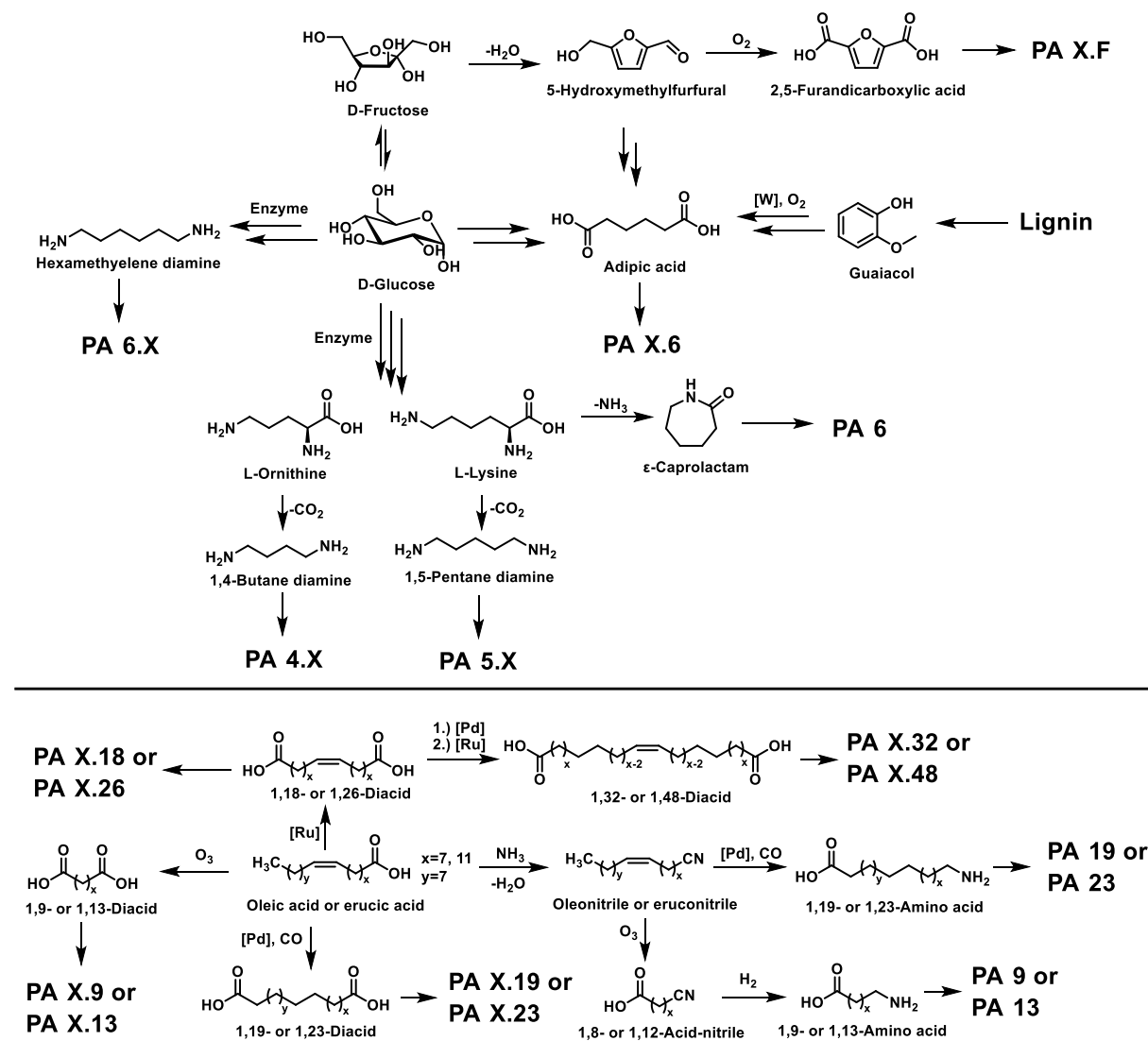
yields of 75% (**Scheme 3**).⁵² The American biotech company *Genomatica* developed a biochemical route towards bio-based ϵ -caprolactam by enzymatic fermentation of adipoyl-CoA to 6-aminohexanoic acid.⁵³ Commercialization of this process is accelerating and the first tons of bio-based PA6 via this route were recently produced.⁵⁴ *Genomatica* also collaborates with polymer companies *Covestro*⁵⁵ and *Asahi Kasei*⁵⁶ for the production of bio-based polyurethanes and PA 6.6 from enzymatically synthesized hexamethylene diamine.^{57–59} Adipic acid, which is used for the synthesis of PA 6.6, has the largest production volume of all aliphatic diacids, exceeding three million tons per year.^{60,61} Commercial production of adipic acid is still relying benzene, which is hydrogenated and oxidized to form the so-called KA-oil (mixture of cyclohexanol and cyclohexanone). Further oxidation of the KA-oil with nitric acid gives adipic acid.⁶² Several bio-based pathways using different feedstocks have been developed, such as 5-hydroxymethylfurfural (HMF),^{63–66} glucose,^{67–72} γ -valerolactone^{73–75} and phenolic compounds (**Scheme 3**).^{76–81} Although many of these processes have cost advantages over conventional adipic acid synthesis, the major challenges for commercial application appear to be product isolation and purification as well as low efficiency of the catalyst.⁸² However, Japanese polymer company *Toray* recently announced successful synthesis of bio-based adipic acid from nonfood-derived sugars by fermentation.⁸³ Commercialization of the bio-derived adipic acid for the production of bio-based PA 6.6 is anticipated by 2030.

Longer-chain diacids are mainly sourced from fatty acids. The 1,9-nonanedioic acid (azelaic acid) for example can be sourced from any C9-unsaturated fatty acid by oxidative cleavage of the double bond. This can be either done by ozonolysis⁸⁴ or by reaction with concentrated hydrogen peroxide at elevated temperatures (**Scheme 3**).⁸⁵ Ozonolysis of oleic acid for the production of azelaic acid is a commercialized synthesis route since the 1950s and mainly performed by *Emery Oleochemicals*.^{86,87} For the oxidative cleavage with hydrogen peroxide, tungsten-based catalysts have proven to be efficient.^{88–93} The Italian company *Novamont* performs this oxidative cleavage commercially, thereby producing bio-based azelaic acid from unsaturated fatty acids and oils without the use of toxic ozone.^{94–98} The resulting partially bio-based PA 6.9 by polycondensation with hexamethylene diamine is also commercially available, although mostly as a copolyamide with PA 6.^{9,25,28,99,100} Oxidative cleavage of erucic acid, a monounsaturated fatty acid with a double bond at the C13 position, yields the 1,13-diacid brassylic acid (**Scheme 3**).¹⁰¹ The subsequent PA X.13 were also synthesized by polycondensation with different diamines, however commercialization is limited to the fully bio-based PA 5.13.^{40,102,103} Starting from sebacic acid, the synthesis of 1,13-tridecane diamine

can be carried out similarly to the amination of the castor oil-based sebacic acid to access PA 13.X and the fully erucic acid-based PA 13.13.^{104–106} 1,12-dodecanedioic acid, which is one methylene-unit shorter, is generally prepared by cyclotrimerization and hydrogenation of conventional 1,3-butadiene and subsequent oxidation of the cyclododecane.¹⁰⁷ However, commercialization of the biochemical production from fatty acids has been done in the last two decades.^{108–110} Leading producer of bio-based 1,12-dodecanedioic acid today is the Chinese company *Cathay Industrial Biotech*.^{111–114} The related polyamides PA 5.12, 6.12, 10.12 and 12.12 have made it into commercialization with the partially bio-based PA 6.12 being the most important one.⁴⁰ Other commercially available partially or fully bio-based polyamides are PA 5.6 and 5.14 made from 1,5-pentane diamine, as well as 4.6 and 4.10 from 1,4-butane diamine. Self-metathesis of monounsaturated fatty acids leads to even longer-chain aliphatic diacids. 1,18-, 1,20-, 1,22- and 1,26-diacids were successfully synthesized by self-metathesis of oleic acid, 10-undecenoic acid, 11-eicosenoic acid and erucic acid respectively (**Scheme 3**).¹¹⁵ The related bio-based polyamides PA X.18,^{116–120} X.20,^{121–123} and X.22¹²⁴ have been synthesized, with the exception of the erucic acid-based PA X.26. Even longer-chain diacids are accessible by chain multiplication of fatty acids.¹²⁵ By combination of metathesis and catalytic dynamic isomerizing crystallization, 1,32- and 1,48-diacids were synthesized from oleic acid. Polyesters were successfully synthesized from those ultra-long-chain diacids, but no polyamides so far (**Scheme 3**). Alternatively, isomerizing carbonylation can also be used to synthesize long-chain aliphatic diacids from fatty acids.¹²⁶ 1,19-nonadecanedioic- and 1,23-tricosanedioic acid can be obtained from oleic acid and erucic acid in this way.¹²⁷ Reductive amination of the diacids also yield the respective long-chain diamines to form the partially and fully bio-based polyamides X.19 and X.23.^{127–129}

The synthesis of bio-based PA 18 and PA 19 from oleonitrile and oleoamide via the respective amino acid can also be achieved by isomerizing carbonylation (**Scheme 3**).¹³⁰ Alternatively, tandem isomerization-hydroformylation of oleonitrile also gives 19-oxononadecanenitrile, a precursor for the synthesis of bio-based PA 19.¹³¹ Using the same strategy with castor oil-based 10-undecenitrile gives 11-cyanoundecanoic acid, a possible monomer for the synthesis of bio-based PA 12.^{132–134} Oxidative ozonolysis of oleonitrile yields 9-aminononanoic acid upon reduction of the nitrile, the monomer for the synthesis of fully bio-based PA 9.¹³⁵ Recently, the synthesis of a bio-based aromatic AB-type polyamide was reported.¹³⁶ Dehydration followed by reductive amination and carbonylation of lignocellulose-based furfural yields the monomer 5-(aminomethyl)-furan-2-carboxylic acid.¹³⁷ AABB-type aromatic polyamides (PA X.F) based

on lignocellulose have also been reported so far using 2,5-furandicarboxylic acid (FDCA) or the corresponding dimethyl ester (DMFD).^{138–143}



Scheme 3. Reaction pathways for the synthesis of bio-based monomers and polyamides.

1.1.2 Oleic acid as a platform chemical

Biologically derived fats and oils play a central role as renewable raw materials for the chemical industry today. In 2021, fats and oils accounted for 36% of renewable feedstocks used in Germany for the production of chemicals, making them the most important resource.¹⁴⁴ About 18% of these were used for the production of bio-based polymers, which is the second most important application of fats and oils in the chemical industry after surfactants. Independent on the source, fats and oils are always made up of fatty acids. While the synthesis of surfactants revolves solely around the carboxy group of the fatty acid, the production of polymers requires unsaturated fatty acids, containing C–C double bonds. The unsaturated fatty acids can be

divided into monounsaturated and polyunsaturated fatty acids depending on their number of C–C double bonds. The most common natural fatty acid is oleic acid, a monounsaturated fatty acid having 18 carbons and a C–C double bond at the C9 position. Apart from plant oils like sunflower, olive or palm oil it can also be produced from microalgae.^{37,145,146} While the aforementioned plant oils are derived from food, microalgae are inedible and therefore a non-food feedstock for the platform chemical oleic acid. Additionally, microalgae do not need to be cultivated on arable land, allowing efficient use of available farmland for food production.

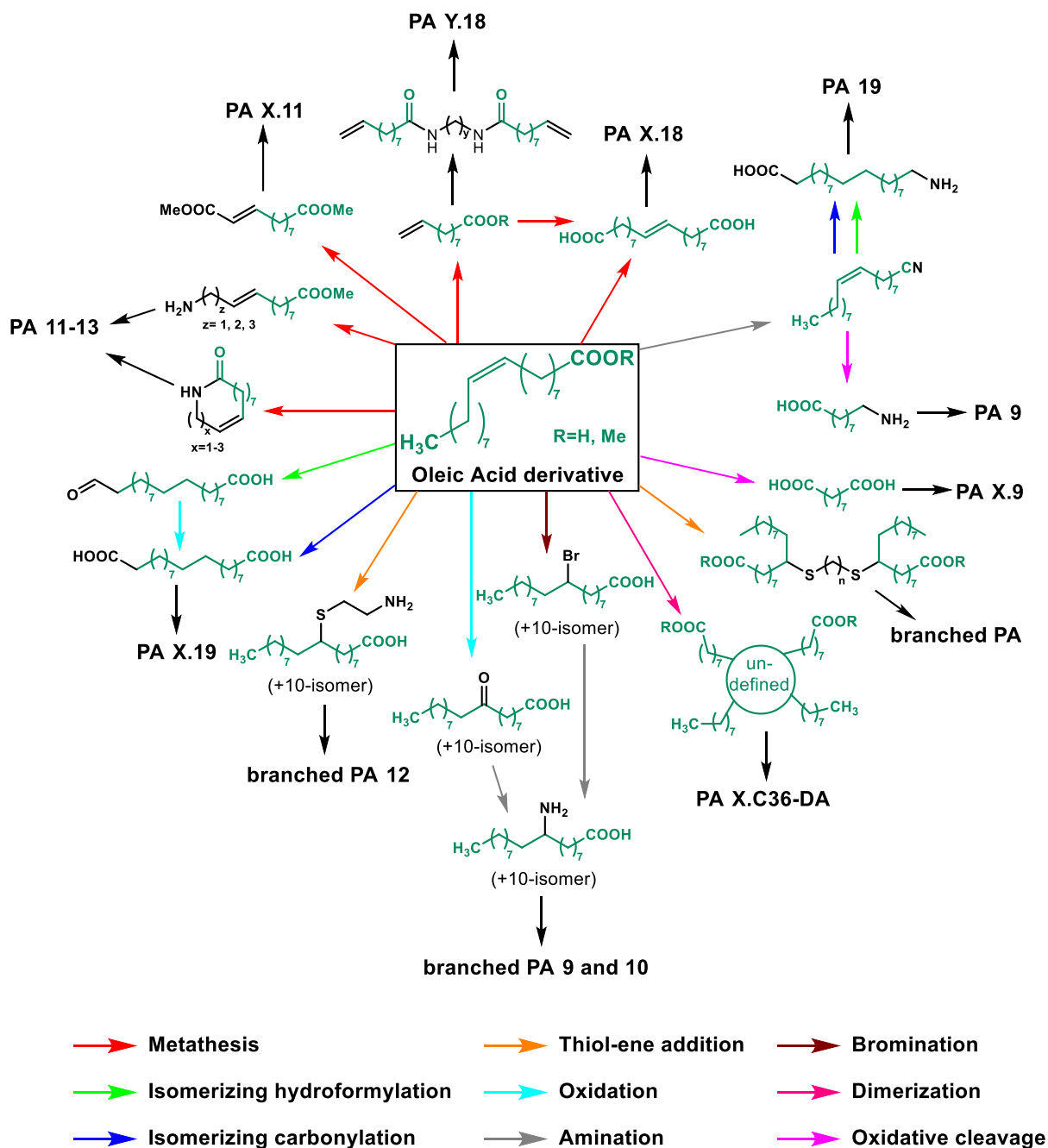
Unsaturated fatty acids like oleic acid can react just like any hydrocarbon having a C–C double bond and allow reactions like oxidation, addition, oxidative cleavage, metathesis, hydroformylation, carbonylation and more. Many of which are useful for the synthesis of monomers for polyamides from unsaturated fatty acids. Oleic acid, for example, can be used to synthesize a variety of novel monomers for polymerization. Cross metathesis with methacrylate or crotonate yields 1,11-undecanedioic acid which can be used for the synthesis of PA X.11 as well as polyesters.^{147–150} Amino acids can be achieved similarly by cross metathesis with alkene cyanides like acrylonitrile, allyl cyanide and homoallyl cyanide.^{151,152} Reduction of the cyanide yields the amino acid, which can be used for the synthesis of AB-type polyamides like PA 12, PA 13 and so on. The use of allyl chloride also leads to amino acids after nucleophilic substitution of the chloride with ammonia.¹⁵³ Cross metathesis with enamines is not possible due to their ability to coordinate to the metal-alkylidene complex, deactivating the Grubbs catalyst.¹⁵⁴ But, amidation of the oleic acid with enamines like allylamine, homoallylamine and pent-4-enylamine followed by ring closing metathesis gives lactams.^{155,156} These lactams can be used for the synthesis of PA 11, 12 and 13 providing a renewable alternative route for the commercial route to PA 12 using petrol-based 1,3-butadiene. Another promising method for the synthesis of monomers from oleic acid is the cross metathesis with ethylene otherwise known as ethenolysis yielding 9-decenoic acid.^{157–160} Amidation with a linear diamine yields a diamide with two terminal C–C double bonds, which can be polymerized by acyclic diene metathesis (ADMET) to give polyamides.²⁰ Self metathesis of the 9-decenoic acid and oleic acid yields the long-chain 1,18-octadec-9-enoic acid, which can then be used for the synthesis of PA X.18.^{115,149,161,162} Polyamides made from the unsaturated diacid¹¹⁶ as well as from the saturated diacid after hydrogenation have already been prepared.^{117–119} Cross metathesis of this long-chain diacid can again be performed analogously to the previously mentioned reactions to yields amino acids.^{152,163,164}

Oxidative cleavage of oleic acid yields the shorter-chain 1,9-nonanedioic acid (azelaic acid), a reaction which is already performed industrially since the 1950s.⁸⁶ This can be achieved by reacting the oleic acid with a strong oxidizer like potassium permanganate,¹⁶⁵ ozone⁸⁶ or hydrogen peroxide.⁸⁵ Ozone and hydrogen peroxide offer better yields and are also considered as green oxidants, in contrast to potassium permanganate and are therefore the preferred choice. The oxidative cleavage by hydrogen peroxide is only possible by addition of transition metal catalysts and due to the health risks associated with ozone desirable in terms of the principles of green chemistry.¹⁶⁶ Many different catalyst systems have been investigated including molybdenum-,^{85,167} ruthenium-,¹⁶⁸ vanadium-¹⁶⁹ and the most promising, tungsten-based catalysts.^{170–173} In recent years, also heterogeneous tungsten-based catalysts have been developed to facilitate product separation and catalyst recycling.^{88,92,174} Performing oxidative cleavage and metathesis reactions on oleic acid always leads to side-products originating from the oleic acid. In both reactions, only half of the available bio-based carbon ends up in the monomer. For the oxidative cleavage a new approach was established based on the synthesis of terephthalic acid from *p*-xylene.¹⁷⁵ The catalyst system consisting of cobalt- and manganese acetates together with hydrobromic acid was able to cleave oleic acid by aerobic oxidation using air. The terminal methyl group of the by-product pelargonic acid was then simultaneously oxidized to also give azelaic acid in high yields of 96%.¹⁷⁶ The resulting PA X.9 have shown to have good mechanical properties combined with a reduced moisture absorption compared to PA 6.6.⁹ Additionally, the combination of reductive amination and oxidative cleavage of oleic acid yields 9-aminononanoic acid, which can be used to synthesize PA 9, a promising candidate for the replacement of PA 6.^{135,177}

Utilization of the complete bio-based carbon should be the goal for further development of synthesis methods towards renewable monomers from oleic acid. Another interesting strategy is the isomerizing carbonylation, where the internal C–C double bond is shifted to a terminal position where a carbonylation reaction with carbon monoxide is facilitated by the catalyst. The use of oleic acid yields the long-chain 1,19-nonadecanedioic acid. The catalyst system, which is also used for the commercial production of methyl methacrylate in the so-called Alpha process, comprises of a palladium-catalyst with the phosphine-ligand 1,2-bis(di-*tert*-butylphosphinomethyl)benzene (DTBPX).¹⁷⁸ This catalyst shows high selectivity of >99% towards linear reaction products suitable for the synthesis of semi crystalline polymers with strong mechanical properties.^{127,128,179,180} Additionally, the isomerizing carbonylation reaction can be performed directly from triglycerides originating from vegetable oils or microalgae to

yield the long-chain diacid in high yield and purity.^{181–183} The resulting PA X.19 have been synthesized and showed lower mechanical properties than conventional PA 6.6, but higher elongation at break and a significantly lower water uptake due to the long alkyl chain.^{127,129,184} Approaches for catalyst recycling have also been made in recent years by selective crystallization of the diacid and the catalyst could be recycled eight consecutive times.¹⁸⁵ Another approach towards 1,19-nonadecanedioic acid is the isomerizing hydroformylation of oleic acid followed by oxidation of the resulting 19-oxononadecanoic acid.¹⁸⁶ Both, the isomerizing carbonylation and hydroformylation can also be applied for the synthesis of 19-aminononadecanedioic acid from oleonitrile¹⁸⁷ for the synthesis of PA 19.^{130,131}

All synthesis routes mentioned yield linear aliphatic monomers, which are suitable for the production of polyamides with high crystallinity. There are however some approaches that yield branched monomers. Thiol-ene addition of oleic acid with cysteamine hydrochloride, for example, yields a thioether-containing amino acid that can be polymerized to a branched polyamide.¹⁸⁸ By the use of a linear dithiol, two oleic acid chains can be connected to form a dimerized fatty acid.¹⁸⁹ Dimerized fatty acids have been commercially available since the 1950s and can be made by a variety of mechanistic pathways, yielding complex product mixtures. Commercial synthesis usually uses tall oil consisting of mostly oleic acid and linoleic acid, the double unsaturated C18-fatty acid. The dimerization of these fatty acids typically proceeds via Diels-Alder cyclization, but the reaction products often consist of acyclic, monocyclic and some bicyclic dimers.^{37,190} The resulting polyamides typically have lower crystallinity and therefore lower melting temperatures due to the bulky structure and the side chains. They are therefore often used as hot-melt adhesives and reactive components for epoxy resins.^{191–193} Recently, the dimerized fatty acids were used for the synthesis of thermoplastic elastomers (TPEs) used for bead foaming and application in midsoles of running shoes.¹⁹⁴ Another approach towards oleic acid-based amino acids is the Wohl-Ziegler bromination and hydrobromination of oleic acid, which can be polymerized after nucleophilic substitution and reduction to yield branched polyamides.¹⁹⁵ Similarly, Wacker oxidation of methyl oleate yields a keto-oleate which can undergo reductive amination to give the branched amino acid and resulting polyamide.¹⁹⁶ Alternatively, the keto-oleate can also be dimerized by reductive amination using a linear diamine to yield a dimerized fatty acid.¹⁹⁷



Scheme 4. Synthesis routes for the synthesis of monomers and resulting polyamides from oleic acid and methyl oleate.

Generally, all the mentioned diacids can also be used to synthesize diamines by reductive amination. This was already shown for the amination of 1,19-nonadecanedioic acid,^{127–129} and is commercially used for the synthesis of 1,10- and 1,13-diamines from fatty acid-based sebacic and erucic acid.^{104–106}

1.2 Fiber-spinning

1.2.1 Melt-spun fibers and applications

For a long time only naturally occurring polymers, like cellulose from cotton, could be used for the production of fibers. With the invention of polyamides by CAROTHERS and SCHLACK, the first synthetic fibers could be produced by a new technique called melt spinning. Today, synthetic fibers dominate the fiber market accounting for approximately 64% of global fiber production in 2021.¹⁹⁸ The majority of which are made by melt spinning of poly(ethylene terephthalate) (PET), polyamides and polypropylene. Melt spinning is considered the simplest process for fiber production and can generally be applied to any thermoplastic polymer with a decomposition temperature above its melting temperature. Additionally, the polymer melt must be viscoelastic, meaning that it must be able to build up tensile stress during the spinning process in order to avoid filament break. The molten polymer is forced under high pressure (100 – 200 bar) through a small orifice called the spinneret. The formed filament is then quenched by drawing through air or in some cases through a liquid to allow the filament to cool down and solidify. No exchange of material takes place during the spinning process, which is why the filament diameter is directly proportional to the filament velocity, which is dependent on the take-up speed and the polymer throughput.¹⁹⁹

The melt-spinning line can be either directly connected to the polycondensation reactor forming a continuous process, or separately fed with granulates or flakes (**Figure 3**). Continuous processes are advantageous for high volume production, while using a hopper to feed polymer flakes or granulates allows for easier material changes often desired for small-volume production. Typically, a melt pump ensures a constant polymer throughput to the spinneret in the spin pack. A screw extruder may be used if the melt-spinning line is used discontinuously to melt the polymer and pressurize it. Additionally, additives or masterbatches can be added and mixed with the polymer in the extruder to improve processability or dye the polymer. The polymer is then pressed through the spinneret, which can either have one or multiple holes. Monofilaments are produced if the spinneret has only one hole, while multiple holes lead to the production of multifilament consisting of sometimes several hundred filaments. The rheological properties of the polymer melt are very important for the choice of spinneret. The polymer experiences high shear flow as it passes through the hole, which increases molecular orientation. The polymer melt releases stored elastic energy as it exits the spinneret, causing the extrudate to have a larger diameter than the spinneret hole. This effect is called die swell

and is only possible for a viscoelastic polymer. The occurrence of the die swell is important to guarantee steady spinning conditions. If the take-up speed is too high, the polymer gets drawn out of the die and die swell can no longer occur. After quenching, a spin finish may be applied to aid filament processing. After solidification and application of the spin finish, the filament may be drawn by several godets to change the molecular orientation and the fiber diameter. This is achieved by stretching the as-spun filament between godets of different revolving speeds. Typically drawing should occur above the glass transition temperature starting from filaments with a low crystallinity.²⁰⁰ If crystallization occurs before drawing, the filaments become brittle, making them impossible to draw.²⁰¹ The amount of drawing greatly influences the mechanical properties of the filaments. Fully drawn fibers for example show no necking, as they have already been stretched beyond their natural draw ratio. This leads to fibers with higher tenacity and stiffness.

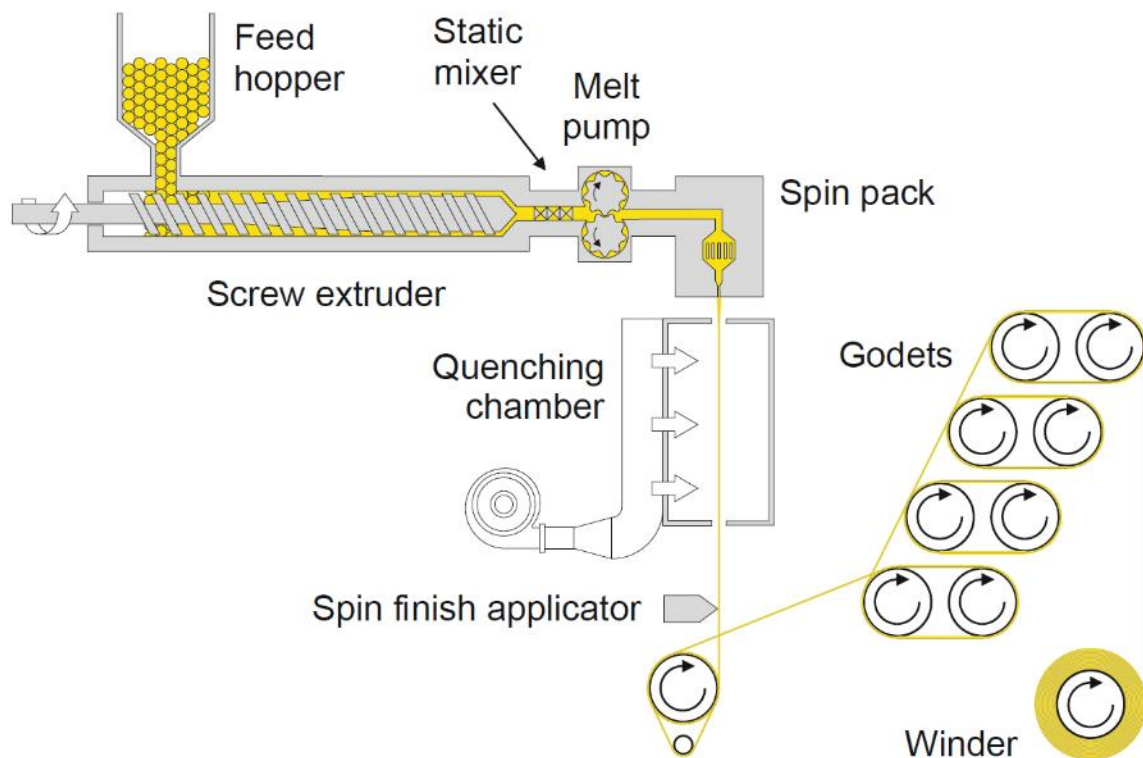


Figure 3. Schematic representation of a melt-spinning line.²⁰²

In order to achieve a stable melt spinning process and sufficient fiber properties, the polymer should withstand high shear strain without decomposition or crosslinking. A molecular weight above the entanglement molecular weight and a low dispersity ensures a stable and high melt viscosity in order to avoid filament break. Linear polymers are preferred due to their high chain mobility, which allows them to withstand high shear forces during processing and to acquire a high orientation in the fiber direction under strain. Furthermore, the polymer needs to have a

high purity in order to prevent fluctuations and blockage of the spinneret.²⁰² Drying of the polymer before extrusion is very important, as remaining moisture can strongly influence the processability by causing degradation of the polymer. Hydrolytic degradation of polyesters like PET can easily happen during melt spinning, causing a considerable reduction in molecular weight and subsequently the melt viscosity. The moisture content is especially important for the melt spinning of polyamides, where so called over-drying can also negatively influence the spinning process. Water acts as a plasticizer in polyamides, reducing the melt viscosity, and also impacts the chemical equilibrium of the polycondensate.²⁰³ Overly dry polyamide leads to more filament breaks interrupting the spinning process. Polyolefins like polypropylene on the other hand do not need to be dried as they are non-hygroscopic.

Semi-crystalline polymers are preferred for melt spinning, as their crystalline structure stabilizes the highly orientated molecular chains during melt spinning. With amorphous polymers, on the other hand, the molecular chains would recoil above their glass transition temperature, resulting in fiber shrinkage.²⁰⁴

1.2.2 Electrospun fibers and applications

Melt spinning is a great technique for fast and continuous production of synthetic fibers in a large quantity and suitable for many applications. However, the smallest fibers obtained often have diameters in the micrometer scale. Certain applications like fiber reinforcement and filtration would benefit from smaller fibers in the nanometer range. One easily accessible technique for the continuous production of such nano- and microfibers is electrospinning. In contrast to conventional spinning techniques, the spinning process is not based on mechanical forces, but on electrical forces.²⁰⁵

The theoretical foundation for the electrospinning process relies on the findings of BOSE and LORD RAYLEIGH. In 1745, BOSE discovered that applying an electrical potential to the surface of droplets causes the formation of an aerosol.²⁰⁶ About 150 years later LORD RAYLEIGH described the calculations for the amount of charge required to cause the deformation of droplets to form a jet.²⁰⁷ Just two years later the first electrospinning process using viscous material like beeswax and pitch was described by BOYS in 1887.²⁰⁸ Shortly after, the first patents regarding electrical dispersion of fluids were filed by COOLEY and MORTON in the early 1900s.^{209–211} About thirty years later FORMHALS described the first application of electrospinning for the production of synthetic fibers.^{212,213} Due to the lacking technology to accurately observe the formed nanofibers, no significant discoveries were made before the

invention of the scanning electron microscope (SEM). In the early 1990s the topic of electrospinning was picked up again by academia due to the works of DOSHI and RENEKKER.^{214,215} With the use of SEM, they were able to determine the fiber diameter and found a correlation between the needle tip to collector distance and the fiber diameter. With the start of the 21st century the interest in electrospinning showed a rapid increase from just a few publications per year to 6500 solely in 2022.²¹⁶

In principle, the electrospinning of a polymer is performed from a solution of the polymer in a suitable solvent (**Figure 4**).^{205,217} Additional salts may be added to increase the conductivity of the solution. The polymer solution is then transferred to a syringe with a metallic canula (spinneret) connected to it. A constant flow of the polymer solution has to be achieved in order to allow a stable electrospinning process. This can be achieved by a syringe pump or a peristaltic pump. Once the solution forms the first droplet at the tip of the spinneret, a high positive voltage of several kilovolt is applied at the spinneret. The high electrostatic charge of the droplet, induced by the high voltage, causes it to deform into a conical shape (Taylor cone).²¹⁸ If the voltage is high enough, a jet will form at the tip of the cone. This jet is then accelerated to the collector, which can either be grounded or a negative charge can be applied to further increase the acceleration. The jet follows a straight path for a short distance, until it begins to spiral with an increasing loop diameter. This is due to the electrostatic repulsion of the charged jet causing deflection and ultimately the spiraling motion. At the same time, the jet becomes thinner due to solvent evaporation. Once the jet reaches the collector, the fiber-formation process is stopped and the solidified fibers are deposited on the surface of the collector. The collector can either be stationary or moving. A moving collector will influence fiber orientation and fast rotating drums can for example lead to highly aligned fibers. Stationary collectors, on the other hand, will result in random deposition of the fibers and form a nonwoven.

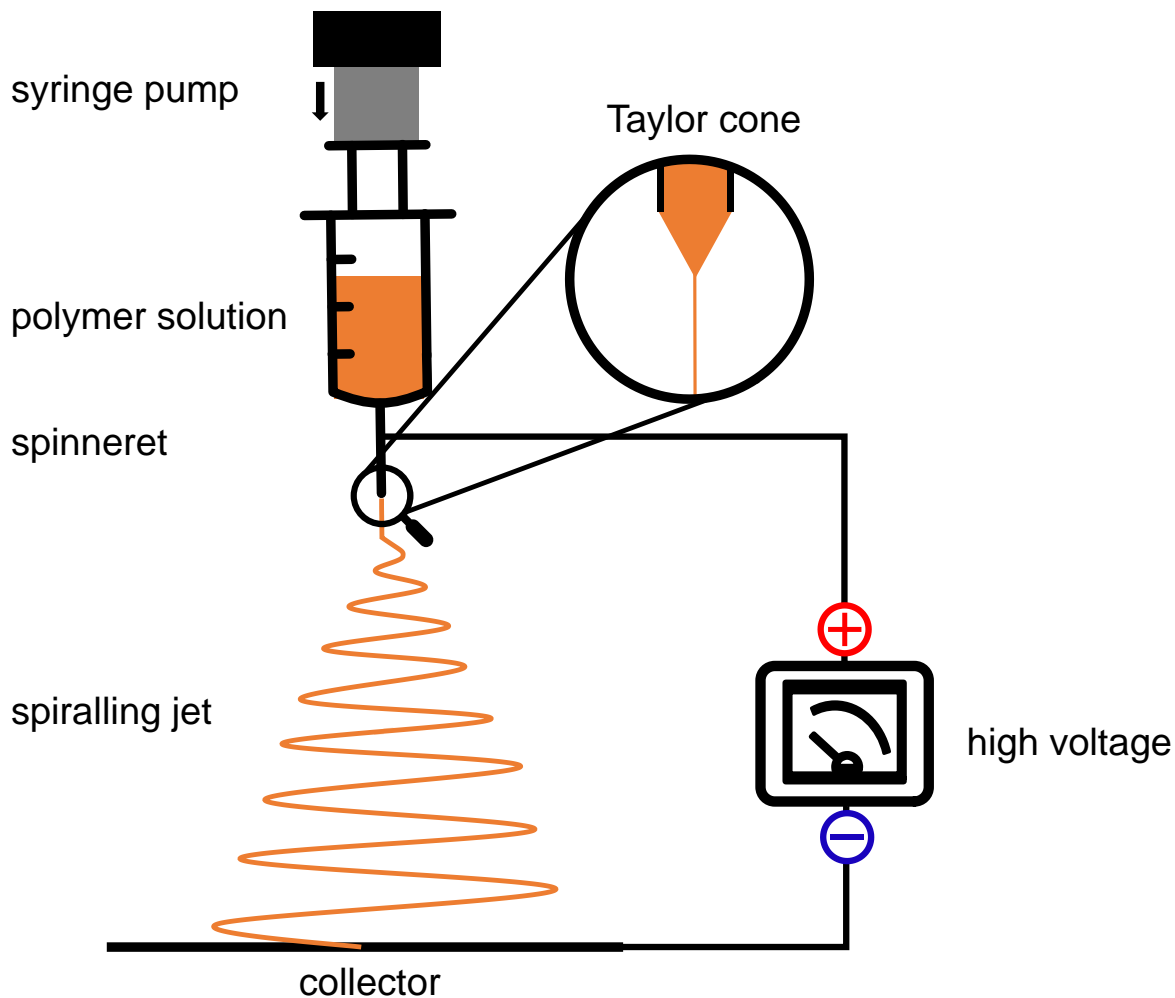


Figure 4. Schematic depiction of an electrospinning apparatus.

There are many factors influencing the electrospinning process. Starting with the solution parameters: viscosity and conductivity of the solution, surface tension, molecular weight and concentration of the polymer and volatility of the solvent. The polymer used needs to have a high enough molecular weight for enough entanglement to ensure the formation of submicrofibers. Additionally, the molecular weight and concentration influences the viscosity of the solution, which might cause clogging if it is too high. The choice of solvent also influences the viscosity, but to a greater extent the conductivity, the surface tension and the ability to evaporate during electrospinning.^{219,220}

Additionally, the ambient conditions are important during the electrospinning process. These include the humidity and the temperature during processing. While the temperature influences the solvent evaporation and the viscosity, the humidity has a strong influence on the conductivity.

Ultimately, the processing parameters need to be chosen according to the aforementioned ambient conditions and solution parameters. These include the applied flow rate of the solution, the applied voltage at the spinneret and the collector, the diameter of the canula, the tip-to-collector distance and the type of collector. While the voltage needs to be high enough to allow formation of the Taylor cone, a too high voltage and/or flow rate will result in bead-formation. Increasing the tip-to-collector distance will result in thinner fibers and vice-versa.²¹⁴

Many different electrospinning techniques have been established since the beginning of the 21st century making it highly versatile. Electrospun nonwovens are especially interesting for membrane technology applications due to their outstanding properties. The electrospinning process allows the continuous production of very thin fibers down to the nanometer-scale, which can then be randomly collected to form a nonwoven. The resulting electrospun membranes have a large specific surface area, as well as high flexibility and porosity.²²¹ These membranes can for example be used as substrates to perform highly efficient catalysis reactions due to their great specific surface area.²²² The highly porous membranes also find applications as solid-state electrolyte in battery cells to improve their safety.²²³ Electrospun membranes are also outstanding filter materials often combining high filtration efficiency with a low pressure drop, resulting in high quality factors.²²⁴ The quality factor combines filtration efficiency and pressure drop and allows comparison between different filters and measurement conditions. The calculation relies on DARCY's law according to which the flow velocity is directly proportional to the pressure difference. It can therefore be calculated using the following formula with f being the filtration efficiency and ΔP being the pressure drop in Pa:

$$QF = - \frac{\ln(1 - f)}{\Delta P}$$

Removal of particles by means of filtration is generally described by either surface-, cake- or depth-filtration and combinations thereof (**Figure 5**). The predominant mechanism is depending on the filter and the particles. If the particle size is larger than the pore size, they cannot penetrate the filter and remain on the surface of the filter media (surface filtration). Particles that have a similar size as the pores are typically separated by cake filtration. These particles accumulate on the surface of the filter and also cannot penetrate the filter. In contrast to surface filtration, the pores of the filter are not blocked by the accumulated particles, due to their smaller size. This results in the formation of a cake layer which can again act as a filter medium for further particles. Lastly, particles smaller than the pore size can penetrate the filter,

but they can still be filtered out by interception with the filter media or electrostatic attraction.^{225,226} Depending on the filtration problem different filtration mechanisms might be preferred. The pore size of the electrospun filter membranes (EFM) can be tailored to match the desired properties. Additionally, the EFM can be chemically modified to allow electrostatic attraction by incorporation of specific functional groups. These affinity membranes can for example be used to selectively remove metal nanoparticles that are much smaller than the pore size.^{227,228} Due to their tailored properties EFMs can be applied for dry^{226,229,230} and wet filtration.^{231–234}

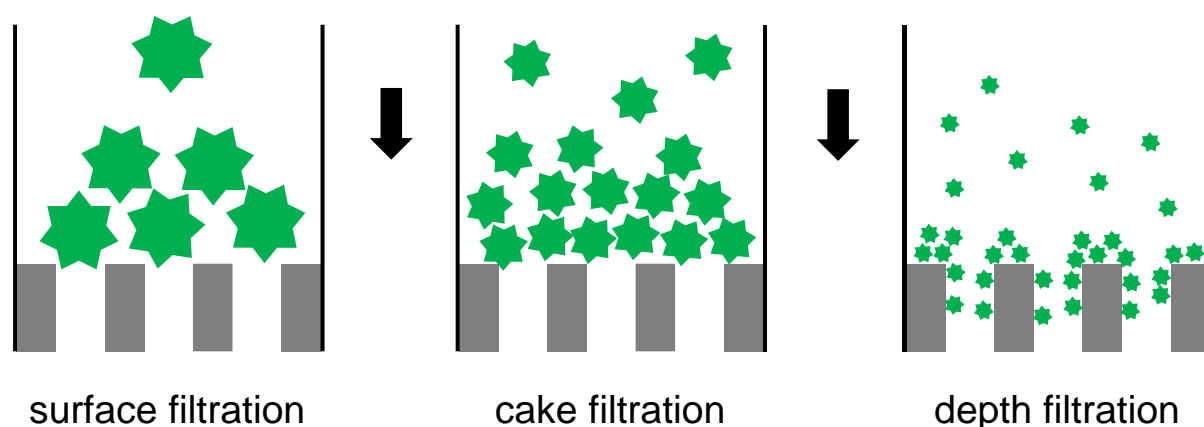


Figure 5. Schematic representation of the three different filtration mechanisms.

Electrospun membranes are already available in commercial air filters and their demand has seen a sharp increase due to the recent COVID-19 pandemic.²²⁹ The requirements for these air filters are high and often times a filtration efficiency of over 99% is expected. HEPA (high-efficiency particulate air) filters, for example, need to be able to remove >99.95% of aerosols with a particle size down to 0.3 μm in diameter.²³⁵ The first reported use of EFMs for air filtration dates back to the 1980s,²³⁶ since then a broad variety of polymers have successfully been applied.²²⁹ EFMs prepared from acrylonitrile-butadiene-styrene (ABS) showed a filtration efficiency of 99% at a pressure drop of under 30 Pa.²³⁷ Electrospun membranes from PA 6 were even able to exceed HEPA standards with an efficiency of 99.993% at a face velocity of 5 $\text{cm}\cdot\text{s}^{-1}$.²³⁸ Multilayered structures are known to perform better than thick single layer membranes.²³⁹ A stack of three electrospun polyacrylonitrile (PAN) membranes of the same thickness had a higher quality factor than a single membrane of triple thickness. Similarly, a sandwich-membrane of PAN in between two layers of PA 6 was able to remove airborne particles with an efficiency of 99.9998%, far exceeding HEPA standards.²⁴⁰

Another problem of rising interest is the availability of drinking water. Most of earth's water is in the oceans and only 2.6% is actually freshwater.²³³ The growing amount of microplastic and other pollutants found in the sea and drinking water makes purification systems more and more important. Electrospun nonwovens are a perfect choice for the removal of microplastic, oil and/or toxic metal nanoparticles for water remediation. EFMs made from functionalized polyacrylates showed excellent filtration properties for the removal of gold and other metal nanoparticles.^{227,228} The affinity membranes reached a filtration efficiency up to 100% and could be regenerated up to three times without significant change in their filtration properties.²²⁷ The major drawback of electrospun membranes is their often lacking mechanical stability.²³¹ So-called hybrid or composite membranes are often used to counter this by electrospinning on a supporting layer providing the mechanical stability. For example, a hybrid membrane of PA 6 electrospun on a PET web could successfully be used to filter oily contaminants from industrial wastewater with a high permeability of over $400 \text{ L}\cdot\text{m}^{-2}\cdot\text{h}^{-1}\cdot\text{bar}^{-1}$ even after 15 h of usage.²⁴¹ Hybrid membranes are also used to increase hydrophilicity and therefore water permeability. A bilayer EFM made from electrospun PA 6 on cellulose showed superhydrophilicity, which resulted in a permeability of $1200 \text{ L}\cdot\text{m}^{-2}\cdot\text{h}^{-1}\cdot\text{bar}^{-1}$ for the filtration of PS microparticles from water.²⁴² Additionally, the prepared membrane was able to remove >99% of the dispersed microparticles. Self-standing membranes of PA 6,²⁴³ PAN,²⁴⁴ polyvinylidene fluoride (PVDF)^{245,246} and even recycled PET²⁴⁷ have also been used to remove PS microparticles dispersed in water to simulate microplastic filtration. All membranes showed good filtration efficiencies of up to >99% with high permeability of up to $45000 \text{ L}\cdot\text{m}^{-2}\cdot\text{h}^{-1}\cdot\text{bar}^{-1}$ for PVDF.²⁴⁶

2 Synopsis

2.1 Aim

The global plastics production is increasing in a seemingly unstoppable manner with an annual growth rate of 4% over the last 20 years.²⁴⁸ It is good to see that bio-based materials are also starting to enter the market with an annual growth rate of 19% in the last three years and a large spike of 51% from 2020 to 2021. This trend is forecasted to increase to an annual growth rate of 29% until 2030.²⁴⁹ One of the biggest drivers for innovation might be the fiber market, where about 20% of all produced plastic is used.¹⁹⁸ Despite the growth in production of bio-based plastics, the share of bio-based materials used for the production of synthetic fibers was below 0.1% in 2021. Clearly, there is a large gap between the application of bio-based materials in the global plastics market and in the synthetic fibers market. In order to close that gap, new materials and feedstocks need to be investigated for their usability in the production of synthetic fibers.

The goal of this work was the synthesis of monomers and polymers from microalgae feedstock and subsequent production of synthetic fibers. Microalgae have several advantages over other crops that are being used for the production of bio-based plastics today. They have a fast growth rate, often 20 times faster than most terrestrial crops.²⁵⁰ Microalgae cultivation also allows more efficient use of available land, as they do not need to be cultivated on arable land and can also be cultivated vertically. Two major benefits are that they are not competing with food production and they also capture carbon dioxide, provided they are cultivated autotrophically.²⁵¹ The choice of algae strain is important for the intended application, as well as the cultivation time and parameters.

In the present work oleic acid was chosen as the platform chemical for the synthesis of monomers. It is the most abundant fatty acid in nature and can also be produced in high quantities by microalgae.^{252,253} Monomers should then be synthesized from oleic acid by introduction of a second functionality. The monomers need to be linear, meaning they cannot have any side-chains or branching points, in order to provide the mechanical stability needed for the production of synthetic fibers from the resulting polymer. To obtain high molecular weight polyamides in melt polycondensation, thorough purification and characterization of the monomers were required. Understanding the structure-property relationship of the resulting polyamides was also important to assess their potential for the production of synthetic fibers.

Maximizing the bio-content in the final polyamide was also a vital part of the thesis to make as much use of the available feedstock as possible. Investigations on potential applications of the fibers prepared from the bio-based polyamides were also of great interest to prove their technical applicability.

2.2 Overview

This work describes the synthesis of bio-based linear diacids and polyamides from oleic acid. Full characterization of the structure-property relationship of the resulting polyamides was performed, as well as the preparation of macro- and submicro-fibers using two different spinning techniques. Possible applications of the bio-based materials for production of sustainable textiles and membranes have been investigated. Additionally, the recyclability of the synthesized polyamides was investigated by chemical recycling to recover pure monomer and highlight the possibility of a closed-loop approach (**Figure 6**). The results of this research led to the publication of three manuscripts in peer-reviewed journals, which are briefly described in the following.

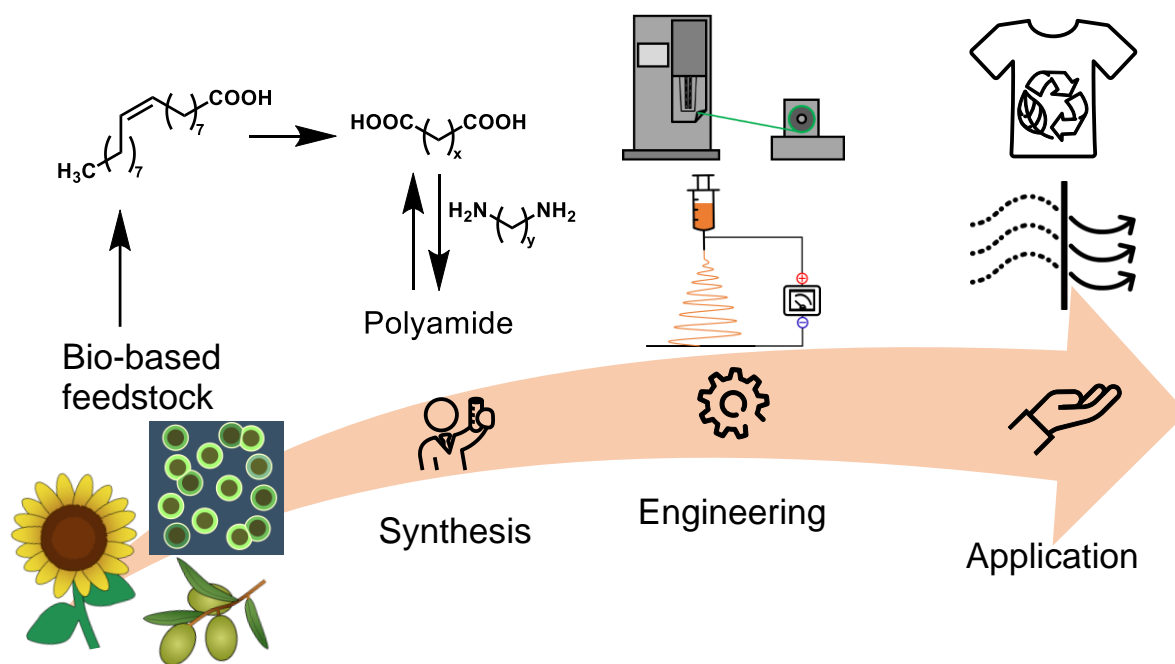


Figure 6. Table of contents graphic of my doctoral thesis.

First, a linear diacid was synthesized from bio-based oleic acid by isomerizing methoxy-carbonylation. Followed by the synthesis of linear polyamides by melt polycondensation with linear aliphatic diamines of different chain-length. The publication focused on the structure-property relationship of these bio-based PA X.19. Chemical recycling of the synthesized diacid

was performed and successfully polymerized to underline the potential for closed-loop recycling.

The second publication focused on improving the mechanical properties of the bio-based polyamides by copolymerization with PA 6.6. Investigations on the structure-property relationship were again an important part of this research. Monofilaments were produced from the best formulation and fabrics were made by knitting. The copolyamides were compared to industrial materials to investigate their potential for application in the textile industry.

For the third publication, oleic acid-based azelaic acid was used to produce bio-based PA 6.9 by melt polycondensation. Electrospinning was performed to produce nonwoven membranes from the shorter-chain polyamide. Full characterization of the nonwovens was performed to tailor membrane properties during preparation. Potential applications as filtration membranes for the remediation of water as well as air purification were assessed. Recyclability of the membranes was also a main focus of the publication in order to provide truly sustainable materials.

2.3 Synthesis, Characterization, and the Potential for Closed Loop Recycling of Plant Oil-Based PA X.19 Polyamides

M. Rist, A. Greiner, *ACS Sustainable Chem. Eng.* **2022**, *10*, 16793 – 16802.

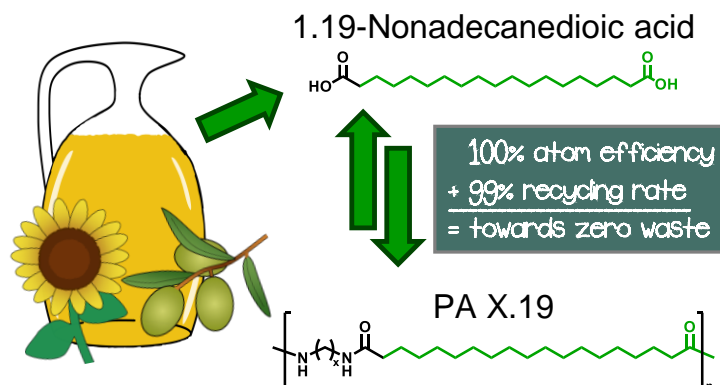


Figure 7. Table of contents graphic of my first publication.

In a two-step reaction the long-chain diacid, 1.19-nonadecanedioic acid, was synthesized from bio-based oleic acid using isomerizing methoxycarbonylation. The catalyst system used showed a high selectivity for the methoxycarbonylation at the terminal position resulting in 99+% linear product. Full use of the available bio-based carbon was achieved with this reaction, as no C–C-bond in the oleic acid structure is being broken during the reaction. Subsequently, four different polyamides (PA X.19) were synthesized using the long-chain diacid by melt polycondensation with linear aliphatic diamines of different chain length. The molecular weight of the resulting polyamides (25 900 – 51 600) met the range of technical grade polyamides.

The resulting polyamides exhibited a high thermal stability with decomposition starting at >400 °C under nitrogen and air atmosphere. Their low melting temperature between 172 °C and 208 °C is beneficial for melt processing in terms of energy consumption. All four polyamides also showed good long term stability at their respective processing temperature with a mass loss of <1% during one hour under nitrogen atmosphere.

In order to investigate the processability for injection molding and melt spinning, the viscoelastic properties of the polyamides were examined using plate-plate rheology. The Arrhenius equation was used to determine the temperature dependent melt viscosity and find the optimal processing window. All four polymers showed a high enough melt viscosity of 300 Pa·s at a shear rate of 10 rad·s⁻¹ in order to be processible by injection molding.

Mechanical properties of the polyamides were determined from injection molded specimens. All oleic acid-based polyamides showed an elongation at break between 93% and 169% with no clear trend regarding the amount of methylene units in the polymer (**Figure 8b**). The ultimate tensile strength of all four polyamides was more or less the same at 36 – 40 MPa. In terms of stiffness, a maximum of 959 ± 39 MPa for the Young's modulus was found for PA 6.19. The results were compared to the commercial PA 10.10, a fully bio-based polyamide sourced from castor oil. The oleic acid-based polyamides were inferior to the commercial product in terms of stiffness and ultimate tensile strength, but exhibited similar elongation at break. On the other hand, the oleic acid-based PA X.19 showed a lower water absorption than the commercial polyamide, with the exception of PA 4.19 (**Figure 8a**). The lower water absorption results in a higher dimensional stability and better processability. Additionally, the amount of water absorbed correlated with the amount of methylene units in the polyamide chain. The increasing hydrophobicity with increasing amount of methylene units resulted in a lower water absorption.

Analysis of the crystal structure by WAXS revealed mostly α -phase structures with some γ -phase present for all PA X.19 except PA 4.19, which only showed α -phase crystalline structures. With the α -form being the most prominent crystal phase in polyamides, these results were rather unsurprising.

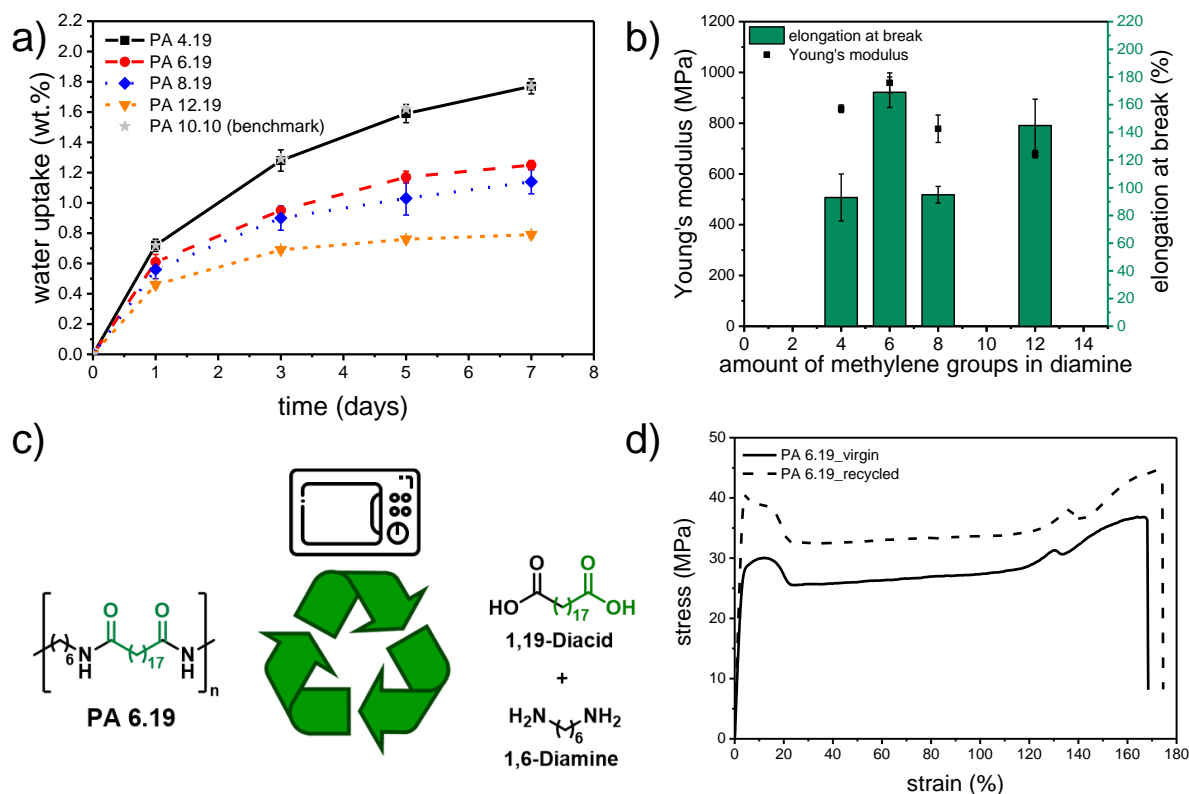


Figure 8. a) Immersed water uptake of PA X.19 and PA 10.10 over time. b) Visualization of the Young's modulus and elongation at break depending on the amount of methylene units in the diamine of the PA X.19. c) Schematic depiction of the chemical recycling of PA 6.19 by microwave assisted hydrolysis. d) Stress-strain curves of virgin and recycled PA 6.19.

Hydrolysis of polyamides is a quite complicated task and often requires harsh conditions and long reaction times. Microwave assisted hydrolysis using diluted hydrochloric acid was proven to be successful in depolymerizing PA 6.19 within 45 minutes reaction time (**Figure 8c**). The resulting 1,19-nonadecanedioic acid was easily recovered in high purity (>99%) by filtration. Formation of PA-salt from the recovered diacid with hexamethylene diamine and subsequent melt polycondensation was successfully performed to yield PA 6.19, again. The recycled polyamide had similar molecular weight as the virgin PA 6.19 and the mechanical properties of the recycled PA 6.19 were comparable with the virgin polymer in every aspect (**Figure 8d**).

2.4 Toughening of bio-based PA 6.19 by copolymerization with PA 6.6 – synthesis and production of melt-spun monofilaments and knitted fabrics

M. Rist, H. Löcken, M. Ortega, A. Greiner, *Macromol. Rapid Commun.* **2023**, *44*, 2300256.

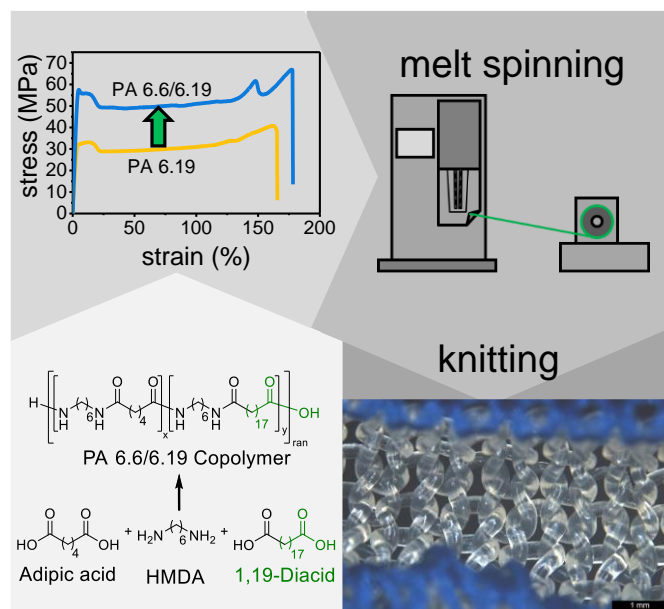


Figure 9. Table of contents graphic of my second publication.

The PA X.19 homopolymers synthesized in the first publication exhibit a lower tensile strength than commercial PA 6, which is commonly used for production of melt-spun polyamide fibers. In order to increase the tensile strength, copolyamides of PA 6.19 and PA 6.6 were synthesized by melt polycondensation of the mixed PA-salts in different ratios. Six copolyamides were synthesized in total with varying PA 6.6 contents of 17 – 88 mol%. Their number average molecular weight ranged from 28600 – 59500, meeting the range of the commercial PA 6 (34900), which was used as benchmark.

The copolyamides showed single-stage degradation under nitrogen and air atmosphere with 5% mass loss at >395 °C, similar to the homopolymers PA X.19. Their thermal stability during processing was also good at temperatures below 270 °C, with a maximum mass loss of 0.5% under air atmosphere over one hour. Processing at higher temperatures resulted in a higher mass loss of up to 4.3%. The melting temperature of the copolyamides showed a high correlation with the PA 6.6 content and was between 177 °C and 248 °C (**Figure 10a**). As expected, the melting temperature decreased upon increasing the PA 6.6 content due to disruption of the crystal structure by the shorter PA 6.6 units. The lowest point was reached for the copolyamide with 31 mol% PA 6.6 and further increasing the PA 6.6 content resulted in an increasing

melting temperature. The disruption of the crystal structure due to the additional PA 6.6 units was also observed in the melting enthalpy, which correlates with the crystallinity of the copolyamides. Here, the melting enthalpy decreased with increasing PA 6.6 content until 55 mol%, then the enthalpy showed an increasing trend.

The copolyamides showed again a much lower water absorption than the commercial benchmark, providing a higher dimensional stability. A correlation of increasing water uptake with the PA 6.6 content was found. This is due to the increased hydrophilicity by introduction of the shorter-chain adipic acid. Their water uptake was still much lower than the benchmark PA 6, which contained more than twice as much water than the worst performing PA 6.6/6.19 copolyamide after one week.

Uniaxial tensile tests of injection molded specimens of the copolyamides revealed an increasing tensile strength and stiffness (Young's modulus) with the PA 6.6 content. Surprisingly, the improved stiffness and strength did not result in a lower elongation at break. The tensile strength could be improved by 58%, while the elongation at break remained between 170% and 200% (**Figure 10b**). The first reduction in tensile strength was observed for the copolyamide with 88 mol% PA 6.6. The combination of increasing tensile strength without change of the elongation properties resulted in an increased toughness. PA 6.6/6.19 copolyamides having 55 – 88 mol% PA 6.6 exhibited a toughness in the range of commercial PA 6. As PA 6.6 is not bio-based, the bio-content of the copolyamide is inversely correlated to the PA 6.6 content. In order to find a sustainable solution, the bio-content needs to be maximized without suffering from weak mechanical properties. Therefore, the best balance between bio-content and toughness was found for the copolyamide having 55 mol% PA 6.6.

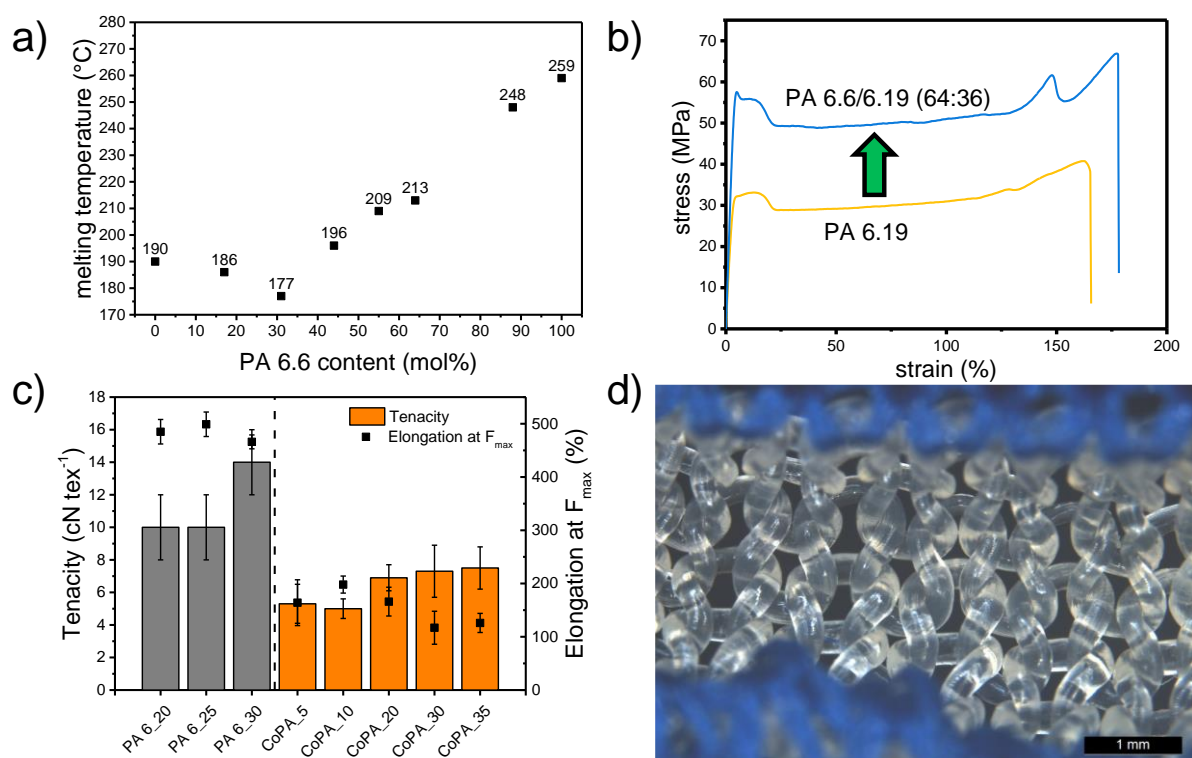


Figure 10. a) Determined melting temperatures of the polyamides as a function of the PA 6.6 content. b) Stress-strain curves of the PA 6.19 homopolymer and the PA 6.6/6.19 copolymer having 64 mol% PA 6.6. c) Tenacity and elongation at maximum force (F_{max}) of melt-spun monofilaments. d) Microscope image of the knitted fabric made from melt-spun monofilament.

The viscoelastic properties of the copolyamides were studied by rheology at different temperatures. Their spinnability was assessed according to their temperature independent loss and storage moduli. All copolyamides with a PA 6.19 content of minimum 56 mol% showed good potential for melt spinning applications according to their viscoelastic properties.

Based on these results, the copolyamide with 55 mol% PA 6.6 was synthesized in a larger scale (CoPA) to perform melt spinning tests. Different draw-down ratios were tested and the material was spinnable in a broad range from 14 to 110. The achieved processing parameters comply with industrial processing conditions for the production of partially oriented yarns (POY). As expected, the fineness of the filament decreases with increasing draw-down ratio due to the higher drawing. A higher draw-down ratio also resulted in a higher tenacity of the monofilament but a lower elongation at break (**Figure 10c**). Unfortunately, the tenacity of the bio-based copolyamide was lower than that of the benchmark PA 6. Nevertheless, these spinning trials prove the suitability of the material for processing on industrial spinning lines.

Knitting trials of the finest monofilaments made from CoPA were performed to produce swatches. No problems occurred during knitting and the resulting swatches show nice loops

without any deformation or yarn breakage (**Figure 10d**). The commercial benchmark on the other hand showed deformations at the touchpoints of the loops and overall a bad loop structure. These trials give a good indication on the suitability of the filaments prepared from the bio-based copolyamides for processing on industrial knitting machines.

2.5 Bio-based electrospun polyamide membrane – sustainable multipurpose filter membranes for microplastic filtration

M. Rist, A. Greiner, *RSC Appl. Polym.* **2024**, Advance Article.

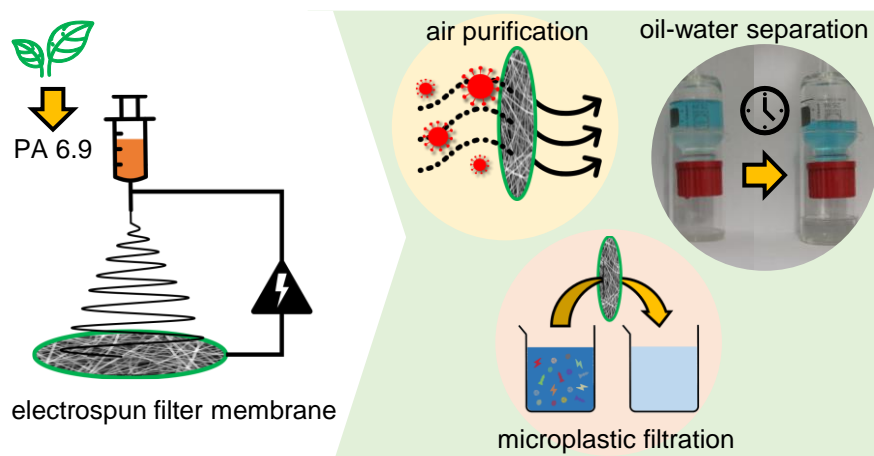


Figure 11. Table of contents graphic of my third publication.

Bio-based PA 6.9 was synthesized from oleic acid-based azelaic acid and hexamethylene diamine by melt polycondensation. The isolated polymer was dissolved in a mixture of formic acid/chloroform 1:1 (v/v). Three different concentrations (10, 12.5 and 15 wt%) of the polymer solutions were used for the electrospinning trials. The solutions were spun onto a rotating disc collector to prepare circular shaped nonwovens. In order to prepare nonwovens of comparable thickness, the total spinning time was varied between the different concentrations. Similar to electrospun nonwovens made from other polyamides, spider net-like structures were observed in all nonwovens. Tailoring of the fiber diameter as well as the resulting pore size was possible upon changing the polymer concentration (**Figure 12a**).

All electrospun filter membranes (EFMs) showed hydrophobic behavior due to their surface roughness. The EFMs also showed better mechanical stability than EFMs made from PVDF and PAN, which are generally used for the preparation of membranes. Due to their good mechanical properties in combination with a narrow pore size distribution and high porosity, their application in wet filtration of microplastic from water was investigated. All three membranes could successfully remove at least 99.7% of the dispersed PS microparticles from the water (**Figure 12b**). The filtration efficiency remained unchanged upon a filtration time of 45 minutes. Additionally, the permeability of the membranes remained unchanged during the filtration tests. The permeability of the commercial filter on the other hand decreased drastically, highlighting the benefit from using an electrospun membrane. Observation of the

cross section of the membranes after filtration suggest a surface filtration mechanism, which would ease recycling of the membranes by back-flushing.

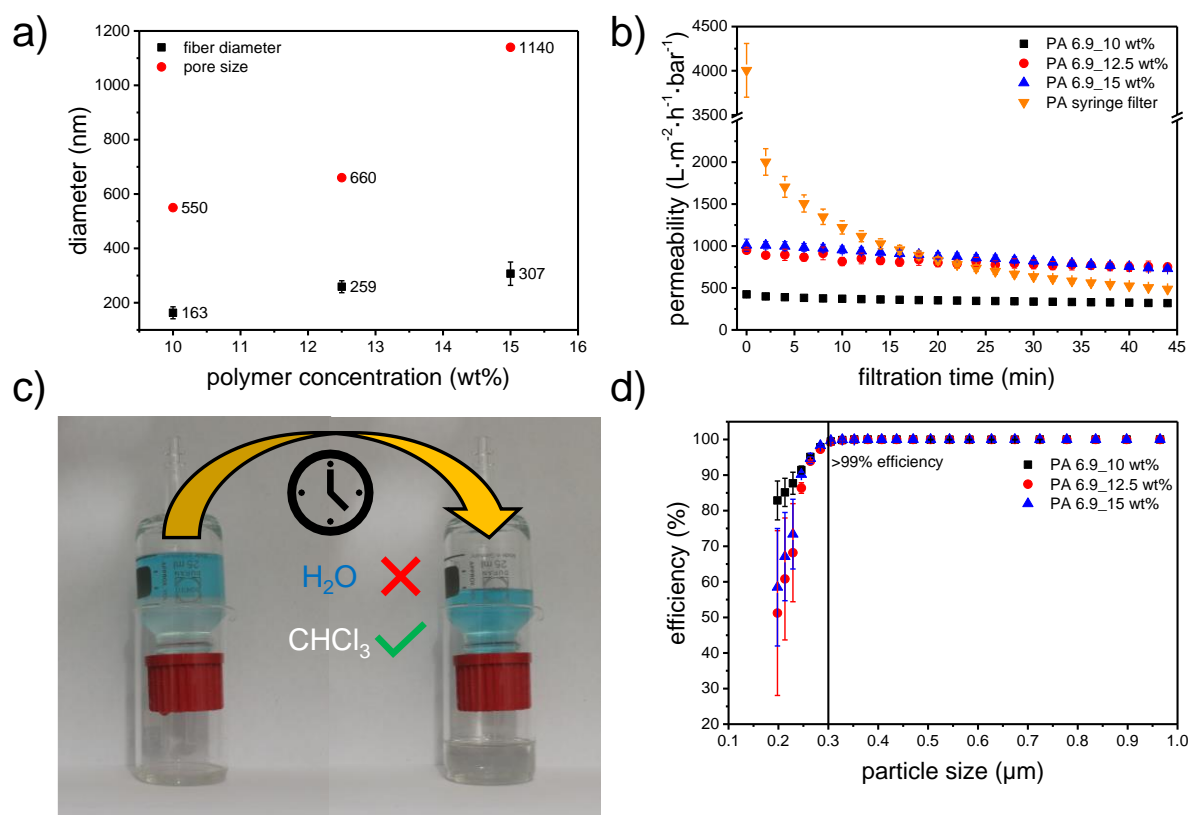


Figure 12. a) Fiber diameter and pore size of the electrospun nonwoven against the polymer concentration. b) Water permeability over time for the filtration of PS microparticles from water using the bio-based EFMs and the PA syringe filter at 1 mL·min⁻¹. c) Representation of the gravity-driven separation of water and oil using the EFMs. d) Particle size dependent filtration efficiency for the removal of aerosols from air using the bio-based EFMs.

Due to their hydrophobic surface, the membranes were used for the separation of water and oil (**Figure 12c**). The membranes were successful at separating 1:1 (v/v) mixtures of chloroform and water with an efficiency of 99.9%. The membranes showed a high permeability for chloroform, which resulted in a high flux. Tailoring of the flux was also possible by changing the polymer concentration, which therefore correlated with the pore size. The EFMs made from PA 6.9 combine a high separation efficiency with a high permeability, making them highly suitable for such separation problems. Recyclability of the membranes was also demonstrated and the membranes could be reused at least ten times without significant influence on their performance.

Additionally, the EFMs were successfully used for the filtration of aerosols from air. They successfully removed >99% of particles down to 0.3 μm in diameter and even up to 83% of

particles of 0.2 μm (**Figure 12d**). In terms of filtration efficiency, the membranes fulfill the technical specifications for FFP3 and EPA (efficient particulate air) filters. However, they suffer from a high pressure drop of 1710 – 2200 Pa, which is four times higher than the limit for FFP3 masks. In order to make these EFMs interesting for filter masks, their pressure drop needs to be lowered.

3 Contribution to the work

3.1 Publication 1

I performed the majority of the work including writing the manuscript and performing the synthesis and purification of the monomers and polymers. I prepared the tensile test specimens and rheology specimens by injection molding and melt pressing. I also performed most of the characterizations of the monomers and polymers using nuclear magnetic resonance spectroscopy (NMR), gas chromatography (GC), thermogravimetric analysis (TGA), differential scanning calorimetry (DSC), dynamic mechanical analysis (DMA), rheology, tensile tester and wide angle x-ray scattering (WAXS) as well as measurement of the water uptake. Size exclusion chromatography measurements were performed by Rika Schneider (Technician, Macromolecular Chemistry II, University of Bayreuth). The injection molding apparatus and hot press I used were kindly provided by the Macromolecular Chemistry I, University of Bayreuth. Prof. Greiner supervised the work and contributed to the work through his discussions and support during preparation of the manuscript.

3.2 Publication 2

The main part of the work was performed by me, including synthesis and purification of the monomers and polymers as well as most characterizations. I prepared tensile test specimens and rheology specimens by injection molding and melt pressing using equipment provided by the Macromolecular Chemistry I, University of Bayreuth. I performed the characterizations of the monomers and polymers using NMR, GC, TGA, DSC, DMA, rheology and tensile tester. In addition, I performed the measurements for the water uptake. Size exclusion chromatography measurements were performed by Rika Schneider (Macromolecular Chemistry II, University of Bayreuth). Melt spinning of the polymer provided by me was performed by Mathias Ortega (Institut für Textiltechnik, RWTH Aachen University), as well as the characterization of the filaments by scanning electron microscopy, tensile tests and measurement of the fineness. Knitting trials of the monofilaments and analysis of the fabrics were performed by Henning Löcken (Institut für Textiltechnik, RWTH Aachen University).

Henning Löcken wrote the knitting trials part of the manuscript and Mathias Ortega the melt spinning part, while the rest, making up most of the manuscript, was written and revised by me.

Prof. Greiner supervised the work and contributed to the work through his discussions and support during preparation of the manuscript.

3.3 Publication 3

I wrote the manuscript and performed the synthesis of the polymer, as well as the manufacturing and testing of the membranes. These involved electrospinning of the polyamide, preparation of a polystyrene latex, water filtration tests and water-oil separation tests. Aerosol filtration trials were performed by Alexander Kern (Technician, Macromolecular Chemistry I, University of Bayreuth). I also performed the majority of the characterization including NMR, uniaxial tensile tests, water contact angle, pore size measurement, evaluation of the fiber thickness, Karl-Fischer titration and UV-Vis measurements. Size exclusion chromatography measurements of the polyamide were performed by Rika Schneider (Technician, Macromolecular Chemistry II, University of Bayreuth). Samples for scanning electron microscopy were prepared by me and measurements were performed by Felix Bretschneider and Chenhui Ding (both, Macromolecular Chemistry II, University of Bayreuth). Prof. Greiner supervised the work and contributed to the work through his discussions and support during preparation of the manuscript.

4 Publications

4.1 Publication 1

Synthesis, Characterization, and the Potential for Closed Loop Recycling of Plant Oil-Based PA X.19 Polyamides

Maximilian Rist and Andreas Greiner*



Cite This: *ACS Sustainable Chem. Eng.* 2022, 10, 16793–16802



Read Online

ACCESS |

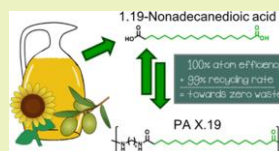
Metrics & More

Article Recommendations

Supporting Information

ABSTRACT: We report on plant oil-based linear aliphatic polyamides from 1.19-nonadecanedioic acid and aliphatic diamines of different chain lengths. Their thermal, mechanical, and rheological properties as well as the water uptake and crystalline structures were analyzed. The polyamides were synthesized with high molecular weights of 26 000 to 52 000. All polyamides showed high thermal stability with $T_{5\%}$ of >400 °C as well as high crystallinities of $\sim 50\%$. Injection molding of the plant-oil-based polyamides was successfully performed to produce tensile test specimens. Chemical recycling of the polyamides was demonstrated by microwave-assisted hydrolysis, with a recovery of 99% for 1.19-nonadecanedioic acid. Melt polycondensation using the recovered monomer was successfully performed to synthesize recycled polyamide in similar quality, which underlines its potential for closed loop recycling.

KEYWORDS: bio-based, fatty acid, polyamide, chemical recycling



Downloaded via UNIV BAYREUTH on April 6, 2023 at 15:22:39 (UTC).
See <https://pubs.acs.org/sharingguidelines> for options on how to legitimately share published articles.

INTRODUCTION

Polyamides are used extensively in engineering applications, such as automotive and electronics, due to their mechanical properties, low weight, and high chemical resistance.¹ They can also be found in our everyday life, such as in tooth brushes, climbing ropes, and clothing.² To date, these polyamides are mostly made from nonrenewable fossil-based feedstock. A shift to renewable resources is needed to produce sustainable polyamides with practical relevance.

The commercially available bio-based polyamides to date are almost exclusively made from plant-based castor oil.² Castor oil consists of mainly ricinoleic acid, a monounsaturated omega-9 fatty acid with a hydroxyl function at the C12 position. The hydroxyl group differentiates this fatty acid from common fatty acids, such as oleic acid and palmitoleic acid, and it enables the synthesis of the platform-chemical 10-undecenoic acid *via* pyrolysis.³ While castor oil does not compete with food, it is, however, the only economically reasonable resource for ricinoleic acid.⁴ Increasing the production volume will result in a high dependency on the cultivation of castor beans as a source for castor oil.

Oleic acid, on the other hand, can be sourced from a wide range of edible and inedible plant oils, resulting in a higher level of diversification of the feedstock.^{5,6} The synthesis of linear amino acids for AB-type polyamides from oleic acid *via* cross-metathesis was extensively studied. Synthesis pathways toward PA 12 using acrylonitrile,^{7–10} allyl chloride,¹¹ and allyl cyanide,¹² as well as PA 13 by the use of homoallyl cyanide, were reported (Scheme 1).¹² The synthesis of lactams *via* ring-closing metathesis was also investigated as precursors for PA 11–13.^{13,14} Cross metathesis using methyl acrylate yields the linear 1.11- and 1.12-diacids for PA X.11^{10,15} and PA

X.12.^{15–17} Self-metathesis of oleic acid and derivatives thereof yields the long-chain linear diacid 1.18-octadecanedioic acid.^{18–23} Polyurethanes,²⁴ polyesters,^{22,25} and polyamides^{26–30} were successfully synthesized using this monomer.

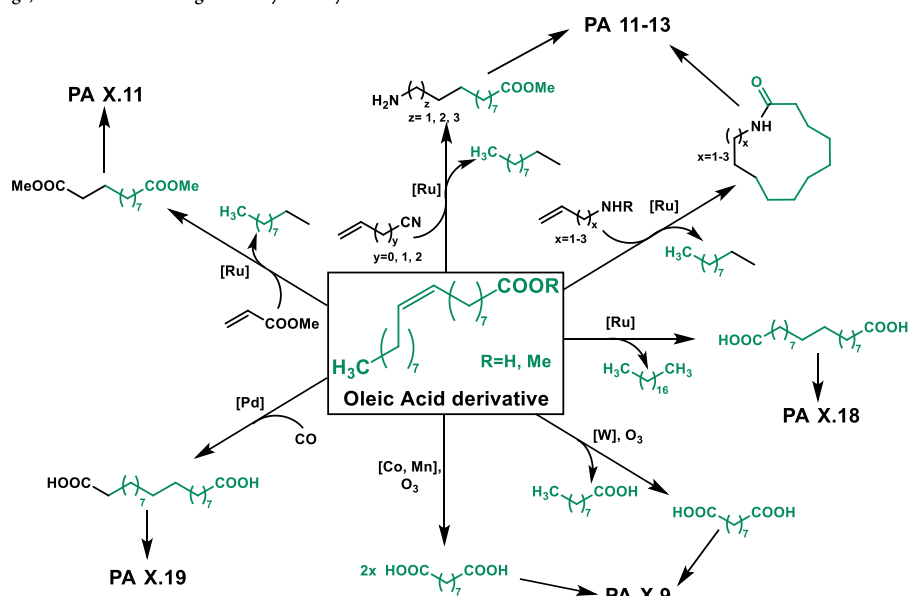
Another approach toward linear diacids is the cleavage of the double bond of oleic acid, yielding azelaic acid. This can be done either *via* ozonolysis³¹ or oxidative cleavage³² using hydrogen peroxide, and both strategies are commercially used by Emery Oleochemicals³³ and Matrica,^{34–38} respectively. At first, ruthenium-based³⁹ catalysts were used, but nowadays tungsten-based catalysts⁴⁰ are more widely used, and, recently, a vanadium-based catalyst system was also published.⁴¹ Azelaic acid-based polyamides using linear diamines with different chain lengths showed good mechanical properties combined with reduced moisture absorption compared to PA 6.6.⁴²

While the aforementioned methods are excellent tools for the synthesis of oleic acid-based monomers, they, however, only utilize 50% of available bio-based carbon of the oleic acid. To be even more sustainable, full use of available bio-based carbon should be achieved for the synthesis of plant oil-based polyamides. The use of cobalt and manganese salts together with hydrogen bromide, for example, enables the full use of bio-based carbon for the synthesis of azelaic acid.^{43,44} In this one-pot reaction, the byproduct pelargonic acid is oxidized to form azelaic acid, reaching 100% atom efficiency. Another

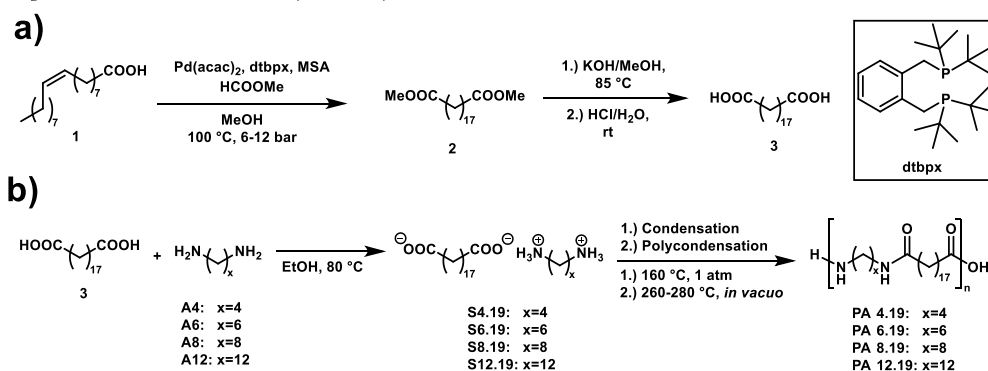
Received: August 29, 2022
Revised: November 17, 2022
Published: December 6, 2022



Scheme 1. Synthesis Routes Toward Oleic Acid-Based Polyamides via Cross-^{7–17} and Self-Metathesis,^{18–23} Oxidative Cleavage,^{40,43} and Isomerizing Methoxycarbonylation^{45,46}



Scheme 2. (a) Synthesis of 1.19-Nonadecanedioic Acid 3 from Oleic Acid 1; (b) Synthesis of PA 4.19–PA 12.19 from 1.19-Nonadecanedioic Acid 3 and Linear Alkyl Diamines A4–A12 Having Different Amounts of Methylene Groups via Their Respective PA-Salts S4.19–S12.19 by Melt Polycondensation



method for the synthesis of linear aliphatic diacids with 100% atom efficiency is isomerizing methoxycarbonylation. The use of a palladium-catalyst together with the phosphine-ligand 1,2-bis(di-*tert*-butylphosphinomethyl)benzene enables the one-step isomerization of the internal double bond to a terminal, and methoxycarbonylation with carbon monoxide to form an ester.⁴⁵ The synthesis of dimethyl-1.19-nonadecanedioate with a high purity of >99% and a high linear selectivity was achieved using this method.⁴⁶ A simple hydrolysis step yields the long-chain diacid 1.19-nonadecanedioic acid, which can then be used for the synthesis of polyamides and polyesters.

The synthesis of fully bio-based polyamides PA 23.23 and PA 23.19 from the methyl esters of oleic acid and erucic acid was reported using isomerizing methoxycarbonylation.⁴⁷ Combining this technique with the “borrowing hydrogen” methodology,^{48–50} the direct amination of the long-chain diacids was reported to synthesize long-chain 1.19-nonadecanediamine for the synthesis of PA X.19.⁵¹

In this work, we investigated the potential of polyamides derived from 1.19-nonadecanedioic acid. The polyamides were synthesized by melt polycondensation with linear diamines having 4, 6, 8, and 12 methylene groups. The focus of our work

is the characterization of those bio-based polyamides in order to understand structure–property relationships, which are fundamental for processing and real-world applications. The decomposition temperature was determined using thermogravimetric analysis (TGA), and thermal properties were analyzed via differential scanning calorimetry (DSC) and dynamic mechanical analysis (DMA). The viscoelastic behavior was analyzed using rheology to determine optimal processing temperatures and residence times for injection molding. The mechanical properties of all polymers were measured using tensile test specimens made by injection molding. Structural characterization was performed using nuclear magnetic resonance spectroscopy (^1H NMR) and wide-angle X-ray diffraction (WAXD). We also report on the microwave-assisted depolymerization of bio-based polyamides with high recovery rates. Polycondensation of recycled monomers was also successfully performed to yield high-performance polyamides in a closed loop approach.

RESULTS AND DISCUSSION

Synthesis of 1.19-Nonadecanedioic Acid and PA X.19. The long-chain diacid, 1.19-nonadecanedioic acid **3**, was synthesized from oleic acid **1** in two steps (Scheme 2a). The first one being an isomerizing methoxycarbonylation of plant oil-based oleic acid **1** by the use of a palladium catalyst in combination with 1,2-bis(di-*tert*-butyl-phosphino-methyl)-benzene (dtbpx) and methyl formate as a source for carbon monoxide in methanol. This catalyst system shows remarkably high selectivity toward α,ω -diesters if used with unsaturated fatty acids.⁴⁵ The unique selectivity of dtbpx is also utilized in the commercial production of methyl methacrylate in the so-called Alpha process.⁵² In the second step, the long-chain diacid was recovered from the long-chain diester **2** by simple hydrolysis using a methanolic solution of potassium hydroxide at elevated temperatures and aqueous hydrochloric acid. Finally, the 1.19-nonadecanedioic acid **3** could be isolated in purities exceeding 99%, as proven by ^1H NMR, with an overall yield of 80%.

PA-salts **S4.19–S12.19** were formed by mixing equimolar amounts of diacid **3** with linear alkyl diamines **A4–A12** having 4, 6, 8, and 12 methylene groups in their alkyl chains in ethanol and heating. After filtration and drying, the polyamides **PA 4.19–PA 12.19** were synthesized from their respective PA-salts **S4.19–S12.19** via melt polycondensation in two steps (Scheme 2b). At first, oligomers were formed at lower temperatures of 160 °C. Then, the polycondensation was performed at 260–280 °C with an applied vacuum. After 8–9 h of reaction time, the synthesis was stopped, and the polymers were received as white solids via precipitation with high yields of up to 97% (Table 1). The structure of the polyamides was verified by ^1H NMR spectra (Figure S8). The molecular weights ranged from 25 900–51 600, which meets the range of technical grade polyamides. In contrast to commercial polycondensation reactions, the PA salts needed to be isolated, as we were not able to perform the polymerization under increased pressure. In order to avoid evaporation of diamine during the precondensation, the temperature was slowly increased until the final temperature was reached. This naturally led to a longer reaction time (8–9 h) compared to commercial processes for the synthesis of PA 6.6 (6 h).¹

The bio-based carbon content focuses solely on the carbon in the polymer without other components such as hydrogen, oxygen, or nitrogen. This allows easier measurement of the

Table 1. Yield, Molecular Weight, and Dispersities of PA X.19

Polyamide	yield (%)	M_n^a	M_w^a	\mathcal{D}^a	biocontent ^b (%)
PA 4.19	76	51 600	92 300	1.8	78
PA 6.19	79	26 000	46 900	1.8	72
PA 8.19	97	25 900	50 000	1.9	67
PA 12.19	88	30 200	49 600	1.6	58
Vestamid Terra DS 16 (PA 10.10)		36 700	86 700	2.4	100

^aSEC (HFIP + 0.1% KTFA, room temperature, PMMA standard).

^bThe percentage of bio-based carbon content of the total carbon content in accordance with DIN EN 16640.

biocontent of polymers, as only the fraction of bio-based carbon needs to be determined by C14 analysis. By means of isomerizing methoxycarbonylation, the complete available bio-based carbon of the oleic acid could be used for the synthesis of diacid **3**. Together with non-bio-based carbon monoxide, this results in a carbon-based biocontent of 95% for diacid **3**. Since the linear alkyl diamines **A4–A12** are sourced from conventional fossil-based feedstock, the carbon-based biocontent of the final PA X.19 decreases as the amount of methylene groups in the diamine increases. Thus, the polymers **PA 4.19–PA 12.19** obtained have a biocontent between 58 and 78% (Table 1). By the use of bio-based diamines, such as pentamethylene diamine and 1.10-diaminododecane, the bio-based carbon-content could be further increased to 96 and 97%. Furthermore, the fully oleic acid-based PA 19.19 could be synthesized by reductive amination of the 1.19-diacid.⁵¹

Thermal Properties of PA X.19. The 5% weight loss ($T_{5\%}$) of the polyamides **PA 4.19–PA 12.19** were under nitrogen as well as air atmosphere above 400 °C. All polyamides are partially crystalline according to DSC analysis, with degrees of crystallinity of approximately 50%. The melting points (T_m) ranged from 172–208 °C (Table 2, Figure 1a). Glass transition temperatures (T_g) were observed only by DMA analysis and ranged from 44–62 °C (Figure S9). The drop of T_g and T_m with increasing number of methylene groups (Figure 1b) can be well understood by the decrease of the amide frequency as reported previously.⁵³

Isothermal TGA measurements of all polyamides were performed to examine the long time stability of the PA X.19 at their respective processing temperature. With the exception of **PA 4.19**, all PA X.19 showed good long time stability with <1% mass loss in 1 h under nitrogen and air atmosphere (Table 2, Figure S6). This deviation is due to the exceptionally high processing temperature (280 °C) necessary for injection molding of **PA 4.19**.

Rheological Properties of PA X.19. The viscoelastic properties of the polyamides **PA 4.19–PA 12.19** were studied in the molten state at different temperatures with a plate–plate rheometer. For all polyamides, a decrease in the complex viscosity with increasing temperature could be observed. This is caused by the increase of the free volume of the polymer melt, which weakens the intermolecular forces and increases the polymer fluidity.⁵⁵ Therefore, the melt viscosity of the polyamides can be adjusted by changing the processing temperature, which is important in injection molding or melt spinning applications. The dependency of the complex viscosity on the temperature can be described with the Arrhenius or the WLF equation. The Arrhenius equation is generally used for temperatures much higher than the glass

Table 2. Thermal Properties of PA X.19

PA X.19	TGA				DSC				DMA
	nitrogen		air		second heating		cooling		second heating
	$T_{5\%}^d$ [°C]	mass loss at T_{process}^e (%)	$T_{5\%}^d$ [°C]	mass loss at T_{process}^e (%)	T_m^b [°C]	ΔH_m^b [J·g ⁻¹]	T_c^c [°C]	X_c^c (%)	T_g^a [°C]
PA 4.19	439	0.6	416	2.7	208	99.2	192	50	62
PA 6.19	445	0.1	410	0.0	190	90.7	173	46	59
PA 8.19	446	0.0	423	0.0	183	99.3	158	50	55
PA 12.19	448	0.3	407	0.5	172	99.4	136	50	44

^aGlass-transition temperature (T_g) determined from the peak of the loss factor ($\tan d$) measured at 2 K·min⁻¹. ^bMelting temperature (T_m), melting enthalpy (ΔH_m), and crystallization temperature (T_c) measured at a rate of ± 20 K·min⁻¹. ^cCrystallinity (X_c) calculated from $\Delta H_m/\Delta H_m^0$, with ΔH_m^0 being the enthalpy of fusion of 100% crystalline PA 6.6, 197 J·g⁻¹. ^d $T_{5\%}$ is the temperature at 5% weight loss, measured at 20 K·min⁻¹. ^eMass loss after 1 h isothermal heating at their respective processing temperature (T_{process}).

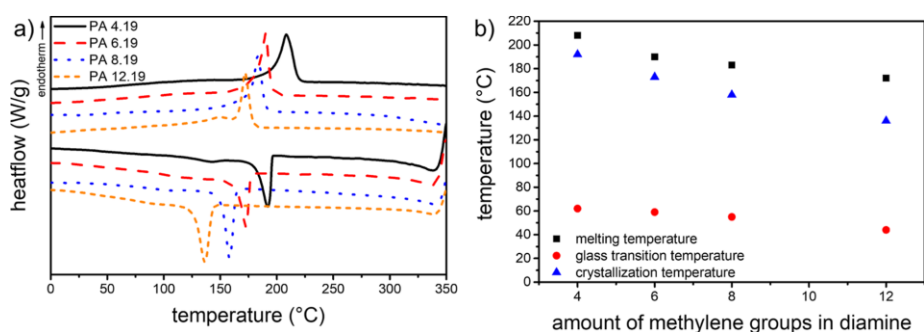


Figure 1. (a) DSC thermograms of the synthesized PA X.19. (b) Determined melting, glass-transition, and crystallization temperatures of the polyamides as a function of the diamine chain-length.

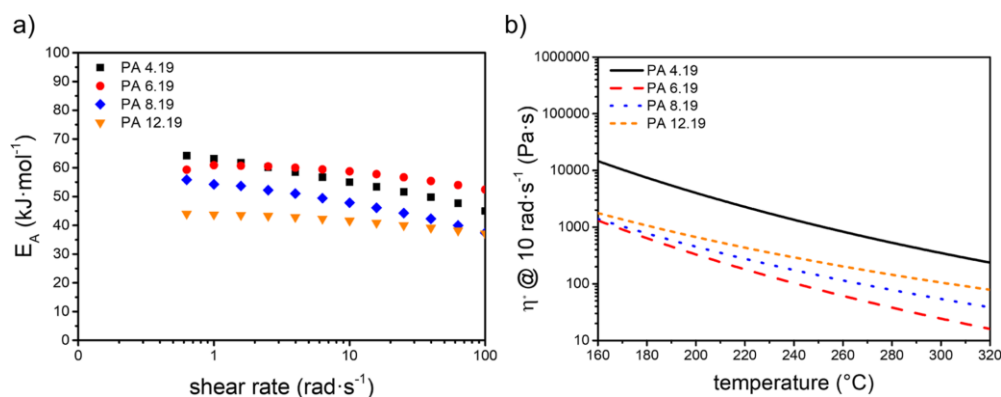


Figure 2. (a) Viscous flow activation energy E_A of PA X.19 against the shear rate. (b) Complex viscosity η^* at 10 rad·s⁻¹ of PA X.19 as a function of temperature, plotted using the Arrhenius equation.

transition temperature of the polymer, and the WLF equation is preferred for temperatures close to the T_g .⁵⁶ As the melting temperatures of the synthesized polyamides PA 4.19–PA 12.19 are much higher than their respective glass transition temperatures, the Arrhenius equation was used

$$\eta^*(T) = C_1 \cdot e^{E_A/R \cdot T}$$

With $\eta^*(T)$ being the complex viscosity at a temperature T , together with the material constant C_1 , the universal gas

constant R (8.314 J·mol⁻¹·K⁻¹), and the viscous flow activation energy E_A . By plotting the logarithm of the complex viscosity against the inverse temperature at a constant shear rate for three different temperatures, E_A for each shear rate was obtained as the slope from the linear curve fit. The viscous flow activation energy represents the dependency of the complex viscosity on the temperature. The resulting plots of E_A against the shear rate can be observed in Figure 2a. A decrease of the viscous flow activation energy with increasing shear rate could

Table 3. Mechanical Properties and Water Uptake of Bio-based PA X.19 and Benchmark PA 10.10

polyamide	Young's modulus ^a [MPa]	ultimate tensile strength ^a [MPa]	elongation at break ^a [%]	toughness ^a [MPa]	water uptake ^b [%]
Vestamid® Terra DS16 (PA 10.10)	1580 ± 39	72 ± 5	103 ± 18	63 ± 12	1.77 ± 0.00
PA 4.19	857 ± 15	40 ± 2	93 ± 17	32 ± 6	1.77 ± 0.05
PA 6.19	959 ± 39	36 ± 1	169 ± 11	47 ± 2	1.25 ± 0.03
PA 8.19	778 ± 54	36 ± 1	95 ± 6	29 ± 2	1.14 ± 0.08
PA 12.19	678 ± 15	40 ± 3	145 ± 19	47 ± 7	0.79 ± 0.02

^aMeasured in accordance with DIN EN ISO 527-2, at 50 mm·min⁻¹ test speed. ^bThe water uptake measured in deionized water at 25 °C for 7 d in accordance with DIN EN ISO 62.

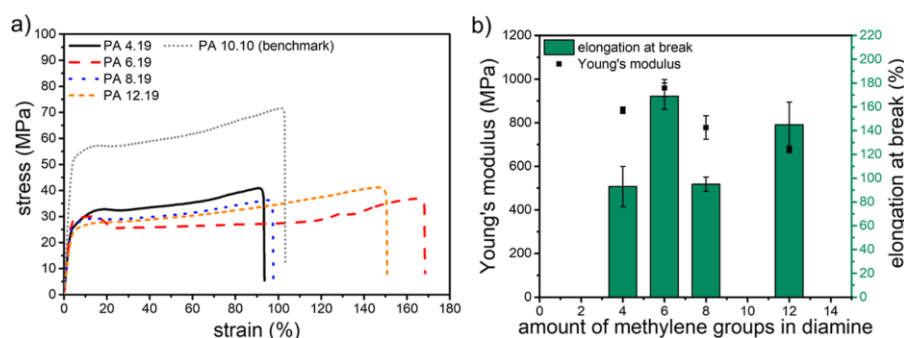


Figure 3. (a) Stress–strain curves of bio-based PA X.19 and commercial Vestamid Terra DS 16 (PA 10.10). (b) Visualization of Young's modulus and the elongation at break in dependence of the amount of methylene groups in the diamine for the synthesized PA X.19. The error bars are sometimes too small to visualize.

be observed, showing that an increase in shear rate reduces the sensitivity to temperature.

With the now known viscous flow activation energy E_A of the polyamides PA 4.19–PA 12.19 for each shear rate, the material constant C_1 can be calculated for the corresponding shear rate. With the completed Arrhenius equation, the temperature-dependent complex viscosity at a shear rate of 10 rad·s⁻¹ was plotted in Figure 2b. PA 4.19 showed a much higher viscosity than the other polyamides at all temperatures, which is due to the increased molecular weight compared to the other PA X.19. Above the entanglement molecular weight, the viscosity of the polymer is dependent on the molecular weight by the power of 3.4.⁵⁷ Using the Arrhenius equation, the optimal processing temperature (T_{process}) for each polymer was calculated, targeting a viscosity of 300 Pa·s at a shear rate of 10 rad·s⁻¹, which was proven to be suitable for injection molding of PA 6. PA 4.19 was therefore processed at 280 °C, PA 6.19 at 210 °C, PA 8.19 at 220 °C, and PA 12.19 at 240 °C.

Mechanical Properties and Water Uptake. Tensile test specimens were processed by injection molding from all polymers, PA 4.19–PA 12.19, at the optimal processing temperatures calculated from the rheology measurements. The results of the tensile tests are depicted in Table 3 and Figure 3b, and the stress–strain curves can be observed in Figure 3a. From the stress–strain curves, no clear trend regarding the amount of methylene groups in the diamine can be observed. While PA 4.19 and PA 8.19 showed an elongation at break of 93 ± 17 and 95 ± 6%, respectively, the polyamides PA 6.19 and PA 12.19 are both more ductile with 169 ± 11% and 145 ± 19%, respectively. A similar observation was made for the ultimate tensile strength, where PA 6.19 and PA 8.19 are both

at 36 ± 1 MPa and PA 4.19 and PA 12.19 show an ultimate tensile strength of 40 ± 3 MPa. This is in contrast to the observations made for the PA X.18²⁸ and recently for the PA X.9.⁴² For both polyamides, a trend toward lower elongation at break and ultimate tensile strength with the increasing diamine chain length was observed. For the Young's modulus, we observed a maximum value for PA 6.19 with 959 ± 39 MPa. Increasing or decreasing the diamine chain-length resulted in a lower Young's modulus.

The mechanical properties of the new bio-based PA X.19 were compared with the commercially available castor oil-based PA 10.10, marketed under the trade name Vestamid Terra DS 16 (Table 3). Vestamid shows a much higher Young's modulus (1580 ± 39 MPa) and ultimate tensile strength (72 ± 5 MPa) than the oleic acid-based PA X.19. Regarding the elongation at break, the PA X.19 are similar to the castor oil-based PA 10.10, with PA 6.19 and PA 12.19 even showing an enhanced elongation of >100%. This might be due to the different number of methylene-units between the amide groups, which affect the formation of hydrogen bonds that strongly influence the mechanical properties. In PA 10.10, the amide groups are distributed very regularly along the polyamide chain, aiding the formation of hydrogen bonds between intermolecular chains. For the PA X.19 this is however not the case, as the diamines are much shorter than the diacid. The amount of amide groups per 100 methylene-units is also lower for the PA X.19 (6.5–8.7) compared to PA 10.10 (10), which results in a lower number of hydrogen bonds along the polymer chains. Similar observations were found for the ultimate tensile strength of the PA X.18.²⁸

The PA X.19 showed mostly lower water absorption than the ricinoleic-based PA 10.10, with the exception of PA 4.19,

which shows the same percentage (Table 3, Figure 4). This can be explained by the similar amounts of methylene groups in

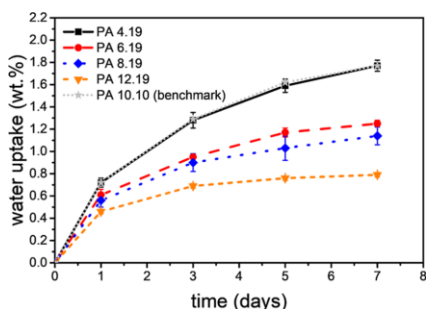


Figure 4. Immersed water uptake of PA X.19 and PA 10.10 over time.

the repeating units of those two polyamides. With the increasing amounts of methylene groups in the polymer backbone, the water uptake decreases due to the increase in hydrophobicity. PA 12.19 shows therefore the lowest water uptake of $0.79 \pm 0.02\%$, which is almost half of PA 4.19. A lower water-uptake is beneficial for the processing of the polymers as this results in better dimensional stability of the material (e.g., fibers). Absorbed water can also act as a plasticizer, reducing the tensile strength while increasing ductility.⁴² The water uptake of polyamides can further be influenced by the crystallinity of the polymer. It was shown that increasing the crystallinity of PA 6 by tempering resulted in a 30% reduction of the water uptake.⁵⁸ The influence of crystallinity can be neglected, though, as the synthesized polyamides all have a similar crystallinity of approximately 50%.

Crystal Structure of PA X.19. The crystal structure of PA X.19 was studied using WAXD analysis (Figure 5). Polyamides

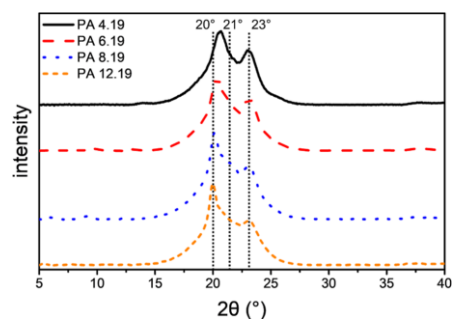


Figure 5. WAXD patterns of PA X.19.

are polymorphic materials and can therefore crystallize in different crystalline structures. The two main crystal structures are the α -crystal form, showing an antiparallel alignment of the polymer chains, and the γ -crystal form with parallel alignment. With the α -crystal form being thermodynamically favored due to easier hydrogen bond formation. However, this is not the case for even–odd and odd–even polyamides, where an all

trans formation hinders the formation of hydrogen bonds in a parallel alignment. Nevertheless, α -crystal structures have still been observed for even–odd polyamides.^{42,59} The postulated structure is based on slightly rotated amide groups of the odd amide unit to enable hydrogen bonding with four neighboring polyamide chains.^{60,61}

All synthesized PA X.19 showed mainly diffraction peaks corresponding to the α -phase at $\sim 20^\circ$ and $\sim 23^\circ$ (Figure 5). Moreover, with the exception of PA 4.19 all polyamides showed also a shoulder at $\sim 21^\circ$, which corresponds to the γ -phase. Similar results were obtained for other even–odd polyamides like PA X.9^{42,60–63} with $X = 4, 6, 8, 10, 12$, and PA 6.13.⁵⁹

Closed Loop Recycling of PA 6.19. Hydrolysis reactions are commonly used for the chemical recycling of polyesters, such as poly(ethylene terephthalate) (PET),⁶⁴ and has also been applied recently for the closed loop recycling of long-chain polyesters.²⁵ The hydrolysis of polyamides, however, is more complicated and often requires long reaction times and harsh conditions.^{65,66} Microwave-assisted hydrolysis is a promising tool for the chemical recycling of polyamides with reduced reaction times and energy consumption.^{67–69}

Chemical recycling of the bio-based PA X.19 was exemplarily performed with PA 6.19 using microwave-assisted hydrolysis in aqueous hydrochloric acid. The oleic acid-based diacid 3 could be recovered with an almost quantitative yield of 99% and a high purity of >99% (¹H NMR). The structure of the recovered diacid 3 was confirmed by ¹H NMR analysis (Figure S4). Similar results were recently published for the microwave-assisted hydrolysis of commercial aliphatic polyamides.⁶⁷

The recovered diacid 3 was used to synthesize PA-salt S6.19 for a following melt polycondensation to form recycled PA 6.19 in order to demonstrate the potential for closed loop recycling of the PA X.19. Finally, the recycled PA 6.19 could be isolated at a high yield of 90%. SEC-analysis of the recycled PA 6.19 confirmed a peak molecular weight (M_p) of 38 500, which is in the range of the virgin PA 6.19 and other commercial polyamides (Figure 6a). Surprisingly, the recycled PA 6.19 shows an increased ultimate tensile strength and Young's modulus compared to the virgin material (Figure 6b). A possible explanation for this could be a difference in the degree of crystallinity of the tensile test specimens. Similar observations were made for the fused filament fabrication of PA 6.6.⁷⁰ Here, an increase in processing temperature by 20 K led to an increase in crystallinity from 47 to 66%, and subsequently, the tensile strength was improved by 30%.

EXPERIMENTAL SECTION

Materials. Oleic acid (99%) was purchased from Jinan Boss Chemical Industry Co., Ltd. 1,2-bis(di-*tert*-butylphosphino-methyl)-benzene (dtbpx) was purchased from Henan Allgreen Chemical Co., Ltd. Methyl formate (97%), 1,4-diaminobutane (99%), hexamethylene diamine (99.5+%), and 1,8-diaminooctane (98%) were purchased from Acros. Methanesulfonic acid (MSA, >99%) and 1,12-diaminododecane (>98%) were purchased from TCI Chemicals. Palladium(II)-acetylacetonate (99%) and calcium hydride (for synthesis) were purchased from Sigma-Aldrich. 1,1,1,3,3,3-Hexafluoro-2-propanol (HFIP, 99%) was purchased from Fluorochem Ltd. Potassium hydroxide (>85%) was purchased from Carl Roth. Aqueous hydrochloric acid (37%) was purchased from VWR. Deuterated chloroform (CDCl₃, 99.8%) and dimethyl sulfoxide (DMSO-*d*₆, 99.8%) were purchased from Deutero. Vestamid Terra DS 16 (PA 10.10, off-white granulates) was kindly provided by

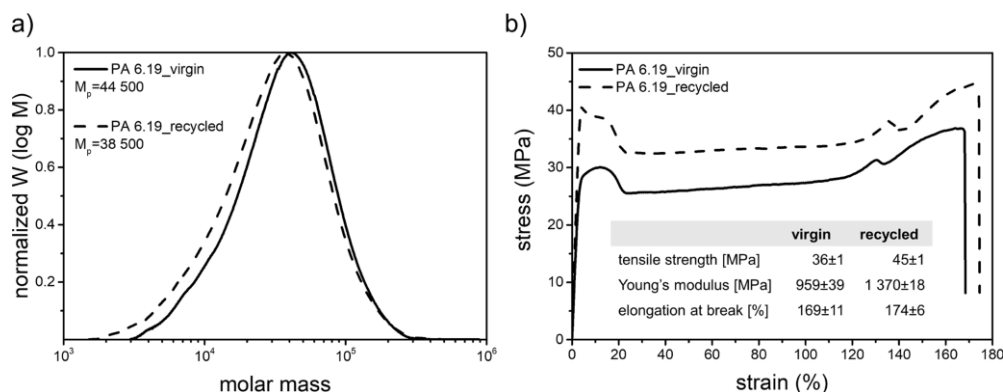


Figure 6. (a) Normalized molecular weight distribution of the virgin and recycled PA 6.19 measured by SEC. (b) Stress–strain curves of the virgin and recycled PA 6.19 and corresponding mechanical properties.

Evonik. All solvents for purification were purchased in technical grade from local suppliers.

Purifications. Methyl formate was degassed by freeze–pump–thaw cycling and stored over molecular sieves 4 Å. Methanol was dried by refluxing with calcium hydride, distilled, and stored over molecular sieves 3 Å. All diamines were distilled and stored under an argon atmosphere.

METHODS

Size Exclusion Chromatography. Size exclusion chromatography (SEC) of the polymers was measured on a 1200 Series system (Agilent Technologies/Gynotek). The instrument was equipped with a PFG 7 μm precolumn and two main columns (PFG 7 μm , 100 Å and PFG 7 μm , 300 Å) (PSS, Mainz, Germany). A refractive index detector (RI, Gynotek SE-61) was used for the detection. The samples were dissolved in HFIP (HPLC grade) with potassium trifluoroacetate (8 $\text{mg}\cdot\text{mL}^{-1}$) and toluene (HPLC grade) as an internal standard in a concentration of 2 $\text{mg}\cdot\text{mL}^{-1}$ and filtered through a 0.22 μm PTFE filter. 20 μL of this solution were injected and measured at a flow rate of 0.5 $\text{mL}\cdot\text{min}^{-1}$ at 23 $^{\circ}\text{C}$. Calibration of the system was performed with poly(methyl methacrylate) (PSS calibration kit, PSS, Mainz, Germany) in a range of 1 720–189 000 Da.

Nuclear Magnetic Resonance Spectroscopy (^1H NMR). ^1H NMR spectra were recorded using an Ultrashield-300 spectrometer (Bruker) at 300 MHz. The spectra of the polymers were recorded in HFIP (99%) with CDCl_3 added as an internal reference. Other spectra were recorded in CDCl_3 or $\text{DMSO}-d_6$.

Thermal Properties. Studies on the thermal stability were performed with thermogravimetric analysis (TGA) on a TG 209 F1 Libra (Netzsch). Approximately 5 mg of the sample were weighed in an aluminum crucible with a pierced lid (Thepro). Dynamic measurements were performed in the range of 20–600 $^{\circ}\text{C}$ using a heating rate of 20 $\text{K}\cdot\text{min}^{-1}$ under nitrogen 5.3 and synthetic air (O₂/N₂, 20/80, v/v), with a flow rate of 50 $\text{mL}\cdot\text{min}^{-1}$. Isothermal measurements were performed for 1 h at the respective processing temperatures of the polymers at 210, 220, 240, and 280 $^{\circ}\text{C}$ under nitrogen 5.3 and synthetic air (O₂/N₂, 20/80, v/v), with a flow rate of 50 $\text{mL}\cdot\text{min}^{-1}$.

Differential scanning calorimetry (DSC) was performed on a DSC 204 F1 Phoenix (Netzsch). Approximately 5 mg of the sample were weighed in a 30/40 μL aluminum crucible with a pierced lid (Thepro). Dynamic measurements were performed in the range of –50–350 $^{\circ}\text{C}$ at a heating rate of 20 $\text{K}\cdot\text{min}^{-1}$ under nitrogen 5.3 with a flow rate of 20 $\text{mL}\cdot\text{min}^{-1}$.

Dynamic Mechanical Analysis (DMA) was performed on a DMA 1 STARE System (Mettler Toledo) in single cantilever mode. The measurements were conducted with a heating rate of 2 $\text{K}\cdot\text{min}^{-1}$ and a frequency of 2 Hz.

Rheology. Test specimens for the rheology were produced with a 25-12-2HC hot press (Carver). The polymers were dried under a vacuum at 80 $^{\circ}\text{C}$ overnight and pressed in between two stainless steel plates separated by Kapton sheets using a circular mold with $d = 25$ mm and $h = 1$ mm at a temperature of $T_m + 30$ K for 5 min. The pressure was increased from 0 to 5 t after 2 min and held for 2 min. Thermal quenching was performed directly afterward on a LaboPress P150H manual lever cold press (Vogt Maschienenbau, Berlin, Germany) until room temperature was reached. Rheology measurements were performed on a MCR302 Rheometer (Anton Paar) using an electrical plate (P-ETD400) and an electrical hood (H-ETD400) in parallel plate geometry with $d = 25$ mm. The dynamic measurements were conducted isothermally at 2% deformation, and the shear rate was varied between 100 and 0.631 $\text{rad}\cdot\text{s}^{-1}$.

Mechanical Properties. The mechanical properties were determined by uniaxial stress–strain testing on a BT1-FR 0.5TND14 (Zwick/Roell) at room temperature. The test specimens of type 5B according to DIN EN ISO 527-2 were produced by injection molding on a Micro Injector 5000 (DACA Instruments) with a 5 mL barrel volume. The dimensions of the test specimens were measured at one sample for each nest with a Series 293 (0–25 mm) digital micrometer (Mitutoyo, Neuss, Germany), taking the average of three different positions in the gauge area. The specimens were conditioned for 48 h at room temperature prior to testing. Tensile tests were performed according to DIN EN ISO 527 at 50 $\text{mm}\cdot\text{min}^{-1}$ at a grip-to-grip separation of 20 mm. The Young's modulus was determined by the slope of the linear region of the stress–strain curves in the range of 0.05–0.25% deformation. At least seven specimens were tested for each material, and the statistical average is given as a result.

Water Uptake. The water uptake tests of the polyamides were performed according to DIN EN ISO 62. Disc-shaped test specimens with $d = 25$ mm and $h = 1$ mm were produced via melt pressing, analogous to the rheology test specimens. The test specimens were dried in a vacuum oven at 80 $^{\circ}\text{C}$ for 48 h prior to testing and weighed after cooling to room temperature in a desiccator to determine the initial weight (m_0). The specimens were then immersed in deionized water at room temperature for seven days. Prior to weighing (m_1), the samples were thoroughly dried with a cloth to remove any surface water. The water uptake was determined using the following formula

$$\text{water uptake} = \frac{m_t - m_0}{m_0} \cdot 100\%$$

Crystal Structure. The analysis of the crystal structure of the polyamides was performed using X-ray diffraction on a D8 ADVANCE diffractometer (Bruker), equipped with Cu K α radiation ($\lambda = 0.154$ nm). The source was operated at 40 kV and 40 mA, and measurements were recorded in a 2θ range of 5 – 40° with a step-size of $0.025^\circ \cdot \text{min}^{-1}$ at room temperature. Disc-shaped test specimens with $d = 25$ mm and $h = 1$ mm were produced *via* melt pressing, analogous to the rheology test specimens.

Gas Chromatography. Purity analysis of dimethyl-1.19-nonadecanedionate **2** was performed on a GC-2010 Plus (Shimadzu) equipped with a ZB-5 ms column ($L = 30$ m, ID = 0.25 mm, FT = 0.25 μm) and a flame-ionization detector (FID). Nitrogen was used as a carrier gas, with a flow of 1.5 mL $\cdot\text{min}^{-1}$. The injection volume was 1 μL , with a split ratio of 5.0 , and the injector temperature was 300 $^\circ\text{C}$. For the column, a temperature program was used to ensure complete separation of possible side-products: 1 min @ 80 $^\circ\text{C}$, then in 10 min to 180 $^\circ\text{C}$ and hold for 5 min, and then in 20 min to 280 $^\circ\text{C}$ and hold for 5 min. The FID temperature was set to 305 $^\circ\text{C}$ for complete detection.

Synthesis of Dimethyl-1.19-Nonadecanedionate 2. The synthesis of dimethyl-1.19-nonadecanedionate **2** was adapted from the method used by Pinggen *et al.*⁷¹ All steps were performed under an inert gas atmosphere. 121 mg (0.40 mmol, 4 mol %) of palladium(II)acetylacetonate and 627 mg (1.59 mmol, 1.6 mol %) of 1,2-bis(di-*tert*-butylphosphino-methyl)benzene (dtbpx) were weighed into a 250 mL stainless steel autoclave equipped with a stirring bar. A solution of 28.04 g (99.27 mmol) of oleic acid **1**, 99% , 48 mL of methyl formate, and 154 μL (2.38 mmol, 6 mol %) of methanesulfonic acid (MSA) in 48 mL of methanol was prepared and directly transferred into the autoclave using a syringe under inert gas counterflow. The autoclave was closed and heated to 100 $^\circ\text{C}$ while being stirred for 24 h. During this period, the pressure gradually increased to 6 – 12 bar. After cooling the autoclave to room temperature, the pressure was carefully released. The reaction products were washed out of the autoclave with 2×40 mL of methylene chloride. The resulting yellow solution was filtered over neutral Al_2O_3 to remove possible Pd black and excess catalyst. The solvent was removed using a rotary evaporator to yield the crude product as yellow crystals. These were purified by two times recrystallization from 200 mL of methanol to isolate the 1.19-nonadecanedionate **2** as white crystals with a purity of $>99\%$ (GC) and a yield of 80% .

¹H NMR: (CDCl_3 , 298 K, 300 MHz, $\delta = \text{ppm}$): 3.66 (s, 6H), 2.30 (t, 4H), 1.61 (m, 4H), 1.25 (m, 26H).

Synthesis of 1.19-Nonadecanedioic Acid 3. The synthesis of 1.19-nonadecanedioic acid **3** was adapted from the method used by Pinggen *et al.*⁷¹ 24.5 g (68.6 mmol) of dimethyl-1.19-nonadecanedionate **2** were transferred into a 1 L round bottom flask equipped with a large stirring bar and a reflux condenser. A solution of 46.2 g potassium hydroxide in 462 mL methanol was added to the flask and heated to 85 $^\circ\text{C}$ with stirring for 12 h to form a white slurry. After cooling to room temperature, the solvent was removed *in vacuo* to yield the potassium salts as white solids. The salts were then dissolved in 236 mL deionized water followed by slow addition of aqueous hydrochloric acid (6 M) until pH ~ 1 , resulting in a white precipitate. The precipitate was washed neutral with deionized water and then dried for 24 h at 80 $^\circ\text{C}$ to obtain the pure 1.19-nonadecanedioic acid **3** as white solids in a yield of 22.5 g (68.4 mmol, 99% yield).

¹H NMR: ($\text{DMSO}-d_6$, 298 K, 300 MHz, $\delta = \text{ppm}$): 11.98 (s, 2H), 2.18 (t, 4H), 1.47 (m, 4H), 1.23 (s, 26H).

Synthesis of Polyamides. The PA-salts **S4.19**–**S12.19** were prepared by dissolving equimolar amounts of the used linear alkyl diamine **A4**–**A12**, which have 4, 6, 8, and 12 methylene groups, and 1.19-nonadecanedioic acid **3** in ethanol to form solutions of 10 wt %. Complete dissolution of the diacid **3** was achieved by heating to 80 $^\circ\text{C}$. Upon complete dissolution of the diacid **3**, the diamine-solution **A4**–**A12** was added, causing the formation of the respective PA-salt

S4.19–**S12.19** as a white precipitate. After another 2 h of heating, the solution was cooled to room temperature. The formed precipitate was recovered by filtration and washed with warm ethanol to yield the desired PA-salts **S4.19**–**S12.19** in $\sim 90\%$ yield.

For the synthesis of polyamides **PA 4.19**–**PA 12.19**, the respective PA-salts **S4.19**–**S12.19** were transferred into a three-necked Schlenk-tube with a mechanical stirrer, and a distillation bridge was attached. Upon exchange of the atmosphere with argon to ensure the exclusion of oxygen, the respective PA-salt was heated to 160 $^\circ\text{C}$ with stirring. The temperature was increased stepwise in 10 K increments to ensure melting until the final temperature of 265 $^\circ\text{C}$ is reached within 4 h. Then, the temperature was held at 265 $^\circ\text{C}$ for 3 h while stirring. Afterward, a vacuum was applied to ensure complete evaporation of water, and the reaction proceeded for another 2 h. Then, the tube was vented with argon and cooled to room temperature. The formed polymer was dissolved in HFIP (1,1,1,3,3,3-hexafluoro isopropanol) and recovered by precipitation in methanol. After drying, the overall yield of recovered polyamides **PA 4.19**–**PA 12.19** was $\sim 90\%$.

Microwave-Assisted Depolymerization Experiments. In a PTFE microwave tube, 3.12 g (7.6 mmol) of **PA 6.19** was weighed in, and 15.0 mL of 6 M hydrochloric acid was added. The tube was closed and placed in a multiwave GO (Anton Paar) microwave, where it was heated to 200 $^\circ\text{C}$ in 5 min; then, the temperature was held for another 20 min. Upon cooling to room temperature, the tube was carefully opened to release leftover pressure, and the reaction products were washed out with water. The resulting slurry was then filtered and washed with water to obtain 2.47 g (7.5 mmol) of diacid **3** in 99% yield.

CONCLUSIONS

Bio-based PA X.19 were synthesized from oleic acid-based 1.19-nonadecanedioic acid **3** with different linear diamines. The polyamides could be obtained with high molecular weights, which fulfill the standard range of technical polyamides. All synthesized polyamides showed high thermal stability, which makes them suitable for melt-processing. Compared to the castor oil-based PA 10.10, they showed improved elongation at break of $>100\%$ but lower tensile strengths of 36 – 40 MPa. Their rheological behavior was analyzed to determine optimal processing temperatures, and they were successfully processed using injection molding. The PA X.19 also showed lower water uptake compared to the castor oil-based benchmark, which is preferred for further processing. Based on these results, we could successfully demonstrate the synthesis of high performance polyamides based on plant oil raw products. Owing to high ductility and Young's modulus, **PA 6.19** can be presented as an interesting material for the production of sustainable textile fibers or packaging material. To further highlight the potential of **PA 6.19** as a sustainable material, we demonstrated the recycling of the polycondensation grade monomer in near quantitative amounts with a yield of 99% . Synthesis of recycled **PA 6.19** was successfully performed in a yield of 90% to highlight the potential for closed loop recycling. The recycled material showed equivalent mechanical properties compared to the virgin material. We are convinced that the **PA 6.19** is a bio-based polyamide, which justifies further investigation in order to provide sustainable polyamides with tailor made properties. Application of these polyamides could be in textile applications as well as engineering plastics wherever closed loop recycling makes sense.

■ ASSOCIATED CONTENT

■ Supporting Information

The Supporting Information is available free of charge at <https://pubs.acs.org/doi/10.1021/acssuschemeng.2c05176>.

¹H NMR spectra of all synthesized monomers and polyamides, GC chromatogram of dimethyl-1,19-nonadecanedionate, and dynamic and isothermal TGA, SEC, and DMA of all synthesized polyamides (PDF)

■ AUTHOR INFORMATION

Corresponding Author

Andreas Greiner — University of Bayreuth, Bayreuth 95440, Germany; Bavarian Polymer Institute, University of Bayreuth, Bayreuth 95440, Germany; orcid.org/0000-0002-5310-3850; Email: greiner@uni-bayreuth.de

Author

Maximilian Rist — University of Bayreuth, Bayreuth 95440, Germany; orcid.org/0000-0002-6008-9583

Complete contact information is available at:

<https://pubs.acs.org/doi/10.1021/acssuschemeng.2c05176>

Author Contributions

The manuscript was written through the contributions of all authors. All authors have given approval to the final version of the manuscript.

Funding

Federal Ministry of Education and Research project Algae Tex, no. 031b1058B

Notes

The authors declare no competing financial interest.

■ ACKNOWLEDGMENTS

The authors are indebted to the Federal Ministry of Education and Research for its financial support.

■ REFERENCES

- (1) Herzog, B.; Kohan, M. I.; Mestemacher, S. A.; Pagilagan, R. U.; Redmond, K.; Sarbandi, R. Polyamides. In *Ullmann's Encyclopedia of Industrial Chemistry*; John Wiley & Sons, Ltd, 2020; pp 1–47.
- (2) TextileExchange. Preferred Fiber & Materials: Market Report 2021. TextileExchange, 2021. https://textileexchange.org/wp-content/uploads/2021/08/Textile-Exchange_Preferred-Fiber-and-Materials-Market-Report_2021.pdf (accessed 2022 26 08).
- (3) Naughton, F. C. Production, chemistry, and commercial applications of various chemicals from castor oil. *J. Am. Oil Chem. Soc.* **1974**, *51*, 65–71.
- (4) Buist, P. H. Unsaturated Fatty Acids. In *Comprehensive natural products II: Chemistry and biology*; Liu, H.-W., Mander, L., Eds.; Elsevier, 2010; Chapter 1.02, pp 5–33.
- (5) Shorland, F. B. *Chemical Plant Taxonomy*; Academic Press, 1963.
- (6) Sievert, C. F. An introduction to the chemistry and biochemistry of fatty acids and their glycerides (Gunstone, F. D.). *J. Chem. Educ.* **1970**, *47*, A314.
- (7) Bruneau, C.; Fischmeister, C.; Miao, X.; Malacea, R.; Dixneuf, P. H. Cross-metathesis with acrylonitrile and applications to fatty acid derivatives. *Eur. J. Lipid Sci. Technol.* **2010**, *112*, 3–9.
- (8) Miao, X.; Fischmeister, C.; Dixneuf, P. H.; Bruneau, C.; Dubois, J.-L.; Couturier, J.-L. Polyamide precursors from renewable 10-undecenenitrile and methyl acrylate via olefin cross-metathesis. *Green Chem.* **2012**, *14*, 2179.
- (9) Miao, X.; Fischmeister, C.; Bruneau, C.; Dixneuf, P. H.; Dubois, J.-L.; Couturier, J.-L. Tandem catalytic acrylonitrile cross-metathesis and hydrogenation of nitriles with ruthenium catalysts: direct access to linear α,ω -aminoesters from renewables. *ChemSusChem* **2012**, *5*, 1410–1414.
- (10) Miao, X.; Malacea, R.; Fischmeister, C.; Bruneau, C.; Dixneuf, P. H. Ruthenium-alkylidene catalysed cross-metathesis of fatty acid derivatives with acrylonitrile and methyl acrylate: a key step toward long-chain bifunctional and amino acid compounds. *Green Chem.* **2011**, *13*, 2911–2919.
- (11) Jacobs, T.; Rybak, A.; Meier, M. A. R. Cross-metathesis reactions of allyl chloride with fatty acid methyl esters: Efficient synthesis of α,ω -difunctional chemical intermediates from renewable raw materials. *Appl. Catal., A* **2009**, *353*, 32–35.
- (12) Abel, G. A.; Oliver Nguyen, K.; Viamajala, S.; Varanasi, S.; Yamamoto, K. Cross-metathesis approach to produce precursors of nylon 12 and nylon 13 from microalgae. *RSC Adv.* **2014**, *4*, 55622–55628.
- (13) Yapa Mudiyansele, A.; Viamajala, S.; Varanasi, S.; Yamamoto, K. Simple Ring-Closing Metathesis Approach for Synthesis of PA11, 12, and 13 Precursors from Oleic Acid. *ACS Sustainable Chem. Eng.* **2014**, *2*, 2831–2836.
- (14) Abel, G. A.; Viamajala, S.; Varanasi, S.; Yamamoto, K. Toward Sustainable Synthesis of PA12 (Nylon-12) Precursor from Oleic Acid Using Ring-Closing Metathesis. *ACS Sustainable Chem. Eng.* **2016**, *4*, 5703–5710.
- (15) Rybak, A.; Meier, M. A. R. Cross-metathesis of fatty acid derivatives with methyl acrylate: renewable raw materials for the chemical industry. *Green Chem.* **2007**, *9*, 1356–1361.
- (16) Forman, G. S.; Toozé, R. P. Improved cross-metathesis of acrylate esters catalyzed by 2nd generation ruthenium carbene complexes. *J. Organomet. Chem.* **2005**, *690*, 5863–5866.
- (17) Vignon, P.; Vancompernelle, T.; Couturier, J.-L.; Dubois, J.-L.; Mortreux, A.; Gauvin, R. M. Cross-metathesis of biosourced fatty acid derivatives: a step further toward improved reactivity. *ChemSusChem* **2015**, *8*, 1143–1146.
- (18) Warwel, S.; Brüse, F.; Demes, C.; Kunz, M.; Klaas, M. Polymers and surfactants on the basis of renewable resources. *Chemosphere* **2001**, *43*, 39–48.
- (19) Warwel, S.; Tillack, J.; Demes, C.; Kunz, M. Polyesters of ω -Unsaturated Fatty Acid Derivatives. *Macromol. Chem. Phys.* **2001**, *202*, 1114–1121.
- (20) Ngo, H. L.; Jones, K.; Foglia, T. A. Metathesis of unsaturated fatty acids: Synthesis of long-chain unsaturated- α,ω -dicarboxylic acids. *J. Am. Oil Chem. Soc.* **2006**, *83*, 629–634.
- (21) Ngo, H. L.; Foglia, T. A. Synthesis of Long Chain Unsaturated- α,ω -Dicarboxylic Acids from Renewable Materials via Olefin Metathesis. *J. Am. Oil Chem. Soc.* **2007**, *84*, 777–784.
- (22) Mutlu, H.; Hofsaß, R.; Montenegro, R. E.; Meier, M. A. R. Self-metathesis of fatty acid methyl esters: full conversion by choosing the appropriate plant oil. *RSC Adv.* **2013**, *3*, 4927–4934.
- (23) Ullah, A.; Arshad, M. Remarkably Efficient Microwave-Assisted Cross-Metathesis of Lipids under Solvent-Free Conditions. *ChemSusChem* **2017**, *10*, 2167–2174.
- (24) Aguilar-Castro, C.; Gomez, M. D.; Nava, M. G.; García, J. M. R.; Uribe, L. E. L. Biobased polyester obtained from bifunctional monomers through metathesis of fatty acids as precursor to synthesis of polyurethanes. *J. Appl. Polym. Sci.* **2019**, *136*, 47095–47106.
- (25) Häußler, M.; Eck, M.; Rothauer, D.; Mecking, S. Closed-loop recycling of polyethylene-like materials. *Nature* **2021**, *590*, 423–427.
- (26) Bennett, C.; Mathias, L. J. Linear Unsaturated Polyamides: Nylons 6 u18 and 18 u18. *Macromol. Chem. Phys.* **2004**, *205*, 2438–2442.
- (27) Bennett, C.; Mathias, L. J. Synthesis and characterization of polyamides containing octadecanedioic acid: Nylon-2,18, nylon-3,18, nylon-4,18, nylon-6,18, nylon-8,18, nylon-9,18, and nylon-12,18. *J. Polym. Sci., Part A: Polym. Chem.* **2005**, *43*, 936–945.
- (28) Bennett, C.; Kaya, E.; Sikes, A. M.; Jarrett, W. L.; Mathias, L. J. Synthesis and characterization of nylon 18 18 and nylon 18 adamantane. *J. Polym. Sci., Part A: Polym. Chem.* **2009**, *47*, 4409–4419.

- (29) Kaya, E.; Mathias, L. J. Investigation of melting behaviors and crystallinity of linear polyamide with high-aliphatic content. *J. Appl. Polym. Sci.* **2012**, *123*, 92–98.
- (30) Cui, X.; Li, W.; Yan, D.; Yuan, C.; Di Silvestro, G. Synthesis and characterization of polyamides X 18. *J. Appl. Polym. Sci.* **2005**, *98*, 1565–1571.
- (31) Atapalkar, R. S.; Athawale, P. R.; Srinivasa Reddy, D.; Kulkarni, A. A. Scalable, sustainable and catalyst-free continuous flow ozonolysis of fatty acids. *Green Chem.* **2021**, *23*, 2391–2396.
- (32) Behr, A.; Tenhumberg, N.; Wintzer, A. An efficient reaction protocol for the ruthenium-catalysed epoxidation of methyl oleate. *Eur. J. Lipid Sci. Technol.* **2012**, *114*, 905–910.
- (33) Goebel, G. C.; Brown, A. C.; Oehlschlaeger, H. F.; Rolfes, R. P. Method of Making Azelaic Acid. US 2,813,113 A, 1957.
- (34) Bieser, A.; Borsotti, G.; Digioia, F.; Ferrari, A.; Pirocco, A. Continuous Process for the Production of Derivatives of Saturated Carboxylic Acids. WO 2011,080,297 A1, 2011.
- (35) Bieser, A.; Borsotti, G.; Digioia, F.; Ferrari, A.; Pirocco, A. Continuous Process for the Production of Derivatives of Saturated Carboxylic Acids. US 8,846,962 B2, 2014.
- (36) Bastioli, C.; Borsotti, G.; Merlin, G.; Milizia, T. Triglycerides containing certain saturated carboxylic acids. US 8,629,290 B2, 2014.
- (37) Bastioli, C.; Borsotti, G.; Merlin, A.; Milizia, T. Catalytic Cleavage Process of Vegetable Oils. ES 2,534,399 T3, 2015.
- (38) Cavani, F.; Vassoio, A. Production of Carboxylic Acids from vicinal Diols. U.S. Patent US 20200,325,095 A1, 2020.
- (39) Behr, A.; Vorholt, A. J.; Rentmeister, N. Recyclable homogeneous catalyst for the hydroesterification of methyl oleate in thermomorphic solvent systems. *Chem. Eng. Sci.* **2013**, *99*, 38–43.
- (40) Melchiorre, M.; Benessere, V.; Cucciolo, M. E.; Melchiorre, C.; Ruffo, F.; Esposito, R. Direct and Solvent-Free Oxidative Cleavage of Double Bonds in High-Oleic Vegetable Oils. *ChemistrySelect* **2020**, *5*, 1396–1400.
- (41) Upadhyay, R.; Rana, R.; Sood, A.; Singh, V.; Kumar, R.; Srivastava, V. C.; Maurya, S. K. Heterogeneous vanadium-catalyzed oxidative cleavage of olefins for sustainable synthesis of carboxylic acids. *Chem. Commun.* **2021**, *57*, 5430–5433.
- (42) Tao, L.; Liu, K.; Li, T.; Xiao, R. Preparation and properties of biobased polyamides based on 1,9-azelaic acid and different chain length diamines. *Polym. Bull.* **2020**, *77*, 1135–1156.
- (43) Hajra, B.; Sultana, N.; Guria, C.; Pathak, A. K.; Saxena, V. K. Liquid Phase Selective Catalytic Oxidation of Oleic Acid to Azelaic Acid Using Air and Transition Metal Acetate Bromide Complex. *J. Am. Oil Chem. Soc.* **2017**, *94*, 1463–1480.
- (44) Sultana, N.; Guria, C.; Saxena, V. K. Selective conversion of stearic acid into high-added value octadecanedioic acid using air and transition metal acetate bromide catalyst: Kinetics, pathway and process optimization. *Arab. J. Chem.* **2020**, *13*, 2368–2383.
- (45) Jiménez-Rodríguez, C.; Eastham, G. R.; Cole-Hamilton, D. J. Dicarboxylic acid esters from the carbonylation of unsaturated esters under mild conditions. *Inorg. Chem. Commun.* **2005**, *8*, 878–881.
- (46) Quinzler, D.; Mecking, S. Linear semicrystalline polyesters from fatty acids by complete feedstock molecule utilization. *Angew. Chem., Int. Ed.* **2010**, *49*, 4306–4308.
- (47) Stempfle, F.; Quinzler, D.; Heckler, I.; Mecking, S. Long-Chain Linear C19 and C23 Monomers and Polycondensates from Unsaturated Fatty Acid Esters. *Macromolecules* **2011**, *44*, 4159–4166.
- (48) Gunanathan, C.; Milstein, D. Selective Synthesis of Primary Amines Directly from Alcohols and Ammonia. *Angew. Chem.* **2008**, *120*, 8789–8792.
- (49) Imm, S.; Bähn, S.; Neubert, L.; Neumann, H.; Beller, M. Eine effiziente und allgemeine Synthese primärer Amine durch Ruthenium-katalysierte Aminierung sekundärer Alkohole mit Ammoniak. *Angew. Chem.* **2010**, *122*, 8303–8306.
- (50) Pinggen, D.; Müller, C.; Vogt, D. Direkte Aminierung von sekundären Alkoholen mit Ammoniak. *Angew. Chem.* **2010**, *122*, 8307–8310.
- (51) Pinggen, D.; Schwaderer, J. B.; Walter, J.; Wen, J.; Murray, G.; Vogt, D.; Mecking, S. Diamines for Polymer Materials via Direct Amination of Lipid- and Lignocellulose-based Alcohols with NH₃. *ChemCatChem* **2018**, *10*, 3027–3033.
- (52) Vondran, J.; Furst, M. R. L.; Eastham, G. R.; Seidensticker, T.; Cole-Hamilton, D. J. Magic of Alpha: The Chemistry of a Remarkable Bidentate Phosphine, 1,2-Bis(di-tert-butylphosphinomethyl)benzene. *Chem. Rev.* **2021**, *121*, 6610–6653.
- (53) Stempfle, F.; Ortmann, P.; Mecking, S. Long-Chain Aliphatic Polymers To Bridge the Gap between Semicrystalline Polyolefins and Traditional Polycondensates. *Chem. Rev.* **2016**, *116*, 4597–4641.
- (54) Elzein, T.; Brogly, M.; Schultz, J. Crystallinity measurements of polyamides adsorbed as thin films. *Polymer* **2002**, *43*, 4811–4822.
- (55) Meng, C.; Liu, X. Study on rheological properties of bio-based semi-aromatic high temperature polyamide PA6T/56 and the effect of PA6T content. *J. Polym. Res.* **2021**, *28*, 466–473.
- (56) Dealy, J. M.; Read, D. J.; Larson, R. G. *Structure and Rheology of Molten polymers: From Structure to Flow Behavior and Back Again*, 2nd ed; Hanser Publishers, 2018.
- (57) Bonten, C. *Kunststofftechnik: Einführung und Grundlagen*; 3 aktualisierte Auflage; Hanser, 2020.
- (58) Dou, Y.; Mu, X.; Chen, Y.; Ning, Z.; Gan, Z.; Jiang, N. Effect of Composition on the Crystallization, Water Absorption, and Biodegradation of Poly(*ε*-caprolactam-co-*ε*-caprolactone) Copolymers. *Polymers* **2020**, *12*, 2488.
- (59) Cui, X.; Li, W.; Yan, D. Investigation on odd-odd nylons based on undecanedioic acid: 1. Synthesis and characterization. *Polym. Int.* **2004**, *53*, 1729–1734.
- (60) Olmo, C.; Rota, R.; Carlos Martínez, J.; Puiggali, J.; Franco, L. Temperature-induced structural changes in even-odd nylons with long polymethylene segments. *J. Polym. Sci., Part B: Polym. Phys.* **2016**, *54*, 2494–2506.
- (61) Olmo, C.; Casas, M. T.; Martínez, J. C.; Franco, L.; Puiggali, J. Thermally Induced Structural Transitions of Nylon 4 9 as a New Example of Even-Odd Polyamides. *Polymers* **2018**, *10*, 198.
- (62) Murase, S. K.; Casas, M. T.; Martínez, J. C.; Estrany, F.; Franco, L.; Puiggali, J. Reversible changes induced by temperature in the spherulitic birefringence of nylon 6 9. *Polymer* **2015**, *76*, 34–45.
- (63) Franco, L.; Cooper, S. J.; Atkins, E. D. T.; Hill, M. J.; Jones, N. A. Nylon 6 9 can crystallize with hydrogen bonding in two and in three interchain directions. *J. Polym. Sci., Part B: Polym. Phys.* **1998**, *36*, 1153–1165.
- (64) Rubio Arias, J. J.; Thielemans, W. Instantaneous hydrolysis of PET bottles: an efficient pathway for the chemical recycling of condensation polymers. *Green Chem.* **2021**, *23*, 9945–9956.
- (65) Booi, M.; Frentzen, Y. H.; Hommez, B. K. S.; Goethals, E. J. Depolymerization of Polyamides. U.S. Patent 5,668,277A, 2000.
- (66) Meng, L.; Zhang, Y.; Huang, Y.; Shibata, M.; Yosomiya, R. Studies on the decomposition behavior of nylon-66 in supercritical water. *Polym. Degrad. Stab.* **2004**, *83*, 389–393.
- (67) Češarek, U.; Pahovnik, D.; Žagar, E. Chemical Recycling of Aliphatic Polyamides by Microwave-Assisted Hydrolysis for Efficient Monomer Recovery. *ACS Sustainable Chem. Eng.* **2020**, *8*, 16274–16282.
- (68) Žagar, E.; Češarek, U.; Drinčić, A.; Sitar, S.; Shlyapnikov, I. M.; Pahovnik, D. Quantitative Determination of PA6 and/or PA66 Content in Polyamide-Containing Wastes. *ACS Sustainable Chem. Eng.* **2020**, *8*, 11818–11826.
- (69) Bäckström, E.; Odelius, K.; Hakkarainen, M. Microwave Assisted Selective Hydrolysis of Polyamides from Multicomponent Carpet Waste. *Global Challenges* **2021**, *5*, 2000119.
- (70) Liao, G.; Li, Z.; Luan, C.; Wang, Z.; Yao, X.; Fu, J. Additive Manufacturing of Polyamide 66: Effect of Process Parameters on Crystallinity and Mechanical Properties. *J. Mater. Eng. Perform.* **2022**, *31*, 191–200.
- (71) Pinggen, D.; Klinkenberg, N.; Mecking, S. Single-Step Catalytic Upgrading of Microalgae Biomass. *ACS Sustainable Chem. Eng.* **2018**, *6*, 11219–11221.

Supporting Information

Synthesis, characterization and the potential for closed loop recycling of plant oil-based PA X.19 polyamides

Maximilian Rist, Andreas Greiner*

E-Mail: greiner@uni-bayreuth.de

University of Bayreuth, Macromolecular Chemistry and Bavarian Polymer Institute,
Universitätsstraße 30, 95440 Bayreuth, Germany

Total pages: 6

Total number of Figures: 9

Table of Contents

Figure S1. ¹H-NMR spectrum of dimethyl-1.19-nonadecanedioate **2** measured in CDCl₃.

Figure S2. Gas chromatogram of dimethyl-1.19-nonadecanedioate **2**.

S1

Figure S3. ¹H-NMR spectrum of 1.19-nonadecanedioic acid **3** measured in DMSO-*d*₆.

Figure S4. ¹H-NMR spectrum of recycled 1.19-nonadecanedioic acid **3** measured in DMSO-*d*₆.

Figure S5. a) Dynamic TGA curves of the PA X.19 under air atmosphere and b) under nitrogen atmosphere.

Figure S6. a) Isothermal TGA curves of the PA X.19 under synthetic air atmosphere and b) under nitrogen atmosphere. Recorded at 280 °C for **PA 4.19**, 210 °C for **PA 6.19**, 220 °C for **PA 8.19** and at 240 °C for **PA 12.19**.

Figure S7. Normalized molecular weight distribution of the PA X.19 measured by SEC.

Figure S8. ¹H-NMR spectra of PA X.19 measured in HFIP+CDCl₃.

Figure S9. a) Loss factor (tan δ) and b) storage modulus (E') of the PA X.19 over the temperature, measured by DMA.

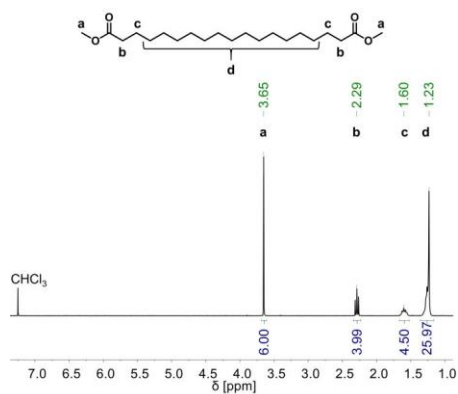


Figure S1. ¹H-NMR spectrum of dimethyl-1,19-nonadecanedioate **2** measured in CDCl₃.

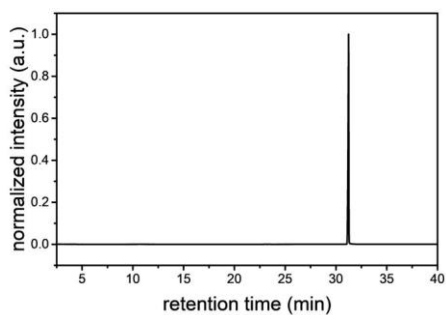
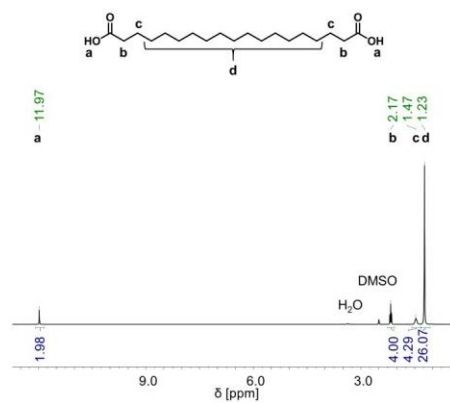


Figure S2. Gas chromatogram of dimethyl-1,19-nonadecanedioate **2**.



S3

Figure S3. ¹H-NMR spectrum of 1.19-nonadecanedioic acid **3** measured in DMSO-*d*₆.

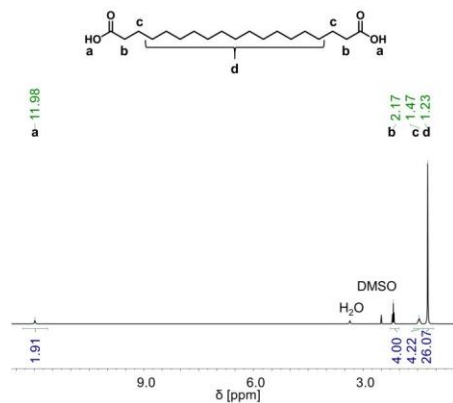


Figure S4. ¹H-NMR spectrum of recycled 1.19-nonadecanedioic acid **3** measured in DMSO-*d*₆.

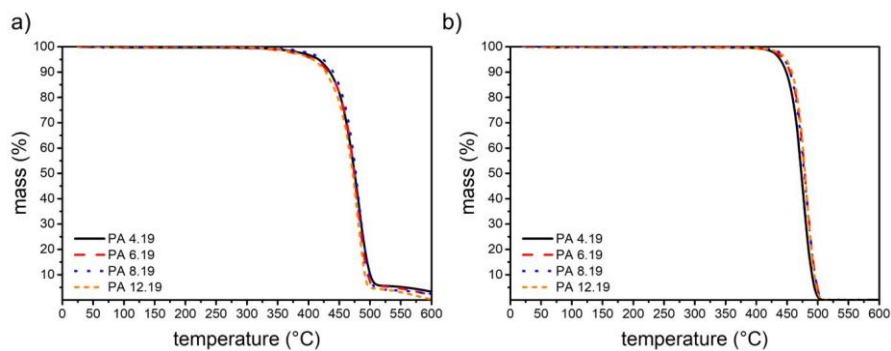


Figure S5. a) Dynamic TGA curves of the PA X.19 under air atmosphere and b) under nitrogen atmosphere.

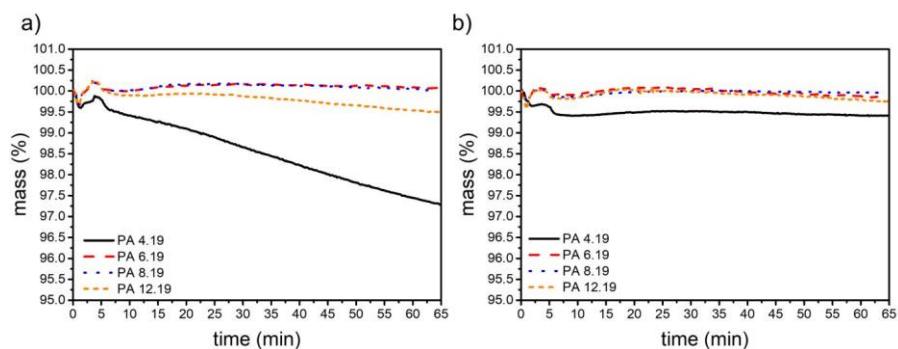


Figure S6. a) Isothermal TGA curves of the PA X.19 under synthetic air atmosphere and b) under nitrogen atmosphere. Recorded at 280 °C for **PA 4.19**, 210 °C for **PA 6.19**, 220 °C for **PA 8.19** and at 240 °C for **PA 12.19**.

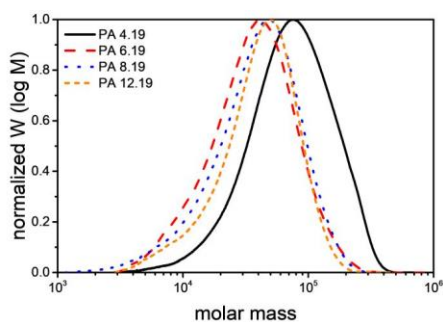


Figure S7. Normalized molecular weight distribution of the PA X.19 measured by SEC.

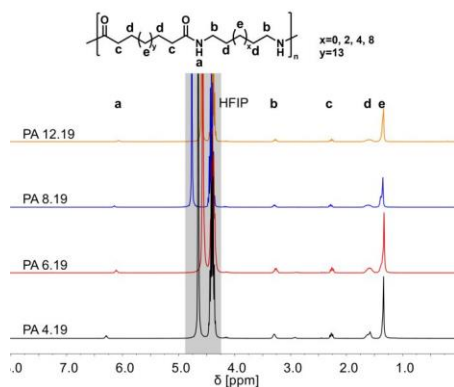


Figure S8. ^1H -NMR spectra of PA X.19 measured in HFIP+ CDCl_3 .

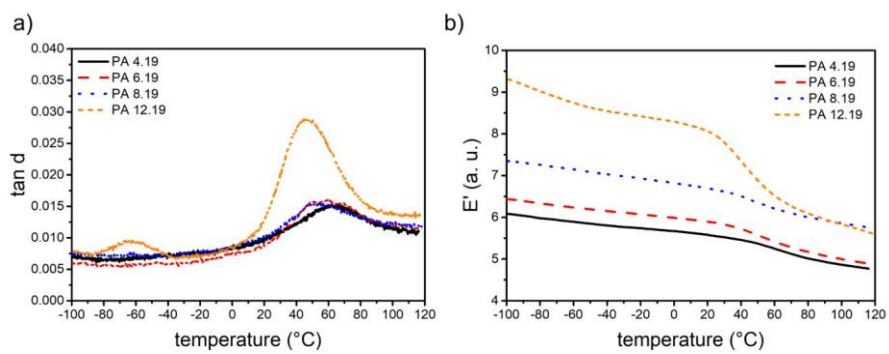


Figure S9. a) Loss factor ($\tan \delta$) and b) storage modulus (E') of the PA X.19 over the temperature, measured by DMA.

Toughening of Bio-Based PA 6.19 by Copolymerization with PA 6.6 – Synthesis and Production of Melt-Spun Monofilaments and Knitted Fabrics

Maximilian Rist, Henning Löcken, Mathias Ortega, and Andreas Greiner*

This work reports on the synthesis of statistical copolymers of bio-based PA 6.19 and PA 6.6 together with the production of melt-spun monofilaments for the production of sustainable textile fibers. The plant oil-based 1.19-nonadecanedioic acid is synthesized from bio-derived oleic acid via isomerizing methoxycarbonylation. The homopolymer PA 6.19 with a carbon-based bio-content of 72% shows a good elongation at break of 166%, but lower tensile strength than commercial PA 6 (43 MPa versus 82 MPa). Addition of adipic acid to form statistical PA 6.6/6.19 copolymers improves toughness while maintaining the high elongation at break. Two PA 6.6/6.19 copolymers with a carbon-based bio-content of 26% and 33% are successfully synthesized and exhibited comparable toughness (94 ± 6 MPa and 92 ± 2 MPa) to the commercial PA 6 (92 ± 15 MPa). The bio-based copolymers also exhibit a much lower water uptake than PA 6 and PA 6.6, resulting in a higher dimensional stability. Melt spinning of the oleic acid-based polyamides is successfully carried out to produce monofilaments with sufficient properties for further processing in a knitting process, demonstrating the capabilities of the bio-based PA 6.6/6.19 copolymers for use in the textile industry.

70 million tons of synthetic fibers in 2020, of which less than 0.5% came from renewable sources.^[2] This is mainly due to the high prices and low availability of bio-based materials. A particularly important material for the production of synthetic fibers is polyamide (PA), with an annual production volume of over 5 million tons.^[2] Only about 0.4% of these polyamides are produced from bio-based raw materials, which are mostly ricinoleic acid. Since castor beans are the only economically viable feedstock for ricinoleic acid, the production of bio-based polyamides depends heavily on this one feedstock.^[3] Expanding the available feedstocks would increase the availability of bio-based raw materials for polyamides and consequently lower prices, making the production of bio-based polyamides more economically viable. Oleic acid, for example, can be found in almost all natural fats and oils, and is thus readily available. Despite the structural similarity to ricinoleic acid,

new synthesis methods need to be developed for the valorization of oleic acid for the synthesis of polymers for synthetic fibers.


Polyamide-based textile fibers are usually produced by melt spinning, where high crystallinity of the polymers is advantageous.^[4] Linear polyamides without side chains are therefore the preferred choice. Numerous synthesis strategies for oleic acid-based monomers such as linear diacids,^[5–7] amino acids,^[6,8] and lactams^[9] have been developed in recent years. However, the actual synthesis of the oleic acid-based polyamides via these linear amino acids and lactams^[10] has often not been described so far. In contrast, the synthesis of linear polyamides from oleic acid-based diacids was described for PA X.9,^[11] PA X.11,^[12] PA X.18,^[13] and PA X.19.^[5,14]

The processing of oleic acid-based polyamides has been described mainly for extruded films for food packaging.^[15] Melt-spun textile fibers from oleic acid-based polyamides have not been described yet. Recently we investigated the mechanical properties of PA X.19 and they showed good melt processability.^[16] However, they exhibited significantly lower tensile strength compared to commercial polyamides such as PA 6. Copolymerization with a tougher material like PA 6.6 could potentially increase the tensile strength and ultimately create a partially bio-based material with comparable or better properties than commercial PA 6. Similar approaches have been

1. Introduction

The need for sustainable materials is greater than ever. With the European Union's goal of being carbon neutral by 2050, extensive research needs to be done in various areas to achieve this goal.^[1] The global fiber industry, for example, produced about

M. Rist, A. Greiner
 University of Bayreuth
 Macromolecular Chemistry and Bavarian Polymer Institute
 Universitätsstrasse 30, 95440 Bayreuth, Germany
 E-mail: greiner@uni-bayreuth.de
 H. Löcken, M. Ortega
 RWTH Aachen University
 Institut fuer Textiltechnik
 Otto-Blumenthal-Strasse 1, 52074 Aachen, Germany

 The ORCID identification number(s) for the author(s) of this article can be found under <https://doi.org/10.1002/marc.202300256>

© 2023 Helmholtz-Zentrum Hereon. Macromolecular Rapid Communications published by Wiley-VCH GmbH. This is an open access article under the terms of the Creative Commons Attribution License, which permits use, distribution and reproduction in any medium, provided the original work is properly cited.

DOI: 10.1002/marc.202300256

Table 1. Feed ratio, yields and molecular weight of the copolymers PA 6.6/6.19, their homopolymers PA 6.6 and PA 6.19 and the benchmark PA 6.

Polyamide	Feed PA 6.6/PA 6.19 [mol%]	Experimental ^{a)} [mol%]	Yield [%]	M_n ^{b)}	M_w ^{b)}	$D^b)$	Bio-content ^{c)} [%]
PA 6 (benchmark)				34 900	58 500	1.7	0
PA 6.19	0/100	0/100	92	28 600	57 100	2.0	72
PA 6.6/6.19 17:83	17/83	17/83	93	30 200	52 400	1.7	60
PA 6.6/6.19 31:69	31/69	31/69	90	29 500	56 600	1.9	50
PA 6.6/6.19 44:56	44/56	44/56	91	44 100	82 400	1.9	41
PA 6.6/6.19 55:45	55/45	54/46	77	30 600	62 000	2.0	33
PA 6.6/6.19 64:36	64/36	64/36	79	48 700	93 200	1.9	26
PA 6.6/6.19 88:12	88/12	87/13	80	49 200	110 100	2.2	9
PA 6.6	100/0	100/0	92	59 500	118 600	2.0	0

^{a)} Calculated by ¹H-NMR spectroscopy, ^{b)} SEC (HFIP + 0.1% KTFA, room temperature, PMMA-standard), ^{c)} The percentage of bio-based carbon content of the total carbon content in accordance with DIN EN 16 640.

described for the toughening of PA 11 by in situ polymerization with PA 6.6,^[17] as well as copolymerization of dimer oleic acid-based PA 6.36 with PA 6.6^[18,19] or PA 11 with PA 6.^[20] An increasing tensile strength was observed with increasing PA 6.6 or PA 6 content in the copolymer.

Herein, we report on the synthesis of bio-based copolymers of oleic acid-based PA 6.19 and PA 6.6. The copolymers were synthesized via melt polycondensation from mixtures of the respective PA-salts to obtain statistical copolymers with molecular weights in the range of common engineering polyamides ($\approx 30\ 000$). Full characterization of the thermal, viscoelastic and mechanical properties of the resulting copolymers was performed by differential scanning calorimetry (DSC), thermogravimetric analysis (TGA), dynamic mechanical analysis (DMA), plate-plate rheology and uniaxial tensile testing. The best performing copolymer formulation was synthesized in a larger scale and melt-spun into monofilaments. In addition, the fineness and the mechanical properties of the monofilaments were characterized. Finally, a knitted fabric was produced from the monofilaments supporting their suitability for the production of oleic acid-based textiles.

2. Results and Discussion

2.1. Synthesis of PA 6.6/6.19 Copolymers

The PA 6.6/6.19 copolymers were synthesized by mixing PA-salts of PA 6.19 and PA 6.6 in the desired ratio. The polymerization was then carried out via melt polycondensation in two steps. At the beginning oligomers were formed in a precondensation step by gradually increasing the temperature from 160 to 260 °C. Then the main polycondensation was performed at 260–280 °C with later application of vacuum. After 8–9 h of reaction time the synthesis was aborted and the polymers were received as white and off-white solids via precipitation in good yields of up to 93% (Table 1).

The number average molecular weight (M_n) of the final polymers ranged from 28 600–59 500, meeting the range of the PA 6 benchmark (34 900) and that of common technical grade polyamides (Table 1). Surprisingly, an increasing molecular weight with increasing PA 6.6 content was observed. A similar observation was made during the copolymerization of PA 11

and PA 6.^[20] It was assumed that the higher hydrophilicity of ϵ -caprolactam inhibits the removal of water during the polycondensation resulting in lower molecular weights for copolymers with high PA 6-content. However, we observed an increasing molecular weight with increasing hydrophilicity of the copolymers, indicating a different cause.

2.2. Thermal Properties

Analysis of the thermal properties of the polyamides was performed via TGA and DSC. The corresponding data are given in Table 2. The thermal stability of the polyamides was observed by TGA under synthetic air and nitrogen atmosphere. All synthesized polyamides showed high thermal stability with a 5% degradation temperature ($T_{5\%}$) of >395 °C under nitrogen and air atmosphere, showing single-stage degradation. Additionally, the thermal stability of the synthesized copolymers at their respective processing temperature was investigated using isothermal TGA analysis. Here, all polyamides showed high stability with a mass loss of less than 1.4% under nitrogen atmosphere. Under air atmosphere the polyamides processable below 270 °C (PA 6.19, PA 6.6/6.19 17:83, 31:69, 55:45) showed again a high thermal stability with a maximum mass loss of 0.5% under air. Processing at higher temperatures led to a mass loss of 1.4% to 4.3% under air atmosphere. The exclusion of oxygen is therefore crucial during processing in order to minimize thermal decomposition of the material.

The melting and crystallization behavior of the polyamides were studied by DSC. Both the melting temperature (T_m) and the crystallization temperature (T_c) of the copolymers showed a strong dependence on the PA 6.6 content (Figure 1). Initially, the melting temperature decreased with increasing PA 6.6 content from 190 °C for the PA 6.19 homopolymer to 177 °C for the copolymer with 31 mol% PA 6.6. From then on, the melting temperature increased in an almost linear trend with the PA 6.6 content to 259 °C for the PA 6.6 homopolymer. A similar trend was observed for the crystallization temperature, with 174 °C for PA 6.19 to 142 °C for the 31:69 copolymer and from there to 216 °C for PA 6.6. This is typical for statistical copolymers and is due to the disruption of the crystal structure by the

Table 2. Thermal Properties of the Polyamides.

Polyamide	TGA				DSC				DMA
	Nitrogen		Air		Second heating		Cooling	X_c^d [%]	Second heating
	$T_{5\%}^a$ [°C]	Mass loss at $T_{process}^b$ [%]	$T_{5\%}^a$ [°C]	Mass loss at $T_{process}^b$ [%]	T_m^c [°C]	ΔH_m^c [J g ⁻¹]	T_c^b [°C]		T_g^e [°C]
PA 6 (benchmark)	406	0.9	404	0.5	219	64	153	34	
PA 6.19	444	0.1	414	0.0	190	86	174	44	59
PA 6.6/6.19 17:83	445	0.0	435	0.1	186	82	161	42	53
PA 6.6/6.19 31:69	415	0.3	397	0.4	177	70	142	35	52
PA 6.6/6.19 44:56	433	0.4	423	1.4	196	63	155	32	52
PA 6.6/6.19 55:45	433	0.3	409	0.5	209	42	161	21	49
PA 6.6/6.19 64:36	428	1.2	413	3.3	213	51	183	26	48
PA 6.6/6.19 88:12	422	1.0	411	2.6	248	56	202	28	63
PA 6.6	416	1.4	398	4.3	259	84	216	43	77

^{a)} $T_{5\%}$ is the temperature at 5% mass loss, measured at 20 K min⁻¹. ^{b)} Mass loss after 1 h isothermal heating at their respective processing temperature ($T_{process}$), 210 °C for PA 6.19; 220 °C for PA 6.6/6.19 17:83 and 31:69; 270 °C for 44:56; 230 °C for 55:45; 280 °C for 64:36; 300 °C for 88:12 and PA 6.6. ^{c)} Melting temperature (T_m), melting enthalpy (ΔH_m) and crystallization temperature (T_c) measured at a rate of ± 20 K min⁻¹. ^{d)} Crystallinity (X_c) is calculated from $\Delta H_m/\Delta H_m^0$, with ΔH_m^0 being the enthalpy of fusion of 100% crystalline PA 6.6, 197 J g⁻¹. ^{e)} Glass transition temperature (T_g) determined from the peak of the tan δ measured at 2 K min⁻¹.

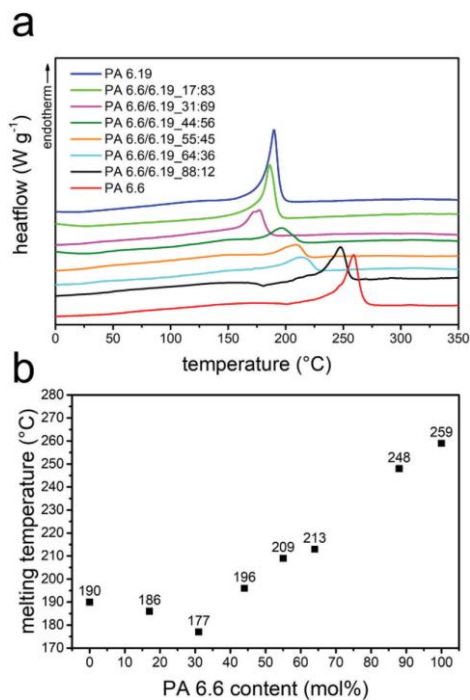


Figure 1. a) DSC thermographs of the synthesized polyamides. b) Determined melting temperatures of the polyamides as a function of the PA 6.6 content.

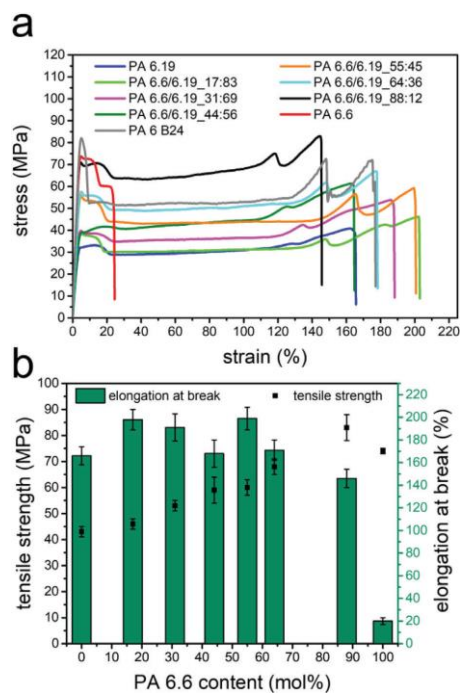


Figure 2. a) Stress-strain curves of synthesized polyamides and benchmark PA 6.6. b) Visualization of the tensile strength and the elongation at break in dependence of the PA 6.6 content. The error bar for the PA 6.6 homopolymer is too small to visualize.

Table 3. Summarized mechanical properties of synthesized polyamides and benchmark PA 6.

Polyamide	Young's modulus ^{a)} [MPa]	Tensile strength ^{a)} [MPa]	Elongation at break ^{a)} [%]	Toughness ^{a)} [MPa]	Water uptake ^{b)} [%]
PA 6 (benchmark)	2200 ± 62	83 ± 3	170 ± 22	92 ± 15	11.33 ± 0.25
PA 6.19	1140 ± 16	43 ± 2	166 ± 8	56 ± 5	1.25 ± 0.03
PA 6.6/6.19 17:83	1220 ± 30	46 ± 2	198 ± 9	68 ± 4	1.86 ± 0.01
PA 6.6/6.19 31:69	1200 ± 25	53 ± 2	191 ± 12	75 ± 6	2.00 ± 0.02
PA 6.6/6.19 44:56	980 ± 60	59 ± 5	168 ± 12	74 ± 9	2.25 ± 0.00
PA 6.6/6.19 55:45	1460 ± 24	60 ± 3	199 ± 10	94 ± 6	2.38 ± 0.04
PA 6.6/6.19 64:36	1460 ± 34	68 ± 3	171 ± 9	92 ± 2	2.69 ± 0.03
PA 6.6/6.19 88:12	2160 ± 35	83 ± 5	146 ± 8	99 ± 7	4.91 ± 0.14
PA 6.6	2080 ± 61	74 ± 1	20 ± 3	12 ± 2	7.90 ± 0.05

^{a)} Measured in accordance with DIN EN ISO 527-2, at 50 mm min⁻¹ test speed ^{b)} The water uptake is measured in deionized water at 25 °C for 7 d in accordance with DIN EN ISO 62.

addition of PA 6.6 units.^[22] Consequently, a decrease in crystallinity was also observed with increasing PA 6.6 content. Starting from the homopolymer PA 6.19, the crystallinity decreased from 44% to 21% for the PA 6.6/6.19 55:45. Further increasing the PA 6.6 content resulted in an increase in crystallinity to 43% for the homopolymer PA 6.6. The local minimal crystallinity was therefore found with 55% PA 6.6, which is significantly higher than the local minimum found for the crystallization and melting temperature. Therefore, the effect of the increased frequency of amide-bonds already outweighs the disruption of the crystallinity. Similar behavior was also observed for the copolymers of polyamide 6 and 11.^[20] In summary, the melting temperature of the PA 6.6/6.19 copolymers can be controlled by the PA 6.6 content. Up to 64 mol% PA 6.6, they also exhibit a lower melting temperature of 177–213 °C compared to the benchmark PA 6 (219 °C). The copolymers may therefore be processable at lower temperatures, which is beneficial in terms of energy consumption.

2.3. Mechanical Properties and Water Uptake

Uniaxial tensile tests were performed on injection molded specimens of the synthesized polyamides. The processing temperatures were adjusted according to the viscosities of the respective polymer sample to ensure processability and were in the range of 210–300 °C. The stress–strain curves can be observed in Figure 2a and the resulting values for the elongation at break and tensile strength are depicted in Figure 2b. The benchmark PA 6 showed an elongation at break of 170 ± 22% with a tensile strength of 83 ± 3 MPa. On the other hand, the bio-based PA 6.19 homopolymer showed a comparable elongation of 166 ± 8% but a significantly lower tensile strength of 43 ± 2 MPa (Table 3). This is, however, comparable to results obtained for similar long-chain polyamides such as PA 6.24 (33 MPa) and PA 6.34 (21 MPa)^[23] and is likely due to the lower frequency of amide-bonds resulting in a lower amount of intermolecular hydrogen bonding.

Increasing the PA 6.6 content in the copolymers resulted in an increase in both tensile strength and Young's modulus. Surprisingly, increasing the PA 6.6 content to 64 mol% did not affect the elongation at break, and all copolymers showed an elongation be-

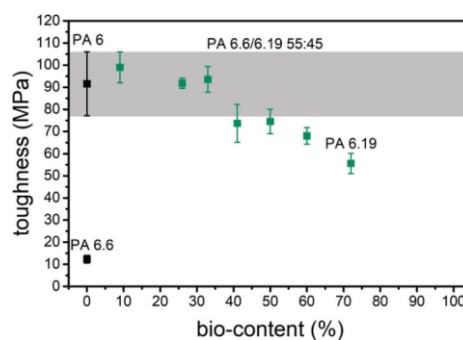


Figure 3. Toughness of the polyamides against the bio-based carbon content.

tween 170–200%. Ultimately, the tensile strength was improved to 68 ± 3 MPa and the Young's modulus to 1460 ± 34 MPa, corresponding to an increase of 58% and 28%, respectively. However, these results are in contrast to prior findings for alloys and blends of PA 11 and PA 6.6, where both elongation at break and tensile strength increased with increasing PA 6.6 content for the alloys.^[17] There was no effect on tensile strength in the blended samples, but the elongation at break decreased.^[17] Increasing the PA 6.6 content to 10% in molecular composites of PA 6 and PA 66 also showed no effect on the tensile strength, but the elongation at break was drastically increased to 502%.^[24] Copolymers of dimerized oleic acid-based PA 6.36 with PA 6.6, on the other hand, showed increasing tensile strength with PA 6.6 content, but a decrease in elongation at break.^[18,19]

In Figure 3, the toughness of the synthesized polyamides together with the benchmark PA 6 is plotted against the bio-content as the percentage of bio-based carbon content in accordance with DIN EN 16 640. As the PA 6.6 content increases, the bio-content decreases since the carbon from the PA 6.6 is not bio-based. The toughness of the copolymers with a PA 6.6 content of 55, 64 and 88 mol% were all within the range of the benchmark PA 6 (92 ± 15 MPa). PA 6.6/6.19 55:45 showed the highest toughness of

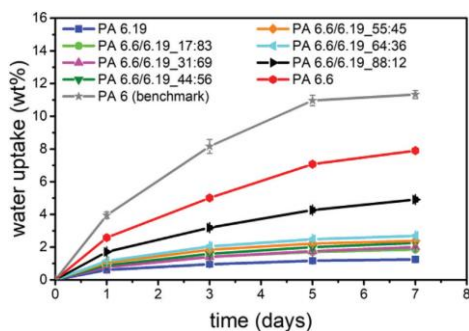


Figure 4. Water uptake of the polyamides over time.

all synthesized polyamides with a bio-content of at least 20% (94 ± 6 MPa). In summary, the copolymers with 55 and 64 mol% PA 6.6 were synthesized as two sustainable alternatives with a bio-content of 33% and 26%, respectively, exhibiting comparable mechanical properties to the benchmark PA 6.

The water uptake of the copolymers was investigated by immersion in water and compared to the PA 6 benchmark, the resulting data can be observed in Figure 4. As expected, the benchmark PA 6 showed a high water uptake of $11.33 \pm 0.25\%$ after 7 days in deionized water. The copolymers, on the other hand, showed a significantly lower water uptake, which can be attributed to the higher hydrophobicity resulting from the long methylene chain of the PA 6.19 moieties. Consequently, the PA 6.19 homopolymer showed the lowest water uptake of $1.25 \pm 0.03\%$, which is an order of magnitude lower than the benchmark PA 6. As the PA 6.6 content in the copolymers increased, the hydrophobicity decreased, which was evident in an increase of the water uptake to $7.90 \pm 0.05\%$ for the PA 6.6 homopolymer. Similar results were reported previously for branched oleic acid-based co-polyamides with PA 6.6.^[25] Polymers having low water absorption are known to have higher dimensional stability, which in turn is advantageous for the production of melt-spun fibers and injection molded parts.^[26] Owing to their low water uptake, the synthesized copolymers therefore offer significant advantages over PA 6 for melt processing applications.

2.4. Rheology

Important characteristics of a thermoplastic polymer suitable for melt spinning include sufficiently high molecular weight, thermal stability during processing, sufficient melt viscosity, high purity and high chain mobility.^[27] All synthesized polyamides show high thermal stability with degradation temperatures ($T_{5\%}$) well over 100 K above their melting temperatures (Table 2). Their molecular weights (28 600–59 500) are also in the range of technical grade polyamides suitable for melt spinning like the benchmark PA 6 (34 900). The synthesized polyamides are also linear, which is favored due to their high chain mobility. In order to investigate on the potential spinnability of the synthesized polyamides their rheological properties were studied in the molten state.

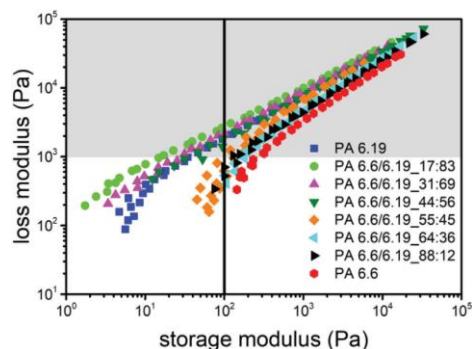


Figure 5. Temperature independent loss modulus versus storage modulus for the polyamides.

Frequency sweeps were recorded for all polyamides at three different temperatures between $T_m + 10$ K and $T_m + 50$ K at 2% deformation. The zero shear viscosity was then obtained by fitting the complex viscosity data from the rheology measurements. The Bird–Carreau–Yasuda model was chosen for fitting, as the model best described the measured data (Equation (2)).^[28] With η_0 as the zero shear viscosity, $\dot{\gamma}$ as the shear rate, n as the Power Law index, accounting for shear thinning, λ as a time constant and the parameter a controlling the curvature.

$$\eta(\dot{\gamma}) = \frac{\eta_0}{(1 + |\lambda\dot{\gamma}|^a)^{\frac{n-1}{a}}} \quad (1)$$

Construction of the temperature independent master curves could then be performed by calculation of the temperature shift factor $a_T(T)$. The master curves for all polymers can be found in Figures S8–S15, Supporting Information. Here, the Arrhenius shift was used, as this model is valid for semi-crystalline polymers such as the polyamides in this work (Equation (3)).^[29] With T_0 being a reference temperature, T being a specific temperature and η_0 as the zero shear viscosity at the respective temperature obtained from the Bird–Carreau–Yasuda model (Equation (2)).

$$a_T(T) = \frac{\eta_0(T)}{\eta_0(T_0)} \quad (2)$$

Using these master curves, the spinnability of the polyamides can be estimated by plotting the loss modulus (G'') against the storage modulus (G'), and the resulting plots can be observed in Figure 5.

Previous studies have shown a correlation between the spinnability of commercial polyamides (PA 6, PA 4.6 and PA 6.6) and their rheological properties.^[30] Polyamides with a G'' of at least 1000 Pa at a G' of 100 Pa showed good spinnability, which deteriorated for polyamides with a lower G'' . According to these results, the copolymers with a PA 6.19 content of at least 56 mol% should show good spinnability, as they all read a G'' of over 1000 Pa at the 100 Pa mark for G' (indicated by the black line). Increasing the PA 6.6 content further seemed to result in

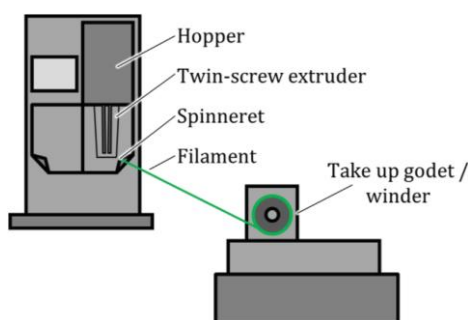


Figure 6. Schematic drawing of the melt spinning process on the micro compounder used for the production of monofilaments.

a more elastic behavior of the polymer melt, indicating poorer spinnability. It was also observed that the PA 6.19 and PA 6.6/6.19 55:45 ceased to be thermo-rheological simple at lower shear rates, which is evident from the deviation of the individual measurements in the master curves in Figures S8 and S12, Supporting Information.

2.5. Melt Spinning

The PA 6.6/6.19 55:45 copolymer (CoPA) was produced in a larger scale of 70 g for the production of monofilaments by melt spinning. Polymerization was performed similar to the small-scale trials from the respective polyamide salt, just in a bigger tube. The final copolymer used for melt spinning had a number average molecular weight of 69 500 with a dispersity of 1.8 (size exclusion chromatography (SEC)).

The most commonly used process for the production of man-made fibers is melt spinning. Here a polymer is either spun directly from the melt after polymer production (direct spinning) or polymer chips are produced first, and then melt-spun using an extruder (extruder spinning).^[31] For extrusion spinning dried polymer chips are melted in an extruder at a specific temperature and transported to the spin head. A constant volume flow is ensured using a spin pump and the polymer melt is filtered and pressed through a spinneret containing one (monofilament) or multiple holes (multifilament). The resulting filaments are cooled by a constant air flow in the quench or with a tempered water bath. The filaments are drawn down by a take-up godet with a constant velocity. If a higher orientation of the polymer chains in the filaments is required, further drafting or drawing can be applied using more (heated) godets with higher rotational velocities. Eventually, the filaments are wound on a winder to receive a spool.^[31] Melt spinning of CoPA and the commercial PA 6 was performed on a micro compounder and the resulting monofilament was taken up by a winder to receive spools (Figure 6).

Typical processing temperatures in melt spinning lie ≈ 40 K above the melting point of the polymer processed. Therefore, spinning trials of the commercial PA 6 and bio-based PA 6.6/6.19 55:45 were performed at 259 and 249 °C respectively. However,

the resulting viscosity of the polymer melt was too low, which resulted in an increased extrusion velocity to an extent that no winding was possible. Therefore, the extrusion temperature was adjusted to 240 °C for the commercial PA 6 and 225 °C for the bio-based copolymer. Monofilaments of both polymers were produced using different wind up speeds. The achieved draw-down ratios, as well as fineness, tenacity and elongation at maximum force can be observed in Table 4. The achieved draw-down ratios of up to 110 comply with industrial processing conditions for partially oriented yarns (POY) and thus prove the suitability of the material for industrial spinning tests.

Analysis of the produced monofilaments by scanning electron microscopy (SEM) revealed a smoother surface for the fibers spun from PA 6 (Figure 7). The surface of the filaments prepared from CoPA on the other hand showed grooves along the fiber. Increasing the wind up speed did not influence the formation of these grooves, the surface of the filament spun at 30 m min⁻¹ and the one spun at 5 m min⁻¹ look identical. For the commercial PA 6, however, a change in the surface morphology was observed for the monofilament spun at 30 m min⁻¹. Here, the surface is not as smooth as for the filaments spun at lower speeds. The filament developed so-called sharkskin, which is caused by a periodic adhesive failure of the polymer melt exiting the die at high velocities.^[4]

For the bio-based CoPA a broad range of wind up speeds could be applied for the production of monofilaments. For both polyamides a general trend of decreasing fineness with increasing wind up speed was observed (Table 4, Figure 8a). The relatively high standard deviations are the result of manual determination of fineness and manual polymer feeding during the spinning process. Increasing the wind up speed also resulted in an increased tenacity of the monofilaments for both materials. This increase was more pronounced for PA 6, where increasing the wind up speed from 20 to 30 m min⁻¹ resulted in a 40% increase in tenacity. The same increase in wind up speed did not result in a significant change in tenacity for the bio-based copolymer (Table 4, Figure 8b). On the other hand, the elongation at break at maximum force showed a decreasing trend with increasing wind up speed for the CoPA. No significant change in elongation was observed for the commercial PA 6 upon increasing the wind up speed from 20 m min⁻¹ (Table 4, Figure 8b). These findings are in contradiction to earlier expectations, since an increase in tenacity and a decrease in elongation are normally accompanied by an increase in wind up speed. However, the high standard deviations due to manual feeding and determination of the fineness must be considered. No standard deviation is available for the copolymer wound at 40 m min⁻¹ (CoPA_40), since not enough filament was produced during melt spinning and only the fineness of one piece could be determined.

2.6. Knitting Trials

In addition to melt spinning, the produced yarns are processed into textiles using the knitting process. Knitting is used for various applications such as t-shirts, socks, shoe-uppers or mattress covers. Since knitting can be generally performed with only one bobbin of material, the knitting process is often used to validate the further textile processing of the developed yarns. In the

Table 4. Characteristics of monofilament spun from PA 6 and PA 6.6/6.19 (CoPA).

Polyamide	Wind up speed [m min ⁻¹]	Draw-down ratio	Fineness [dtex]	Tenacity [cN tex ⁻¹]	Elongation at max. force [%]
PA 6_20	20	55.1	624 ± 69	10 ± 2	485 ± 23
PA 6_25	25	68.9	663 ± 89	10 ± 2	499 ± 23
PA 6_30	30	82.6	437 ± 161	14 ± 2	466 ± 13
CoPA_5	5	13.8	1146 ± 179	5.3 ± 1.2	164 ± 43
CoPA_10	10	27.5	1665 ± 131	5.0 ± 0.6	198 ± 16
CoPA_20	20	55.1	879 ± 253	6.9 ± 0.8	166 ± 27
CoPA_30	30	82.6	725 ± 247	7.3 ± 1.6	117 ± 31
CoPA_35	35	96.4	720 ± 199	7.5 ± 1.3	126 ± 18
CoPA_40	40	110.2	644 ^{a)}	-	-

^{a)} Only one measurement was possible, due to lack of material.

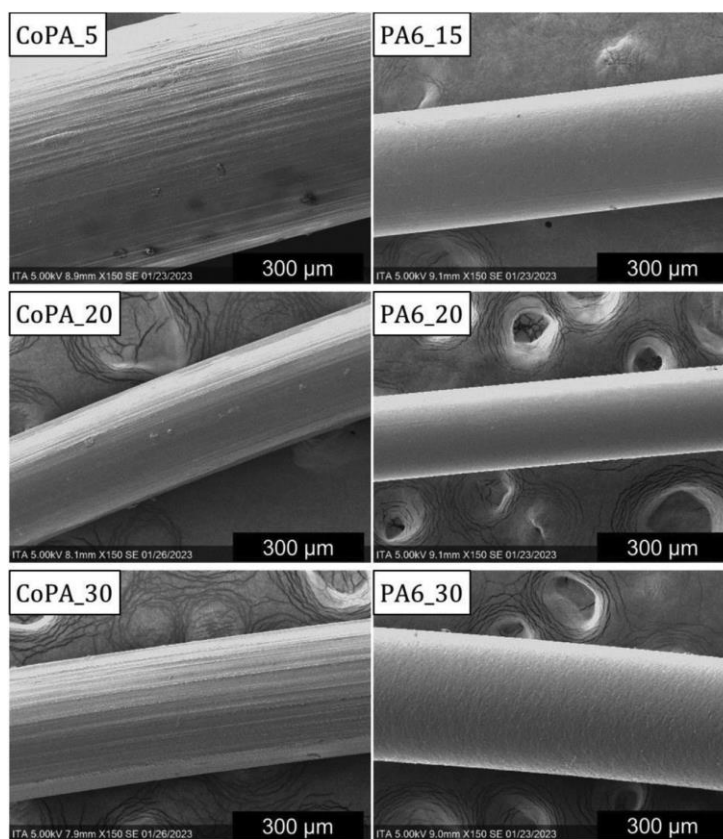


Figure 7. SEM pictures of produced monofilaments at different wind up speeds.

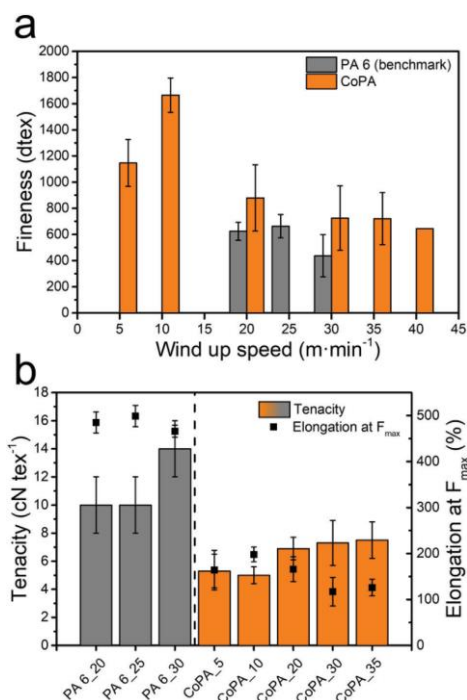


Figure 8. a) Fineness of melt-spun monofilaments in relation to the wind up speed. b) Tenacity and elongation at maximum force (F_{max}) of the melt-spun monofilaments.

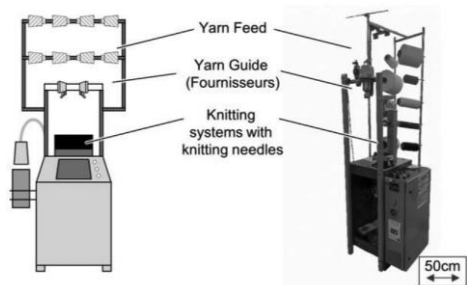


Figure 9. Small circular knitting machine used for the production of knitted fabrics.

knitting process the yarns are formed to loops interlinked to each other, forming a flexible and adaptive textile.^[31]

The spun monofilament yarns of PA 6 and CoPA were processed on a laboratory circular knitting machine with a fineness of E16 (16 needles per inch) (Figure 9). Due to the equipped fineness of the knitting machine and knitting needles used, only the

monofilament yarns made from PA 6 and the finer yarns of the bio-based CoPA₃₀₋₄₀ could be processed. A courser knitting machine would be required for knitting of the thicker yarns. Nevertheless, the processability respectively knittability of the commercial PA 6 and the bio-based CoPA₃₀ was investigated. In general, all yarns used were knittable with the given parameters, although a major difference in the knitting loop build-up was observed.

During processing of the monofilaments from commercial PA 6, the material was visibly deformed to form the loops of the knitted textile (Figure 10d, red circle). In contrast, the monofilaments made from the bio-based CoPA did not show any deformation (Figure 10a,c). Such deformations occur due to the take down force of the knitting needle forming the knitted loop if the material still exhibits plastic deformation properties at low elongations. Since the CoPA does not deform during knitting, plastic deformation at low elongations is not present, thus making it in principle suitable for use in the textile industry. Given that the knitting process was only carried out with laboratory spun monofilaments, the generalization of the results is not necessarily given, but gives a first good indication.

3. Conclusion

Bio-based copolymers were synthesized from oleic acid by isomerizing methoxycarbonylation and melt polycondensation with adipic acid and hexamethylene diamine in bulk. The PA 6.6/6.19 copolymers were successfully obtained with number average molecular weights suitable for melt processing applications (28 600–59 500) and in high yields. Their melting temperature could be controlled by the PA 6.6 content between 177 and 259 °C. The copolymers showed an improvement in mechanical properties compared to the PA 6.19 homopolymer. Thus, the tensile strength was improved by 58% and the Young's modulus by 28%. Surprisingly, the elongation at break was not affected by the increasing PA 6.6 content up to 64 mol%, and remained between 170 and 200%. This resulted in a large increase in toughness of the copolymers, with the copolymers having 55 and 64 mol% PA 6.6 exhibiting similar toughness (94 MPa and 92 MPa) as the commercial PA 6 (92 MPa) with a carbon-based bio-content of 33% and 26% respectively. The bio-based copolymers also exhibit four times lower water absorption than the commercial PA 6, due to the long methylene chains. Their viscoelastic properties suggest good spinnability, which was further evidenced by melt spinning of the exemplary PA 6.6/6.19 55:45 copolymer. Draw-down ratios of up to 110 could be achieved, indicating the suitability of the material for industrial spinning trials. The resulting monofilaments were also successfully knitted on a circular knitting machine to produce fabrics, further underlining the suitability of these copolymers for the production of textiles.

Surely, the copolymerization of bio-based and fossil-based monomers opens for copolyamides with tailored property profiles comprising the lack of performance of many bio-based polyamides and lack of sustainability of high-performance fossil-based polyamides. There is still plenty of room to further tune the property of copolyamides of these types of copolyamides by control of the macromolecular structure. Nevertheless, it is important at this stage, to show also potential for applications which will require the engineering input as well.

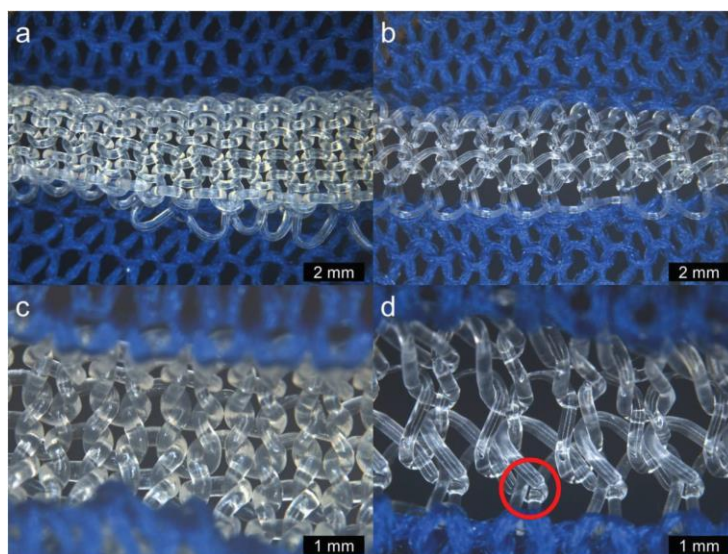


Figure 10. Microscope images of knitted fabrics of a,c) CoPA_30 and b,d) PA 6_25.

4. Experimental Section

Materials: Oleic acid (99%) was purchased from Jinan Boss Chemical Industry Co., Ltd. 1,2-Bis(di-*tert*-butylphosphinomethyl)benzene was purchased from Henan Allgreen Chemical Co., Ltd. Methyl formate (97%) and hexamethylene diamine (99.5+%) were purchased from Acros. Methanesulfonic acid (>99%) was purchased from TCI Chemicals. Palladium(II)acetylacetonate (99%) was purchased from Sigma-Aldrich. 1,1,1,3,3,3-Hexafluoro-2-propanol (99%) was purchased from Fluorochem Ltd. Potassium hydroxide (>85%) was purchased from Carl Roth. Deuterated chloroform (CDCl_3 , 99.8%) and dimethyl sulfoxide ($\text{DMSO-}d_6$, 99.8%) were purchased from Deutero. Aqueous hydrochloric acid (37%) was purchased from VWR. PA 6.6-salt and PA 6 Ultramid B24 N 03 was kindly provided by BASF. All solvents for purification were purchased in technical grade from local suppliers.

Purifications: Methyl formate was degassed by freeze-pump-thaw and stored over molecular sieves 4 Å. Methanol was dried by refluxing with calcium hydride, distilled and stored over molecular sieves 3 Å. Hexamethylene diamine was distilled and stored under argon atmosphere.

Size exclusion Chromatography: The number and weight average molar masses and molar mass distributions were measured on a 1200 Infinity (Agilent Technologies/Cyrotek) gel permeation chromatography (SEC). The instrument was equipped with a PFG 7 μm precolumn and two main columns (PFG 7 μm 100 Å and PFG 7 μm 300 Å) (PSS, Mainz, Germany). A refractive index detector (RI, Gynotek SE-61) was used for the detection. The samples were dissolved in HFIP (HPLC grade) with potassium trifluoroacetate (8 mg mL^{-1}) and toluene (HPLC grade) as an internal standard in a concentration of 2 mg mL^{-1} and filtered through a 0.22 μm PTFE filter. 20 μL of this solution were injected and measured at a flow rate of 0.5 mL min^{-1} at 23 °C. Calibration of the system was performed with Poly(methyl methacrylate) (PSS calibration kit, PSS, Mainz, Germany) in a range of 1720–189 000 Da.

Nuclear Magnetic Resonance Spectroscopy ($^1\text{H-NMR}$): $^1\text{H-NMR}$ spectra were recorded using a Ultrashield-300 spectrometer (Bruker) at

300 MHz in HFIP with added CDCl_3 as an internal reference, for the polymers, and $\text{DMSO-}d_6$ or CDCl_3 for the monomers.

Thermal Properties: Studies on the thermal stability were performed with thermogravimetric analysis (TGA) on a TG 209 F1 Libra (Netzsch). ≈ 5 mg of the sample was weighed in an aluminum crucible with a pierced lid (Thepro). Dynamic measurements were performed in the range of 20–600 °C using a heating rate of 20 K min^{-1} under nitrogen 5.3 and synthetic air (O_2/N_2 , 20/80, v/v) with a flow rate of 50 mL min^{-1} . Isothermal measurements were performed for 1 h at the respective processing temperatures of the polymers (210 °C for PA 6.19; 220 °C for PA 6.6/6.19 17:83; 270 °C for 44:56; 230 °C for 55:45; 280 °C for 64:36; 300 °C for 88:12 and PA 6.6) under nitrogen 5.3 and synthetic air (O_2/N_2 , 20/80, v/v) with a flow rate of 50 mL min^{-1} .

Differential scanning calorimetry (DSC) was performed on a DSC 204 F1 Phoenix (Netzsch). ≈ 5 mg of the sample were weighed in a 30/40 μL aluminum crucible with a pierced lid (Thepro). Dynamic measurements were performed in the range of 0–350 °C at a heating rate of 20 K min^{-1} under nitrogen 5.3 with a flow rate of 20 mL min^{-1} .

Dynamic Mechanical Analysis (DMA) was performed on a DMA 1 STARe System (Mettler Toledo) in single cantilever modus. The measurements were conducted with a heating rate of 2 K min^{-1} and a frequency of 2 Hz.

Rheology: Test specimens for the rheology were produced with a 25-12-2HC hot press (Carver). The polymers were dried in a vacuum at 80 °C overnight and pressed in between two stainless steel plates separated by Kapton sheets using a circular mold with $d = 25$ mm and $h = 1$ mm at a temperature of $T_m + 30$ K for 5 min. The pressure was increased from 0 to 5 t after 2 min and held for 2 min. Thermal quenching was performed directly afterward on a LaboPress P150H manual lever cold press (Vogt Maschinenbau, Berlin, Germany) until room temperature was reached. Rheology measurements were performed on a MCR302 Rheometer (Anton Paar) using an electrical plate (P-ETD400 and an electrical hood (H-ETD400) in parallel plate geometry with $d = 25$ mm. The dynamic measurements were conducted isothermal at 2% deformation and the shear rate was varied between 100 and 0.63 1 rad s^{-1} .

Mechanical Properties of the Polymers: The mechanical properties of the bulk materials were determined by uniaxial stress-strain testing on a BT1-FR 0.5TND14 (Zwick/Roell) at room temperature. The test specimens of type 5B according to DIN EN ISO 527-2 were produced by injection molding on a Micro Injector 5000 (DACA Instruments) with 5 mL barrel-volume. The dimensions of the test specimens were measured at one sample for each nest with a Series 293 (0–25 mm) digital micrometer (Mitutoyo, Neuss, Germany), taking the average of three different positions in the gauge area. The specimens were dried for 48 h at 80 °C under applied vacuum prior to testing. Tensile tests were performed according to DIN EN ISO 527 at 50 mm min⁻¹ at a grip to grip separation of 20 mm. The Young's modulus was determined by the slope of the linear region of the stress-strain curves in range of 0.05%–0.25% deformation. At least seven specimens were tested for each material and the statistical average is given as a result.

Water Uptake: The water uptake tests of the polyamides were performed in triplicate according to DIN EN ISO 62. Disc-shaped test specimens with $d = 25$ mm and $h = 1$ mm were produced via melt pressing analogous to the rheology test specimens. The test specimens were dried in a vacuum oven at 80 °C for 48 h prior to testing and weighed after cooling to room temperature in a desiccator to determine the initial weight (m_0). The specimens were then immersed in deionized water at room temperature for 7 days. Prior to weighing (m_1), the samples were thoroughly dried with a cloth to remove any surface water. The water uptake was determined using Equation (1):

$$\text{water uptake} = \frac{m_1 - m_0}{m_0} \cdot 100\% \quad (3)$$

Crystal Structure: The analysis of the crystal structure of the polyamides was performed using an X-ray diffraction on a D8 ADVANCE diffractometer (Bruker), equipped with Cu K α radiation ($\lambda = 0.154$ nm). The source was operated at 40 kV and 40 mA and measurements were recorded in a 2θ range of 5–40° with a step-size of 0.025° min⁻¹ at room temperature. Disc-shaped test specimens with $d = 25$ mm and $h = 1$ mm were produced via melt pressing analogous to the rheology test specimens.

Scanning Electron Microscopy: Scanning electron microscopy of the monofilaments was performed using a FlexSEM 1000 II (Hitachi High-Tech Corporation) with an acceleration voltage of 5 kV at high vacuum. The samples were sputtered with gold and the pictures were recorded in secondary electron (SE) mode.

Monofilament Characterization: The fineness of the monofilaments was analyzed according to DIN 53830–3. The monofilaments were tested under norm climate with 25 h of acclimatization in accordance with DIN EN ISO 139. 100 mm samples were analyzed in triplicate with a pre-tension of 0.5 cN tex⁻¹.

Tensile tests of the monofilaments were performed according to DIN EN 13 895 on a Statimat 4U (Textechno Herbert Stein GmbH und Co. KG) using a sample length of 100 mm at 100 mm min⁻¹ testing speed and a pre-tension of 0.5 cN tex⁻¹. 10 specimens were tested for each material and the statistical average is given as a result.

Synthesis of Dimethyl-1.19-Nonadecanedionate: The synthesis of dimethyl-1.19-nonadecanedionate was performed as previously reported.^[16] All steps were performed under inert gas atmosphere. 121 mg (0.40 mmol, 4 mol%) palladium(II)acetylacetonate and 627.0 mg (1.59 mmol, 1.6 mol%) 1,2-Bis(di-*tert*-butylphosphino-methyl)benzene (dtbpx) were weighed into a 250 mL stainless steel autoclave equipped with a stirring bar. A solution of 28.04 g (99.27 mmol) oleic acid, 99%, 48 mL methyl formate and 154 μ L (2.38 mmol, 6 mol%) methanesulfonic acid (MSA) in 48 mL methanol was prepared and directly transferred into the autoclave using a syringe under inert gas counterflow. The autoclave was closed and heated to 100 °C while stirring for 24 h. During this period, the pressure gradually increased to 6–12 bar. After cooling the autoclave to room temperature, the pressure was carefully released. The reaction products were washed out of the autoclave with 2 \times 40 mL methylene chloride. The resulting yellow solution was filtered over neutral Al₂O₃ to remove possible Pd black and excess catalyst. The solvent was removed

using a rotary evaporator to yield the crude product as yellow crystals. These were purified by two times recrystallization from 200 mL methanol to isolate the 1.19-nonadecanedionate **2** as white crystals with a purity of >99% (GC) and a yield of 80%.

¹H-NMR: (300 MHz, CDCl₃, 298 K, δ): 3.66 (s, 6H, O-CH₃), 2.30 (t, $J = 7.6$ Hz, 4H, CH₂), 1.61 (m, 4H, CH₂), 1.25 (m, 26H, CH₂).

Synthesis of 1.19-Nonadecanedioic Acid: The synthesis of 1.19-nonadecanedioic acid was performed as previously reported.^[16] 24.5 g (68.6 mmol) dimethyl-1.19-nonadecanedionate were transferred into a 1 L round bottom flask equipped with a large stirring bar. A solution of 46.2 g potassium hydroxide in 462 mL methanol was added to the flask and heated to 85 °C while stirring for 12 h to form a white slurry. After cooling to room temperature, the solvent was removed in vacuo to yield the potassium salt as white solids. The salt was then dissolved in 236 mL deionized water followed by slow addition of aqueous hydrochloric acid (6 m) until pH \approx 1, resulting in a white precipitate. The precipitate was washed neutral with deionized water and then dried for 24 h at 80 °C to obtain the pure 1.19-nonadecanedioic acid as white solids in a yield of 22.5 g (68.4 mmol, 99% yield).

¹H-NMR: (300 MHz, DMSO-*d*₆, 298 K, δ): 11.98 (s, 2H, COOH), 2.18 (t, $J = 7.3$ Hz, 4H, CH₂), 1.47 (m, 4H, CH₂), 1.23 (s, 26H, CH₂).

Synthesis of Copolymers: The PA-salts of PA 6.19 and PA 6.6 were prepared by dissolving equimolar amounts of hexamethylene diamine and 1.19-diacid or adipic acid respectively in ethanol for PA 6.19 or water for PA 6.6 to form solutions of 10 wt%. Complete dissolution of the diacid was achieved by heating to 80 °C. Upon complete dissolution, the diamine solution was added, causing the formation of the PA-salt as a white precipitate. After another 2 h of heating the solution was cooled to room temperature. The formed PA-salt was recovered by filtration and washed with warm ethanol respectively water to yield the desired PA-salts in \approx 90 % yield.

For the synthesis of PA 6.6/6.19 copolymers the PA-salts of PA 6.6 and PA 6.19 were mixed in the desired ratio with a spatula. This mixture was then transferred into a three-necked Schlenk-tube with a mechanical stirrer and distillation bridge attached. Upon exchange of atmosphere with argon to ensure exclusion of oxygen the mixture was heated to 160 °C under stirring. The temperature was increased stepwise in 10 K increments to ensure melting until the final temperature of 265 °C is reached within 4 h. Then the temperature was held at 265 °C for 3 h under stirring. Afterward vacuum was applied to ensure complete evaporation of water and the reaction proceeded for another 2 h. Then the tube was vented with argon and cooled to room temperature. The formed polymer was dissolved in HFIP (hexafluoro isopropanol) and recovered by precipitation in methanol. After drying the overall yield of recovered polymer was \approx 90%.

Melt Spinning: Melt spinning of the polyamides was performed using a MC 15 HT micro compounder (Xplore Instruments BV) with a batch-wise manual polymer feed and a twin-screw setup. A monofilament spinneret hole with a diameter of 3 mm was used and the take-up godet served as the winder. The polymers were dried prior to processing at 80 °C under applied vacuum overnight. The residual moisture content was determined by Karl Fischer titration using a C30 Coulometric Karl Fischer titrator (Mettler-Toledo).

Knitting Trials: The melt-spun monofilaments were processed on a laboratory circular knitting machine TK 83 (Maschinenfabrik Harry Lucas GmbH & Co. KG), with a fineness of E16 (16 needles per inch). The yarn feeding was controlled by a EFS 820 Fournisseur (Memminger-Iro GmbH) to maintain a constant yarn tension of 1.5 cN.

Supporting Information

Supporting Information is available from the Wiley Online Library or from the author.

Acknowledgements

The authors are indebted for financial support to the Federal Ministry of Education and Research (Research project Algae Tex, no. 03 1b1058B).

The authors gratefully acknowledge the use of equipment and assistance offered by the Keylab "Small Scale Polymer Processing" of the Bavarian Polymer Institute at the University of Bayreuth.
Open access funding enabled and organized by Projekt DEAL.

Conflict of Interest

The authors declare no conflict of interest.

Data Availability Statement

The data that support the findings of this study are available in the supplementary material of this article.

Keywords

copolyamide, low water uptake, oleic acid, polymer engineering, vegetable oil-based materials

Received: May 5, 2023

Revised: May 9, 2023

Published online: June 4, 2023

- [1] E. Commission, *Publications Office* **2019**.
- [2] TextileExchange, Preferred Fiber & Materials, https://textileexchange.org/wp-content/uploads/2021/08/Textile-Exchange-Preferred-Fiber-and-Materials-Market-Report_2021.pdf, accessed: 08.2022.
- [3] M. Winnacker, B. Rieger, *Macromol. Rapid Commun.* **2016**, *37*, 1391.
- [4] R. Hufenus, Y. Yan, M. Dauner, T. Kikutani, *Materials* **2020**, *13*, 4298.
- [5] F. Stempfle, D. Quinzler, I. Heckler, S. Mecking, *Macromol. Chem. (Oxford)* **2011**, *44*, 4159.
- [6] X. Miao, R. Malacea, C. Fischmeister, C. Bruneau, P. H. Dixneuf, *Green Chem.* **2011**, *13*, 2911.
- [7] a) H. Mutlu, R. Hofstätter, R. E. Montenegro, M. A. R. Meier, *RSC Adv.* **2013**, *3*, 4927; b) X. Li, J. Choo Ping Syong, Y. Zhang, *Green Chem.* **2018**, *20*, 3619; c) R. S. Atapalkar, P. R. Athawale, D. Srinivasa Reddy, A. A. Kulkarni, *Green Chem.* **2021**, *23*, 2391.
- [8] a) T. Witt, F. Stempfle, P. Roesle, M. Häußler, S. Mecking, *ACS Catal.* **2015**, *5*, 4519; b) G. A. Abel, K. O. Nguyen, S. Viamajala, S. Varanasi, K. Yamamoto, *RSC Adv.* **2014**, *4*, 55622.
- [9] a) A. Y. Mudiyansele, S. Viamajala, S. Varanasi, K. Yamamoto, *ACS Sustainable Chem. Eng.* **2014**, *2*, 2831; b) G. A. Abel, S. Viamajala, S. Varanasi, K. Yamamoto, *ACS Sustainable Chem. Eng.* **2016**, *4*, 5703.
- [10] M. A. R. Meier, *Macromol. Rapid Commun.* **2019**, *40*, 1800524.
- [11] L. Tao, K. Liu, T. Li, R. Xiao, *Polym. Bull.* **2020**, *77*, 1135.
- [12] X. Cui, W. Li, D. Yan, *Polym. Int.* **2004**, *53*, 1729.
- [13] a) C. Bennett, E. Kaya, A. M. Sikes, W. L. Jarrett, L. J. Mathias, *J. Polym. Sci., Part A: Polym. Chem.* **2009**, *47*, 4409; b) C. Bennett, L. J. Mathias, *J. Polym. Sci., Part A: Polym. Chem.* **2005**, *43*, 936; c) C. Bennett, L. J. Mathias, *Macromol. Chem. Phys.* **2004**, *205*, 2438; d) X. Cui, W. Li, D. Yan, C. Yuan, G. Di Silvestro, *J. Appl. Polym. Sci.* **2005**, *98*, 1565.
- [14] D. Pinggen, J. B. Schwaderer, J. Walter, J. Wen, G. Murray, D. Vogt, S. Mecking, *ChemCatChem* **2018**, *10*, 3027.
- [15] B. Cornils, P. Lappe, in *Ullmann's Encyclopedia of Industrial Chemistry*, 7th ed., Wiley-VCH, Weinheim **2010**.
- [16] M. Rist, A. Greiner, *ACS Sustainable Chem. Eng.* **2022**, *10*, 16793.
- [17] Q. Guo, C. Fan, H. Liu, Y. Cai, *Polym. Polym. Compos.* **2011**, *19*, 69.
- [18] F. Jia, J.-L. Mao, X.-Y. Yang, Y. Ma, C. Yao, *Chin. Chem. Lett.* **2013**, *24*, 654.
- [19] F. Jia, J. L. Mao, Y. Ma, C. Yao, *J. Appl. Polym. Sci.* **2014**, *131*, 39845.
- [20] P. Zierdt, E. Mitzner, A. Gomoll, T. Theumer, A. Lieske, *J. Appl. Polym. Sci.* **2016**, *133*, 44155.
- [21] T. Elzein, M. Brogly, J. Schultz, *Kobunja Kwahak Kwa Kisul* **2002**, *43*, 4811.
- [22] S. Koltzenburg, M. Maskos, O. Nuyken, *Polymere: Synthese, Eigenschaften und Anwendungen*, Springer, Berlin, Heidelberg **2014**.
- [23] M. Ehrenstein, S. Dellsperger, C. Kocher, N. Stutzmann, C. Weder, P. Smith, *Kobunja Kwahak Kwa Kisul* **2000**, *41*, 3531.
- [24] Y. Li, G. Yang, *Macromol. Rapid Commun.* **2004**, *25*, 1714.
- [25] M. Winkler, M. A. R. Meier, *Green Chem.* **2014**, *16*, 1784.
- [26] a) I. Clavería, D. Elduque, J. Santolaria, C. Pina, C. Javierre, A. Fernandez, *Polym. Test.* **2016**, *50*, 15; b) V. Venoor, J. H. Park, D. O. Kazmer, M. J. Sobkowicz, *Polym. Rev.* **2021**, *61*, 598.
- [27] a) F. Fourné, *Synthetic fibers: Machines and equipment, manufacture, properties*, Hanser, Munich **1999**; b) Z. K. Walczak, *Processes of fiber formation*, 1st ed., Elsevier, Amsterdam, New York **2002**.
- [28] a) P. J. Carreau, D. C. de Kee, R. P. Chhabra, *Rheology of Polymeric Systems: Principles and applications*, 2nd ed. Carl Hanser Verlag GmbH & Co. KG, München **2021**; b) K. Yasuda, R. C. Armstrong, R. E. Cohen, *Rheol. Acta* **1981**, *20*, 163.
- [29] T. A. Osswald, N. Rudolph, *Polymer Rheology: Fundamentals and applications*, Hanser, Munich, Cincinnati **2015**.
- [30] R. Beyreuther, R. Vogel, *Int. Polym. Proc.* **1996**, *11*, 154.
- [31] T. Gries, D. Veit, B. Wulfhorst, *Textile Technology: An Introduction*, 2nd ed. Hanser, Munich, Cincinnati, Ohio **2017**.

[M]acro-
[M]olecular
Rapid Communications

Supporting Information

for *Macromol. Rapid Commun.*, DOI 10.1002/marc.202300256

Toughening of Bio-Based PA 6.19 by Copolymerization with PA 6.6 – Synthesis and Production of Melt-Spun Monofilaments and Knitted Fabrics

*Maximilian Rist, Henning Löcken, Mathias Ortega and Andreas Greiner**

Supporting Information

Toughening of bio-based PA 6.19 by copolymerization with PA 6.6 – synthesis and production of melt-spun monofilaments and knitted fabrics

*Maximilian Rist, Henning Löcken, Mathias Ortega and Andreas Greiner**

M. Rist, A. Greiner

University of Bayreuth, Macromolecular Chemistry and Bavarian Polymer Institute,
Universitätsstrasse 30, 95440 Bayreuth, Germany.

E-mail: greiner@uni-bayreuth.de

H. Löcken, M. Ortega

Institut fuer Textiltechnik, RWTH Aachen University, Otto-Blumenthal-Strasse 1, 52074
Aachen, Germany

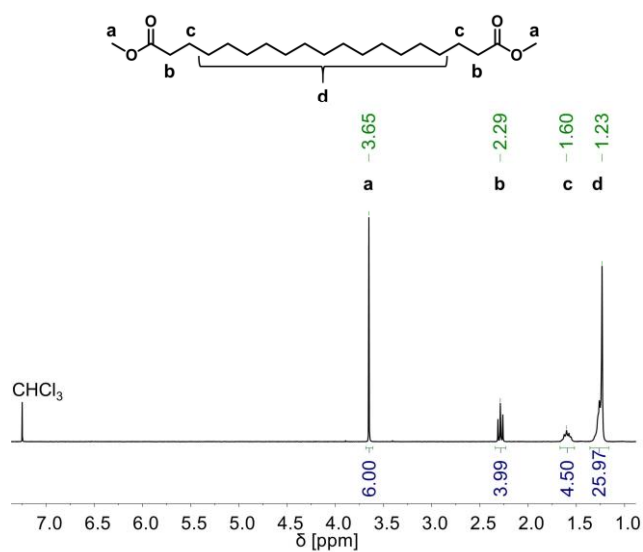


Figure S1. ¹H-NMR spectrum of dimethyl-1,19-nonadecanedioate recorded in CDCl₃.

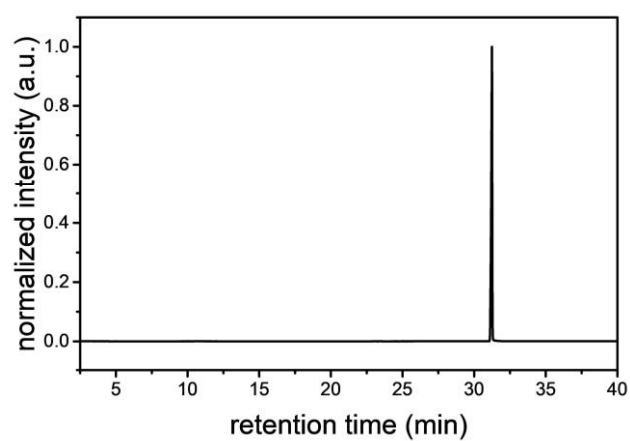


Figure S2. Gas chromatogram of dimethyl-1,19-nonadecanedioate.

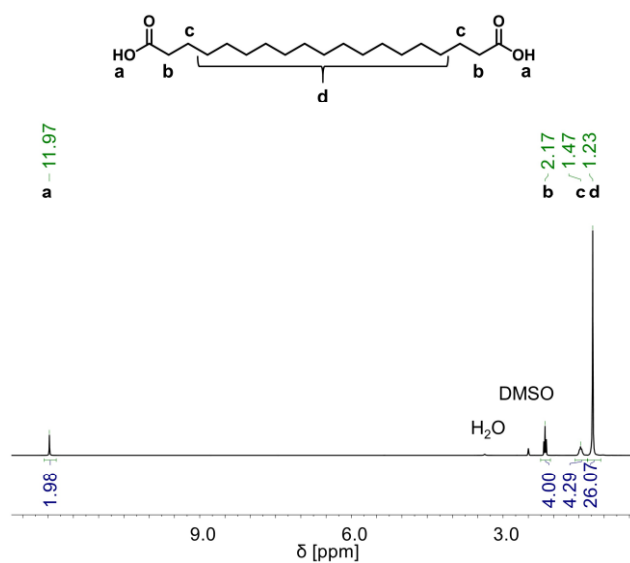


Figure S3. $^1\text{H-NMR}$ spectrum of 1,19-nonadecanedioic acid recorded in $\text{DMSO-}d_6$.

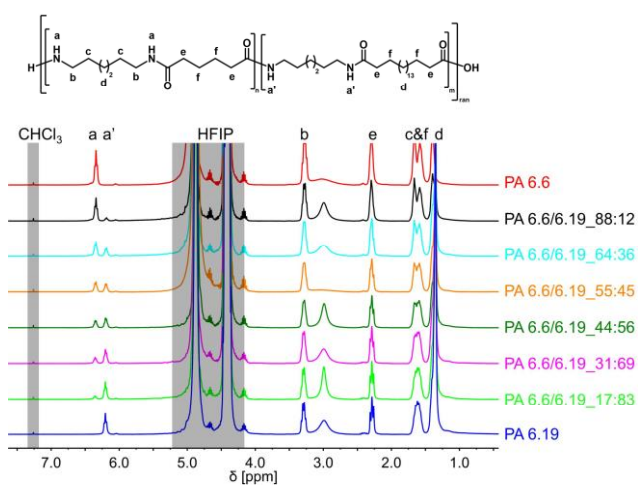


Figure S4. $^1\text{H-NMR}$ spectrum of PA 6.6/6.19 copolymers recorded in $\text{HFIP}/\text{CDCl}_3$ 9:1.

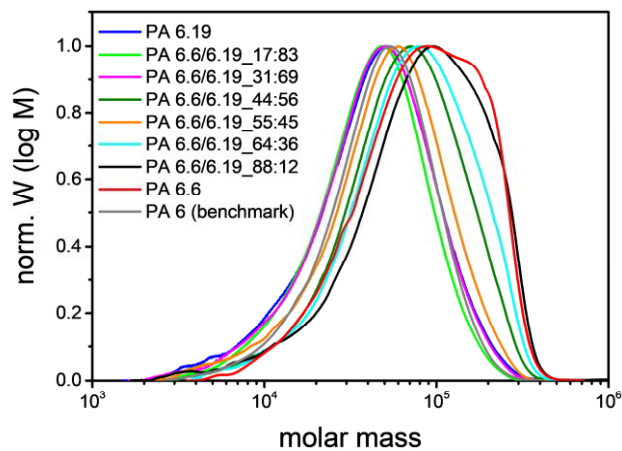


Figure S5. Normalized molecular weight distribution of the polyamides measured by HFIP-GPC.

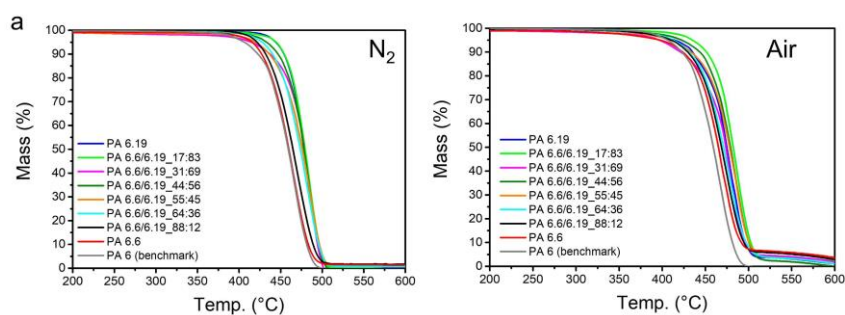


Figure S6. a) Dynamic TGA curves of the polyamides under synthetic air atmosphere and b) under nitrogen atmosphere, recorded at 20 K min^{-1} .

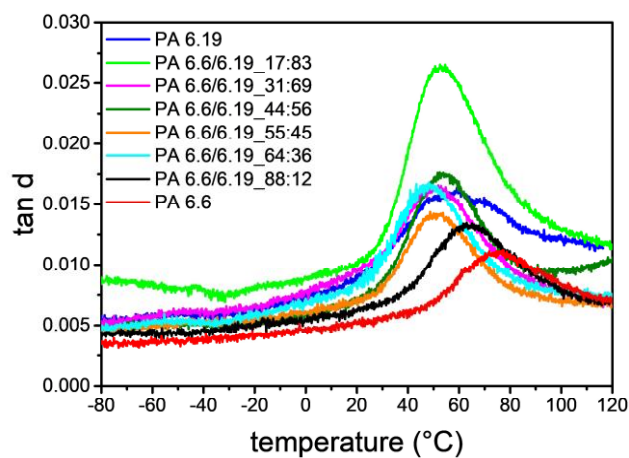


Figure S7. Loss factor (tan δ) of the PA 6.6/6.19 copolymers over the temperature, measured by DMA.

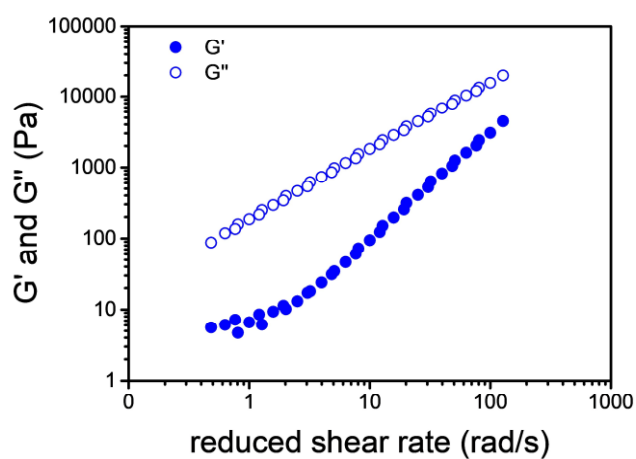


Figure S8. Temperature independent master curve of PA 6.19.

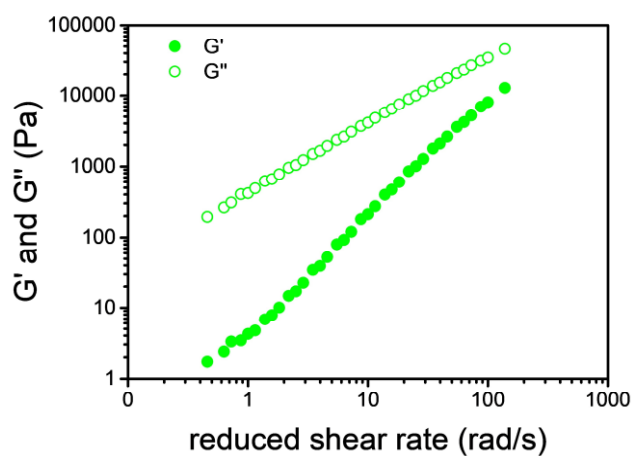


Figure S9. Temperature independent master curve of PA 6.6/6.19 17:83.

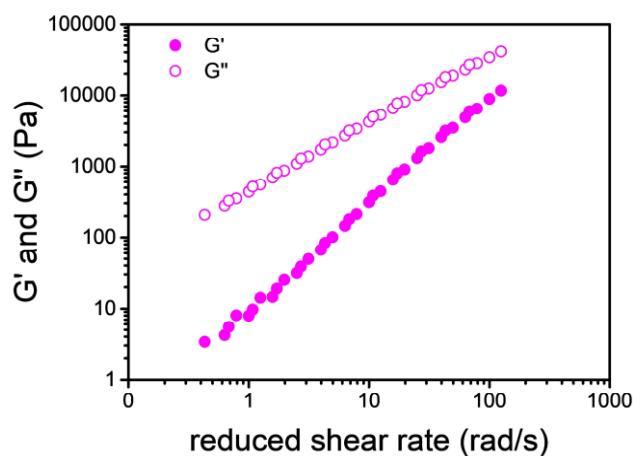


Figure S10. Temperature independent master curve of PA 6.6/6.19 31:69.

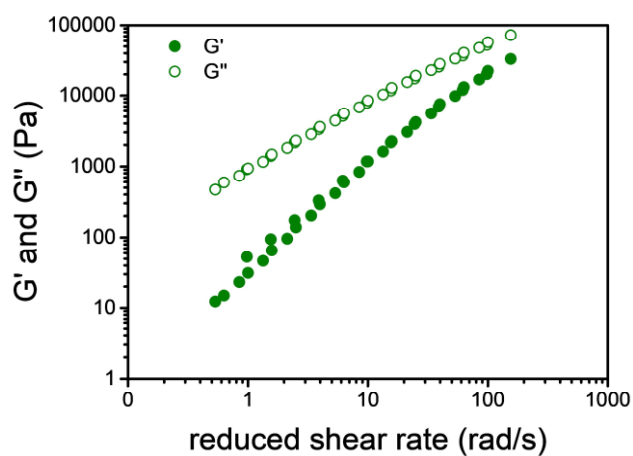


Figure S11. Temperature independent master curve of PA 6.6/6.19 44:56.

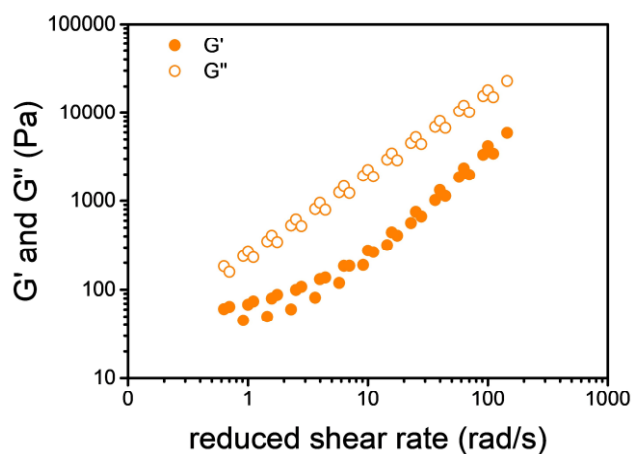


Figure S12. Temperature independent master curve of PA 6.6/6.19 55:45.

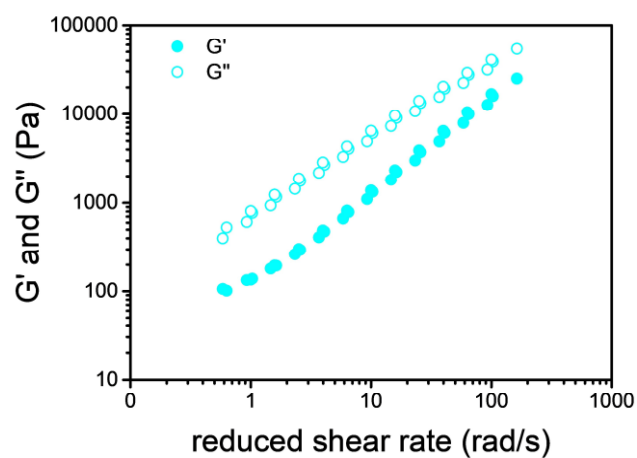


Figure S13. Temperature independent master curve of PA 6.6/6.19 64:36.

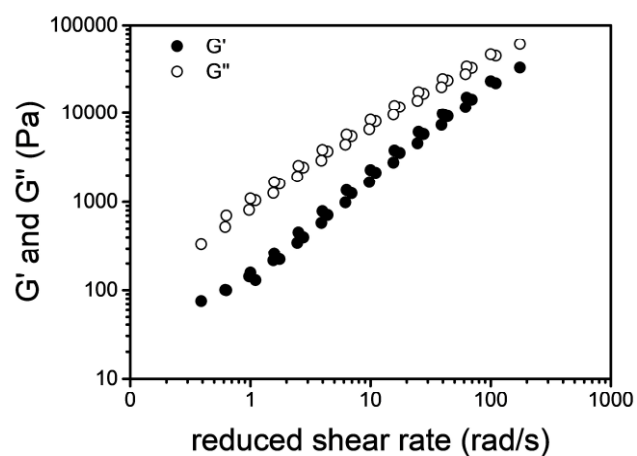


Figure S14. Temperature independent master curve of PA 6.6/6.19 88:12.

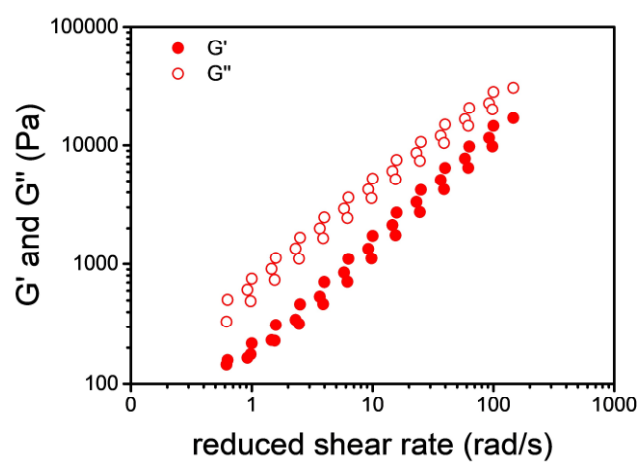


Figure S15. Temperature independent master curve of PA 6.6.


Table S1. Residual moisture contents of polyamides used for melt spinning determined by Karl Fischer Titration.

Polyamide	Drying time (vacuum) [h]	Mean residual moisture content [ppm]	Standard deviation [ppm]
PA 6 (benchmark)	18	546	34.7
PA 6.6/6.19 55:45	18	1296	69.8



Cite this: DOI: 10.1039/d3lp00201b

Bio-based electrospun polyamide membrane – sustainable multipurpose filter membranes for microplastic filtration†

Maximilian Rist  and Andreas Greiner *

Electrospinning is a highly versatile method for manufacturing filter membranes, contributing to advanced concepts for the production of sustainable membranes for waste water treatment. The use of bio-based polymers could expand the sustainability of such filter membranes significantly. Bio-based PA 6,9, for example, shows great potential for the creation of bio-sourced electrospun filter membranes (EFMs) with high mechanical properties and high resistance to solvents. The polyamide is synthesized from plant oil-based azelaic acid and electrospun from chloroform/formic acid to produce self-standing electrospun nonwovens. These highly porous membranes show high efficiencies of up to 99.8% for the filtration of polystyrene microparticles (PS-MPs) from water. Additionally, the electrospun nonwovens exhibit comparable filtration efficiencies to FFP3 masks for the removal of 0.3 μm particles from air. The membranes show hydrophobic surface behavior (water contact angle of $>120^\circ$) making them suitable for water oil separation. Efficiencies of up to 99.9% can be achieved for the separation of water and chloroform from 50 vol% mixtures, while maintaining a high permeate flux of up to 5345 $\text{L m}^{-2} \text{h}^{-1}$. Additionally, the membranes can be reused for at least ten times without any significant reduction in efficiency or flux.

Received 11th October 2023,

Accepted 2nd January 2024

DOI: 10.1039/d3lp00201b

rsc.li/rscapppolym

Introduction

Electrospinning is the state-of-the-art method for the production of nonwovens composed of polymer nano- or microfibers.¹ These nonwovens find many different applications including catalysis,^{2–4} energy storage^{5–7} or filtration.^{8–10} Cutting of nonwovens yield short microfibers which can be processed in dispersions. Such dispersions were used for the preparation of sponges or wet-laid membranes.^{11,12} Due to their high flexibility, porosity, and specific surface area, electrospun filter membranes (EFMs) often combine high permeability with high rejection rate, making them promising materials for filtration purposes.^{13,14} Such EFMs have been successfully used for the filtration of particles from water^{8,9,15,16} as well as air^{10,17,18} and for the separation of oil and water.^{19–23}

Recently, the demand for air filters has seen a sharp increase due to the COVID-19 pandemic.¹⁰ Face masks, in particular, were necessary to prevent spreading of the virus in close quarters. The filters in these face masks must have a high efficiency for the exclusion of particles while having a low

pressure drop or high permeability to allow free breathing. The use of electrospun nonwovens as air filtration membranes offers these properties at a lower cost than conventional air filters.¹⁰ In addition, the electrospinning process enables continuous fiber production, which results in very long fibers and prevents them from going airborne.¹³ Electrospinning also allows tailoring of the fiber diameter and pore size of the EFM in a wide range reaching three orders of magnitude.¹⁰ Many different polymers have been used to successfully produce EFMs for air filtration, including poly(vinylidene difluoride) (PVDF), polyacrylonitrile (PAN) and polyamides (PA). PA and PAN are especially useful to produce robust filters that need to be used in harsh environments.^{24–26} PVDF on the other hand is selected for its hydrophobicity.^{27,28} Electrospun membranes for air filtration are usually composites, where the nonwoven is deposited on top of a porous substrate to enhance the generally poor mechanical stability of electrospun nonwovens.²⁹ On the flipside, self-standing membranes made from only one component can be made in a simpler process, which is more attractive for large-scale production.¹⁰ Additionally, the material can be recycled more easily as the used filter can just be dissolved and the resulting solution used for electrospinning again.^{30,31}

While most of the earth is covered by water, only 2.6% of all water on earth is freshwater, and only 0.3% of that is available in liquid form and can be used directly by humans.⁹ This

University of Bayreuth, Macromolecular Chemistry and Bavarian Polymer Institute, Universitätsstrasse 30, 95440 Bayreuth, Germany. E-mail: greiner@uni-bayreuth.de
† Electronic supplementary information (ESI) available. See DOI: <https://doi.org/10.1039/d3lp00201b>



makes drinking water a scarce resource and local availability is often not given. Studies from 2020 show that every fourth human doesn't have access to safe drinking water, and every tenth person lacks even basic water supply.³² The removal of pollutants from available freshwater is essential for the supply of clean drinking water. Filtration membranes are the choice for the removal of solid particles like microplastics and metal nanoparticles.^{33,34} The membranes need to have a high filtration efficiency together with a high water permeability, which is why EFMs are interesting materials for such applications. EFMs for water filtration are commonly prepared from poly(vinyl alcohol) (PVA),³⁵ PAN,³⁶ polysulfone (PSF),³⁷ PVDF,³⁸ and polyurethane (PU).³⁹ Self-standing EFMs made of PA have been used for water filtration,⁴⁰ however, they are mostly applied in composite membranes where they provide the surface hydrophilicity to achieve high water permeability.^{41–46}

Another challenging task for the purification of water is the separation of oil from oily wastewater and polluted oceans due to oil spills. The methods currently used are still a challenge.^{20,47} Electrospun nonwoven membranes are promising materials for the separation of water and oil. Selective wettability of the EFM can be tailored by choice of material and surface morphology to allow separation of water and oil.⁴⁸ EFMs made from poly(vinylidene fluoride-co-hexafluoropropylene) (PVDF-HFP) with superhydrophobic surface properties were able to separate oil from water with high efficiency and high flux.^{49,50} Similar results were obtained for EFMs made from polylactide (PLA),^{51–53} acrylonitrile-butadiene-styrene (ABS)⁵⁴ and PA.^{55–57} Polyamides can also be used in composite membranes with hydrophobic materials like PVDF to make hydrophilic membranes, where only water is able to penetrate the membrane.⁵⁸

So far, mostly conventional polymers are used for the production of such EFMs, but the availability of bioplastics is growing and their potential application for filtration membranes need to be investigated. PLA-, cellulose- or chitosan-based EFMs are among the most studied bio-based and/or -degradable materials for the production and application of filtration membranes.^{59–63} Self-standing membranes made of these materials often lack mechanical stability, making them prone to rupture. Polyamides on the other hand exhibit high

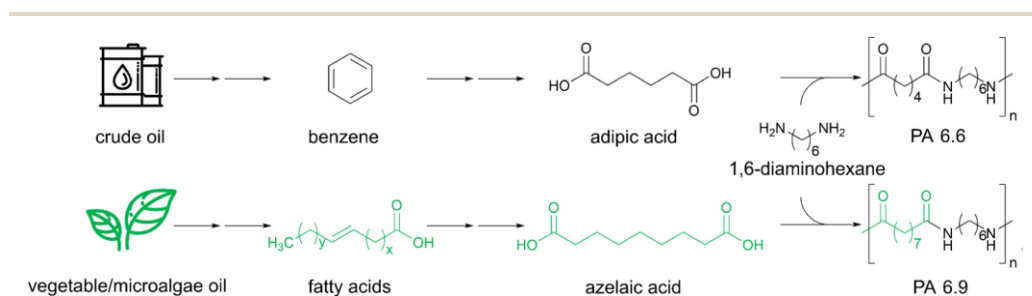
mechanical stability due to intermolecular hydrogen bonding. One particularly interesting polyamide is PA 6.9 which is synthesized from bio-based azelaic acid and 1,6-diaminohexane (Scheme 1).⁶⁴ The azelaic acid can be sourced from various vegetable and microalgae oils as it is synthesized from common fatty acids like oleic acid. PA 6.9 is structurally similar to PA 6.6, but owing to the extra methylene units in the diacid and the even-odd structure it possesses some unique properties. The PA 6.9 exhibits increased hydrophobicity, resulting in greater dimensional stability, which is advantageous for the production of composites and application in aqueous media.⁶⁵ It also has a higher chain flexibility than PA 6.6 because of the greater separation of the amide bonds along the polymer chain.⁶⁶ Additionally, production of the bio-based azelaic acid is already commercialized since the 1950s and PA 6.9 is also commercially available.⁶⁷

Herein, we report the preparation of sustainable self-standing EFMs from bio-based PA 6.9. The polyamide was synthesized from hexamethylene diamine and plant oil-based azelaic acid. Nonwovens were prepared by electrospinning from polymer solutions in formic acid/chloroform at different concentrations and cut into membranes. The morphology as well as the surface wettability and the mechanical properties of the prepared membranes were analyzed. The influence of the polymer concentration on the resulting properties was evaluated and discussed. Their potential application as filtration membranes for the filtration of microplastic particles from water and air as well as for the separation of water and oil was investigated. Important filtration properties including flux, permeability, and filtration/separation efficiency were analyzed and compared to existing conventional and bio-based EFMs.

Experimental

Materials

Azelaic acid (technical grade for synthesis), styrene (>99%) and potassium persulfate (99+%) were purchased from Sigma-Aldrich. Hexamethylene diamine (99.5+%) and basic aluminum oxide (5–200 μm , 60A) was purchased from Acros. Chloroform (>99.8%) was purchased from fisher scientific.



Scheme 1 Synthesis of crude oil-based adipic acid and PA 6.6 in comparison to vegetable/microalgae oil-based azelaic acid and PA 6.9.



Formic acid (99–100%) was purchased from VWR. 1,1,1,3,3,3-Hexafluoro-2-propanol (HFIP, 99%) was purchased from Fluorochem Ltd. Deuterated chloroform (CDCl_3 , 99.8%) was purchased from Deutero. All solvents for purification were purchased in technical grade from local suppliers.

Purifications

Azelaic acid was recrystallized from ethyl acetate with the addition of activated charcoal. Hexamethylene diamine was distilled and stored under argon atmosphere.

Synthesis of polyamide 6.9

The synthesis of PA 6.9 was adapted from the method used by Tao *et al.*⁶⁸ The PA-salt of PA 6.9 was prepared by dissolving equimolar amounts of hexamethylene diamine and azelaic acid in ethanol to form solutions of 10 wt%. Complete dissolution of the diacid was achieved by heating to 40 °C. Upon complete dissolution of the diacid the diamine-solution was added, causing the formation of the PA-salt as a white precipitate. After 1 hour of heating the solution was cooled to 0 °C. The formed PA-salt was recovered by filtration and washed with ethanol to yield the desired PA-salt with a yield of 93%.

For the synthesis of PA 6.9, 400 g of the PA-salt was transferred into a 1 L stainless steel reactor with a mechanical stirrer. Upon exchange of atmosphere with argon to ensure exclusion of oxygen 270 mL of degassed water was added. The resulting slurry was then heated at maximum heating (310 °C jacket temperature) while stirring until a pressure of 15 bar was reached. Then the water steam was slowly removed to keep the reaction running isobar at *ca.* 15 bar, until there was no more water left in the reaction vessel and atmospheric pressure was reached (6 h). Then, the reactor was slowly evacuated over the course of one hour. The polycondensation was proceeded for another three hours at a final melt temperature of 240 °C. Once the torque of the stirrer reached 100 N cm the reaction was stopped by slowly purging with argon until a pressure of 0.2 bar. The polymer was recovered by opening a valve on the bottom of the reaction vessel and quenching of the polymer melt in ice water. The solid polymer was then grinded to receive polymer particles with a maximum diameter of 2 mm. After drying at 70 °C *in vacuo* for 24 h 285 g of PA 6.9 was received as an off-white powder.

Electrospinning of PA 6.9

Polyamide 6.9 was dissolved in 5 mL of a mixture of formic acid and chloroform 1 : 1 v/v (FA/CHCl_3) in the specific concentrations. Electrospinning was performed at 24 kV positive voltage for 10 wt% solutions, 25 kV for 12.5 wt% and 26 kV for 15 wt% solutions. The negative voltage was -0.8 kV and the tip to collector distance was 20 cm for all experiments. A rotary disc collector was used as a collector and the flow rate used was 0.4 mL h^{-1} for the 10 and 12.5 wt% solutions and 0.65 mL h^{-1} for the 15 wt% solutions. The total collection time was 1.5 hours for the 10 wt% solutions, 2 hours for the 12.5 wt% and 1 hour for the 15 wt% solutions.

Emulsion polymerization

15.4 g (148 mmol) styrene (destabilized by filtration over basic aluminum oxide) was dispersed in 150 mL of degassed deionized water at 80 °C and a stirrer speed of 200 rpm. A solution of 3.2 mg (0.012 mmol) potassium persulfate in 5 mL degassed deionized water was added quickly. The resulting mixture was stirred over night at 80 °C to form a milky emulsion. The emulsion was filtered over a kitchen sieve to remove larger agglomerated polystyrene particles. The concentration of polystyrene micro-particles was determined gravimetrically by taking an aliquot of 5 mL from the dispersion, followed by freeze-drying. The hydrodynamic diameter of the particles was determined *via* dynamic light scattering (DLS) using a PN3704 Zetasizer (Malvern).

Characterizations

Size exclusion chromatography (SEC). The number and weight average molar mass and molar mass distribution of PA 6.9 was measured on a 1200 Infinity (Agilent Technologies/Gynotek) gel permeation chromatography (GPC). The instrument was equipped with a PFG 7 μm precolumn and two main columns (PFG 7 μm 100 Å and PFG 7 μm 300 Å) (PSS, Mainz, Germany). A refractive index detector (RI, Gynotek SE-61) was used for the detection. The sample was dissolved in HFIP (HPLC grade) with potassium trifluoroacetate (8 mg mL^{-1}) and toluene (HPLC grade) as an internal standard in a concentration of 2 mg mL^{-1} and filtered through a $0.22 \mu\text{m}$ PTFE filter. 20 μL of this solution were injected and measured at a flow rate of 0.5 mL min^{-1} at 23 °C. Calibration of the system was performed with poly(methyl methacrylate) (PSS calibration kit, PSS, Mainz, Germany) in a range of 1720–189 000 Da.

Scanning electron microscopy (SEM). The electrospun membranes were placed onto stubs and sputtered with 1.3 nm platinum using a platinum-sputter coater 208HR (Cressington). Recordings were performed with a Leo 1530 (Zeiss) with 3 kV acceleration voltage and at a pressure of 2.0×10^{-5} bar. Images were taken with an inlens and secondary electron detector (Everhart Thornley). A backscattering detector (Centaurus) was used at 10 kV acceleration voltage under the same pressure.

Mechanical properties of membranes. The mechanical properties were determined by uniaxial stress–strain testing on a BT1-FR 0.5TND14 (Zwick/Roell) at room temperature. Test specimens were prepared by cutting out rectangular shaped stripes from the electrospun nonwoven using a scalpel. The dimensions of the test specimens were 5 mm in width with a gauge length of 20 mm. The height of the specimens was measured using a Series 293 (0–25 mm) digital micrometer (Mitutoyo, Neuss, Germany), taking the average of three different positions in the gauge area. The specimens were conditioned for 48 h at room temperature prior to testing. Tensile tests were performed according at 2 mm min^{-1} at a grip to grip separation of 20 mm. The Young's modulus was determined by the slope of the linear region of the stress–strain curves in range of 0.05%–0.25% deformation. At least five specimens were tested for each material and the statistical average is given as a result.



Contact angle measurement. The contact angle measurement for all membranes were performed using a drop shape analyzer (Krüss). For measurement, small rectangular pieces of the nonwovens were cut out and placed on a flat surface. A drop of 4 μL water was produced and placed on top of the membrane and the contact angle was measured after 30 s.

Pore size measurement. Measurement of the pore size distributions were performed using a porometer PSM165 (Topas). Circular-shaped samples (20 mm diameter) were cut out with a scalpel and placed into a measuring adapter with a flow cross-section of 11 mm. For the measurement of the bubble-point, about 5 drops of Topor liquid (surface tension 16.0 mN m^{-1}) was dropped onto the membrane. The used airflow-rate was in the range of 3.6–4200 L h^{-1} and adjusted automatically by the instrument.

Microparticle filtration in water. Circular shaped filters with a diameter of 30 mm were cut out of the membranes using a scalpel. The cut out filters were then placed on a metal mesh and then fixed into a reusable filtering apparatus (Satorius AG), limiting the available filtration area to 3.14 cm^2 . The flow rate was adjusted to 1 mL min^{-1} using a LA100 syringe pump (Landgraf Laborsysteme). For each filtration experiment, 45 mL polystyrene microparticle dispersion (300 $\mu\text{g mL}^{-1}$) were used and the filtrate was collected in intervals of two minutes. The remaining polystyrene concentration in the filtrate was then analyzed *via* UV-Vis to determine the filtration efficiency.

During the experiment, the transmembrane pressure was recorded with a battery powered digital manometer (digi-04) with an accuracy of 0.4% in the range of 0–2.5 bar. The manometer was installed between the syringe pump and the filtering apparatus, and the measured value was noted every minute to calculate the membrane permeability ($\text{L m}^{-2} \text{h}^{-1} \text{bar}^{-1}$) according to the formula:

$$\text{Permeability} = \frac{V}{A \times \Delta t \times \Delta p}$$

where V is the total volume of the organic phase (L), A is the available area (m^2), Δt is the total filtration time (h) and Δp is the transmembrane pressure (bar).

Quantification of the filtration efficiency. A linear calibration was performed by measurement of the absorption at the absorption maximum of polystyrene (280 nm, Fig. S6†).⁶⁹ The polystyrene dispersion was diluted with distilled water to yield five calibration dispersions. The calibration was performed in a range between 1.88 $\mu\text{g mL}^{-1}$ and 30 $\mu\text{g mL}^{-1}$. The calibration curve is depicted in the ESI,† as well as the absorption spectrum of the polystyrene dispersion.

Aerosol filtration. For the aerosol filtration tests, a Palas MFP 2000 filter test station was used. The test was performed with bis(2-ethylhexyl)sebacate (PALAS DEHS) as a test aerosol. The total volume flow was 8.5 L min^{-1} at a flow velocity of 5 cm s^{-1} and a filter area of 28.3 cm^2 . A total number of ca. 30 000 particles was measured per filtration test (PALAS aerosol sensor welas® 2100) and at least three filters were tested for each material.

Water-oil separation. For each experiment 4 mL of a mixture of water (colored with methylene blue) and chloroform was used 1:1 (v/v). Circular shaped filters with a diameter of 10 mm were cut out of the membranes using a scalpel and placed in a filtration apparatus, limiting the available filtration area to 0.38 cm^2 . Each membrane was tested in triplicate and the membranes were reused 10 times. The total time to complete separation of chloroform and water was noted to calculate the flux ($\text{L m}^{-2} \text{h}^{-1}$) according to the formula:

$$\text{Flux} = \frac{V}{A \times \Delta t}$$

where V is the total volume of the organic phase (L), A is the available area (m^2) and Δt is the total separation time (h).

Measurement of the water content. A Karl-Fischer titrator 831KF Coulometer (Metrohm) with diaphragm was used to measure the residual water content in the organic phase. Coulomat AG and Coulomat CG were used as anolyte and catholyte for the measurement at 25 $^{\circ}\text{C}$. Measurements were performed in duplicates and the statistical average is given as the result.

Ultraviolet/visible light spectroscopy (UV-Vis). UV-Vis measurements were performed on a V-630 spectrometer (Jasco) using a quartz cuvette with a measurement depth of 10 mm. The spectrum of the polystyrene-microparticles (PS-MP) was measured in the range of 200–800 nm, with a resolution of 2 nm. Quantitative measurements were performed at the absorption maximum of 280 nm. A calibration was performed in the range of 1.875 ppm to 30 ppm in triplicate. The calibration standards were prepared by dilution of a concentrated PS-MP dispersion with water.

Results and discussion

Evaluation of optimal electrospinning parameters

PA 6.9 was synthesized by melt polycondensation of the PA-salt formed by mixing azelaic acid and hexamethylene diamine in ethanolic solution as previously shown by Tao *et al.*⁶⁸ The polymer was drawn out in molten state and grinded to receive granulates with a maximum diameter of 2 mm. SEC measurement of the PA 6.9 confirmed a molecular weight of 34 800 with a dispersity of 2.2, consistent with standard commercial polyamides (Fig. S2†). The PA 6.9 was readily soluble in formic acid/chloroform 1:1 (v/v) (FA/ CHCl_3) with concentrations of up to 20 wt%. The resulting polymer solutions were increasing in viscosity with increasing polymer content. Electrospinning of the final solutions was performed to adjust the parameters for a stable process. It was found, that the viscosity had a great influence on the electrospinning process and no stable jet was formed for the solution with 20 wt% PA 6.9. The growth of stactite-like structures at the tip of the needle resulting from evaporation of the solvent was observed, which partly blocked the needle. In contrast, the viscosity of the 5 wt% solution was too low and resulted in strong droplet formation. These results are in line with the observations made for the electrospinning



of PA 6.9 from mixtures of formic acid and acetic acid, where solutions between 10 and 20 wt% were spinnable.⁶⁶ Finally, steady state electrospinning could be performed for solutions of PA 6.9 with 10, 12.5 and 15 wt% in FA/CHCl₃ 1 : 1 (v/v) to form a self-standing membrane. The duration of the electrospinning process of the polymer solutions was adjusted to prepare nonwoven membranes with a comparable thickness in the range of 54–60 μm.

Membrane characterization

The morphology and fiber diameter of the electrospun membranes were analyzed *via* SEM. From the SEM images uniform and smooth fibers can be seen and no formation of beads (Fig. 1). Increasing the polymer concentration also led to an increase of the fiber diameter, which is typical for electrospun polymer fibers. Similar observations were made for electrospun fibers of PA 6.6 from formic acid/chloroform 3 : 1 (v/v)⁷⁰ and PA 6.9 from formic acid/acetic acid 1 : 1 (v/v).⁶⁶ This might be due to the increased viscosity with increasing polymer concentration, resulting in a lower stretching of the fibers in the Taylor cone. Additionally, a higher polymer concentration also means a lower solvent to polymer ratio. As the solvent evaporates during the electrospinning process, the polymer spends less time in the dissolved state if there is less solvent to begin with, leading again to a lower stretching and thus thicker fibers. Hence, a higher polymer concentration, meaning less solvent per polymer, leads to thicker fibers. Furthermore, the distribution of the fiber diameter is quite narrow for all EFMs made from PA 6.9 with standard deviations of <15%. This shows the great potential of electrospinning for the production of uniform sub-microfibers. Spider net-like structures were observed in all electrospun nonwovens, with a higher prevalence with increasing polymer concentration (Fig. S1†). Similar observations were made in earlier publications for EFMs made from PA 6 and PA 6.6 with increasing polymer concentration.⁷¹ The presence of these structures may be advantageous in terms of filtration performance and they have also been shown to improve the mechanical properties of EFMs.⁷²

The mean pore size of the electrospun nonwovens was determined with a capillary flow porometer. Similar to the fiber diameter, the pore size increases with the polymer concentration from 0.55 μm to 1.14 μm (Table 1 and Fig. 2D). The pore structure of electrospun membranes is based on the number of fiber to fiber contacts, as the fibers act as pore boundaries and define the pore.^{73,74} The increased viscosity of the polymer solution due to the increased concentration impacts the bending stability of the fibers during solidification between the nozzle and the receiver.^{75,76} The resulting change in packing density leads to a lower number of fiber to fiber contacts and ultimately to an increase in pore size.⁷⁷ Hence, the pore size of the EFMs prepared from PA 6.9 can be adjusted by the polymer concentration, much like the fiber diameter. Additionally, the pore size distribution was very narrow for all EFMs, which is advantageous for particle filtration (Fig. S3†). Particles having a larger diameter than the pore size will therefore be filtered more easily and with a high

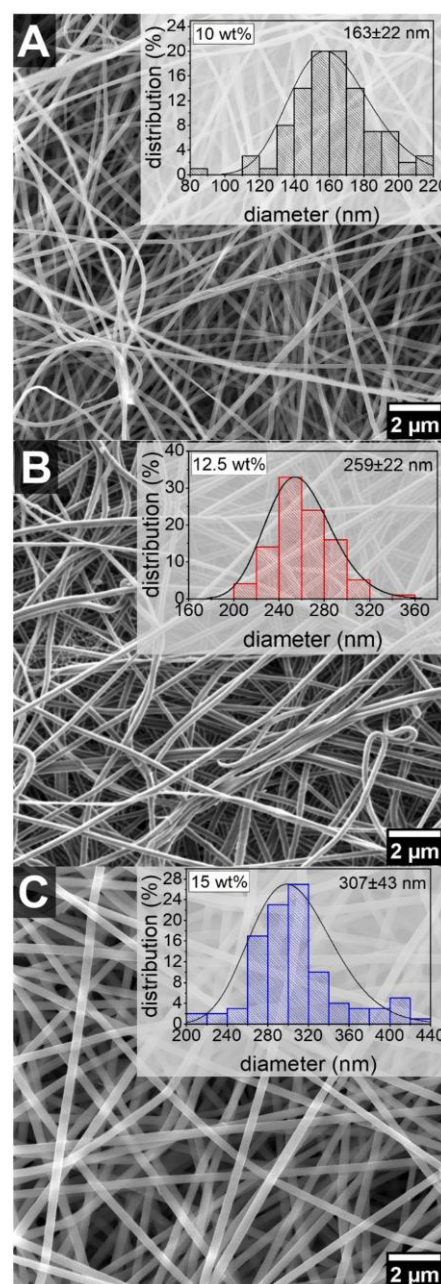
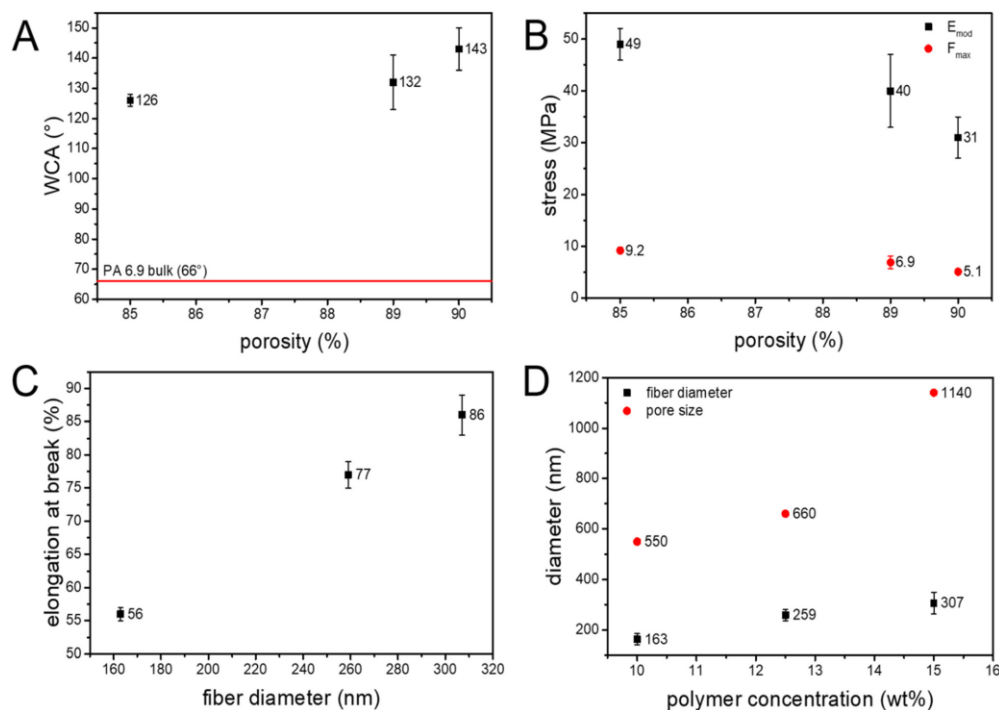


Fig. 1 SEM images and fiber diameter distributions of EFMs prepared from (A) 10 wt%, (B) 12.5 wt% and (C) 15 wt% solutions of PA 6.9 in formic acid/chloroform 1 : 1 v/v.



Table 1 Membrane properties of the PA 6.9 electrospun nonwovens and commercial syringe filter

Material	Thickness [μm]	Average fiber diameter [nm]	Mean pore size [μm]	Areal density [g m ⁻²]	Porosity [%]	Water contact angle [°]
PA 6.9_10 wt%	54 ± 4	163 ± 22	0.55	6.4 ± 0.4	89	132 ± 9
PA 6.9_12.5 wt%	62 ± 2	259 ± 22	0.66	9.7 ± 0.4	85	126 ± 2
PA 6.9_15 wt%	60 ± 3	307 ± 43	1.14	6.8 ± 0.6	90	143 ± 7
PA syringe filter	131 ± 3		0.2			22 ± 2

**Fig. 2** Different membrane characteristics of the EFMs made from PA 6.9, (A) water contact angle (WCA) and (B) stiffness (E_{mod}) and ultimate tensile strength (F_{max}) in dependence of the porosity, (C) elongation at break against the fiber diameter and (D) fiber diameter and pore size against the polymer concentration.

efficiency. The pore size of the prepared membranes is also in the range of typical microfiltration membranes.⁷⁸

The wettability of electrospun membranes was investigated by measurement of the water contact angle. Interestingly, the electrospun nonwovens showed hydrophobic surface properties with contact angles of $>120^\circ$. In contrast, PA 6.9 films have a water contact angle of 66° .⁷⁹ This is due to the high dependency of the water contact angle on the surface morphology of the electrospun nonwoven. Decreasing the surface roughness of an EFM prepared from PA 6.6 resulted in a 40% lower water contact angle, making the membrane more hydrophilic.⁸⁰ The high contact angle and resulting hydrophobic be-

havior of the EFMs made from PA 6.9 can therefore be explained by their surface roughness. The electrospun nonwovens produced are highly porous structures ($>85\%$ porosity) with a high surface roughness.⁷⁴ As these pores are typically filled with air (contact angle of 180°), the Cassie-Baxter equation needs to be applied to describe the contact angle of these electrospun membranes.^{81,82}

$$\cos \theta = \sigma_1 \times (1 + \cos \theta_1) - 1$$

With θ as the resulting contact angle of the EFM, σ_1 as the solids content of the material and θ_1 as the bulk contact angle of the solid material.



For the EFMs made from PA 6.9 a dependency of the contact angle on the porosity of the membrane could be observed, where an increasing porosity resulted in an increasing contact angle (Table 1 and Fig. 2A). This is further evidence that the Cassie–Baxter model should be applied here, since increasing porosity leads to a lower solids content of the material at the surface of the membrane and thus to an increased hydrophobicity.

The mechanical stability of a filtration membrane is of great importance for its performance. A high mechanical stability prevents the pores from widening due to increased backpressure and ultimately from rupturing during use. Typically EFMs are known to have poor mechanical properties due to their high porosity, random orientation and poor fiber to fiber bonding.^{45,83} Several different attempts have been made to improve the mechanical properties of EFMs including UV-cross-linking,^{33,34} and solvent vapor treatment.⁸⁰ Owing to the generally good mechanical properties of polyamides the EFMs prepared from PA 6.9 showed a much higher tensile strength than membranes prepared from other typical materials like polyvinylidene fluoride (PVDF) and polyacrylonitrile (PAN) (Table 2). Additionally, the results from uniaxial tensile testing of the PA 6.9 membranes are comparable to EFMs made from PA 6.6.⁸⁴

The prepared EFMs showed increasing stiffness (E_{mod}) and tensile strength (F_{max}) with decreasing porosity of the nonwoven (Fig. 2B). Interfiber bond fracture has been proven to be the major damage mechanism for electrospun nonwovens.⁸⁵ It was shown, that less interfiber bonds are broken in denser networks, resulting in a higher mechanical stability. Therefore, nonwovens having a lower porosity are stronger and stiffer than ones with a higher porosity.^{86,87} Additionally, the nonwovens showed an increasing elongation at break with the fiber diameter (Fig. 2C). This is again in line with observations made for EFMs made from PA 6.6.⁷⁰ This could be explained by the also larger pore size leading to a smaller number of loops between the nonwovens, resulting in a longer elongation until the fibers are aligned. Additionally, the thicker fibers could potentially be cold stretched to a greater extent than thinner fibers.

Microplastic particle filtration in water

The filtration performance of the bio-based EFMs for the removal of microplastics from aqueous media was investigated

Table 2 Mechanical properties of EFMs made from PA 6.9 compared to existing materials

Material	F_{max} [MPa]	Elongation at break [%]	E_{mod} [MPa]	Ref.
PA 6.9_10 wt%	6.9 ± 1.2	56 ± 1	40 ± 7	This work
PA 6.9_12.5 wt%	9.2 ± 0.6	77 ± 2	49 ± 3	This work
PA 6.9_15 wt%	5.1 ± 0.4	86 ± 3	31 ± 4	This work
PA 6.6	6.5 ± 0.6	67 ± 11	45 ± 2	84
PVDF	2.8	76	58	88
PAN	4.9	23	—	89
PLA	1.8	200	15	90

using a dispersion of polystyrene microparticles (PS-MP) in water. Therefore, polystyrene microspheres were prepared by surfactant-free emulsion polymerization in water using the initiator potassium persulfate.⁹¹ The resulting polystyrene spheres had a hydrodynamic diameter of 679 ± 4 nm and formed a stable emulsion in water with a concentration of 300 ppm (Fig. S5†). All three bio-based membranes and the commercial syringe filter were able to remove the PS-MP during filtration with a remarkable efficiency of >99.7%, even after a prolonged filtration time of 45 minutes (Fig. 3A). Comparison with other electrospun membranes reveals that the bio-based EFMs prepared from PA 6.9 show similar performance for the removal of microparticles as EFMs made from conventional materials (Table 3). See Fig. S7† for the experimental setup used for the microplastic particle filtration tests.

There was a large difference in the permeability during microplastic filtration between the EFMs with a pore size of 0.55 μm (PA 6.9_10 wt%) and 0.66 μm (PA 6.9_12.5 wt%). A 0.11 μm larger pore size resulted in a 123% higher initial permeability (Fig. 3B). Further increasing the pore size, on the other hand, did not lead to a significant change of the permeability. Furthermore, only a small decrease of the per-

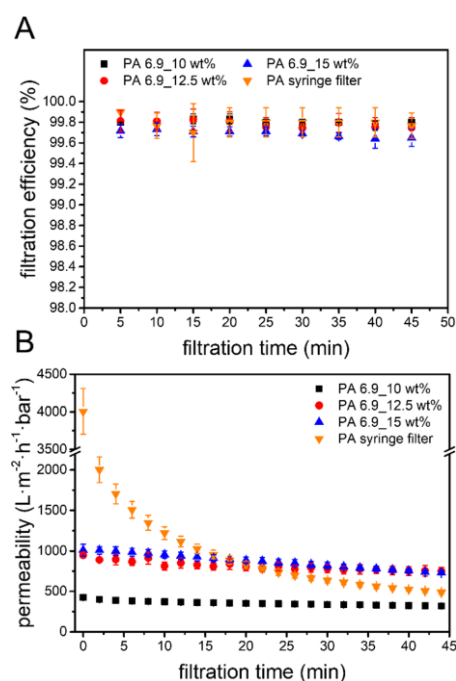


Fig. 3 (A) Filtration efficiency and (B) permeability over time for PS-MP removal using the bio-based EFMs and the PA syringe filter at 1 mL min⁻¹.



Table 3 Filtration performance of different EFMs for the removal of microplastic particles from aqueous media

Material	Membrane thickness [μm]	Particle type and (size) [μm]	Mean pore size [μm]	Filtration efficiency [%]	Initial permeability [$\text{L m}^{-2} \text{h}^{-1} \text{bar}^{-1}$]	Ref.
PA 6.9_10 wt%	54 \pm 4	PS-MP (0.7)	0.55	99.8	424 \pm 5	This work
PA 6.9_12.5 wt%	62 \pm 2	PS-MP (0.7)	0.66	99.8	949 \pm 35	This work
PA 6.9_15 wt%	60 \pm 3	PS-MP (0.7)	1.14	99.7	1011 \pm 73	This work
PA 6	150 \pm 50	PS-MP (1)	0.006	95.9	—	40
PA 6/cellulose	97	PS-MP (0.5)	0.64	>99	570	41
rPET	—	PS-MP (0.5)	0.2	>99	3336 \pm 870	92
PAN	ca. 70	Unspecified MP (10)	0.15–2	93	22 733	89
PVDF	300	PS-MP (1)	4–11	98	1985	38
PVDF	220	PS-MP (3)	3.59	99.0	45 200	88

meability was observed for all bio-based EFMs during the filtration trials. In contrast, the commercial PA syringe filter showed a much steeper decrease of the permeability, especially in the first 10 minutes. As a result, the performance of the syringe filter became worse than the bio-based EFMs with longer filtration time. After 20 minutes, the bio-based EFMs with a pore size of $>0.66 \mu\text{m}$ showed a higher permeability and therefore better performance. These results indicate a possible application of the bio-based EFMs for the removal of microplastics from aqueous media.

Observation of the membrane cross-section after filtration shows a cake layer of PS microparticles on the top and only a few particles on the bottom side of the membrane (Fig. 4A and Fig. S8†). In the close-up image of the membrane cross section (Fig. 4B and Fig. S8†) some layer separation in the membrane can be observed, allowing a look inside of the membrane. In between the layers, no particles can be observed. This would indicate a surface filtration mechanism which is typical for membranes with smaller or similar pores than the particle size. A surface filtration mechanism would be beneficial in terms of sustainability, as it opens up the possibility of back-flushing the membrane in order to reactivate and reuse it. But, these results are only an indication. A closer examination of the inside of the membrane after filtration could provide a better understanding of the filtration mechanism.

Aerosol filtration

The suitability for the removal of aerosols from air was also investigated using the bio-based EFMs from PA 6.9. All three membranes showed excellent efficiency ($>99.3\%$) for the removal of the test aerosol particles down to $0.3 \mu\text{m}$ (Fig. 5A). With smaller particles the filtration efficiency decreases to 51–83% for $0.2 \mu\text{m}$ particles. For comparison, FFP3 masks are defined by DIN EN 149 to have a filtration efficiency of $>99\%$ for particles sizes down to $0.6 \mu\text{m}$. The bio-based EFMs therefore exceed the requirements for these face masks in terms of filtration efficiency. They are more comparable to so-called EPA (efficient particulate air) filters, which are defined by the ISO 29463-1 to have a filtration efficiency of greater 99.5% for particles with a diameter of $0.3 \mu\text{m}$.

A good air filtration membrane not only needs to have a high filtration efficiency, but also a low pressure drop. EPA

filters should have a maximum pressure drop of 300 Pa and FFP3 masks are not allowed to have a pressure drop of over 500 Pa. In comparison, the prepared EFMs exhibit much higher pressure drops of $2090 \pm 286 \text{ Pa}$ for PA 6.9_10 wt%, $1710 \pm 182 \text{ Pa}$ for 12.5 wt% and $2200 \pm 381 \text{ Pa}$ for 15 wt%, exceeding those limitations. This might be due to the thickness of the membrane, which is known to influence the pressure drop of EFMs.³⁰ Thinner membranes might still be able to show high filtration efficiency with a reduced pressure drop. Additionally, an increasing trend of the pressure drop with decreasing porosity was observed for the bio-based EFMs (Fig. 5B). This is not surprising, however, since a higher porosity offers less resistance to air flow, a well-known effect in air filtration membranes.^{28,93,94} The quality factor is a useful parameter to compare the performance of different filtration membranes, as it combines filtration efficiency and pressure drop. Commercial air filters such as HEPA (high efficiency particulate air), cabin air filters and FFP3 face masks have high quality factors of 15, 10 and 19 kPa^{-1} respectively.^{95,96} Compared to these, the bio-based EFMs exhibit lower performance with quality factors ranging between 2.5 and 2.9 kPa^{-1} for particles of $0.3 \mu\text{m}$ in diameter (Fig. 5B). This is mainly due to the high pressure drop, as the filtration efficiency for all three membranes was $>99.3\%$. Other air filtration EFMs made from PA, PAN or poly(ethylene oxide) (PEO) often have quality factors between 15 and 50 kPa^{-1} , compared to which the bio-based EFMs from PA 6.9 are also inferior.⁷¹

Water–oil separation

Polyamides generally show a high stability against solvents, making them interesting materials for applications in harsh environments. The EFMs prepared from bio-based PA 6.9 also show hydrophobic surface behavior, making them promising candidates for the separation of water from oil. In order to highlight their potential application, the performance for the separation of chloroform and water in gravity driven filtration was investigated. All three membranes showed excellent separation efficiencies of $>99\%$ independent of their pore size and porosity. This is comparable with results obtained for other electrospun, hydrophobic membranes like polyimide (PI) modified with thiolated graphene (GSH/PI) and PVDF-HFP (Table 4). The PVDF-HFP membrane shows a good separation



Open Access Article. Published on 16 January 2024. Downloaded on 3/10/2024 5:46:11 PM.
This article is licensed under a Creative Commons Attribution 3.0 Unported Licence.

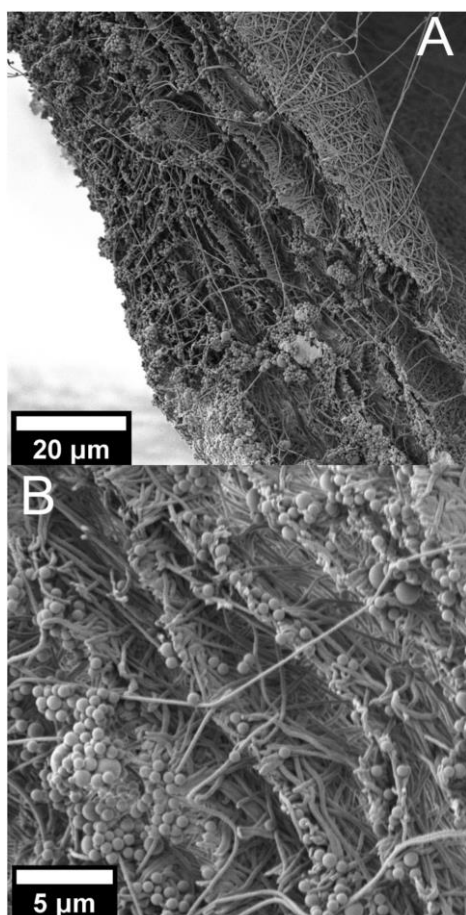


Fig. 4 SEM pictures of the cross section of the PA 6.9_12.5 wt% membrane after filtration, (A) at 1000 \times magnification and (B) at 3500 \times magnification.

efficiency, but at a much lower flux than the membranes prepared from PA 6.9 ($120 \text{ L m}^{-2} \text{ h}^{-1}$).⁵⁰ The lower flux could be due to the higher membrane thickness, which is twice that of the PA 6.9 membranes. The modified GSH/PI membranes on the other hand shows a high flux of $2744 \text{ L m}^{-2} \text{ h}^{-1}$ together with an excellent separation efficiency of 99.9%. However, the modification of the electrospun PI membranes to achieve the GSH/PI membranes involves multiple reaction steps. The PA 6.9 membranes on the other hand can be easily produced by electrospinning. Furthermore, they are self-standing membranes without modifications, which facilitates recycling of the membranes considerably. They also combine a high separation efficiency of 99.9% with a high flux ranging from 985 to 5345

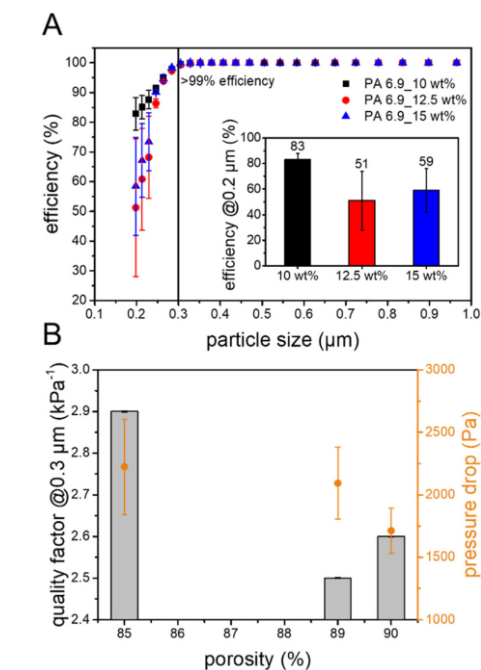


Fig. 5 (A) Particle size dependent filtration efficiency and (B) pressure drop and quality factor against porosity for the aerosol filtration using the bio-based EFMs.

Table 4 Performance of different hydrophobic EFMs for the separation of water and oil

Material	Mean pore size [μm]	Separation efficiency [%]	Initial flux [$\text{L m}^{-2} \text{ h}^{-1}$]	Ref.
PA 6.9_10 wt%	0.55	99.9 ± 0.0	2878	This work
PA 6.9_12.5 wt%	0.66	99.9 ± 0.1	985	This work
PA 6.9_15 wt%	1.14	99.9 ± 0.0	5345	This work
GSH/PI	—	99.9	2744	97
PVDF-HFP	1.8	99	120	50

$\text{m}^{-2} \text{ h}^{-1}$. We observed an increasing permeate flux with the porosity of the membranes. This can be explained by the lower drag acting on the permeate during the flow through the membrane with a higher porosity.

The reusability of the membranes was investigated by repeating the separation tests ten times using the same membrane (Fig. 6). No significant loss in separation efficiency was observed during the cycles. The permeate flux was also very stable during the cycles and only a slight decrease could be observed over ten cycles.

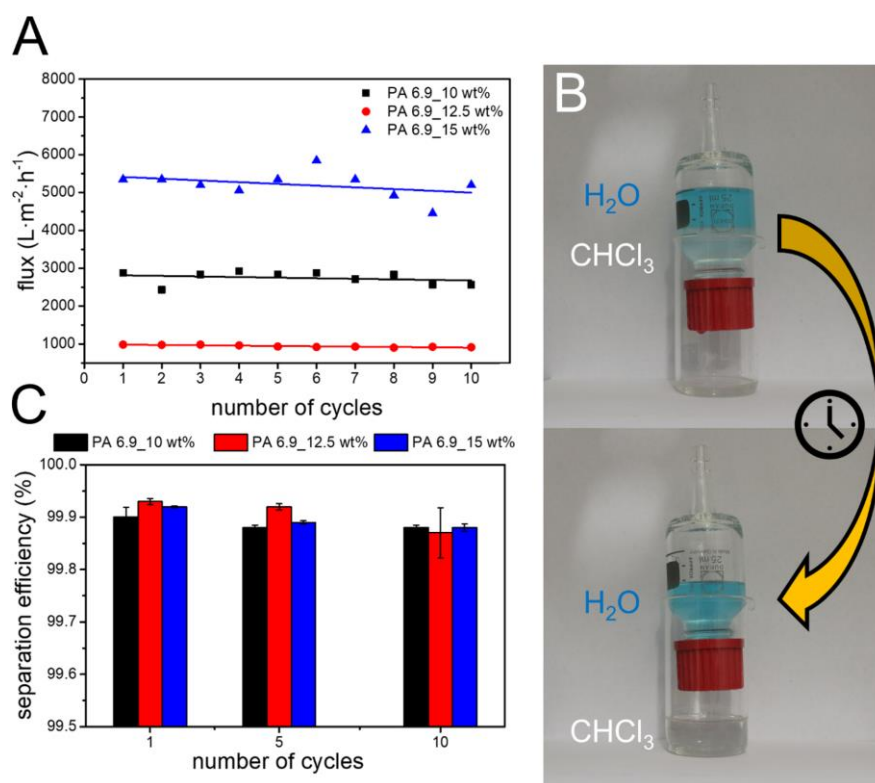


Fig. 6 Results for the separation of water and chloroform, (A) the initial permeate flux for each separation cycle (linear fit), (B) filtration setup with a mixture of chloroform and water before and after filtration, (C) separation efficiency during the first, fifth and tenth cycle.

Conclusions

Bio-based EFMs were prepared by electrospinning from solutions of vegetable oil-sourced PA 6.9 in chloroform/formic acid. Their morphology, as well as their mechanical properties and surface properties were analyzed and tailored by changing the polymer concentration during the electrospinning process. A great influence of the porosity on the mechanical strength and the surface hydrophobicity was observed. The EFMs also showed high efficiency for the removal of microplastic particles from water under prolonged time. Additionally, the membranes showed comparable water permeability to PA composite membranes and better performance than commercial syringe filters. The possible surface filtration mechanism also opens the opportunity of recycling by back-flushing. This highlights the potential of sustainable EFMs prepared from PA 6.9 for the removal of microplastics from polluted water. Furthermore, the membranes were successfully applied for the removal of aerosols from air. The EFMs achieved a filtration efficiency of >99.3% for aerosol particles down to 0.3 μm , the

industry standard most penetrating particle size, and up to 83% for 0.2 μm particles. However, the pressure drop of the as-spun membranes was too high for commercial application as air filters. Thinner membranes might be able to achieve similar filtration efficiencies at a lower pressure drop. Due to their high hydrophobicity, the EFMs showed excellent performance for the separation of water and oil with separation efficiencies of 99.9% while maintaining a high permeate flux of up to 5345 $\text{L m}^{-2} \text{h}^{-1}$. Reusability of the EFMs for the separation of water and oil was also proven and the membranes could be reused up to 10 times without any significant loss in separation efficiency and permeate flux. In conclusion, this work highlights the potential of PA 6.9 for the production of sustainable filter membranes.

Author contributions

All authors contributed to the manuscript. All authors have given approval to the final version of the manuscript.



Conflicts of interest

There are no conflicts to declare.

Acknowledgements

The authors are indebted for partial financial support to the Federal Ministry of Education and Research (Research project Algae Tex, no. 031b1058B).

This study was cofunded by the Deutsche Forschungsgemeinschaft (DFG, German Research Foundation) – SFB 1357-391977956.

The authors gratefully acknowledge the use of equipment and assistance offered by the Keylab “Small Scale Polymer Processing” and by the Keylab “Electron- and Optical Microscopy” of the Bavarian Polymer Institute at the University of Bayreuth.

References

- 1 K. D. Patel, H.-W. Kim, J. C. Knowles and A. Poma, Molecularly Imprinted Polymers and Electrospinning: Manufacturing Convergence for Next-Level Applications, *Adv. Funct. Mater.*, 2020, **30**, 2001955.
- 2 M. O. Pretschner, G. Sitaru, M. Dietel, H. Schmalz, S. Gekle and S. Agarwal, Post-Process-Functionalized Catalytic Electrospun and 2D-Printed Structures for Wolf-Lamb-Type Catalysis, *ACS Appl. Polym. Mater.*, 2021, **3**, 1349–1357.
- 3 W. Shi, H. Li, R. Zhou, X. Qin, H. Zhang, Y. Su and Q. Du, Preparation and characterization of phosphotungstic acid/PVA nanofiber composite catalytic membranes via electrospinning for biodiesel production, *Fuel*, 2016, **180**, 759–766.
- 4 E. Formo, E. Lee, D. Campbell and Y. Xia, Functionalization of electrospun TiO₂ nanofibers with Pt nanoparticles and nanowires for catalytic applications, *Nano Lett.*, 2008, **8**, 668–672.
- 5 S. Pazhaniswamy, S. A. Joshi, H. Hou, A. K. Parameswaran and S. Agarwal, Hybrid Polymer Electrolyte Encased Cathode Particles Interface-Based Core-Shell Structure for High-Performance Room Temperature All-Solid-State Batteries, *Adv. Energy Mater.*, 2023, **13**, 2202981.
- 6 A. Laezza, A. Celeste, M. Curcio, R. Teghil, A. de Bonis, S. Brutti, A. Pepe and B. Bochicchio, Cellulose Nanocrystals as Additives in Electrospun Biocompatible Separators for Aprotic Lithium-Ion Batteries, *ACS Appl. Polym. Mater.*, 2023, **5**, 1453–1463.
- 7 H. Cai, X. Tong, K. Chen, Y. Shen, J. Wu, Y. Xiang, Z. Wang and J. Li, Electrospun Polyethylene Terephthalate Nonwoven Reinforced Polypropylene Separator: Scalable Synthesis and Its Lithium Ion Battery Performance, *Polymers*, 2018, **10**, 574.
- 8 A. A. Nayl, A. I. Abd-Elhamid, N. S. Awwad, M. A. Abdelgawad, J. Wu, X. Mo, S. M. Gomha, A. A. Aly and S. Bräse, Review of the Recent Advances in Electrospun Nanofibers Applications in Water Purification, *Polymers*, 2022, **14**, 1594.
- 9 Z. Uddin, F. Ahmad, T. Ullan, Y. Nawab, S. Ahmad, F. Azam, A. Rasheed and M. S. Zafar, Recent trends in water purification using electrospun nanofibrous membranes, *Int. J. Environ. Sci. Technol.*, 2021, 1–28.
- 10 I. A. Borojeni, G. Gajewski and R. A. Riahi, Application of Electrospun Nonwoven Fibers in Air Filters, *Fibers*, 2022, **10**, 15.
- 11 P. Risch and C. Adlhart, A Chitosan Nanofiber Sponge for Oyster-Inspired Filtration of Microplastics, *ACS Appl. Polym. Mater.*, 2021, **3**, 4685–4694.
- 12 F. Kessel, M. Friefel, O. Hohn, L. Klopsch, C. Zöllner, C. Dirks, M. Scheiffel, F. Vogel and R. Jemmali, Three-dimensional preforming via wet-laid nonwoven technology for ceramic matrix composites, *J. Eur. Ceram. Soc.*, 2023, **43**, 5148–5158.
- 13 R. Asmatulu and W. S. Khan, in *Synthesis and applications of electrospun nanofibers*, ed. R. Asmatulu and W. S. Khan, Elsevier, Oxford, United Kingdom, 2019, pp. 135–152.
- 14 G. Nallathambi, D. Baskar and A. K. Selvam, Preparation and characterization of triple layer membrane for water filtration, *Environ. Sci. Pollut. Res.*, 2020, **27**, 29717–29724.
- 15 X. Xu, Y. Yang, T. Liu and B. Chu, Cost-effective polymer-based membranes for drinking water purification, *Giant*, 2022, **10**, 100099.
- 16 T. M. Subrahmanya, A. Bin Arshad, P. T. Lin, J. Widakdo, H. K. Makari, H. F. M. Austria, C.-C. Hu, J.-Y. Lai and W.-S. Hung, A review of recent progress in polymeric electrospun nanofiber membranes in addressing safe water global issues, *RSC Adv.*, 2021, **11**, 9638–9663.
- 17 A. Mamun, T. Blachowicz and L. Sabantina, Electrospun Nanofiber Mats for Filtering Applications-Technology, Structure and Materials, *Polymers*, 2021, **13**, 1368.
- 18 J. Matulevicius, L. Kliucininkas, T. Prasauskas, D. Buivydiene and D. Martuzevicius, The comparative study of aerosol filtration by electrospun polyamide, polyvinyl acetate, polyacrylonitrile and cellulose acetate nanofiber media, *J. Aerosol Sci.*, 2016, **92**, 27–37.
- 19 M. Y. Ghadhbhan, K. T. Rashid, A. A. AbdulRazak and Q. F. Alsahy, Recent progress and future directions of membranes green polymers for oily wastewater treatment, *Water Sci. Technol.*, 2023, **87**, 57–82.
- 20 Y. Su, T. Fan, W. Cui, Y. Li, S. Ramakrishna and Y. Long, Advanced Electrospun Nanofibrous Materials for Efficient Oil/Water Separation, *Adv. Fiber Mater.*, 2022, **4**, 938–958.
- 21 H. M. Mousa, H. S. Fahmy, G. A. M. Ali, H. N. Abdelhamid and M. Ateia, Membranes for Oil/Water Separation: A Review, *Adv Mater. Interfaces*, 2022, **9**, 2200557.
- 22 J. Zhang, F. Zhang, J. Song, L. Liu, Y. Si, J. Yu and B. Ding, Electrospun flexible nanofibrous membranes for oil/water separation, *J. Mater. Chem. A*, 2019, **7**, 20075–20102.
- 23 W. Ma, Q. Zhang, D. Hua, R. Xiong, J. Zhao, W. Rao, S. Huang, X. Zhan, F. Chen and C. Huang, Electrospun



- fibers for oil–water separation, *RSC Adv.*, 2016, **6**, 12868–12884.
- 24 R. S. Barhate, C. K. Loong and S. Ramakrishna, Preparation and characterization of nanofibrous filtering media, *J. Membr. Sci.*, 2006, **283**, 209–218.
- 25 Y. C. Ahn, S. K. Park, G. T. Kim, Y. J. Hwang, C. G. Lee, H. S. Shin and J. K. Lee, Development of high efficiency nanofilters made of nanofibers, *Curr. Appl. Phys.*, 2006, **6**, 1030–1035.
- 26 C. Liu, P.-C. Hsu, H.-W. Lee, M. Ye, G. Zheng, N. Liu, W. Li and Y. Cui, Transparent air filter for high-efficiency PM2.5 capture, *Nat. Commun.*, 2015, **6**, 6205.
- 27 X. Wang, H. Xiang, C. Song, D. Zhu, J. Sui, Q. Liu and Y. Long, Highly efficient transparent air filter prepared by collecting-electrode-free bipolar electrospinning apparatus, *J. Hazard. Mater.*, 2020, **385**, 121535.
- 28 D. Buivydiene, A. M. Todea, C. Asbach, E. Krugly, D. Martuzevicius and L. Kliucininkas, Composite micro/nano fibrous air filter by simultaneous melt and solution electrospinning, *J. Aerosol Sci.*, 2021, **154**, 105754.
- 29 W. W.-F. Leung, C.-H. Hung and P.-T. Yuen, Effect of face velocity, nanofiber packing density and thickness on filtration performance of filters with nanofibers coated on a substrate, *Sep. Purif. Technol.*, 2010, **71**, 30–37.
- 30 A. Rajak, D. A. Hapidin, F. Iskandar, M. M. Munir and K. Khairurrijal, Electrospun nanofiber from various source of expanded polystyrene (EPS) waste and their characterization as potential air filter media, *Waste Manage.*, 2020, **103**, 76–86.
- 31 J. Xue, T. Wu, Y. Dai and Y. Xia, Electrospinning and Electrospun Nanofibers: Methods, Materials, and Applications, *Chem. Rev.*, 2019, **119**, 5298–5415.
- 32 Change, Environment, Climate and Health, State of the world's drinking water: An urgent call to action to accelerate progress on ensuring safe drinking water for all, *World Health Organization*, 2022.
- 33 A.-K. Müller, Z.-K. Xu and A. Greiner, Preparation and Performance Assessment of Low-Pressure Affinity Membranes Based on Functionalized, Electrospun Polyacrylates for Gold Nanoparticle Filtration, *ACS Appl. Mater. Interfaces*, 2021, **13**, 15659–15667.
- 34 A.-K. Müller, Z.-K. Xu and A. Greiner, Sustainable Electrospun Affinity Membranes for Water Remediation by Removing Metal and Metal Oxide Nanoparticles, *ACS Appl. Polym. Mater.*, 2021, **3**, 5739–5748.
- 35 K. Razmgar and M. Nasirae, Polyvinyl alcohol -based membranes for filtration of aqueous solutions: A comprehensive review, *Polym. Eng. Sci.*, 2022, **62**, 25–43.
- 36 S. A. Parekh, R. N. David, K. K. R. Bannuru, L. Krishnaswamy and A. Baji, Electrospun Silver Coated Polyacrylonitrile Membranes for Water Filtration Applications, *Membranes*, 2018, **8**, 59.
- 37 P. Arribas, M. C. García-Payo, M. Khayet and L. Gil, Heat-treated optimized polysulfone electrospun nanofibrous membranes for high performance wastewater microfiltration, *Sep. Purif. Technol.*, 2019, **226**, 323–336.
- 38 R. Gopal, S. Kaur, Z. Ma, C. Chan, S. Ramakrishna and T. Matsuura, Electrospun nanofibrous filtration membrane, *J. Membr. Sci.*, 2006, **281**, 581–586.
- 39 J. Lev, M. Holba, M. Došek, L. Kalhotka, P. Mikula and D. Kimmmer, A novel electrospun polyurethane nanofibre membrane—production parameters and suitability for wastewater (WW) treatment, *Water Sci. Technol.*, 2014, **69**, 1496–1501.
- 40 D. Aussawasathien, C. Teerawattananon and A. Vongachariya, Separation of micron to sub-micron particles from water: Electrospun nylon-6 nanofibrous membranes as pre-filters, *J. Membr. Sci.*, 2008, **315**, 11–19.
- 41 A. Fauzi, D. A. Hapidin, M. M. Munir, F. Iskandar and K. Khairurrijal, A superhydrophilic bilayer structure of a nylon 6 nanofiber/cellulose membrane and its characterization as potential water filtration media, *RSC Adv.*, 2020, **10**, 17205–17216.
- 42 F. Yalcinkaya, B. Yalcinkaya and J. Hruza, Electrospun Polyamide-6 Nanofiber Hybrid Membranes for Wastewater Treatment, *Fibers Polym.*, 2019, **20**, 93–99.
- 43 N. S. Abd Halim, M. D. H. Wirzal, M. R. Bilad, N. A. H. Md Nordin, Z. Adi Putra, A. R. Mohd Yusoff, T. Narkkun and K. Faungnawakij, Electrospun Nylon 6,6/ZIF-8 Nanofiber Membrane for Produced Water Filtration, *Water*, 2019, **11**, 2111.
- 44 A. R. Jabur, L. K. Abbas and S. A. Moosa, Fabrication of Electrospun Chitosan/Nylon 6 Nanofibrous Membrane toward Metal Ions Removal and Antibacterial Effect, *Adv. Mater. Sci. Eng.*, 2016, **2016**, 1–10.
- 45 L. Huang and J. R. McCutcheon, Hydrophilic nylon 6,6 nanofibers supported thin film composite membranes for engineered osmosis, *J. Membr. Sci.*, 2014, **457**, 162–169.
- 46 J.-C. Chen, J.-A. Wu, K.-H. Lin, P.-J. Lin and J.-H. Chen, Preparation of microfiltration membranes with controlled pore sizes by interfacial polymerization on electrospun nanofibrous membranes, *Polym. Eng. Sci.*, 2014, **54**, 430–437.
- 47 X. Wang, J. Yu, G. Sun and B. Ding, Electrospun nanofibrous materials: a versatile medium for effective oil/water separation, *Mater. Today*, 2016, **19**, 403–414.
- 48 X. Han and Z. Guo, Graphene and its derivative composite materials with special wettability: Potential application in oil-water separation, *Carbon*, 2021, **172**, 647–681.
- 49 Z. Liu, B. Gao, X. Huang, H. Ke and J. Xu, Scale-up fabrication of PVDF-HFP nanofibrous membrane with unique surface properties for efficient separation of oil from water, *Text. Res. J.*, 2022, **92**, 1830–1842.
- 50 L. Zaidouny, M. Abou-Daher, A. R. Tehrani-Bagha, K. Ghali and N. Ghaddar, Electrospun nanofibrous polyvinylidene fluoride-co-hexafluoropropylene membranes for oil–water separation, *J. Appl. Polym. Sci.*, 2020, **137**, 49394.
- 51 C. Eang, B. Nim, P. Sreearunothai, A. Petchsuk and P. Opaprakasit, Chemical upcycling of polylactide (PLA) and its use in fabricating PLA-based super-hydrophobic and oleophilic electrospun nanofibers for oil absorption and oil/water separation, *New J. Chem.*, 2022, **46**, 14933–14943.



- 52 Z. Zhou, L. Liu and W. Yuan, A superhydrophobic poly (lactic acid) electrospun nanofibrous membrane surface-functionalized with TiO₂ nanoparticles and methyl-trichlorosilane for oil/water separation and dye adsorption, *New J. Chem.*, 2019, **43**, 15823–15831.
- 53 L. Liu and W. Yuan, A hierarchical functionalized biodegradable PLA electrospun nanofibrous membrane with superhydrophobicity and antibacterial properties for oil/water separation, *New J. Chem.*, 2018, **42**, 17615–17624.
- 54 S. Jiang, H. Schmalz, S. Agarwal and A. Greiner, Electrospinning of ABS nanofibers and their high filtration performance, *Adv. Fiber Mater.*, 2020, **2**, 34–43.
- 55 P. Sobolčiak, A. Tanvir, A. Popelka, J. Moffat, K. A. Mahmoud and I. Krupa, The preparation, properties and applications of electrospun co-polyamide 6,12 membranes modified by cellulose nanocrystals, *Mater. Des.*, 2017, **132**, 314–323.
- 56 P. Zhao, N. Qin, C. L. Ren and J. Z. Wen, Polyamide 6.6 separates oil/water due to its dual underwater oleophobicity/underoil hydrophobicity: Role of 2D and 3D porous structures, *Appl. Surf. Sci.*, 2019, **466**, 282–288.
- 57 S. Bhagyaraj, P. Sobolčiak, M. A. Al-Ghouti and I. Krupa, Copolyamide-Clay Nanotube Polymer Composite Nanofiber Membranes: Preparation, Characterization and Its Asymmetric Wettability Driven Oil/Water Emulsion Separation towards Sewage Remediation, *Polymers*, 2021, **13**, 3710.
- 58 R. Lv, M. Yin, W. Zheng, B. Na, B. Wang and H. Liu, Poly (vinylidene fluoride) fibrous membranes doped with polyamide 6 for highly efficient separation of a stable oil/water emulsion, *J. Appl. Polym. Sci.*, 2017, **134**, 44980.
- 59 V. K. Thakur and S. I. Voicu, Recent advances in cellulose and chitosan based membranes for water purification: A concise review, *Carbohydr. Polym.*, 2016, **146**, 148–165.
- 60 N. Fiol, Q. Tarrés, M. G. Vásquez, M. A. Pereira, R. T. Mendonça, P. Mutjé and M. Delgado-Aguilar, Comparative assessment of cellulose nanofibers and calcium alginate beads for continuous Cu(II) adsorption in packed columns: the influence of water and surface hydrophobicity, *Cellulose*, 2021, **28**, 4327–4344.
- 61 H. N. Chang, S. X. Hou, Z. C. Hao and G. H. Cui, Ultrasonic green synthesis of an Ag/CP nanocomposite for enhanced photodegradation effectiveness, *Ultrason. Sonochem.*, 2018, **40**, 1039–1048.
- 62 R. E. Abou-Zeid, A. Salama, Z. A. Al-Ahmed, N. S. Awwad and M. Youssef, Carboxylated cellulose nanofibers as a novel efficient adsorbent for water purification, *Cellul. Chem. Technol.*, 2020, **54**, 237–245.
- 63 W. Wang, J. Lin, J. Cheng, Z. Cui, J. Si, Q. Wang, X. Peng and L.-S. Turng, Dual super-amphiphilic modified cellulose acetate nanofiber membranes with highly efficient oil/water separation and excellent antifouling properties, *J. Hazard. Mater.*, 2020, **385**, 121582.
- 64 A. Todea, C. Deganutti, M. Spennato, F. Asaro, G. Zingone, T. Milizia and L. Gardossi, Azelaic Acid: A Bio-Based Building Block for Biodegradable Polymers, *Polymers*, 2021, **13**, 4091.
- 65 B. de Schoenmaker, L. van der Schueren, S. de Vrieze, P. Westbroek and K. de Clerck, Wicking properties of various polyamide nanofibrous structures with an optimized method, *J. Appl. Polym. Sci.*, 2011, **120**, 305–310.
- 66 B. de Schoenmaker, A. Goethals, L. van der Schueren, H. Rahier and K. de Clerck, Polyamide 6.9 nanofibres electrospun under steady state conditions from a solvent/non-solvent solution, *J. Mater. Sci.*, 2012, **47**, 4118–4126.
- 67 G. C. Goebel, A. C. Brown, H. F. Oehlschlaeger and R. P. Rolfes, *US Pat*, 2813113, 1957.
- 68 L. Tao, K. Liu, T. Li and R. Xiao, Preparation and properties of biobased polyamides based on 1,9-azelaic acid and different chain length diamines, *Polym. Bull.*, 2020, **77**, 1135–1156.
- 69 Y. Zhang, T. Paul, J. Brehm, M. Völk, V. Jérôme, R. Freitag, C. Laforsch and A. Greiner, Role of Residual Monomers in the Manifestation of (Cyto)toxicity by Polystyrene Microplastic Model Particles, *Environ. Sci. Technol.*, 2023, **57**, 9925–9933.
- 70 M. Afshari, R. Kotek, A. E. Tonelli and D.-W. Jung, in *Nanofibers and Nanotechnology in Textiles*, Elsevier, 2007, pp. 71–89.
- 71 J. Matulevicius, L. Kliucininkas, D. Martuzevicius, E. Krugly, M. Tichonovas and J. Baltrusaitis, Design and Characterization of Electrospun Polyamide Nanofiber Media for Air Filtration Applications, *J. Nanomater.*, 2014, **2014**, 1–13.
- 72 N. A. Barakat, M. A. Kanjwal, F. A. Sheikh and H. Y. Kim, Spider-net within the N6, PVA and PU electrospun nanofiber mats using salt addition: Novel strategy in the electrospinning process, *Polymer*, 2009, **50**, 4389–4396.
- 73 R. Bagherzadeh, S. S. Najari, M. A. Latifi, M. A. Tehran and L. Kong, A theoretical analysis and prediction of pore size and pore size distribution in electrospun multilayer nanofibrous materials, *J. Biomed. Mater. Res., Part A*, 2013, **101**, 2107–2117.
- 74 J. H. Wendorff, S. Agarwal and A. Greiner, *Electrospinning. Materials, processing, and applications*, John Wiley & Sons, Weinheim, Hoboken, N.J., 2012.
- 75 K. P. Feltz, E. A. Growney Kalaf, C. Chen, R. S. Martin and S. A. Sell, A review of electrospinning manipulation techniques to direct fiber deposition and maximize pore size, *Electrospinning*, 2017, **2**, 46–61.
- 76 C. Mit-uppatham, M. Nithitanakul and P. Supaphol, Ultrafine Electrospun Polyamide-6 Fibers: Effect of Solution Conditions on Morphology and Average Fiber Diameter, *Macromol. Chem. Phys.*, 2004, **205**, 2327–2338.
- 77 J. L. Lowery, N. Datta and G. C. Rutledge, Effect of fiber diameter, pore size and seeding method on growth of human dermal fibroblasts in electrospun poly(epsilon-caprolactone) fibrous mats, *Biomaterials*, 2010, **31**, 491–504.
- 78 R. W. Baker, *Membrane technology and applications*, Wiley-Blackwell, Oxford, 3rd edn, 2012.
- 79 D. I. Richter, *Oberflächencharakterisierung von aliphatischen Polyamiden zur Bewertung adhäsiver Wechselwirkungen in Carbonfaserverbunden*, Berlin, 2004.



- 80 N. S. Abd Halim, M. D. H. Wirzal, M. R. Bilad, N. A. H. Md Nordin, Z. Adi Putra, N. S. Sambudi and A. R. Mohd Yusoff, Improving Performance of Electrospun Nylon 6,6 Nanofiber Membrane for Produced Water Filtration via Solvent Vapor Treatment, *Polymers*, 2019, **11**, 2117.
- 81 A. B. D. Cassie and S. Baxter, Wettability of porous surfaces, *Trans. Faraday Soc.*, 1944, **40**, 546.
- 82 H. Y. Erbil and C. E. Cansoy, Range of applicability of the Wenzel and Cassie-Baxter equations for superhydrophobic surfaces, *Langmuir*, 2009, **25**, 14135–14145.
- 83 L. Huang, S. S. Manickam and J. R. McCutcheon, Increasing strength of electrospun nanofiber membranes for water filtration using solvent vapor, *J. Membr. Sci.*, 2013, **436**, 213–220.
- 84 M. M. Mannarino, R. Katsumata and G. C. Rutledge, Structural, mechanical, and tribological properties of electrospun poly(hexamethylene adipamide) fiber mats, *Wear*, 2013, **305**, 58–68.
- 85 S.-S. Choi, S. G. Lee, C. W. Joo, S. S. Im and S. H. Kim, Formation of interfiber bonding in electrospun poly(etherimide) nanofiber web, *J. Mater. Sci.*, 2004, **39**, 1511–1513.
- 86 N. Chen, M. K. Koker, S. Uzun and M. N. Silberstein, *In situ* X-ray study of the deformation mechanisms of non-woven polypropylene, *Int. J. Solids Struct.*, 2016, **97–98**, 200–208.
- 87 N. Chen and M. N. Silberstein, A micromechanics-based damage model for non-woven fiber networks, *Int. J. Solids Struct.*, 2019, **160**, 18–31.
- 88 M. Li, J. Li, M. Zhou, Y. Xian, Y. Shui, M. Wu and Y. Yao, Super-hydrophilic electrospun PVDF/PVA-blended nanofiber membrane for microfiltration with ultrahigh water flux, *J. Appl. Polym. Sci.*, 2020, **137**, 48416.
- 89 A. M. Bazargan, M. Keyanpour-rad, F. A. Hesari and M. E. Ganji, A study on the microfiltration behavior of self-supporting electrospun nanofibrous membrane in water using an optical particle counter, *Desalination*, 2011, **265**, 148–152.
- 90 L. Li, R. Hashaiekeh and H. A. Arafat, Development of eco-efficient micro-porous membranes via electrospinning and annealing of poly (lactic acid), *J. Membr. Sci.*, 2013, **436**, 57–67.
- 91 P. T. Flaviana Yohanala, R. Mulya Dewa, K. Quarta, W. Widiyastuti and S. Winardi, Preparation of Polystyrene Spheres Using Surfactant-Free Emulsion Polymerization, *Mod. Appl. Sci.*, 2015, **9**, 121.
- 92 N. E. Zander, M. Gillan and D. Sweetser, Recycled PET Nanofibers for Water Filtration Applications, *Materials*, 2016, **9**, 247.
- 93 N. Wang, Y. Si, N. Wang, G. Sun, M. El-Newehy, S. S. Al-Deyab and B. Ding, Multilevel structured polyacrylonitrile/silica nanofibrous membranes for high-performance air filtration, *Sep. Purif. Technol.*, 2014, **126**, 44–51.
- 94 Z. Wang, C. Zhao and Z. Pan, Porous bead-on-string poly (lactic acid) fibrous membranes for air filtration, *J. Colloid Interface Sci.*, 2015, **441**, 121–129.
- 95 H.-J. Kim, D.-I. Choi, S.-K. Sung, S.-H. Lee, S.-J. Kim, J. Kim, B.-S. Han, D.-I. Kim and Y. Kim, Eco-Friendly Poly(Vinyl Alcohol) Nanofiber-Based Air Filter for Effectively Capturing Particulate Matter, *Appl. Sci.*, 2021, **11**, 3831.
- 96 A. Sharma, H. Omidvarborna and P. Kumar, Efficacy of facemasks in mitigating respiratory exposure to submicron aerosols, *J. Hazard. Mater.*, 2022, **422**, 126783.
- 97 W. Ma, Y. Li, M. Zhang, S. Gao, J. Cui, C. Huang and G. Fu, Biomimetic Durable Multifunctional Self-Cleaning Nanofibrous Membrane with Outstanding Oil/Water Separation, Photodegradation of Organic Contaminants, and Antibacterial Performances, *ACS Appl. Mater. Interfaces*, 2020, **12**, 34999–35010.



Electronic Supplementary Information

Bio-based electrospun polyamide membrane – sustainable multipurpose filter membranes for microplastic filtration

*Maximilian Rist and Andreas Greiner**

M. Rist, A. Greiner

University of Bayreuth, Macromolecular Chemistry and Bavarian Polymer Institute,
Universitätsstrasse 30, 95440 Bayreuth, Germany.

E-mail: greiner@uni-bayreuth.de

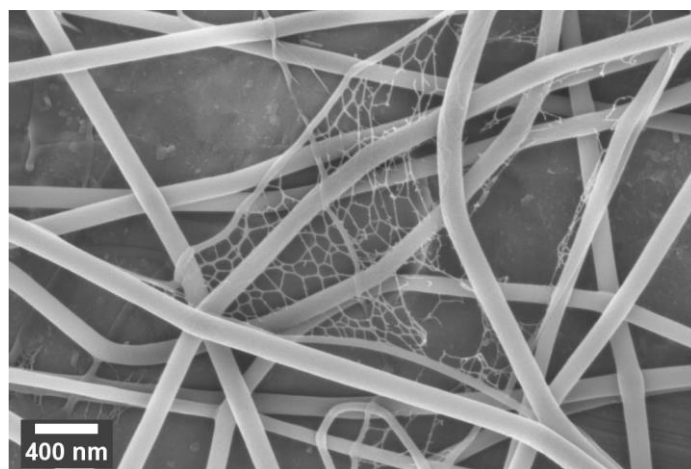


Figure S1. SEM image of spider web-like structure found in PA 6,9 membrane prepared from 10 wt% solution in FA/ CHCl_3 .

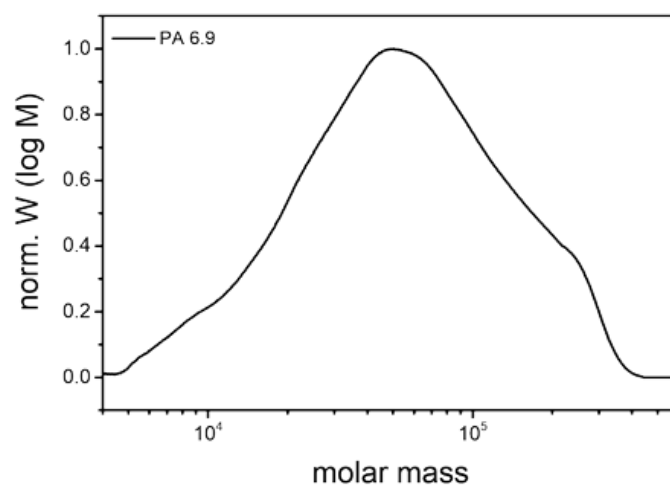


Figure S2. Normalized molecular weight distribution of PA 6,9 measured by SEC.

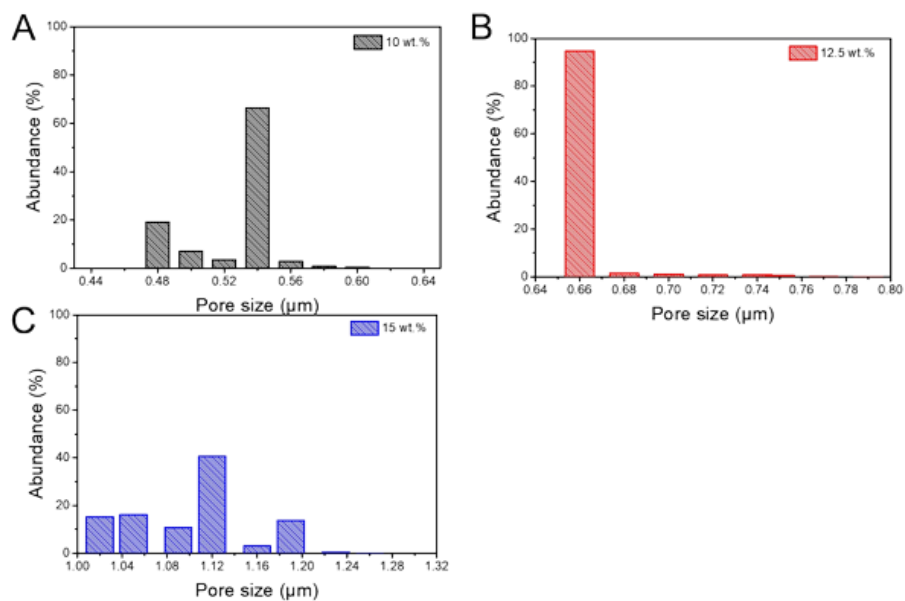


Figure S3. Pore size distribution of the nonwovens measured by capillary flow porometry.

Table S1. Average weight and resulting density determined by gravimetrically weighing the tensile test specimens (30 × 5 mm) prior to being measured. At least 5 samples were measured and the statistical average is given.

Material	Thickness [μm]	Average weight [mg]	Average density [kg m ⁻³]	Basis weight [g m ⁻²]	Porosity ^a [%]
PA 6.9_10 wt%	54±4	0.97±0.06	119±10	6.4±0.4	89
PA 6.9_12.5 wt%	62±2	1.46±0.06	157±5	9.7±0.4	85
PA 6.9_15 wt%	60±3	1.01±0.09	112±7	6.8±0.6	90

^a Calculated from the density of bulk PA 6.9 (1080 kg m⁻³) and the average density of the membrane.

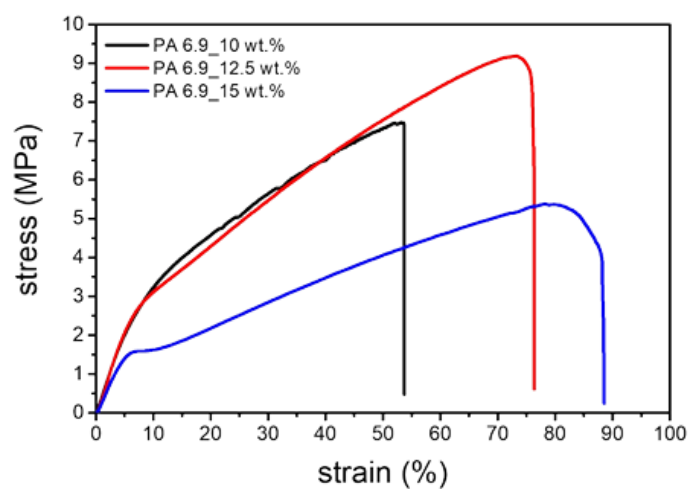


Figure S4. Stress-strain curves of the electrospun membranes prepared from PA 6.9.

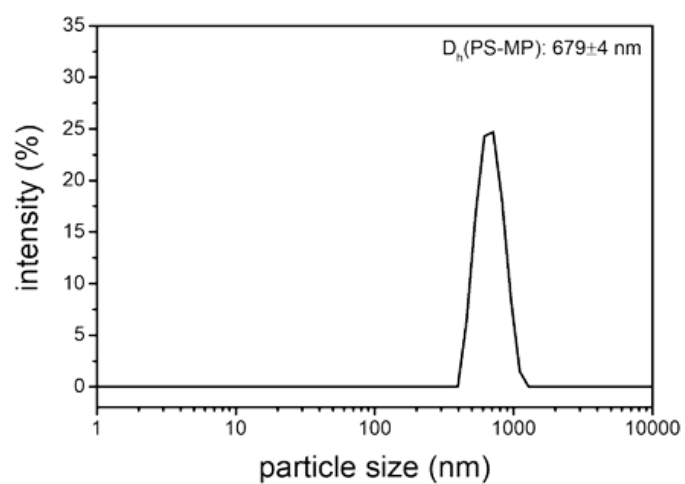


Figure S5. DLS measurement of the prepared PS microparticle dispersion in water.

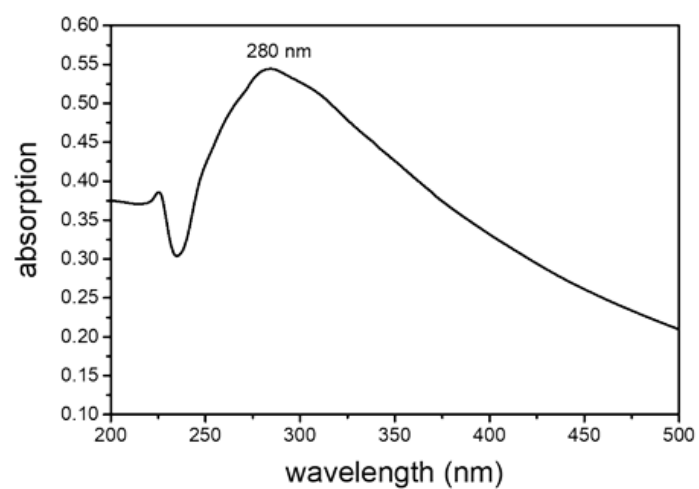


Figure S6. Absorption spectrum of the prepared PS microparticle dispersion in water.



Figure S7. Measurement setup for the aqueous filtration of PS microparticles from water with parallel measurement of the pressure drop.

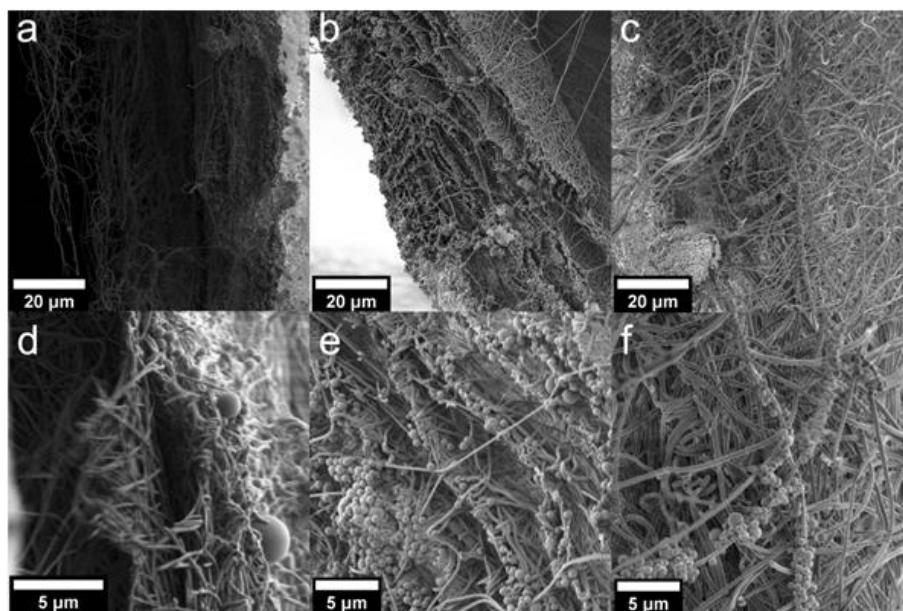


Figure S8. SEM pictures of the cross section of the electrospun filter membranes prepared from PA 6,9 solutions in formic acid chloroform 1:1 v/v a & d) 10 wt%, b & e) 12,5 wt% and c & f) 15 wt%.

5 List of publications

- (1) **Synthesis, characterization and the potential for closed loop recycling of plant oil-based PA X.19 polyamides**

M. Rist, A. Greiner, *ACS Sustainable Chem. Eng.* **2022**, *10*, 16793 – 16802.

<https://doi.org/10.1021/acssuschemeng.2c05176>

- (2) **Toughening of bio-based PA 6.19 by copolymerization with PA 6.6 – synthesis and production of melt-spun monofilaments and knitted fabrics**

M. Rist, H. Löcken, M. Ortega, A. Greiner, *Macromol. Rapid Commun.* **2023**, *44*, 2300256.

<https://doi.org/10.1002/marc.202300256>

- (3) **Bio-based electrospun polyamide membrane – sustainable multipurpose filter membranes for microplastic filtration**

M. Rist, A. Greiner, *RSC Appl. Polym.* **2024**, Advance Article.

<https://doi.org/10.1039/D3LP00201B>

6 Supplementary Information

Abbreviations

ABS	acrylonitrile-butadiene-styrene
ADMET	acyclic diene metathesis
C36-DA	dimerized oleic acid
CoPA	PA 6.6/6.19 copolyamide with 55 mol% PA 6.6
DMA	dynamic mechanical analysis
DMFD	dimethyl-2,5-furandicarboxylate
DSC	differential scanning calorimetry
DTBPX	1,2-bis(di- <i>tert</i> -butylphosphinomethyl)benzene
EFM	electrospun filter membrane
FDCA	2,5-furandicarboxylic acid
F_{\max}	ultimate tensile strength
GC	gas chromatography
HDPE	high density polyethylene
HEPA	high-efficiency particulate air
HMF	5-hydroxymethylfurfural
KA-oil	mixture of cyclohexanol and cyclohexanone
NMR	nuclear magnetic resonance
PA	polyamide
PAN	polyacrylonitrile
PCL	polycaprolactone
PET	poly(ethylene terephthalate)
POY	partially oriented yarn
PS	polystyrene
PVDF	polyvinylidene fluoride
SEM	scanning electron microscope
TGA	thermogravimetric analysis
T_m	melting temperature
TPE	thermoplastic elastomer

UV-Vis ultraviolet-visible
WAXS wide angle x-ray scattering

7 References

- (1) Carothers, W. H. Studies on Polymerization and Ring Formation. I. An Introduction to the General Theory of Condensation Polymers. *J. Am. Chem. Soc.* **1929**, *51* (8), 2548–2559. DOI: 10.1021/ja01383a041.
- (2) Carothers, W. H.; Arvin, J. A. Studies on Polymerization and Ring Formation. II. Polyesters. *J. Am. Chem. Soc.* **1929**, *51* (8), 2560–2570. DOI: 10.1021/ja01383a042.
- (3) Osswald, T. A.; Baur, E.; Brinkmann, S.; Oberbach, K.; Schmachtenberg, E., *International Plastics Handbook: The Resource for Plastics Engineers*, 4. Aufl.; Carl Hanser Fachbuchverlag, **2006**. DOI: 10.3139/9783446407923.
- (4) Abdellah Ali, S. F. Mechanical and thermal properties of promising polymer composites for food packaging applications. *IOP Conf. Ser.: Mater. Sci. Eng.* **2016**, *137*, 12035. DOI: 10.1088/1757-899X/137/1/012035.
- (5) Brown, J. R.; Ennis, B. C. Thermal Analysis of Nomex® and Kevlar® Fibers. *Textile Research Journal* **1977**, *47* (1), 62–66. DOI: 10.1177/004051757704700113.
- (6) Herzog, B.; Kohan, M. I.; Mestemacher, S. A.; Pagilagan, R. U.; Redmond, K.; Sarbandi, R. Polyamides. In *Ullmann's Encyclopedia of Industrial Chemistry*; Wiley VCH, **2020**; pp 1–47. DOI: 10.1002/14356007.a21_179.pub4.
- (7) Palmer, R. J.; Staff, U. b. Polyamides, Plastics. In *Kirk-Othmer Encyclopedia of Chemical Technology*; Kirk, R. E., Othmer, D. F., Eds.; Wiley online library; Wiley, **2013**. DOI: 10.1002/0471238961.1612011916011213.a01.pub2.
- (8) Stempfle, F.; Ortmann, P.; Mecking, S. Long-Chain Aliphatic Polymers To Bridge the Gap between Semicrystalline Polyolefins and Traditional Polycondensates. *Chem. Rev.* **2016**, *116* (7), 4597–4641. DOI: 10.1021/acs.chemrev.5b00705.
- (9) Tao, L.; Liu, K.; Li, T.; Xiao, R. Preparation and properties of biobased polyamides based on 1,9-azelaic acid and different chain length diamines. *Polym. Bull.* **2020**, *77* (3), 1135–1156. DOI: 10.1007/s00289-019-02791-2.
- (10) Venoor, V.; Park, J. H.; Kazmer, D. O.; Sobkowicz, M. J. Understanding the Effect of Water in Polyamides: A Review. *Polym. Rev.* **2021**, *61* (3), 598–645. DOI: 10.1080/15583724.2020.1855196.
- (11) Arhant, M.; Le Gac, P.-Y.; Le Gall, M.; Burtin, C.; Briançon, C.; Davies, P. Effect of sea water and humidity on the tensile and compressive properties of carbon-polyamide 6 laminates. *Compos Part A Appl Sci Manuf* **2016**, *91*, 250–261. DOI: 10.1016/j.compositesa.2016.10.012.

- (12) El-Mazry, C.; Correc, O.; Colin, X. A new kinetic model for predicting polyamide 6-6 hydrolysis and its mechanical embrittlement. *Polym. Degrad. Stab.* **2012**, *97* (6), 1049–1059. DOI: 10.1016/j.polymdegradstab.2012.03.003.
- (13) Carothers, W. H. Synthetic Fiber, US2130948, **1937**.
- (14) Schlack, P. Preparation of polyamides, US2241321, **1941**.
- (15) Kunststoffe International, *SPECIAL K 2019:Plastics World Market*. Carl Hanser Verlag, **2019**. https://res.cloudinary.com/sternwald-systems/raw/upload/v1/hugoprdr/ARTIKEL_ATTACH/0022D011_39DF787EF0CA/266230ff0f35fa4cdabcf5a0ebb42648c290f31/Polyamide%20and%20PA6_%20PA66_%20Kunststoffe%202019.pdf (accessed 2023-02-14).
- (16) Genas, M. Rilsan (Polyamid 11), Synthese und Eigenschaften. *Angew. Chem.* **1962**, *74* (15), 535–540.
- (17) Griehl, W.; Ruestem, D. Nylon-12-Preparation, Properties, and Applications. *Ind. Eng. Chem.* **1970**, *62* (3), 16–22. DOI: 10.1021/ie50723a005.
- (18) Tey, W. S.; Cai, C.; Zhou, K. A Comprehensive Investigation on 3D Printing of Polyamide 11 and Thermoplastic Polyurethane via Multi Jet Fusion. *Polymers* **2021**, *13* (13). DOI: 10.3390/polym13132139. Published Online: Jun. 29, 2021.
- (19) Ehrenstein, M.; Smith, P.; Weder, C. Polyamides X.34: A New Class of Polyamides with Long Alkane Segments. *Macromol. Chem. Phys.* **2003**, *204* (13), 1599–1606. DOI: 10.1002/macp.200350026.
- (20) Ortmann, P.; Lemke, T. A.; Mecking, S. Long-Spaced Polyamides: Elucidating the Gap between Polyethylene Crystallinity and Hydrogen Bonding. *Macromolecules* **2015**, *48* (5), 1463–1472. DOI: 10.1021/acs.macromol.5b00060.
- (21) Marchildon, K. Polyamides - Still Strong After Seventy Years. *Macromolecular Reaction Engineering* **2011**, *5* (1), 22–54. DOI: 10.1002/mren.201000017.
- (22) Kunststoffe International, *SPECIAL K 2016:Plastics World Market*. Carl Hanser Verlag, **2016**. https://res.cloudinary.com/sternwald-systems/raw/upload/v1/hugoprdr/ARTIKEL_ATTACH/002424A4_66AFF183BD0/ef2fd1b9b5f09b43766f0ec5258fd16365978308/KUint_2016_10_Polyamide-6-and-66-PA6-and-PA66.pdf (accessed 2023-02-14).
- (23) Saotome, K.; Komoto, H. Polyamides having long methylene chain units. *J. Polym. Sci. A-1 Polym. Chem.* **1966**, *4* (6), 1463–1473. DOI: 10.1002/pol.1966.150040611.

- (24) Novitsky, T. F.; Mathias, L. J. One-pot synthesis of polyamide 12,T–polyamide-6 block copolymers. *J. Polym. Sci. A Polym. Chem.* **2011**, *49* (10), 2271–2280. DOI: 10.1002/pola.24660.
- (25) Bertolla, M.; Cecchetto, M.; Comotto, M.; Dal Moro, A. Comparison of the Properties of a Random Copolymer and a Molten Blend PA6/PA6.9. *Polymers* **2022**, *14* (19). DOI: 10.3390/polym14194115. Published Online: Oct. 1, 2022.
- (26) Allen, S. J. *J. Text. Inst. Proc.* **1953**, *44*, 8.
- (27) Harvey, E. D.; Hybart, F. J. Rates of crystallization of copolyamides. II. Random copolymers of nylons 66 and 6. *J. Appl. Polym. Sci.* **1970**, *14* (8), 2133–2143. DOI: 10.1002/app.1970.070140821.
- (28) Zilberman, M.; Siegmann, A.; Narkis, M. Structure and properties of 6/6.9 copolyamide series. II. The crystalline phase. *J. Macromol. Sci., Part B, Phys.* **1996**, *35* (1), 1–21. DOI: 10.1080/00222349608220373.
- (29) Johnson, C. G.; Cypcar, C. C.; Mathias, L. J. ¹³C and ¹⁵N Solid-State NMR of Copolymers of Nylons 6 and 7: Observation of a Stable Pseudo-hexagonal Phase. *Macromolecules* **1995**, *28* (25), 8535–8540. DOI: 10.1021/ma00129a011.
- (30) Zierdt, P.; Mitzner, E.; Gomoll, A.; Theumer, T.; Lieske, A. Synthesis of polyamide 6/11 copolymers and their use as matrix polymer in wood-plastic composites. *J. Appl. Polym. Sci.* **2016**, *133* (46), 44155. DOI: 10.1002/app.44155.
- (31) Garner, D. P.; Fasulo, P. D. The effect of composition on the properties of nylon 612 copolymers. *J. Appl. Polym. Sci.* **1988**, *36* (3), 495–509. DOI: 10.1002/app.1988.070360304.
- (32) Goodman, I.; Kehayoglou, A. H. Anionic copolymers of caprolactam with lauro-lactam (nylon copolymers) II. Crystallisation, glass transitions and tensile properties. *Eur. Polym. J.* **1983**, *19* (4), 321–325. DOI: 10.1016/0014-3057(83)90167-2.
- (33) Jia, F.; Mao, J. L.; Ma, Y.; Yao, C. Mechanical and thermal properties of dimer acid based nylon 636/Nylon 66 copolymers. *J. Appl. Polym. Sci.* **2014**, *131* (6), 39845. DOI: 10.1002/app.39845.
- (34) Jia, F.; Mao, J.-L.; Yang, X.-Y.; Ma, Y.; Yao, C. Thermal, physical and mechanical properties of hydrogenated dimer acid-based Nylon 636/Nylon 66 copolymers. *Chinese Chemical Letters* **2013**, *24* (7), 654–658. DOI: 10.1016/j.ccl.2013.04.012.

- (35) American Chemical Society National Historic Chemical Landmarks, *Bakelite: The World's First Synthetic*, **08.03.2023**. <https://www.acs.org/education/whatischemistry/landmarks/bakelite.html> (accessed 2023-03-08).
- (36) Naik, S. N.; Saxena, D. K.; Dole, B. R.; Khare, S. K. Potential and Perspective of Castor Biorefinery. In *Waste Biorefinery: Potential and Perspectives*; Pandey, A., Bhaskar, T., Mohan, S. V., Lee, D.-J., Khanal, S. K., Eds.; Elsevier, **2018**; pp 623–656. DOI: 10.1016/B978-0-444-63992-9.00021-5.
- (37) Kenar, J. A.; Moser, B. R.; List, G. R. Naturally Occurring Fatty Acids. In *Fatty acids: Chemistry, synthesis, and applications*; Ahmad, M. U., Ed.; Academic Press an imprint of Elsevier; AOCs Press an imprint of Elsevier, **2017**; pp 23–82. DOI: 10.1016/B978-0-12-809521-8.00002-7.
- (38) Naughton, F. C. Production, chemistry, and commercial applications of various chemicals from castor oil. *J Am Oil Chem Soc* **1974**, *51* (3), 65–71. DOI: 10.1007/BF00000015.
- (39) Wang, M.-S.; Huang, J.-C. Nylon 1010 Properties and Applications. *Journal of Polymer Engineering* **1994**, *13* (2). DOI: 10.1515/POLYENG.1994.13.2.155.
- (40) Kyulavska, M.; Toncheva-Moncheva, N.; Rydz, J. Biobased Polyamide Ecomaterials and Their Susceptibility to Biodegradation. In *Handbook of Ecomaterials*; Martínez, L. M. T., Kharissova, O. V., Kharisov, B. I., Eds.; SpringerLink Bücher; Springer International Publishing, **2019**; pp 2901–2934. DOI: 10.1007/978-3-319-68255-6_126.
- (41) Winnacker, M.; Rieger, B. Biobased Polyamides: Recent Advances in Basic and Applied Research. *Macromol. Rapid Commun.* **2016**, *37* (17), 1391–1413. DOI: 10.1002/marc.201600181. Published Online: Jul. 26, 2016.
- (42) Qian, Z.-G.; Xia, X.-X.; Lee, S. Y. Metabolic engineering of *Escherichia coli* for the production of putrescine: a four carbon diamine. *Biotechnology and Bioengineering* **2009**, *104* (4), 651–662. DOI: 10.1002/bit.22502.
- (43) Lammens, T. M.; Le Nôtre, J.; Franssen, M. C. R.; Scott, E. L.; Sanders, J. P. M. Synthesis of biobased succinonitrile from glutamic acid and glutamine. *ChemSusChem* **2011**, *4* (6), 785–791. DOI: 10.1002/cssc.201100030. Published Online: May. 10, 2011.
- (44) Froidevaux, V.; Negrell, C.; Caillol, S.; Pascault, J.-P.; Boutevin, B. Biobased Amines: From Synthesis to Polymers; Present and Future. *Chem. Rev.* **2016**, *116* (22), 14181–14224. DOI: 10.1021/acs.chemrev.6b00486. Published Online: Nov. 3, 2016.

- (45) Huang, Y.; Ji, X.; Ma, Z.; Łężyk, M.; Xue, Y.; Zhao, H. Green chemical and biological synthesis of cadaverine: recent development and challenges. *RSC Adv.* **2021**, *11* (39), 23922–23942. DOI: 10.1039/D1RA02764F.
- (46) Hashimoto, M.; Eda, Y.; Osanai, Y.; Iwai, T.; Aoki, S. A Novel Decarboxylation of α -Amino acids. A facile Method of Decarboxylation by the Use of 2-Cyclohex en-1-one as a Catalyst. *Chem. Lett.* **1986**, *15* (6), 893–896. DOI: 10.1246/cl.1986.893.
- (47) Laval, G.; Golding, B. T. One-pot Sequence for the Decarboxylation of α -Amino Acids. *Synlett* **2003** (4), 542–546. DOI: 10.1055/s-2003-37512.
- (48) Xie, S.; Jia, C.; Wang, Z.; Ong, S. S. G.; Zhu, M.; Lin, H. Mechanistic Insight into Selective Deoxygenation of l -Lysine to Produce Biobased Amines. *ACS Sustainable Chem. Eng.* **2020**, *8* (31), 11805–11817. DOI: 10.1021/acssuschemeng.0c04052.
- (49) 路飞; 周豪宏; 刘修才. A kind of method of fermenting and producing 1,5-pentanediamineCN110468167A, **2019**.
- (50) Qian, Z.-G.; Xia, X.-X.; Lee, S. Y. Metabolic engineering of Escherichia coli for the production of cadaverine: a five carbon diamine. *Biotechnology and Bioengineering* **2011**, *108* (1), 93–103. DOI: 10.1002/bit.22918.
- (51) Kind, S.; Wittmann, C. Bio-based production of the platform chemical 1,5-diaminopentane. *Appl Microbiol Biotechnol* **2011**, *91* (5), 1287–1296. DOI: 10.1007/s00253-011-3457-2. Published Online: Jul. 15, 2011.
- (52) Frost, J. W. Synthesis of caprolactam from lysine, WO2005123669A1, **2005**.
- (53) Burgard, A. P.; Pharkya, P.; Osterhout, R. E. Microorganisms for the production of adipic acid and other compoundsUS7799545B2, **2010**.
- (54) Sherman, L. M., *Genomatica and Aquafil Start Pre-Commercial Plant-Based Nylon 6 Production*. *Plastics Technology*, **2022**. <https://www.ptonline.com/blog/post/genomatica-and-aquafil-start-pre-commercial-plant-based-nylon-6-production-> (accessed 2023-03-09).
- (55) Covestro AG, *Covestro and Genomatica produce important chemical raw material using biotechnology*. Covestro AG, **2022**. <https://www.covestro.com/press/covestro-and-genomatica-produce-important-chemical-raw-material-using-biotechnology/> (accessed 2023-03-09).
- (56) Asahi Kasei, *Genomatica and Asahi Kasei Partner on Renewably-Sourced Nylon 6,6*. Asahi Kasei, **2022**. https://www.asahi-kasei.com/news/2021/e220316_2.html (accessed 2023-03-09).

- (57) Burk, M. J.; Burgard, A. P.; Osterhout, R. E.; Pharkya, P. Microorganisms and methods for the biosynthesis of adipate, hexamethylenediamine and 6-aminocaproic acid, US20230022727A1, **2023**.
- (58) Suominen, L. H.; Galleher, C. J.; Japs, M.; Burk, M. J.; Tracewell, C. Method of producing and processing diamines from an engineered microorganismUS10711289B2, **2020**.
- (59) Suominen, L. H.; Galleher, C. J.; Japs, M.; Burk, M. J.; Tracewell, C. Method of producing & processing diamines, US20210130861A1, **2021**.
- (60) Skoog, E.; Shin, J. H.; Saez-Jimenez, V.; Mapelli, V.; Olsson, L. Biobased adipic acid - The challenge of developing the production host. *Biotechnol. Adv.* **2018**, *36* (8), 2248–2263. DOI: 10.1016/j.biotechadv.2018.10.012. Published Online: Oct. 30, 2018.
- (61) Rios, J.; Lebeau, J.; Yang, T.; Li, S.; Lynch, M. D. A critical review on the progress and challenges to a more sustainable, cost competitive synthesis of adipic acid. *Green Chem.* **2021**, *23* (9), 3172–3190. DOI: 10.1039/D1GC00638J.
- (62) Deng, W.; Yan, L.; Wang, B.; Zhang, Q.; Song, H.; Wang, S.; Zhang, Q.; Wang, Y. Efficient Catalysts for the Green Synthesis of Adipic Acid from Biomass. *Angew. Chem. Int. Ed.* **2021**, *60* (9), 4712–4719. DOI: 10.1002/anie.202013843. Published Online: Jan. 14, 2021.
- (63) Gilkey, M. J.; Balakumar, R.; Vlachos, D. G.; Xu, B. Adipic acid production catalyzed by a combination of a solid acid and an iodide salt from biomass-derived tetrahydrofuran-2,5-dicarboxylic acid. *Catal. Sci. Technol.* **2018**, *8* (10), 2661–2671. DOI: 10.1039/C8CY00379C.
- (64) Wei, L.; Zhang, J.; Deng, W.; Xie, S.; Zhang, Q.; Wang, Y. Catalytic transformation of 2,5-furandicarboxylic acid to adipic acid over niobic acid-supported Pt nanoparticles. *ChemComm.* **2019**, *55* (55), 8013–8016. DOI: 10.1039/c9cc02877c.
- (65) Tuteja, J.; Choudhary, H.; Nishimura, S.; Ebitani, K. Direct synthesis of 1,6-hexanediol from HMF over a heterogeneous Pd/ZrP catalyst using formic acid as hydrogen source. *ChemSusChem* **2014**, *7* (1), 96–100. DOI: 10.1002/cssc.201300832. Published Online: Nov. 20, 2013.
- (66) He, J.; Burt, S. P.; Ball, M.; Zhao, D.; Hermans, I.; Dumesic, J. A.; Huber, G. W. Synthesis of 1,6-Hexanediol from Cellulose Derived Tetrahydrofuran-Dimethanol with Pt-WO_x/TiO₂ Catalysts. *ACS Catal.* **2018**, *8* (2), 1427–1439. DOI: 10.1021/acscatal.7b03593.

- (67) Zhou, Y.; Zhao, M.; Zhou, S.; Zhao, Y.; Li, G.; Deng, Y. Biosynthesis of adipic acid by a highly efficient induction-free system in *Escherichia coli*. *J. Biotechnol.* **2020**, *314-315*, 8–13. DOI: 10.1016/j.jbiotec.2020.03.011. Published Online: Apr. 7, 2020.
- (68) Jin, X.; Liu, M.; Zhang, G.; Wang, J.; Xia, Q.; Sun, Y.; Zhou, Z.; Zhang, W.; Wang, S.; Lam, C. H.; Shen, J.; Yang, C.; Chaudhari, R. V. Chemical Synthesis of Adipic Acid from Glucose and Derivatives: Challenges for Nanocatalyst Design. *ACS Sustainable Chem. Eng.* **2020**, *8* (51), 18732–18754. DOI: 10.1021/acssuschemeng.0c04411.
- (69) Zhao, M.; Huang, D.; Zhang, X.; Koffas, M. A.; Zhou, J.; Deng, Y. Metabolic engineering of *Escherichia coli* for producing adipic acid through the reverse adipate-degradation pathway. *Metab. Eng.* **2018**, *47*, 254–262. DOI: 10.1016/j.ymben.2018.04.002.
- (70) Raj, K.; Partow, S.; Correia, K.; Khusnutdinova, A. N.; Yakunin, A. F.; Mahadevan, R. Biocatalytic production of adipic acid from glucose using engineered *Saccharomyces cerevisiae*. *Metab. Eng. Commun.* **2018**, *6*, 28–32. DOI: 10.1016/j.meteno.2018.02.001. Published Online: Feb. 3, 2018.
- (71) Larson, R. T.; Samant, A.; Chen, J.; Lee, W.; Bohn, M. A.; Ohlmann, D. M.; Zuend, S. J.; Toste, F. D. Hydrogen Gas-Mediated Deoxydehydration/Hydrogenation of Sugar Acids: Catalytic Conversion of Glucarates to Adipates. *J. Am. Chem. Soc.* **2017**, *139* (40), 14001–14004. DOI: 10.1021/jacs.7b07801. Published Online: Oct. 3, 2017.
- (72) Niu, W.; Draths, K. M.; Frost, J. W. Benzene-free synthesis of adipic acid. *Biotechnol. Prog.* **2002**, *18* (2), 201–211. DOI: 10.1021/bp010179x.
- (73) Burke, P. M.; Sieja, J. B. Verfahren zur Herstellung von 5-Cyanovaleriansäure und ihrer Ester unter Verwendung von zyklischen Co-Lösungsmitteln EP0373579A1, **1993**.
- (74) Han, J. A bio-based ‘green’ process for catalytic adipic acid production from lignocellulosic biomass using cellulose and hemicellulose derived γ -valerolactone. *Energy Convers. Manag.* **2016**, *129*, 75–80. DOI: 10.1016/j.enconman.2016.10.019.
- (75) Zhao, L.; Pudasaini, B.; Genest, A.; Nobbs, J. D.; Low, C. H.; Stubbs, L. P.; van Meurs, M.; Rösch, N. Palladium-Catalyzed Hydroxycarbonylation of Pentenoic Acids. Computational and Experimental Studies on the Catalytic Selectivity. *ACS Catal.* **2017**, *7* (10), 7070–7080. DOI: 10.1021/acscatal.7b02278.
- (76) Liu, H.; Jiang, T.; Han, B.; Liang, S.; Zhou, Y. Selective phenol hydrogenation to cyclohexanone over a dual supported Pd-Lewis acid catalyst. *Science* **2009**, *326* (5957), 1250–1252. DOI: 10.1126/science.1179713.

- (77) Wang, J.; Wang, X.; Wan, L.; Yang, Y.; Wang, S. An Effective Method for Bulk Obtaining Graphene Oxide Solids. *Chin. J. Chem.* **2010**, *28* (10), 1935–1940. DOI: 10.1002/cjoc.201090322.
- (78) Patra, A. K.; Dutta, A.; Bhaumik, A. Mesoporous core–shell Fenton nanocatalyst: a mild, operationally simple approach to the synthesis of adipic acid. *Chem. Eur. J.* **2013**, *19* (37), 12388–12395. DOI: 10.1002/chem.201301498.
- (79) Bhanja, P.; Chatterjee, S.; Patra, A. K.; Bhaumik, A. A new microporous oxyfluorinated titanium(IV) phosphate as an efficient heterogeneous catalyst for the selective oxidation of cyclohexanone. *J. Colloid Interface Sci.* **2018**, *511*, 92–100. DOI: 10.1016/j.jcis.2017.09.115. Published Online: Sep. 30, 2017.
- (80) Sutor, J. T.; Varzandeh, S.; Wallace, S. One-Pot Synthesis of Adipic Acid from Guaiacol in *Escherichia coli*. *ACS Synth. Biol.* **2020**, *9* (9), 2472–2476. DOI: 10.1021/acssynbio.0c00254. Published Online: Aug. 7, 2020.
- (81) Li, T.; Li, H.; Huang, G.; Shen, X.; Wang, S.; Li, C. Transforming biomass tar into a highly active Ni-based carbon-supported catalyst for selective hydrogenation-transalkylation of guaiacol. *J. Anal. Appl. Pyrolysis* **2021**, *153*, 104976. DOI: 10.1016/j.jaap.2020.104976.
- (82) Lang, M.; Li, H. Sustainable Routes for the Synthesis of Renewable Adipic Acid from Biomass Derivatives. *ChemSusChem* **2022**, *15* (1), e202101531. DOI: 10.1002/cssc.202101531. Published Online: Nov. 30, 2021.
- (83) Toray Industries, Inc., *Toray Invents 100% Bio-Based Adipic Acid from Sugars Derived from Inedible Biomass, Scaling Up for Application to Eco-Friendly Nylon 66*. Toray Industries, Inc., **2022**. <https://www.toray.com/global/news/details/20220818103248.html> (accessed 2023-03-10).
- (84) Ackman, R. G.; Retson, M. E.; Gallay, L. R.; Vandenheuvel, F. A. Ozonolysis of Unsaturated Fatty Acids: I. Ozonolysis of Oleic Acid. *Can. J. Chem.* **1961**, *39* (10), 1956–1963. DOI: 10.1139/v61-262.
- (85) Turnwald, S. E.; Lorier, M. A.; Wright, L. J.; Mucalo, M. R. Oleic Acid Oxidation Using Hydrogen Peroxide in Conjunction with Transition Metal Catalysis. *J. Mater. Sci. Lett.* **1998**, *17* (15), 1305–1307. DOI: 10.1023/A:1006532314593.
- (86) Goebel, G. C.; Brown, A. C.; Oehlschlaeger, H. F.; Rolfes, R. P. Method of Making Azelaic Acid US2813113, **1957**.

- (87) Oehlschlaeger, H. F.; Rodenberg, H. G. Process for the production of a purified grade of azelaic acid by treatment with ozone during purification US3402108, **1968**.
- (88) Yun, D.; Zhang, Z.; Flaherty, D. W. Catalyst and reactor design considerations for selective production of acids by oxidative cleavage of alkenes and unsaturated fatty acids with H₂O₂. *React. Chem. Eng.* **2022**, *7* (9), 2054–2065. DOI: 10.1039/D2RE00160H.
- (89) Melchiorre, M.; Benessere, V.; Cucciolito, M. E.; Melchiorre, C.; Ruffo, F.; Esposito, R. Direct and Solvent-Free Oxidative Cleavage of Double Bonds in High-Oleic Vegetable Oils. *ChemistrySelect* **2020**, *5* (4), 1396–1400. DOI: 10.1002/slct.201903516.
- (90) Araj, N.; Chatel, G.; Moores, A.; Jérôme, F.; Oliveira Vigier, K. de. Selective dihydroxylation of methyl oleate to methyl-9,10-dihydroxystearate in the presence of a recyclable tungsten based catalyst and hydrogen peroxide. *New J. Chem.* **2020**, *44* (27), 11507–11512. DOI: 10.1039/D0NJ02167A.
- (91) Masyithah, Z.; Ginting, A. Optimization of A Two-Step Method to Synthesize Azelaic Acid from Oleic Acid. *Orient. J. Chem* **2018**, *34* (3), 1249–1256. DOI: 10.13005/ojc/340307.
- (92) Li, X.; Syong, J. C. P.; Zhang, Y. Sodium stannate promoted double bond cleavage of oleic acid by hydrogen peroxide over a heterogeneous WO₃ catalyst. *Green Chem.* **2018**, *20* (15), 3619–3624. DOI: 10.1039/C8GC00949J.
- (93) Enferadi Kerenkan, A.; Ello, A. S.; Do, T.-O. Synthesis, Organo-Functionalization, and Catalytic Properties of Tungsten Oxide Nanoparticles As Heterogeneous Catalyst for Oxidative Cleavage of Oleic Acid As a Model Fatty Acid into Diacids. *Ind. Eng. Chem. Res.* **2017**, *56* (38), 10639–10647. DOI: 10.1021/acs.iecr.7b03001.
- (94) Bastioli, C.; Borsotti, G.; Merlin, A.; Milizia, T. Catalytic Cleavage Process of Vegetable Oils, ES2534399T3, **2015**.
- (95) Bieser, A.; Borsotti, G.; Digioia, F.; Ferrari, A.; Pirocco, A. Continuous Process for the Production of Derivatives of Saturated Carboxylic Acids, US8846962B2, **2014**.
- (96) Bastioli, C.; Borsotti, G.; Merlin, G.; Milizia, T. Triglycerides containing certain saturated carboxylic acids, US8629290B2, **2014**.
- (97) Bieser, A.; Borsotti, G.; Digioia, F.; Ferrari, A.; Pirocco, A. Continuous Process for the Production of Derivatives of Saturated Carboxylic Acids, WO2011080297A1, **2011**.
- (98) Cavani, F.; Vassoi, A. Production of Carboxylic Acids from vicinal Diols, US20200325095A1, **2020**.

- (99) Cotarca, L.; Delogu, P.; Nardelli, A.; Maggioni, P.; Bianchini, R.; Sguassero, S.; Alini, S.; Dario, R.; Clauti, G.; Pitta, G.; Duse, G.; Goffredi, F. Efficient and Scaleable Methods for ω -Functionalized Nonanoic Acids: Development of a Novel Process for Azelaic and 9-Aminononanoic Acids (Nylon-6,9 and Nylon-9 Precursors). *Org. Process Res. Dev.* **2001**, *5* (1), 69–76. DOI: 10.1021/op000081j.
- (100) Scarfato, P.; Di Maio, L.; Incarnato, L.; Acierno, D.; Mariano, A. Influence of co-monomer structure on properties of co-polyamide packaging films. *Packag. Technol. Sci.* **2002**, *15* (1), 9–16. DOI: 10.1002/pts.561.
- (101) Nieschlag, H. J.; Wolff, I. A.; Manley, T. C.; Holland, R. J. Brassylic Acid from Ozonolysis of Erucic Acid. *Ind. Eng. Chem. Prod. Res. Dev.* **1967**, *6* (2), 120–123. DOI: 10.1021/i360022a009.
- (102) Cui, X.; Yan, D.; Xiao, D. Synthesis and characterization of novel polyamides based on tridecanedioic acid: Nylons 3 13, 5 13, 6 13, 7 13, 9 13, 10 13, 11 13. *e-Polymers* **2004**, *4* (1). DOI: 10.1515/epoly.2004.4.1.784.
- (103) H. J. Nieschlag; J. A. Rothfus; V. E. Sohns. Nylon-1313 from Brassylic Acid. *Ind. Eng. Chem. Prod. Res. Dev.* **1977**, *16* (1), 101–107.
- (104) Samanta, S.; He, J.; Selvakumar, S.; Lattimer, J.; Ulven, C.; Sibi, M.; Bahr, J.; Chisholm, B. J. Polyamides based on the renewable monomer, 1,13-tridecane diamine II: Synthesis and characterization of nylon 13,6. *Polymer* **2013**, *54* (3), 1141–1149. DOI: 10.1016/j.polymer.2012.12.034.
- (105) Greene, J. L., JR.; Huffman, E. L.; Burks, R. E., JR.; Sheehan, W. C. Nylon 1313: Synthesis and polymerization of monomers. *J. Polym. Sci. A-1* **1967**, *5*, 391–394.
- (106) Greene, J. L.; Burks, R. E.; Wolff, I. A. 13-Aminotridecanoic Acid from Erucic Acid. *Product R&D* **1969**, *8* (2), 171–176. DOI: 10.1021/i360030a015.
- (107) Elvers, B.; Ullmann, F., *Ullmann's fine chemicals*, Vol. 3; Wiley-VCH, **2014**.
- (108) Cyranoski, D. China's patent boom brings legal wrangles. *Nature* **2012**, *492* (7429), 323. DOI: 10.1038/492323a.
- (109) Laplaza, J.; Beardslee, T.; Eirich, D.; Picataggio, S. Biological methods for preparing a fatty dicarboxylic acidWO2014100461A2, **2014**.
- (110) Beardslee, T.; Picataggio, S.; Hutagalung, A.; Fahland, T. Biological methods for preparing a fatty dicarboxylic acidUS9957512B2, **2018**.
- (111) Liu, C.; Liao, J.; Wang, J.; Qin, H.; Li, N. Candida sake strain for producing long chain dicarboxylic acids, US9388378B2, **2016**.

- (112) 刘文波; 徐敏; 杨晨; 周豪宏; 刘修才. Long-chain dibasic acid with low content of monobasic acid impurities and production method thereof, CN110684784A, **2020**.
- (113) Liu, W.; Xu, M.; Chou, H.; Liu, X. Directed evolution of cyp52a12 gene and its use in dicarboxylic acid productionUS20210340506A1, **2021**.
- (114) Xu, M.; Yang, C.; Qin, B.; Li, N.; Liu, X. Method for producing a long chain dicarboxylic acid by fermentation, fermentation broth, treated fermentation broth and wastewaterUS11319561B2, **2022**.
- (115) Ngo, H. L.; Jones, K.; Foglia, T. A. Metathesis of unsaturated fatty acids: Synthesis of long-chain unsaturated- α,ω -dicarboxylic acids. *J Am Oil Chem Soc* **2006**, 83 (7), 629–634. DOI: 10.1007/s11746-006-1249-0.
- (116) Bennett, C.; Mathias, L. J. Linear Unsaturated Polyamides: Nylons 6 u18 and 18 u18. *Macromol. Chem. Phys.* **2004**, 205 (18), 2438–2442. DOI: 10.1002/macp.200400351.
- (117) Bennett, C.; Mathias, L. J. Synthesis and characterization of polyamides containing octadecanedioic acid: Nylon-2,18, nylon-3,18, nylon-4,18, nylon-6,18, nylon-8,18, nylon-9,18, and nylon-12,18. *J. Polym. Sci. A Polym. Chem.* **2005**, 43 (5), 936–945. DOI: 10.1002/pola.20550.
- (118) Cui, X.; Li, W.; Yan, D.; Yuan, C.; Di Silvestro, G. Synthesis and characterization of polyamides X 18. *J. Appl. Polym. Sci.* **2005**, 98 (4), 1565–1571. DOI: 10.1002/app.22160.
- (119) Bennett, C.; Kaya, E.; Sikes, A. M.; Jarrett, W. L.; Mathias, L. J. Synthesis and characterization of nylon 18 18 and nylon 18 adamantane. *J. Polym. Sci. A Polym. Chem.* **2009**, 47 (17), 4409–4419. DOI: 10.1002/pola.23494.
- (120) Ahmadi, R.; Ullah, A. Synthesis and Characterization of Unsaturated Biobased-Polyamides from Plant Oil. *ACS Sustainable Chem. Eng.* **2020**, 8 (21), 8049–8058. DOI: 10.1021/acssuschemeng.0c02692.
- (121) Huang, Y.; Li, W.; Yan, D. Preparation and characterization of a series of polyamides with long alkylene segments: Nylons 12 20, 10 20,s 20,6 20, 4 20 and 2 20. *Polym. Bull.* **2002**, 49 (2-3), 111–118. DOI: 10.1007/s00289-002-0090-3.
- (122) Cui, X.; Yan, D. Synthesis and characterization of novel odd-even nylons based on eicosanedioic acid. *J. Appl. Polym. Sci.* **2004**, 93 (5), 2066–2071. DOI: 10.1002/app.20676.
- (123) Mutlu, H.; Meier, M. A. R. Unsaturated PA X,20 from Renewable Resources via Metathesis and Catalytic Amidation. *Macromol. Chem. Phys.* **2009**, 210 (12), 1019–1025. DOI: 10.1002/macp.200900045.

- (124) Zhang, G.; Yan, D. Morphology and Structure of Chain-Folded Lamellar Crystals of Nylons 2 22, 4 22, 6 22, 8 22, 10 22, and 12 22. *Cryst. Growth Des.* **2004**, *4* (2), 383–387. DOI: 10.1021/cg034177r.
- (125) Witt, T.; Häußler, M.; Kulpa, S.; Mecking, S. Chain Multiplication of Fatty Acids to Precise Telechelic Polyethylene. *Angew. Chem. Int. Ed.* **2017**, *56* (26), 7589–7594. DOI: 10.1002/anie.201702796.
- (126) Jiménez-Rodríguez, C.; Eastham, G. R.; Cole-Hamilton, D. J. Dicarboxylic acid esters from the carbonylation of unsaturated esters under mild conditions. *Inorg. Chem. Comm.* **2005**, *8* (10), 878–881. DOI: 10.1016/j.inoche.2005.06.005.
- (127) Stempfle, F.; Quinzler, D.; Heckler, I.; Mecking, S. Long-Chain Linear C19 and C23 Monomers and Polycondensates from Unsaturated Fatty Acid Esters. *Macromolecules* **2011**, *44* (11), 4159–4166. DOI: 10.1021/ma200627e.
- (128) Walther, G.; Deutsch, J.; Martin, A.; Baumann, F.-E.; Fridag, D.; Franke, R.; Köckritz, A. α,ω -Functionalized C19 monomers. *ChemSusChem* **2011**, *4* (8), 1052–1054. DOI: 10.1002/cssc.201100187. Published Online: Jun. 7, 2011.
- (129) Pinggen, D.; Schwaderer, J. B.; Walter, J.; Wen, J.; Murray, G.; Vogt, D.; Mecking, S. Diamines for Polymer Materials via Direct Amination of Lipid- and Lignocellulose-based Alcohols with NH₃. *ChemCatChem* **2018**, *10* (14), 3027–3033. DOI: 10.1002/cctc.201800365.
- (130) Witt, T.; Stempfle, F.; Roesle, P.; Häußler, M.; Mecking, S. Unsymmetrical α,ω -Difunctionalized Long-Chain Compounds via Full Molecular Incorporation of Fatty Acids. *ACS Catal.* **2015**, *5* (8), 4519–4529. DOI: 10.1021/acscatal.5b00825.
- (131) Le Goanvic, L.; Ternel, J.; Couturier, J.-L.; Dubois, J.-L.; Carpentier, J.-F. Rhodium-Biphephos-Catalyzed Tandem Isomerization–Hydroformylation of Oleonitrile. *Catalysts* **2018**, *8* (1), 21. DOI: 10.3390/catal8010021.
- (132) Ternel, J.; Couturier, J.-L.; Dubois, J.-L.; Carpentier, J.-F. Rhodium-Catalyzed Tandem Isomerization/Hydroformylation of the Bio-Sourced 10-Undecenitrile: Selective and Productive Catalysts for Production of Polyamide-12 Precursor. *Adv. Synth. Catal.* **2013**, *355* (16), 3191–3204. DOI: 10.1002/adsc.201300492.
- (133) Le Goanvic, L.; Couturier, J.-L.; Dubois, J.-L.; Carpentier, J.-F. Ruthenium-catalyzed hydroformylation of the functional unsaturated fatty nitrile 10-undecenitrile. *Journal of Molecular Catalysis A: Chemical* **2016**, *417*, 116–121. DOI: 10.1016/j.molcata.2016.02.030.

- (134) Le Goanvic, L.; Couturier, J.-L.; Dubois, J.-L.; Carpentier, J.-F. Insights in the Rhodium-Catalyzed Tandem Isomerization-Hydroformylation of 10-Undecenitrile: Evidence for a Fast Isomerization Regime. *Catalysts* **2018**, *8* (4), 148. DOI: 10.3390/catal8040148.
- (135) Perkins, R. B.; Roden, J. J.; Pryde, E. H. Nylon-9 from unsaturated fatty derivatives: Preparation and characterization. *J Am Oil Chem Soc* **1975**, *52* (11), 473–477. DOI: 10.1007/BF02637493.
- (136) Woroch, C. P.; Cox, I. W.; Kanan, M. W. A Semicrystalline Furanic Polyamide Made from Renewable Feedstocks. *J. Am. Chem. Soc.* **2023**, *145* (1), 697–705. DOI: 10.1021/jacs.2c11806. Published Online: Dec. 27, 2022.
- (137) Lankenau, A. W.; Kanan, M. W. Polyamide monomers via carbonate-promoted C-H carboxylation of furfurylamine. *Chem. Sci.* **2019**, *11* (1), 248–252. DOI: 10.1039/c9sc04460d. Published Online: Nov. 11, 2019.
- (138) Cousin, T.; Galy, J.; Rousseau, A.; Dupuy, J. Synthesis and properties of polyamides from 2,5-furandicarboxylic acid. *J. Appl. Polym. Sci.* **2018**, *135* (8), 45901. DOI: 10.1002/app.45901.
- (139) Huang, W.; Zhai, J.; Zhang, C.; Hu, X.; Zhu, N.; Chen, K.; Guo, K. 100% Bio-Based Polyamide with Temperature/Ultrasound Dually Triggered Reversible Cross-Linking. *Ind. Eng. Chem. Res.* **2020**, *59* (30), 13588–13594. DOI: 10.1021/acs.iecr.0c02028.
- (140) Mao, L.; Pan, L.; Ma, B.; He, Y. Synthesis and Characterization of Bio-Based Amorphous Polyamide From Dimethyl furan-2,5-dicarboxylate. *J Polym Environ* **2021**, 1–8. DOI: 10.1007/s10924-021-02265-5.
- (141) Ai, T.; Zou, G.; Feng, W.; Wang, P.; Lu, B.; Ren, Z.; Ji, J. Biobased Semiaromatic Polyamides Derived from Dimethyl Furan-2,5-Dicarboxylate: Influence of the Composition on Their Properties. *ACS Sustainable Chem. Eng.* **2022**, *10* (41), 13792–13804. DOI: 10.1021/acssuschemeng.2c04129.
- (142) Kamran, M.; Davidson, M. G.; Tsanaktis, V.; van Berkel, S.; Vos, S. de. Structure-property insights of semi-aromatic polyamides based on renewable furanic monomer and aliphatic diamines. *Eur. Polym. J.* **2022**, *178*, 111496. DOI: 10.1016/j.eurpolymj.2022.111496.
- (143) Kamran, M.; Davidson, M. G.; Vos, S. de; Tsanaktis, V.; Yeniad, B. Synthesis and characterisation of polyamides based on 2,5-furandicarboxylic acid as a sustainable

- building block for engineering plastics. *Polym. Chem.* **2022**, *13* (23), 3433–3443. DOI: 10.1039/D2PY00189F.
- (144) Fachagentur Nachwachsende Rohstoffe e. V, *Anbau und Verwendung nachwachsender Rohstoffe in Deutschland*, **2023**. <https://www.fnr.de/fileadmin/Statistik/2023.pdf> (accessed 2023-04-01).
- (145) Moazami, N.; Ashori, A.; Ranjbar, R.; Tangestani, M.; Eghtesadi, R.; Nejad, A. S. Large-scale biodiesel production using microalgae biomass of *Nannochloropsis*. *Biomass and Bioenergy* **2012**, *39*, 449–453. DOI: 10.1016/j.biombioe.2012.01.046.
- (146) Li, T.; Xu, J.; Wu, H.; Wang, G.; Dai, S.; Fan, J.; He, H.; Xiang, W. A Saponification Method for Chlorophyll Removal from Microalgae Biomass as Oil Feedstock. *Marine drugs* **2016**, *14* (9). DOI: 10.3390/md14090162. Published Online: Sep. 7, 2016.
- (147) Forman, G. S.; Tooze, R. P. Improved cross-metathesis of acrylate esters catalyzed by 2nd generation ruthenium carbene complexes. *J. Organomet. Chem.* **2005**, *690* (24-25), 5863–5866. DOI: 10.1016/j.jorganchem.2005.07.107.
- (148) Rybak, A.; Meier, M. A. R. Cross-metathesis of fatty acid derivatives with methyl acrylate: renewable raw materials for the chemical industry. *Green Chem.* **2007**, *9* (12), 1356–1361. DOI: 10.1039/b712293d.
- (149) Yinghuai, Z.; Kuijin, L.; Huimin, N.; Chuanzhao, L.; Stubbs, L. P.; Siong, C. F.; Muihua, T.; Peng, S. C. Magnetic Nanoparticle Supported Second Generation Hoveyda-Grubbs Catalyst for Metathesis of Unsaturated Fatty Acid Esters. *Adv. Synth. Catal.* **2009**, *351* (16), 2650–2656. DOI: 10.1002/adsc.200900370.
- (150) Vignon, P.; Vancompernelle, T.; Couturier, J.-L.; Dubois, J.-L.; Mortreux, A.; Gauvin, R. M. Cross-metathesis of biosourced fatty acid derivatives: a step further toward improved reactivity. *ChemSusChem* **2015**, *8* (7), 1143–1146. DOI: 10.1002/cssc.201403170.
- (151) Abel, G. A.; Oliver Nguyen, K.; Viamajala, S.; Varanasi, S.; Yamamoto, K. Cross-metathesis approach to produce precursors of nylon 12 and nylon 13 from microalgae. *RSC Adv.* **2014**, *4* (98), 55622–55628. DOI: 10.1039/C4RA10980E.
- (152) Miao, X.; Malacea, R.; Fischmeister, C.; Bruneau, C.; Dixneuf, P. H. Ruthenium-alkylidene catalysed cross-metathesis of fatty acid derivatives with acrylonitrile and methyl acrylate: a key step toward long-chain bifunctional and amino acid compounds. *Green Chem.* **2011**, *13* (10), 2911–2919. DOI: 10.1039/c1gc15569e.

- (153) Jacobs, T.; Rybak, A.; Meier, M. A. R. Cross-metathesis reactions of allyl chloride with fatty acid methyl esters: Efficient synthesis of α,ω -difunctional chemical intermediates from renewable raw materials. *Appl. Catal. A: Gen.* **2009**, *353* (1), 32–35. DOI: 10.1016/j.apcata.2008.10.026.
- (154) Compain, P. Olefin Metathesis of Amine-Containing Systems: Beyond the Current Consensus. *Adv. Synth. Catal.* **2007**, *349* (11-12), 1829–1846. DOI: 10.1002/adsc.200700161.
- (155) Yapa Mudiyansele, A.; Viamajala, S.; Varanasi, S.; Yamamoto, K. Simple Ring-Closing Metathesis Approach for Synthesis of PA11, 12, and 13 Precursors from Oleic Acid. *ACS Sustainable Chem. Eng.* **2014**, *2* (12), 2831–2836. DOI: 10.1021/sc500599u.
- (156) Abel, G. A.; Viamajala, S.; Varanasi, S.; Yamamoto, K. Toward Sustainable Synthesis of PA12 (Nylon-12) Precursor from Oleic Acid Using Ring-Closing Metathesis. *ACS Sustainable Chem. Eng.* **2016**, *4* (10), 5703–5710. DOI: 10.1021/acssuschemeng.6b01648.
- (157) Bosma, R. H. A.; van den Aardweg, F.; Mol, J. C. Cometathesis of methyl oleate and ethylene; a direct route to methyl dec-9-enoate. *J. Chem. Soc., Chem. Commun.* **1981** (21), 1132. DOI: 10.1039/c39810001132.
- (158) Warwel, S.; Bavaj, P.; Rüschen, Klaas, M.; Wolff, B. Polymerbausteine aus Pflanzenölen durch katalytische Reaktionen. In *Perspektiven nachwachsender Rohstoffe in der Chemie*; Eierdanz, H., Ed.; VCH, **1996**; 119-135.
- (159) Warwel, S.; Brüse, F.; Demes, C.; Kunz, M.; Rüschen, Klaas, M. Polymers and surfactants on the basis of renewable resources. *Chemosphere* **2001**, *43* (1), 39–48. DOI: 10.1016/S0045-6535(00)00322-2.
- (160) Warwel, S.; Tillack, J.; Demes, C.; Kunz, M. Polyesters of ω -Unsaturated Fatty Acid Derivatives. *Macromol. Chem. Phys.* **2001**, *202* (7), 1114–1121. DOI: 10.1002/1521-3935(20010401)202:7<1114:AID-MACP1114>3.0.CO;2-T.
- (161) Ngo, H. L.; Foglia, T. A. Synthesis of Long Chain Unsaturated- α,ω -Dicarboxylic Acids from Renewable Materials via Olefin Metathesis. *J Am Oil Chem Soc* **2007**, *84* (8), 777–784. DOI: 10.1007/s11746-007-1089-6.
- (162) Mutlu, H.; Hofstätter, R.; Montenegro, R. E.; Meier, M. A. R. Self-metathesis of fatty acid methyl esters: full conversion by choosing the appropriate plant oil. *RSC Adv.* **2013**, *3* (15), 4927–4934. DOI: 10.1039/c3ra40330k.
- (163) Miao, X.; Blokhin, A.; Pasynskii, A.; Nefedov, S.; Osipov, S. N.; Roisnel, T.; Bruneau, C.; Dixneuf, P. H. Alkylidene-Ruthenium-Tin Catalysts for the Formation of Fatty Nitriles

- and Esters via Cross-Metathesis of Plant Oil Derivatives. *Organometallics* **2010**, *29* (21), 5257–5262. DOI: 10.1021/om100372b.
- (164) Miao, X.; Fischmeister, C.; Bruneau, C.; Dixneuf, P. H.; Dubois, J.-L.; Couturier, J.-L. Tandem catalytic acrylonitrile cross-metathesis and hydrogenation of nitriles with ruthenium catalysts: direct access to linear α,ω -aminoesters from renewables. *ChemSusChem* **2012**, *5* (8), 1410–1414. DOI: 10.1002/cssc.201200086. Published Online: Jun. 15, 2012.
- (165) Garti, I.; Avni, E. Permanganate oxidation of oleic acid using emulsion technology. *J Am Oil Chem Soc* **1981**, *58* (8), 840–841. DOI: 10.1007/BF02665593.
- (166) Anastas, P.; Eghbali, N. Green chemistry: principles and practice. *Chem. Soc. Rev.* **2010**, *39* (1), 301–312. DOI: 10.1039/b918763b. Published Online: Nov. 20, 2009.
- (167) Ello, A. S.; Enferadi Kerenkan, A.; Trokourey, A.; Do, T.-O. Sustainable Oxidative Cleavage of Vegetable Oils into Diacids by Organo-Modified Molybdenum Oxide Heterogeneous Catalysts. *J Am Oil Chem Soc* **2017**, *94* (12), 1451–1461. DOI: 10.1007/s11746-017-3047-2.
- (168) Behr, A.; Tenhumberg, N.; Wintzer, A. Efficient ruthenium-catalysed oxidative cleavage of methyl oleate with hydrogen peroxide as oxidant. *RSC Adv.* **2013**, *3* (1), 172–180. DOI: 10.1039/C2RA22370H.
- (169) Nocito, F.; Orlando, I.; Digioia, F.; Aresta, M.; Dibenedetto, A. One-Pot Aerobic Cleavage of Monounsaturated Lipids Catalyzed by Mixed Oxides. *ACS Sustainable Chem. Eng.* **2021**, *9* (18), 6459–6469. DOI: 10.1021/acssuschemeng.1c01457.
- (170) Antonelli, E.; D'Aloisio, R.; Gambaro, M.; Fiorani, T.; Venturello, C. Efficient Oxidative Cleavage of Olefins to Carboxylic Acids with Hydrogen Peroxide Catalyzed by Methyltrioctylammonium Tetrakis(oxodiperoxotungsto)phosphate(3-) under Two-Phase Conditions. Synthetic Aspects and Investigation of the Reaction Course. *J. Org. Chem.* **1998**, *63* (21), 7190–7206. DOI: 10.1021/jo980481t.
- (171) Godard, A.; Caro, P. de; Thiebaud-Roux, S.; Vedrenne, E.; Mouloungui, Z. New Environmentally Friendly Oxidative Scission of Oleic Acid into Azelaic Acid and Pelargonic Acid. *J Am Oil Chem Soc* **2013**, *90* (1), 133–140. DOI: 10.1007/s11746-012-2134-7.
- (172) Kadyrov, R.; Hackenberger, D. Oxidative Cleavage of Long Chain Olefins to Carboxylic Acids with Hydrogen Peroxide. *Top Catal* **2014**, *57* (17-20), 1366–1371. DOI: 10.1007/s11244-014-0304-6.

- (173) Benessere, V.; Cucciolito, M. E.; Santis, A. de; Di Serio, M.; Esposito, R.; Ruffo, F.; Turco, R. Sustainable Process for Production of Azelaic Acid Through Oxidative Cleavage of Oleic Acid. *J Am Oil Chem Soc* **2015**, *92* (11-12), 1701–1707. DOI: 10.1007/s11746-015-2727-z.
- (174) Enferadi Kerenkan, A.; Béland, F.; Do, T.-O. Chemically catalyzed oxidative cleavage of unsaturated fatty acids and their derivatives into valuable products for industrial applications: a review and perspective. *Catal. Sci. Technol.* **2016**, *6* (4), 971–987. DOI: 10.1039/C5CY01118C.
- (175) Trebellas, J. C.; Thigpen, H. H. Liquid Phase Oxidation of p-Xylene to Terephthalic Acid US3860981, **1974**.
- (176) Hajra, B.; Sultana, N.; Guria, C.; Pathak, A. K.; Saxena, V. K. Liquid Phase Selective Catalytic Oxidation of Oleic Acid to Azelaic Acid Using Air and Transition Metal Acetate Bromide Complex. *J Am Oil Chem Soc* **2017**, *94* (12), 1463–1480. DOI: 10.1007/s11746-017-3048-1.
- (177) Miller, W. R.; Pryde, E. H.; Awl, R. A.; Kohlhase, W. L.; Moore, D. J. Nylon-9 Via 9-Aminononanoic Acid from Soybean Oil. *Product R&D* **1971**, *10* (4), 442–447. DOI: 10.1021/i360040a022.
- (178) Vondran, J.; Furst, M. R. L.; Eastham, G. R.; Seidensticker, T.; Cole-Hamilton, D. J. Magic of Alpha: The Chemistry of a Remarkable Bidentate Phosphine, 1,2-Bis(di-tert-butylphosphinomethyl)benzene. *Chem. Rev.* **2021**, *121* (11), 6610–6653. DOI: 10.1021/acs.chemrev.0c01254.
- (179) Quinzler, D.; Mecking, S. Linear semicrystalline polyesters from fatty acids by complete feedstock molecule utilization. *Angew. Chem. Int. Ed.* **2010**, *49* (25), 4306–4308. DOI: 10.1002/anie.201001510.
- (180) Goldbach, V.; Falivene, L.; Caporaso, L.; Cavallo, L.; Mecking, S. Single-Step Access to Long-Chain α,ω -Dicarboxylic Acids by Isomerizing Hydroxycarbonylation of Unsaturated Fatty Acids. *ACS Catal.* **2016**, *6* (12), 8229–8238. DOI: 10.1021/acscatal.6b02622.
- (181) Furst, M. R. L.; Le Goff, R.; Quinzler, D.; Mecking, S.; Botting, C. H.; Cole-Hamilton, D. J. Polymer precursors from catalytic reactions of natural oils. *Green Chem.* **2012**, *14* (2), 472–477. DOI: 10.1039/C1GC16094J.

- (182) Roesle, P.; Stempfle, F.; Hess, S. K.; Zimmerer, J.; R o B artulos, C.; Lepetit, B.; Eckert, A.; Kroth, P. G.; Mecking, S. Synthetic Polyester from Algae Oil. *Angew. Chem.* **2014**, *126* (26), 6918–6922. DOI: 10.1002/ange.201403991.
- (183) Pinggen, D.; Klinkenberg, N.; Mecking, S. Single-Step Catalytic Upgrading of Microalgae Biomass. *ACS Sustainable Chem. Eng.* **2018**, *6* (9), 11219–11221. DOI: 10.1021/acssuschemeng.8b02939.
- (184) Rist, M.; Greiner, A. Synthesis, Characterization, and the Potential for Closed Loop Recycling of Plant Oil-Based PA X.19 Polyamides. *ACS Sustainable Chem. Eng.* **2022**, *10* (50), 16793–16802. DOI: 10.1021/acssuschemeng.2c05176.
- (185) Herrmann, N.; K ohnke, K.; Seidensticker, T. Selective Product Crystallization for Concurrent Product Separation and Catalyst Recycling in the Isomerizing Methoxycarbonylation of Methyl Oleate. *ACS Sustainable Chem. Eng.* **2020**. DOI: 10.1021/acssuschemeng.0c03432.
- (186) Behr, A.; Obst, D.; Westfechtel, A. Isomerizing hydroformylation of fatty acid esters: Formation of ω -aldehydes. *Eur. J. Lipid Sci. Technol.* **2005**, *107* (4), 213–219. DOI: 10.1002/ejlt.200401123.
- (187) Mekki-Berrada, A.; Bennici, S.; Gillet, J.-P.; Couturier, J.-L.; Dubois, J.-L.; Auroux, A. Ammoniation-dehydration of fatty acids into nitriles: heterogeneous or homogeneous catalysis? *ChemSusChem* **2013**, *6* (8), 1478–1489. DOI: 10.1002/cssc.201300210. Published Online: Jun. 21, 2013.
- (188) T ur un , O.; Firdaus, M.; Klein, G.; Meier, M. A. R. Fatty acid derived renewable polyamides via thiol–ene additions. *Green Chem.* **2012**, *14* (9), 2577. DOI: 10.1039/c2gc35982k.
- (189) Unverferth, M.; Meier, M. A. R. Selective formation of C 36 -dimer fatty acids via thiol-ene addition for copolyamide synthesis. *Eur. J. Lipid Sci. Technol.* **2016**, *118* (10), 1470–1474. DOI: 10.1002/ejlt.201600003.
- (190) Leonard, E. C. Polymerization-dimer acids. *J Am Oil Chem Soc* **1979**, *56* (11Part2), 782A–785A. DOI: 10.1007/BF02667445.
- (191) Hablot, E.; Donnio, B.; Bouquey, M.; Av erous, L. Dimer acid-based thermoplastic bio-polyamides: Reaction kinetics, properties and structure. *Polymer* **2010**, *51* (25), 5895–5902. DOI: 10.1016/j.polymer.2010.10.026.
- (192) Freitas, R.; Klein, C.; Pereira, M. P.; Duczinski, R. B.; Einloft, S.; Seferin, M.; Ligabue, R. Lower purity dimer acid based polyamides used as hot melt adhesives: synthesis and

- properties. *J Adhes Sci Technol.* **2015**, 29 (17), 1860–1872. DOI: 10.1080/01694243.2014.1001961.
- (193) Reulier, M.; Avérous, L. Elaboration, morphology and properties of renewable thermoplastics blends, based on polyamide and polyurethane synthesized from dimer fatty acids. *Eur. Polym. J.* **2015**, 67, 418–427. DOI: 10.1016/j.eurpolymj.2014.11.036.
- (194) Ranganathan, P.; Chen, C.-W.; Tasi, M.-C.; Rwei, S.-P.; Lee, Y.-H. Biomass Thermoplastic (Co)polyamide Elastomers Synthesized from a Fatty Dimer Acid: a Sustainable Route toward a New Era of Uniform and Bimodal Foams. *Ind. Eng. Chem. Res.* **2021**, 60 (33), 12139–12154. DOI: 10.1021/acs.iecr.1c01533.
- (195) Winkler, M.; Steinbiß, M.; Meier, M. A. R. A more sustainable Wohl-Ziegler bromination: Versatile derivatization of unsaturated FAMES and synthesis of renewable polyamides. *Eur. J. Lipid Sci. Technol.* **2014**, 116 (1), 44–51. DOI: 10.1002/ejlt.201300126.
- (196) Winkler, M.; Meier, M. A. R. Highly efficient oxyfunctionalization of unsaturated fatty acid esters: an attractive route for the synthesis of polyamides from renewable resources. *Green Chem.* **2014**, 16 (4), 1784–1788. DOI: 10.1039/C3GC41921E.
- (197) Czapiewski, M. von; Meier, M. A. R. Synthesis of Dimer Fatty Acid Methyl Esters by Catalytic Oxidation and Reductive Amination: An Efficient Route to Branched Polyamides. *Eur. J. Lipid Sci. Technol.* **2018**, 120 (1), 1700350. DOI: 10.1002/ejlt.201700350.
- (198) TextileExchange, *Preferred Fiber & Materials:Market Report 2022*. TextileExchange, **2022**. https://textileexchange.org/app/uploads/2022/10/Textile-Exchange_PFMR_2022.pdf (accessed 2023-04-16).
- (199) Stibal, W.; Schwarz, R.; Kemp, U.; Bender, K.; Weger, F.; Stein, M. Fibers, 3. General Production Technology. In *Ullmann's Encyclopedia of Industrial Chemistry*; Bohnet, M., Ullmann, F., Eds.; Wiley VCH, **2003**. DOI: 10.1002/14356007.a10_511.
- (200) Salem, D. R., *Structure Formation in Polymeric Fibers*; Carl Hanser Verlag GmbH & Co. KG, **2001**. DOI: 10.3139/9783446456808.
- (201) Bessey, W.; Jaffe, M. Solid State Processing of Fibers. In *Solid phase processing of polymers*; Ward, I. M., Ed.; Progress in polymer processing; Hanser; Hanser Gardner, **2000**; pp 85–119. DOI: 10.3139/9783446401846.004.
- (202) Hufenus, R.; Yan, Y.; Dauner, M.; Kikutani, T. Melt-Spun Fibers for Textile Applications. *Materials* **2020**, 13 (19), 4298. DOI: 10.3390/ma13194298.

- (203) Giles, H. F.; Wagner, J. R.; Mount, E. M., *Extrusion: The definitive processing guide and handbook*; PDL handbook series; William Andrew, **2004**.
- (204) Prevorsek, D. C.; Tirpak, G. A.; Harget, P. J.; Reimschuessel, A. C. Effects of thermal contraction on structure and properties of PET fibers. *J. Macromol. Sci., Part B, Phys.* **1974**, 9 (4), 733–759. DOI: 10.1080/00222347408204559.
- (205) Wendorff, J. H.; Agarwal, S.; Greiner, A., *Electrospinning: Materials, processing, and applications*; John Wiley & Sons, **2012**. DOI: 10.1002/9783527647705.
- (206) Bose, G. M., *Recherches sur la cause et sur la véritable théorie de l'électricité*, **1745**.
- (207) Lord Rayleigh, F. R. S. On the equilibrium of liquid conducting masses charged with electricity. *Phil. Mag.* **1882**, 14 (87), 184–186. DOI: 10.1080/14786448208628425.
- (208) Boys, C. V. On the Production, Properties, and some suggested Uses of the Finest Threads. *Proc. Phys. Soc. London* **1887**, 9 (1), 8–19. DOI: 10.1088/1478-7814/9/1/303.
- (209) Morton, W. J. Method of dispersing fluids, US705691, **1902**.
- (210) Cooley, J. F. Apparatus for Electrically Dispersing Fluids, US692631, **1902**.
- (211) Cooley, J. F. Electrical Method of Dispersing Fluids, US745276, **1903**.
- (212) Formhals, A. Method and apparatus for the production of artificial fibers, US2158416, **1937**.
- (213) Formhals, A. Process and apparatus for preparing artificial threads, US1975504, **1934**.
- (214) Doshi, J.; Reneker, D. H. Electrospinning process and applications of electrospun fibers. *Journal of Electrostatics* **1995**, 35 (2-3), 151–160. DOI: 10.1016/0304-3886(95)00041-8.
- (215) Fong, H.; Chun, I.; Reneker, D. H. Beaded nanofibers formed during electrospinning. *Polymer* **1999**, 40 (16), 4585–4592. DOI: 10.1016/S0032-3861(99)00068-3.
- (216) Keirouz, A.; Wang, Z.; Reddy, V. S.; Nagy, Z. K.; Vass, P.; Buzgo, M.; Ramakrishna, S.; Radacsi, N. The History of Electrospinning: Past, Present, and Future Developments. *Adv Materials Technologies* **2023**, 8 (11), 2201723. DOI: 10.1002/admt.202201723.
- (217) Agarwal, S.; Burgard, M.; Greiner, A.; Wendorff, J. H., *Electrospinning: A practical guide to nanofibers*; De Gruyter Graduate; De Gruyter, **2016**. DOI: 10.1515/9783110333510.
- (218) Taylor, G. I. Disintegration of water drops in an electric field. *Proc. R. Soc. Lond. A* **1964**, 280 (1382), 383–397. DOI: 10.1098/rspa.1964.0151.

- (219) Wang, Y.; Wang, C. Extension rate and bending behavior of electrospinning jet: The role of solution conductivity. *Polymer* **2021**, *222*, 123672. DOI: 10.1016/j.polymer.2021.123672.
- (220) Inamuddin, I.; Boddula, R.; Ahamed, M. I.; Asiri, A. M., *Electrospun materials and their allied applications*; Wiley; Scrivener Publishing, **2020**.
- (221) Asmatulu, R.; Khan, W. S. Electrospun nanofibers for filtration applications. In *Synthesis and applications of electrospun nanofibers*; Asmatulu, R., Khan, W. S., Eds.; Micro & nano technologies series; Elsevier, **2019**; pp 135–152. DOI: 10.1016/B978-0-12-813914-1.00007-9.
- (222) Pretscher, M. O.; Sitaru, G.; Dietel, M.; Schmalz, H.; Gekle, S.; Agarwal, S. Post-Process-Functionalized Catalytic Electrospun and 2D-Printed Structures for Wolf–Lamb-Type Catalysis. *ACS Appl. Polym. Mater.* **2021**, *3* (3), 1349–1357. DOI: 10.1021/acsapm.0c01197.
- (223) Pazhaniswamy, S.; Joshi, S. A.; Hou, H.; Parameswaran, A. K.; Agarwal, S. Hybrid Polymer Electrolyte Encased Cathode Particles Interface-Based Core–Shell Structure for High-Performance Room Temperature All-Solid-State Batteries. *Adv. Energy Mater.* **2023**, *13* (1), 2202981. DOI: 10.1002/aenm.202202981.
- (224) Nallathambi, G.; Baskar, D.; Selvam, A. K. Preparation and characterization of triple layer membrane for water filtration. *Environ. Sci. Pollut. Res.* **2020**, *27* (24), 29717–29724. DOI: 10.1007/s11356-019-06254-z. Published Online: Aug. 24, 2019.
- (225) Gough, C. R.; Callaway, K.; Spencer, E.; Leisy, K.; Jiang, G.; Yang, S.; Hu, X. Biopolymer-Based Filtration Materials. *ACS Omega* **2021**, *6* (18), 11804–11812. DOI: 10.1021/acsomega.1c00791. Published Online: Apr. 26, 2021.
- (226) Mamun, A.; Blachowicz, T.; Sabantina, L. Electrospun Nanofiber Mats for Filtering Applications-Technology, Structure and Materials. *Polymers* **2021**, *13* (9). DOI: 10.3390/polym13091368. Published Online: Apr. 22, 2021.
- (227) Müller, A.-K.; Xu, Z.-K.; Greiner, A. Sustainable Electrospun Affinity Membranes for Water Remediation by Removing Metal and Metal Oxide Nanoparticles. *ACS Appl. Polym. Mater.* **2021**, *3* (11), 5739–5748. DOI: 10.1021/acsapm.1c00990.
- (228) Müller, A.-K.; Xu, Z.-K.; Greiner, A. Preparation and Performance Assessment of Low-Pressure Affinity Membranes Based on Functionalized, Electrospun Polyacrylates for Gold Nanoparticle Filtration. *ACS Appl. Mater. Interfaces* **2021**, *13* (13), 15659–15667. DOI: 10.1021/acsmi.1c01217. Published Online: Mar. 24, 2021.

- (229) Borojeni, I. A.; Gajewski, G.; Riahi, R. A. Application of Electrospun Nonwoven Fibers in Air Filters. *Fibers* **2022**, *10* (2), 15. DOI: 10.3390/fib10020015.
- (230) Matulevicius, J.; Kliucininkas, L.; Prasauskas, T.; Buivydiene, D.; Martuzevicius, D. The comparative study of aerosol filtration by electrospun polyamide, polyvinyl acetate, polyacrylonitrile and cellulose acetate nanofiber media. *Journal of Aerosol Science* **2016**, *92*, 27–37. DOI: 10.1016/j.jaerosci.2015.10.006.
- (231) Xu, X.; Yang, Y.; Liu, T.; Chu, B. Cost-effective polymer-based membranes for drinking water purification. *Giant* **2022**, *10*, 100099. DOI: 10.1016/j.giant.2022.100099.
- (232) Nayl, A. A.; Abd-Elhamid, A. I.; Awwad, N. S.; Abdelgawad, M. A.; Wu, J.; Mo, X.; Gomha, S. M.; Aly, A. A.; Bräse, S. Review of the Recent Advances in Electrospun Nanofibers Applications in Water Purification. *Polymers* **2022**, *14* (8). DOI: 10.3390/polym14081594. Published Online: Apr. 14, 2022.
- (233) Uddin, Z.; Ahmad, F.; Ullan, T.; Nawab, Y.; Ahmad, S.; Azam, F.; Rasheed, A.; Zafar, M. S. Recent trends in water purification using electrospun nanofibrous membranes. *Int. J. Environ. Sci. Technol.* **2021**, 1–28. DOI: 10.1007/s13762-021-03603-9.
- (234) Subrahmanya, T. M.; Arshad, A. B.; Lin, P. T.; Widakdo, J.; H K, M.; Austria, H. F. M.; Hu, C.-C.; Lai, J.-Y.; Hung, W.-S. A review of recent progress in polymeric electrospun nanofiber membranes in addressing safe water global issues. *RSC Adv.* **2021**, *11* (16), 9638–9663. DOI: 10.1039/d1ra00060h. Published Online: Mar. 4, 2021.
- (235) ISO 29463-1, *High efficiency filters and filter media for removing particles from air: Part 1: Classification, performance, testing*, **2017**.
- (236) Homaeigohar, S.; Elbahri, M. Nanocomposite Electrospun Nanofiber Membranes for Environmental Remediation. *Materials* **2014**, *7* (2), 1017–1045. DOI: 10.3390/ma7021017. Published Online: Feb. 10, 2014.
- (237) Jiang, S.; Schmalz, H.; Agarwal, S.; Greiner, A. Electrospinning of ABS nanofibers and their high filtration performance. *Adv. Fiber Mater.* **2020**, *2* (1), 34–43. DOI: 10.1007/s42765-019-00026-7.
- (238) Ahn, Y. C.; Park, S. K.; Kim, G. T.; Hwang, Y. J.; Lee, C. G.; Shin, H. S.; Lee, J. K. Development of high efficiency nanofilters made of nanofibers. *Current Applied Physics* **2006**, *6* (6), 1030–1035. DOI: 10.1016/j.cap.2005.07.013.
- (239) Zhang, Q.; Welch, J.; Park, H.; Wu, C.-Y.; Sigmund, W.; Marijnissen, J. C. Improvement in nanofiber filtration by multiple thin layers of nanofiber mats. *Journal of Aerosol Science* **2010**, *41* (2), 230–236. DOI: 10.1016/j.jaerosci.2009.10.001.

- (240) Yang, Y.; Zhang, S.; Zhao, X.; Yu, J.; Ding, B. Sandwich structured polyamide-6/polyacrylonitrile nanonets/bead-on-string composite membrane for effective air filtration. *Sep. Purif. Technol.* **2015**, *152*, 14–22. DOI: 10.1016/j.seppur.2015.08.005.
- (241) Yalcinkaya, F.; Yalcinkaya, B.; Hruza, J. Electrospun Polyamide-6 Nanofiber Hybrid Membranes for Wastewater Treatment. *Fibers Polym* **2019**, *20* (1), 93–99. DOI: 10.1007/s12221-019-8820-4.
- (242) Fauzi, A.; Hapidin, D. A.; Munir, M. M.; Iskandar, F.; Khairurrijal, K. A superhydrophilic bilayer structure of a nylon 6 nanofiber/cellulose membrane and its characterization as potential water filtration media. *RSC Adv.* **2020**, *10* (29), 17205–17216. DOI: 10.1039/D0RA01077D.
- (243) Aussawasathien, D.; Teerawattananon, C.; Vongachariya, A. Separation of micron to sub-micron particles from water: Electrospun nylon-6 nanofibrous membranes as pre-filters. *J. Membr. Sci.* **2008**, *315* (1-2), 11–19. DOI: 10.1016/j.memsci.2008.01.049.
- (244) Bazargan, A. M.; Keyanpour-rad, M.; Hesari, F. A.; Ganji, M. E. A study on the microfiltration behavior of self-supporting electrospun nanofibrous membrane in water using an optical particle counter. *Desalination* **2011**, *265* (1-3), 148–152. DOI: 10.1016/j.desal.2010.07.045.
- (245) R. Gopal; S. Kaur; Z. Ma; C. Chan; S. Ramakrishna; T. Matsuura. Electrospun nanofibrous filtration membrane. *J. Membr. Sci.* **2006**, *281* (1-2), 581–586. DOI: 10.1016/j.memsci.2006.04.026.
- (246) Li, M.; Li, J.; Zhou, M.; Xian, Y.; Shui, Y.; Wu, M.; Yao, Y. Super-hydrophilic electrospun PVDF/PVA-blended nanofiber membrane for microfiltration with ultrahigh water flux. *J. Appl. Polym. Sci.* **2020**, *137* (9), 48416. DOI: 10.1002/app.48416.
- (247) Zander, N. E.; Gillan, M.; Sweetser, D. Recycled PET Nanofibers for Water Filtration Applications. *Materials* **2016**, *9* (4). DOI: 10.3390/ma9040247. Published Online: Mar. 30, 2016.
- (248) Plastics Europe, *Plastics - The Facts 2022*. https://plasticseurope.org/de/wp-content/uploads/sites/3/2022/10/PE-PLASTICS-THE-FACTS_20221017.pdf (accessed 2023-06-20).
- (249) KPMG FAS, *KPMG FAS Newsletter Driver*. <https://assets.kpmg.com/content/dam/kpmg/jp/pdf/2019/jp-en-consumer-retail-esg.pdf> (accessed 2023-06-20).

- (250) Mayfield, S.; Burkart, M. The algae revolution 2.0: the potential of algae for the production of food, feed, fuel and bioproducts – why we need it now. *The Biochemist* **2021**, *43* (6), 34–38. DOI: 10.1042/bio_2021_190.
- (251) Hess, S. K.; Lepetit, B.; Kroth, P. G.; Mecking, S. Production of chemicals from microalgae lipids - status and perspectives. *Eur. J. Lipid Sci. Technol.* **2018**, *120* (1), 1700152. DOI: 10.1002/ejlt.201700152.
- (252) Shorland, F. B., *Chemical Plant Taxonomy*; Academic Press, **1963**. DOI: 10.1016/B978-0-12-395540-1.X5001-5.
- (253) Sievert, C. F. An introduction to the chemistry and biochemistry of fatty acids and their glycerides (Gunstone, F. D.). *J. Chem. Educ.* **1970**, *47* (4), A314. DOI: 10.1021/ed047pA314.

8 Conclusion

This thesis presents a comprehensive exploration of the synthesis, characterization, and potential applications of bio-based linear diacids and polyamides derived from oleic acid. Utilization of the isomerizing methoxycarbonylation enabled full use of the available bio-based carbon for the synthesis of aliphatic polyamides. The investigation into the structure-property relationship of these bio-based polyamides shed light on their unique characteristics and potential applications as fiber materials. Additionally, the thesis highlights the viability of a closed-loop approach, emphasizing the potential for these bio-based materials to be recycled and reprocessed, aligning with principles of circular economy.

Furthermore, the study advanced beyond synthesis by examining the spinnability and knittability of these oleic acid-based polyamides, leading to the production of monofilaments and fabrics suitable for the textile industry. This interdisciplinary approach showcased the potential of these bio-based materials to compete with conventional polyamides.

Moreover, the utilization of oleic acid-based azelaic acid for the production of bio-based PA 6.9 extended the application spectrum. Electrospun filter membranes from this polyamide demonstrated the suitability of these materials for water remediation and air purification. The meticulous characterization of these nonwovens ensured the tailoring of membrane properties for optimal performance. Additionally, the focus on recyclability highlighted the commitment to sustainable practices, as demonstrated by the successful recycling of the membranes.

The integration of these findings resulted in the publication of two peer-reviewed manuscripts and one soon to be published manuscript. Collectively, they highlight the potential of oleic acid-based polyamides for the production of synthetic fibers and their applications. Overall, this work represents a significant advance in the development of bio-based polyamides, which have a wide range of applications in sustainable textiles, membranes and potentially other industries, paving the way for more environmentally friendly and resource-efficient materials in the future.

9 Outlook

Looking ahead, the results presented in this thesis offer a promising outlook for the continued development and application of bio-based linear diacids and polyamides derived from oleic acid. The challenges posed by the finite nature of crude oil-based materials are being met with innovative solutions, as exemplified by the utilization of oleic acid. Furthermore, the potential of algae-derived feedstock presents a compelling avenue to address concerns regarding competition with food production, ensuring the viability of bio-based polyamides without compromising vital resources.

The monofilaments produced in this work gave a good indication for the general production of melt-spun fibers. Multifilament yarns, on the other hand, would open up a wider field of applications in the textile and automotive sectors. Additionally, melt spinning of the PA X.19 homopolymers might result in fibers having good mechanical properties together with a higher bio-content.

The polyamides also showed good potential for the production of films by solvent casting or melt pressing. The resulting films might exhibit interesting barrier properties together with high mechanical stability.

Furthermore, the emerging field of 3D printing also offers an exciting opportunity for the application of oleic acid-based polyamides. The fast and flexible production of customized parts made from bio-based polyamides might attract various sectors, such as automotive, aerospace, and medical. This avenue of exploration could significantly expand the scope of applications for bio-based polyamides.

Electrospinning of the PA X.19 homopolymers might result in nonwovens with unique properties due to their lower hydrophilicity. Improved air purification membranes might be accessible by preparation of a composite membrane by electrospinning the bio-based polyamide on a support layer. The thin polyamide layer could result in a lower pressure drop, while maintaining a high separation efficiency. Regarding water remediation, the separation of emulsified oil in water should be investigated in a continuous setup and compared to industrial standards.

10 Acknowledgements

First of all, I want to thank Prof. Greiner for giving me the opportunity of working with this great topic. I very much enjoyed the freedom you have offered me during my research and am grateful for all the constructive discussions we had. The collaboration with so many talented individuals in our interdisciplinary project was inspiring and a great pleasure to me. Thank you for all your support you have given me during my time at the chair.

Additionally, I want to thank Prof. Agarwal for all her backup and support. Thank you for the fruitful discussions and the resulting inspiration for new ideas.

Thank you to everyone at the chair of MC 2 for the great time that I had during the last 3.5 years with you. A special thank you goes out to the game night regulars Sophie, Tasmai, Hendrik, Yannick, Sören, Elmar, Marcel and Benedict. Thank you for keeping me company and mentally sane virtually during the pandemic and later on also in person.

I also want to thank the technical staff at the chair. Thank you, Annette for the quick ordering of all the necessary chemicals and equipment and her overall positive energy she brought to the lab. Also, a big thank you to Lothar for his help setting up bigger reactions at the reactors and his advice. Thank you, Holger for the valuable discussions and the new ideas that came from these. Additionally, I want to thank Reiner Giesa from MC 1 for basically teaching me everything I needed to know for the testing of mechanical properties and interpretation of results. Thank you, Rika for all the GPC measurements and for your help with the ozonolysis reactions. Another big thank you goes out to our secretaries Christina and Ramona for dealing with all of the paper work and planning in lightning speed, and also for the many great talks we had during my time at the chair.

An additional thank you goes to my students, Merlin, Leo and Tino, who have performed excellent work and have all contributed to this work in their own way.

Special thanks to my lab buddies from 796, Benedict, Dipannita and Dan. Thank you for the great atmosphere, whether it was saturated with thiols, amines, sulfoxides or just loud music. Thank you for all the great times and being there during the not so great times.

Last but not least I want to thank my family for all the support they have given me during my chemistry studies over the last 13 years. I would also like to thank Carlotta for her patience in difficult times and for helping me to refocus myself when necessary.

11 Eidesstattliche Versicherungen und Erklärungen

(§ 9 Satz 2 Nr. 3 PromO BayNAT)

Hiermit versichere ich eidesstattlich, dass ich die Arbeit selbstständig verfasst und keine anderen als die von mir angegebenen Quellen und Hilfsmittel benutzt habe (vgl. Art. 97 Abs. 1 Satz 8 BayHIG).

(§ 9 Satz 2 Nr. 3 PromO BayNAT)

Hiermit erkläre ich, dass ich die Dissertation nicht bereits zur Erlangung eines akademischen Grades eingereicht habe und dass ich nicht bereits diese oder eine gleichartige Doktorprüfung endgültig nicht bestanden habe.

(§ 9 Satz 2 Nr. 4 PromO BayNAT)

Hiermit erkläre ich, dass ich Hilfe von gewerblichen Promotionsberatern bzw. -vermittlern oder ähnlichen Dienstleistern weder bisher in Anspruch genommen habe noch künftig in Anspruch nehmen werde.

(§ 9 Satz 2 Nr. 7 PromO BayNAT)

Hiermit erkläre ich mein Einverständnis, dass die elektronische Fassung meiner Dissertation unter Wahrung meiner Urheberrechte und des Datenschutzes einer gesonderten Überprüfung unterzogen werden kann.

(§ 9 Satz 2 Nr. 8 PromO BayNAT)

Hiermit erkläre ich mein Einverständnis, dass bei Verdacht wissenschaftlichen Fehlverhaltens Ermittlungen durch universitätsinterne Organe der wissenschaftlichen Selbstkontrolle stattfinden können.

.....

Ort, Datum, Unterschrift